Template-Assisted Patterning of Functional Polymers

Dissertation

zur Erlangung des Grades
“Doktor der Naturwissenschaften“
im Promotionsfach Chemie

am Fachbereich Chemie, Pharmazie und Geowissenschaften
der Johannes Gutenberg-Universität Mainz

Niko Haberkorn

geb. in Lauterbach

Mainz, 2010

Die vorliegende Arbeit wurde unter der Betreuung von [redacted] in der Zeit von Mai 2007 bis Juli 2010 am Institut für Organische Chemie der Johannes Gutenberg-Universität Mainz, am Max-Planck-Institut für Polymerforschung in Mainz und der Seoul National University in Südkorea angefertigt.

Dekan:	[redacted]
Erster Berichterstatter:	[redacted]
Zweiter Berichterstatter:	[redacted]
Tag der mündlichen Prüfung:	13.08.2010

Table of Contents

List of Abbreviations

a.u.	arbitrary units
AAO	anodic aluminum oxide
AFM	atomic force microscopy
AIBN	azoisobutyronitrile
AM	air mass
ATO	anodic titanium oxide
ATR	attenuated total reflectance
b	*block*
br	broad (NMR spectroscopy)
$CDCl_3$	deuterated chloroform
CLSM	confocal laser scanning microgaphy
CPMAS NMR	charge polarized magic angle spinning nuclear magnetic resonance
CV	cyclovoltammetry
d	distance
d	duplet (multiplicity in NMR spectroscopy)
dba	dibenzylideneacetone
DCM	dichloromethane
d_{Int}	interpore distance
DMF	dimethylformamide
dp	pore diameter
d_p	pore diameter
DPPF	1,1’-bis(diphenylphosphino)-ferrocene
DSC	differential scanning calorimetry
DTMS-TPD	*N,N′-bis(4-methoxyphenyl)-N,N′-bis(4-((3-(trimethoxysilyl) propoxy) methyl)-phenyl)- (1,1′-biphenyl)-4,4′-diamine*
DVTPA	4,4’-divinyltriphenylamine
DVTPD	*N,N′-bis(4-methoxyphenyl)-N,N′-bis(4-vinylphenyl-(1,1′-biphenyl)-4,4′-diamine)*
E	electrical field
EA	electron affinity
eq.	equivalent
EQE	external quantum efficiency

eV	electron volt
F8BT	poly(9,9′-dioctylfluorene-co-benzothiadiazole)
FD	field desorption (mass spectroscopy)
FF	fill factor
FFT	fast fourier transformation
FIB	focused ion beam
FTO	fluorine doped oxide
FTO	fluorine doped tin oxide
γ	surface tension
g	gravitational acceleration
g	gram
GPC	gel permeation chromatography
h	height
η	efficiency
h	hours
HA	hard anodization
HBC	hexa-*peri*-hexabenzocoronenes
HOMO	highest occupied molecular orbital
Hz	hertz
I	current
IPCE	incident power to current efficiency
IR	infrared
I_{SC}	short circuit current
ITO	indium tin oxide
J	coupling constant (NMR spectroscopy)
L	liter
lc	capillary length
LC	liquid crystal
LCE	liquid crystalline elastomers
LCST	lower critical solution temperature
LUMO	lowest unocupied molecular orbital
M	molar
m	multiplet (multiplicity in NMR spectroscopy)
MDMO-PPV	poly[2-methoxy-5-(3,7-dimethyloctyloxy)]-1,4-phenylenevinylene

Ni-BNc	tetrakis(*tert*-butyl)-naphthalocyaninato nickel
NIPAM	*N*-isopropylacrylamide
NLO	non-lnear optic
nm	nanometer
NMR	nuclear magnetic resonance
OFET	organic field emitting transistor
OLED	organic light emitting devices
OPV	organic photovoltaic device
P2VP	poly(2-vinylpyridine)
P3HT	poly(3-hexylthiophene)
PANI	polyaniline
PCBM	1-(3- methoxycarbonyl) propyl-1-phenyl[6,6]C_{61}
PDI	polydispersity index
PDMS	polydimethylsiloxane
PEDOT	poly(3,4-ethylenedioxythiophene)
PEO	poly(ethylene oxide)
PFS	poly(4-fluorostyrene)
Pip-NBD	piperazinyl-4-chloro-7-nitrobenzofurane
PLA	poly(lactide acid)
P_{max}	maximum power
PMDDOPP	poly(2-methoxy-5-dodecyloxy-p-phenylenevinylene)
PMMA	poly(methylmethacylate)
POM	polarized optical microscopy
POOPPV	poly(2,5-dioctyloxy-p-phenylenevinylene)
PPerAcry	poly(perylene bisimide acrylate)
PPFPA	pentafluorophenylacrylate
PPFPVB	poly(pentafluorophenyl 4-vinylbenzoate)
ppm	parts per million (NMR spectroscopy)
PS	polystyrene
PSA	phenolsulfonate
PVDF	poly(vinylidene fluoride)
θ	contact angle
ρ	density
RAFT	reversible addition-fragmentation chain transfer
RT	room temperature

s	singlet (multiplicity in NMR spectroscopy)
S101C	sulforhodamine 101 cadervarine
SCTMM	conductive scanning torsion mode microscopy
SEM	scanning electron microscopy
t	triplet (multiplicity in NMR spectroscopy)
TEM	transmission electron microscopy
TGA	thermo gravimetrical analysis
THF	tetrahydrofurane
TPA	triphenylamine
TPD	tetraphenylbenzidene
U	voltage
UV	ultraviolett
UV	ultraviolett
V	volt
v	volume
V_{OC}	open circuit voltage
Wc	capillary interaction energy
wt%	weight percent
ξ	volume expansion coefficient
λ	wavelength

1 Introduction

1.1 Nanoporous Templates

In the following chapter the most commonly used porous templates, like ion-track etched membranes, anodic metal oxides, such as anodic aluminum oxide (AAO) or anodic titanium oxide (ATO), macroporous silicon and block copolymer templates are presented (see Figure 1). These templates can be employed in order to pattern inorganic and organic materials on the nanometer scale and are used to fabricate one-dimensional nanostructures such as fibers and tubules with a well-controllable size and shape. The focus lays on anodic aluminum oxide (AAO) since they were chosen to be the most suitable in regard to the needs for the patterning steps, which are presented in this thesis.

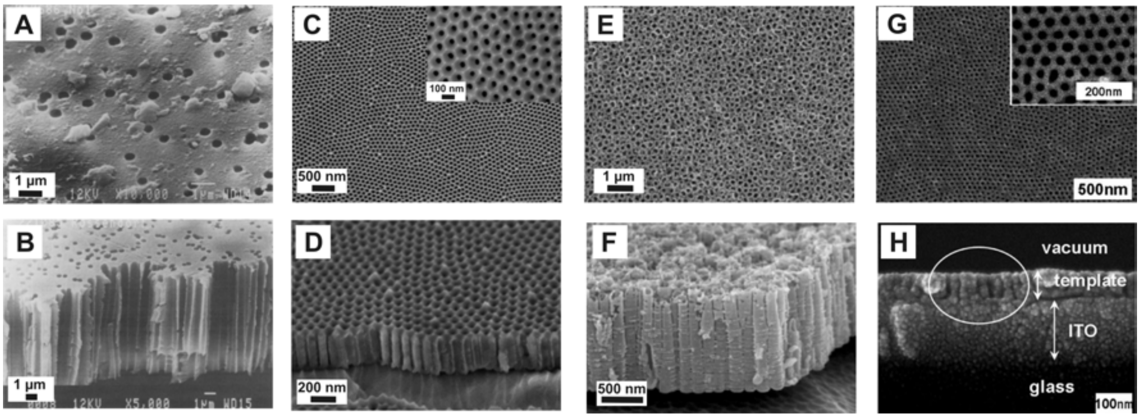

Figure 1. *Scanning electron micrographs of nanoporous templates: Top view (A) and cross-sectional view (B) of track-etched membranes. Reproduced from [1]; AAO templates anodized with an oxalic acid electrolyte at 40 V (C and D)[2]; Nanotube arrays of anodic titanium oxide (ATO) templates (E and F). Reproduced from [3]; Block copolymer templates prepared by PS-b-PMMA/PMMA mixture film on ITO/glass (G and H). Reproduced from [4].*

1.1.1 Anodic Aluminum Oxide (AAO)

1.1.1.1 History and General Remarks

Due to the high affinity of aluminum surfaces for oxygen a very thin and highly resistant oxide film is formed on aluminum upon exposure to air.[5] *Via* an electrochemical oxidation, so-called anodization, which was already reported at the beginning of the last century, the thickness of the native oxide film can be increased.[6] For aluminum but also for various other metals like magnesium, titanium, silicon, tungsten, vanadium etc. this process is commercially used to increase the resistance of the metal to corrosion and wear. Further electrochemically-fabricated aluminum oxide has been applied in rectifiers and as dielectrics in aluminum capacitors.[7-9]

The anodization of aluminum gained increasing attention after the discovery of unordered porous oxide films that are formed *via* anodization in electrolytes like sulphuric, oxalic and phosphoric acid (see Figure 3A). The unordered porous oxide films provide excellent corrosion and abrasion resistance and form a good base for paints and dyes.[5] Further the deposition of metal salts like copper, silver, tin etc. into porous alumina was intensively used for the coloring of anodized surfaces.[10-12]

In the 1970s nanoporous AAO filled with electrodeposited metals were also considered to be used as magnetic memories and recording devices.[13, 14] However at this time the ordering of the porous aluminum oxide was still poor and consequently only a low storage density could have been realized. At present AAO membranes with irregularly ordered pores and a broad size distribution are commercially available from *Whatman* and mainly find application as filters.[15]

A major breakthrough for the preparation of AAO was made by *Masuda* and *Fukuda* in the 1990s. They reported on the fabrication of highly ordered porous AAO with a low pore size distribution by utilizing a two-step anodization process (see Figure 2).[16, 17] Briefly described, the first anodization step initially results in disordered pores, which self-assemble into a regular hexagonal lattice after longer anodization times. In a subsequent wet-chemical etching step of the alumina layer the disordered pores on the surface of the layer are removed and leave hexagonally arranged indentions in the remaining aluminum layer behind. In the following second anodization step, these indentions act as seeds for the pore growth and results in an array of columnar hexagonal packed cells with central, cylindrical, uniformly sized pores.

Self-ordered anodic aluminum oxide that is fabricated by a two-step anodization process exhibits a poly-domain structure (see Figure 3 B). Each domain with a highly ordered array of pores is separated with neighboring domains by grain boundaries. At these boundaries the hexagonal order is interrupted and defects are present. By combining self-ordered anodization with prepatterning of the aluminum substrates *Masuda* demonstrated the fabrication of AAO with a long-range order.[18] Techniques like nanoimprinting,[19] focused ion beam,[20] holographic[21] and microsphere lithography[22] were employed for the prepatterning. The nanoindentions on the surface that were formed by the prepatterning step initiates the pore nucleation and leads to the long-range order. AAO with square and triangular array architectures are also feasible by utilizing prepatterning anodization.[23]

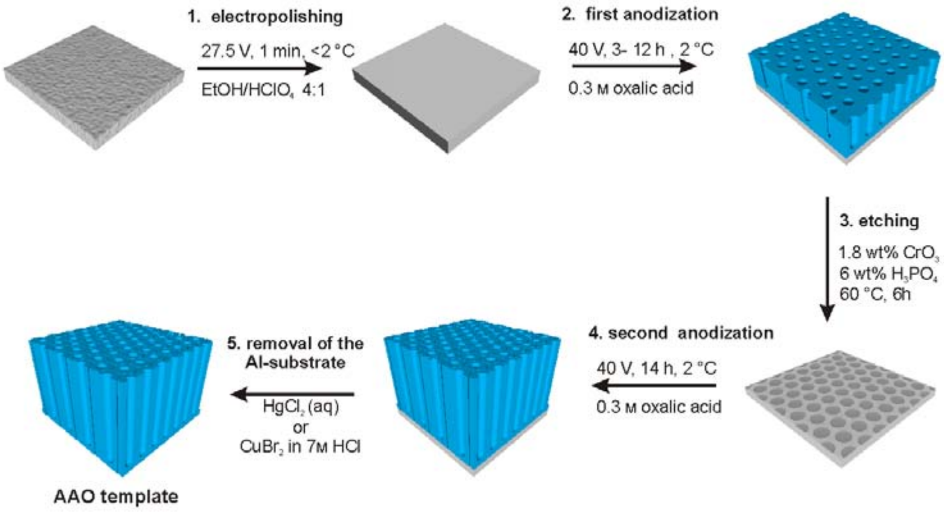

Figure 2. *Schematic diagram of the fabrication of hexagonally-ordered AAO templates by utilizing a two-step anodization: (1) Cleaning and smoothing of the surface of high-purity aluminum via electro polishing; (2) first anodization step results in partially unordered pores; (3) selective etching of the porous alumina by treatment in aqueous chromic acid; (4) formation of hexagonally-ordered pores during the second anodization since the ordered indentions on the aluminum surface act as seeds for the pore growth; (5) Selective removal of the residual aluminum layer via treatment with aqueous mercury-(II)-chloride or acidic copper-(II)-bromide solution.*

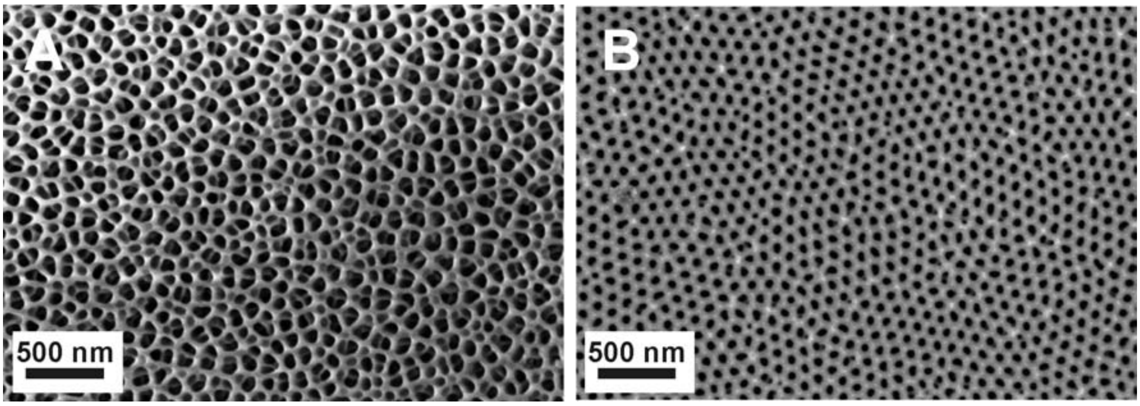

Figure 3. *Scanning electron micrographs of (A) AAO anodized in aqueous phosphoric acid (1 wt%) at 80 V. The experimental parameters are within the regime for an ordered pore growth. (B) Anodization in oxalic acid (c = 0.3 M) at 40 V results in well-ordered AAO templates with a polydomain structure. Defects can form at the grain boundaries.*

Up to now the fabrication of well-ordered AAO has been intensively investigated and AAO templates with very high lateral pore densities of up to 10^{11} cm^{-2} and a broad range of pore sizes ranging from 10 nm to 200 nm in diameter and up to 100 μm in length are accessible.[24-27]

The pore diameter d_p and the inter-pore distance d_{Int}, mainly depend on the applied voltage, the nature of the electrolyte and the electrolyte concentration (see Figure 4). Three different self-ordering regimes can be distinguished, which are commonly used for the fabrication of self-ordered AAO arrays:[28] Anodization in (i) phosphoric acid (0.1 M) at 195 V (d_{Int}≈500 nm; d_p≈160 nm),[29, 30] (ii) oxalic acid (0.3 M) at 40 V (d_{Int}≈100 nm; d_p≈40 nm)[31, 32] and (iii) sulfuric acid (0.3 M) at 25 V (d_{Int}≈65 nm; d_p≈30 nm).[17, 33]

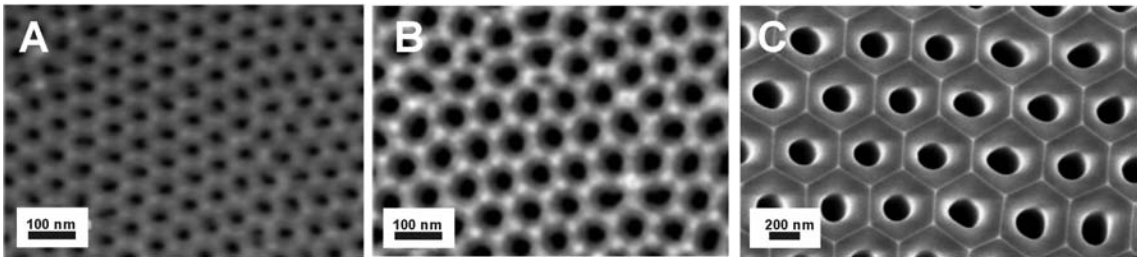

Figure 4. *Top-view scanning electron micrographs of well-ordered AAO that was anodized within the self-ordering parameters: Anodization in (A) sulfuric acid (c = 0.3 mol L^{-1}) at 25 V yield pores with d_{Int}≈65 nm; d_p≈30 nm; (B) oxalic acid (c = 0.3 mol L^{-1}) at 40V generates well-ordered AAO with d_{Int}≈100 nm and d_p≈40 nm; (C) phosphoric acid (1 wt%) at 195 V results in the formation of pores with d_{Int}≈500 nm; d_p≈160 nm.*

Further, by a subsequent partial wet-chemical etching step the pores could also be post-widened or the pore bottom can be removed, resulting in porous structures opened on both sides. The fabrication of well-ordered AAO was also investigated in other electrolytes in order to broaden the range of accessible pore parameters.[34-37] More sophisticated well-ordered porous structures, like branched and bamboo-like architectures have been demonstrated recently by sequential change of the applied voltage and pulsed anodization procedures respectively.[38, 39] A more detailed overview about the pore dimensions at various anodization parameters can be found in the following references.[25, 40, 41]

Besides the mentioned conventional – so-called "mild anodization" – process, which can only be performed in a narrow range of voltage for the given electrolyte *Lee et al.* recently introduced a "hard anodization" (HA) process to form well-ordered porous alumina structures.[38] This approach is much faster than the fabrication under mild conditions and allows the fabrication of AAO membranes with interpore distances of d_{Int}=200–300 nm, which have not been accessible by mild anodization so far.

Besides the feasibility to easily tune their pore parameters, AAO templates offer a thermal and mechanical stability as well as potential low fabrication costs and a high resistance to organic solvents. Therefore at present self-ordered AAO is one of the most frequently used kind of template for the fabrication of one-dimensional nanostructures composed of a number of different materials like metals, carbon, inorganic semiconductors, nanoparticles, low-molecular organic materials, polymers, metal-polymer amphiphiles etc.

1.1.1.2 Electrochemical Priciples of Aluminum Oxide Formation

If aluminum is electrochemically oxidized in a conductive aqueous electrolyte the oxidation can be written as:

$$2Al + 3H_2O \rightarrow Al_2O_3 + 6H^+ + 6e^- \tag{1}$$

At the cathode hydrogen is formed by reduction of H^+-ions:

$$6H^+ + 6e^- \longrightarrow 3H_2 \tag{2}$$

Although these simplified redox equations correctly describe the anodization of aluminum, they do not give any information about the detailed oxidation mechanism and the morphology of the formed aluminum oxide.

Depending on the properties of the electrolyte that is used for the anodization of aluminum, two different types of oxide layers can be formed. In near-neutral electrolytes (5<pH<7), such as aqueous tartaric acid, boric acid and ammonium tetraborate solutions, a homogenous, nonporous oxide barrier is generated. In contrast a porous aluminum oxide layer is obtained by performing the anodization in weakly acidic electrolytes, e.g., sulfuric, oxalic and phosphoric acid. The porosity of the resulting layer is mainly caused by a partial dissolution of the aluminum oxide during the anodization process. However the detailed oxidation reactions and the formation of ordered porous morphologies are not fully understood and several mechanisms have been proposed[7, 42-52] the formation of the morphologically different layers can be well explained by the newly established equifield strength model.[53, 54] It is taken into account that two basic chemical processes take place during the anodization process: (i) the oxidation of aluminum into Al^{3+} cations at the metal/oxide interface

$$Al \longrightarrow Al^{3+} + 3e^- \tag{3}$$

and (ii) the dissolution of aluminum oxide at the interface between electrolyte and oxide.

The formed Al^{3+} ions can either migrate through the oxide layer and dissolve into the electrolyte or they remain at the metal/oxide interface and directly form Al_2O_3 with oxide anions (O^{2-} and OH^-) migrated from the electrolyte/oxide interface.

$$2Al^{3+} + 3O^{2-} \longrightarrow 2Al_2O_3 \tag{4}$$

$$2Al^{3+} + 3OH^- \longrightarrow Al_2O_3 + 3H^+ \tag{5}$$

These oxide anions migrate induced by the high electric field and are formed by partial dissolution of Al_2O_3 and dissociation of water at the electrolyte/oxide interface and the overall reaction can be written as:[53, 55]

$$Al_2O_3 + nH_2O \longrightarrow 2Al^{3+} + (3+n-x)O^{2-} + xOH^- + (2n-x)H^+ \qquad (6)$$

where x is introduced as an indicator for the ratio of O^{2-} and OH^- that has not yet been exactly determined and n indicates the ratio of the dissociation rate of water and the rate of Al_2O_3 dissolution. The oxide layer thickness is increased by the formation of Al_2O_3 in reaction (4) and (5), and decreased by the described dissolution process in reaction (6).

In a near-neutral solution the dissolution of aluminum oxide in reaction (6) is very slow and if the applied voltage is sufficient to generate an electric field that carries on the anion migration, the thickness of the flat Al_2O_3 layer will continuously increase. However the thickness of the generated layer is limited since the electric field strength can be written as $E = U/d$, where U is the applied voltage and d the thickness of the oxide layer. If a constant voltage is applied and d approaches a critical value d_c the electrical field strength E_C becomes to weak to sustain the anion migration and the oxide growth eventually stops. For near-neutral electrolytes the value for U/d_c was experimentally determined to be approximately 0.7 V nm^{-1}.[5] Thus by applying a constant voltage of about 800 V a homogenous oxide barrier layer with a thickness of 1 μm can be fabricated. For even higher voltages a dielectrical breakdown occurs.[5] Figure 5 shows the equifield strength model for a non-porous oxide layer. For the flat non-porous morphology the electric field has a constant strength at any point across the oxide layer.

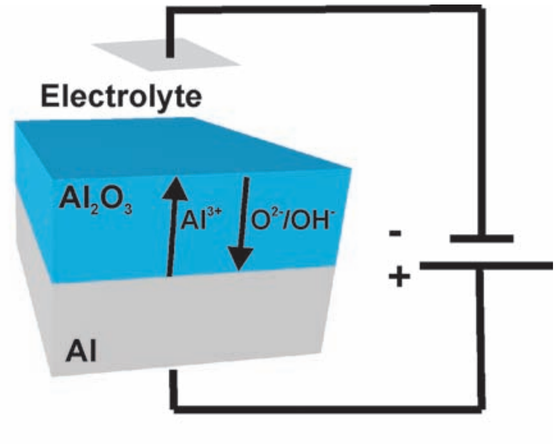

Figure 5. *Schematic diagram of anodization of aluminum in near neutral electrolytes. A uniform planar oxide layer is formed. The applied voltage promotes the migration of* Al^{3+} *and* O^{2-}/OH^- *ions through the oxide layer.*

In contrast to the near-neutral electrolytes the dissolution of the oxide layer at the oxide/electrolyte interface is significantly increased in weakly acidic electrolytes. Further by applying an electrical field that results in a more severe polarization and impairment of the Al-O bond the dissolution rate can be even increased.[7] Due to the increased dissolution rate the critical value for the oxide layer thickness d_c can never be approached. Both the oxidation and the dissolution process can continue indefinitely. After some time a steady state with constant dissolution and oxidation rates is achieved. The thickness of the corresponding oxide layer d_B is smaller than d_C and the electrical field E_B is larger than E_C under near-neutral conditions. Theoretically the anodization still generates a flat nonporous oxide film in weakly acidic electrolytes. In fact, even high purity aluminum exhibits several kinds of defects on their surface, such as impurities, dislocation, grain boundaries, nonmetallic inclusions and a certain roughness. It has also been reported that high-density voids in the oxide layer are formed when Al^{3+} ions are ejected from the oxide layer.[56, 57] Pretreatment of aluminum in phosphoric acid or sodium hydroxide can also result in the formation of voids.[58, 59] Induced by these defects the dissolution rate of the oxide layer is normally not homogeneous all over the surface and leads to a pit growth as an initial step of pore growth.[60]

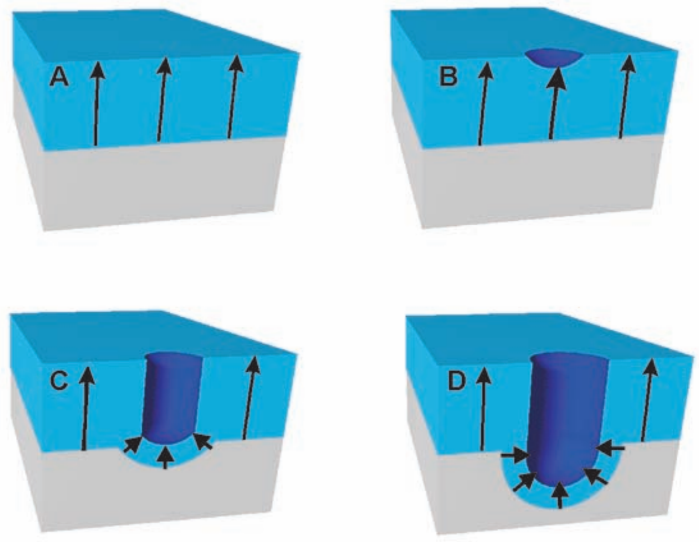

Figure 6. *Schematic representation of the pore formation mechanism in weak acidic electrolytes. (A) Planar oxide layer with a uniform thickness and a uniform electric-field strength distribution (B) Formation of a corrosive pit. The electric-field strength below the pit is enhanced which consequently increased the local oxidation and field-assisted dissolution rate. (C) The indention of the corrosive pit on the oxide/electrolyte interface is replicated at the metal/oxide interface. (D) A cylindrical pore with a hemispherical base is formed.*

As shown in Fig. 6B, the oxide layer below the formed pit is thinner than that of the homogenous layer and consequently the electrical field is stronger, which results in an enhanced oxidation rate. While further anodization the pit at the electrolyte/oxide interface is replicated to the oxide/metal interface in order to rebalance the areal inhomogeneous field strength. The formed hemispherical shape of the pore provides a uniform oxide thickness and consequently a uniform electrical field strength on the surface. After further growth of the pore the characteristic cylindrical shape is obtained. Noteworthy, since the electrical field strength at the sidewalls is equal to that at the hemispherical bottom, the pores cannot exclusively grow downwards but also sideward. This lateral growth would result in a continuous increase of the diameter of a single pore. However this pore widening effect is restricted due to the high lateral pore density and stops after two walls of neighbored pores merge together. For a better clarity the approach and the merging of separated pores is discussed in a simplified two-pore model (see Figure 7). Directly after the pores move towards each other and merge the total wall thickness will be $2d_B$ (see Figure 7). However the oxidation rate at the joint position B is larger than on the other positions since the anions can migrate from both sides to B. Consequently the joint position will shift downwards to point D and the total wall thickness will slightly decease to $2d_w$.

In the case of two pores are being to close according to the equifield strength model the wall will also increase until the balanced total wall thickness $2d_w$ has reached. The pore architecture, which is derived from the equifield strength model and is shown in Figure 7C, is in accordance with cross-sectional scanning electron micrographs of the AAO. Figure 7D shows a SEM image of the AAO morphology after anodization in oxalic acid. Instead of the completely hemispherical shape of pores, which was proposed for the growth of a single pore, the balanced curvature became more fattened with spherical angle of 2θ.

As described by the equifield strength model each pore can shift laterally in order to balance its distance to the neighboring pores. Applied to a two dimensional ordering of pores this self-ordering can explain the formation of hexagonally ordered pores.

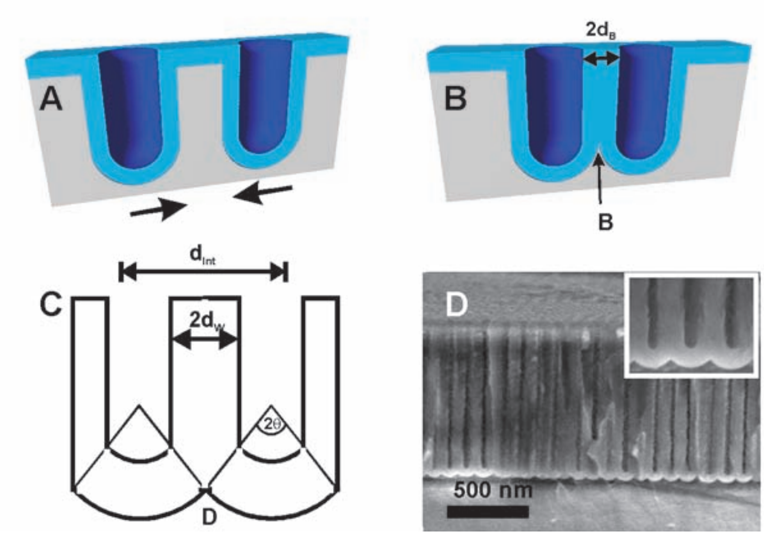

Figure 7. *Schematic illustration for the self-ordering mechanism of two-pores. (A)Two single pores having an interpore distance larger than $2d_B$ are formed and move towards according to the equifield strength model. (B) Merging of the oxide walls of two pores with a total wall thickness of $2d_w$. The electric field strength at point B is larger than at other positions of the oxide/metal interface and in order to balance the electric-field strength a pore morphology with a curvature of 2θ is formed (C). (D) Cross-sectional scanning electron micrograph of aluminum oxide pores formed in oxalic acid ($c = 0.3\ \text{mol L}^{-1}$) at 40.0 V. The inset shows the pore bases whose architecture is in accordance to (C).*

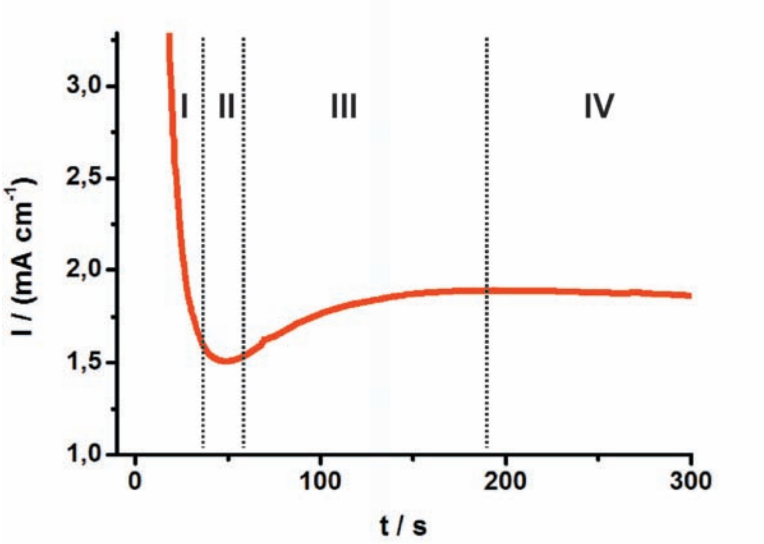

Figure 8. Current–time transient for the potentiostatic anodization of aluminum in oxalic acid *(c = 0.3 mol L*$^{-1}$*) at 40.0 V*.

The different steps of pore formation that are illustrate in Figure 2 can be used to describe the shape of the characteristic time-current transient for the potentiostatic anodization of aluminum (see Figure 8). At the very beginning of the anodization (phase I) a thin barrier oxide layer forms and its constant growth results in an exponential decrease of the current. Due to the formation of corrosion pits the exponential current decay stops in phase II and the curve exhibits a minimum. The further formation of pores increases the local electrical field strength and also the oxidation rate (see figure 2C) and the recorded current consequently increases. After formation of a balanced pore growth, the current maintains an equilibrated state (Phase IV). For long time anodization the current density slightly decreases due to diffusion limits in the long pore channels.

Alternatively to the equifield strength model the formation of a hexagonally ordered porous structure can be explained by the mechanical stress model that was proposed by *Jessensky et al.* [41, 61, 62] and *Li et al.*[32] They suggested that the self-ordering is caused by repulsive forces between neighboring pores, which are generated due to the volume expansion during the oxidation process. According to their studies, the degree of volume expansion that is described by the volume expansion coefficient ξ, varies with the anodization parameters, like electrolyte concentration and applied voltage, and determines whether self-ordered or disordered pores are formed. For the oxidation in near-neutral electrolytes the volume expansion coefficient is almost ξ=2 since the density of Al_2O_3 is by a factor 2 lower than in metallic aluminum. The induced mechanical stress due to the volume expansion is maximal and no pores are generated. While anodization in weakly acidic electrolytes the generated Al^{3+} ions are partially dissolved in the electrolyte and therefore ξ is decreased and depending on the anodization parameters in the range between 0.8 and 1.8. However an ordered pores growth can only be observed for a moderate mechanical stress forces ($\xi \approx 1.2$-1.5). If the volume expansion is low ($\xi < 1.2$), the stress forces are too small and disordered porous AAO is formed. For $\xi > 1.6$ the high stress forces cause a high amount of lattice defects and the size of ordered domains will decrease and finally disappear. A volume expansion coefficient of $\xi \approx 1.2$ corresponds to a porosity of the formed AAO of approximately 10%. *Nielsch et al.* consequently proposed the 10% porosity rule.[29] It says that in order to obtain self-ordered porous alumina the applied voltage, which mainly determines the interpore distance, and the pH value of the electrolyte that mainly defines the pore diameter, have to be tuned in a way that the fulfill the 10% porosity rule.

In contrast to the equifield strength model the mechanical stress model in combination with the 10% porosity rule provides a plausible explanation why self-ordering of porous alumina only occurs for quite small processing windows.

1.1.1.3 Experimental Set-up

The experimental set-up that is used for the fabrication of well-ordered nanoporous AAO templates is illustrated in Figure 10. It basically consists of a two-electrode system that is connected to power supply with computer interface. For the anodization an aluminum disc (anodization area: 2.27 cm^2) is inserted between the electrolyte container and a copper plate that is connected to the anode of the power supply. The interface between the aluminum plate and the container is sealed with a gasket and the container is fixed and tightly pressed onto the ground plate in order to prevent leakage of the electrolyte. For the anodization process the set-up is surrounded with a cooling bath, whose temperature was regulated with a cryostatic temperature regulator. The electrolyte is continuously agitated by a motor-controlled stirrer. The time-current transient is recorded with a multimeter that is connected to a computer.

The described set-up has several advantages over a conventional set-up, which consists of a cooled beaker filled with the electrolyte and the two electrodes that are dipped into the electrolyte from the top. With the employed apparatus a precise area can be anodized, which features a better comparability of the current values for different anodization steps. In addition the edges of the aluminum sheet are not contacted to the electrolyte, which drastically decreases the probability of a local electrical breakdown during the anodization at high voltages. These breakdowns are usually caused by an inhomogeneous electric field distribution during the anodization, e.g. at the edges of an aluminum sheet, and require the complete replacement of the damaged sample. Anodization in phosphoric acid (1 wt%) and applied voltages up to 200 V could be realized with the describe set-up and a proper cooling.

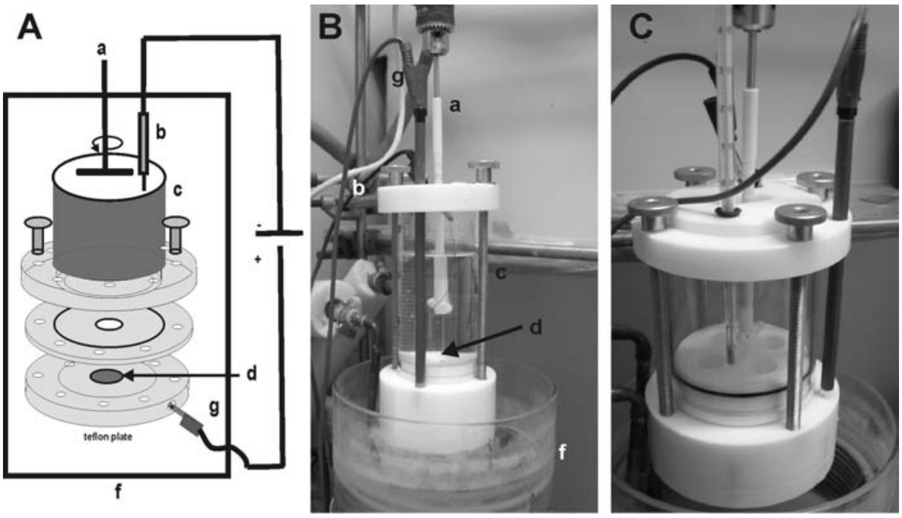

Figure 10. *Experimental set up for the fabrication of AAO templates. (A) Schematic diagram of the self-build apparatus (a) Motor-controlled stirrer for continuous agitating of the electrolyte; (b) Pt-wire as cathode; (c) Container for the electrolyte made of glass; (d) Aluminum plate that is anodized; (e) Potentiostat/galvanostat with computer interface; (f) cryostatic bath for cooling of the anodization apparatus; (g) Teflon plate with an integrated copper plate where the aluminum sheet is place while anodization. (B) Image of the apparatus. While anodization the apparatus is surrounded by the cooling bath that can be seen at the lower part of the image. (C) Apparatus for the simultaneous anodization four aluminum sheets.*

1.1.2 Anodic Titanium Oxide (ATO)

Due to the numerous potential applications in several research areas, such as gas sensors[63, 64], photoelectrolysis[65, 66] and particularly photovoltaics[3, 67], great efforts have been made to fabricate highly-ordered nanoporous titania (see Figure 1 E and F) by applying an anodization process similar to the anodization of aluminum.[68, 69] In 2001 *Gong et al.* showed the fabrication of arrays of vertically aligned titania nanotubes up to a length of 0.5 µm by anodization of titanium foil in an aqueous KF containing electrolyte.[70] The formation of self-ordered nanopore arrays in titania is based on a mechanism similar to that described for AAO[71-73]. By buffering the pH value of the electrolyte[74-76], or by using different nonaqueous fluoride containing electrolytes, such as dimethyl sulfoxide, formamide or ethylene glycol[77, 78], nanopores in titania ranging from several µm up to 220 µm in length were successfully fabricated. The diameter of the nanopore structures, which can be varied from about 10 nm to about 250 nm, depends amongst others on the used cathode material[79] and the applied anodization voltage.[80] For optoelectronic applications, *Grimes* and coworkers have fabricated titania nanoporous arrays on fluorine doped tin oxide (FTO) conducting glass substrates by anodization of a thin sputtered Ti film on the substrate.[3, 67, 81]

1.1.3 Macroporous Silicon

Well-ordered porous structures in silicon can also be fabricated by a self-ordering anodization. The process, which was developed by *Lehmann* et al., is based on the electrochemical oxidation of silicon and simultaneous dissolution of the formed silicon oxide or silicon fluoride in fluoride containing electrolyte.[82, 83] However, in contrast to the anodization of aluminum or titanium, the electrochemical oxidation of silicon results in macroporous membranes. Typically, macropores with typical diameter of 20 µm down to a minimum of 200 nm and a length up to the wafer thickness can be formed.[84] To vary the inter-pore distance and to generate large pore monodomains with lateral dimensions reaching the square centimeter range, ordered arrays of etch pits on the silicon wafer, which are used to initiate the pore formation, were generated lithographically prior anodization.[85]

1.1.4 Track-etched Membranes

The fabrication of track-etched polymer membranes is meanwhile an established technique and these membranes have become commercially available, for example as filter materials from several companies, e.g. Nuclepore®[86] and Poretics®.[87] They are commonly produced by a two-step process starting from irradiation of a polymer film with energetic heavy ions, which results in the creation of linear damage tracks. In the following step, these linear but randomly distributed spaced tracks are converted to pores by means of chemical etching.[88-90] The track-etched process is a very versatile method to fabricate polymeric membranes and was successfully applied to a broad range of polymers, such as poly(vinylidene fluoride) (PVDF)[91, 92], polyimide[93], and most commonly used polyethylene terephthalate[1] (Figure 1 A and B) and polycarbonate[94]. By controlling the conditions of irradiation and chemical etching, the pore size and pore density can be independently varied over a large range. The pore diameter can be adjusted from 10 nm to tens of micrometers, whereas the pore density can be varied from 1 to 10^{10}/cm^2.[95] However, it has to be mentioned that track-etched membranes possess a non-ordered porous structure due to the random bombardment with ions.

1.1.5 Diblock Copolymer Templates

Another class of nanoporous templates, which has recently drawn great attention, is based on block copolymer films.[96] Block copolymer thin films, in which the individual blocks self-assemble into arrays of nanoscopic domains, can be used to prepare a nanoporous template. By using high-molecular block copolymers with an appropriate volume ratio of the individual blocks (major block of A and minor block of B), cylinders of B with a nanoscopic diameter can form in a continuous matrix of A in a hexagonal lattice.[97] These cylindrical domains can be oriented and vertically aligned by use of electric fields[98-102], chemically patterned substrates[103, 104], underlying neutral random copolymer films[105], surfactant-assisted orientation[106], solvent evaporation[107, 108], an array of nanoscale topographical elements[109] or controlled interfacial interaction[110], to mention a few, generating arrays with more than 10^{11} elements per cm^2. After selectively removing the minor block, a nanoporous templates with pore dimensions ranging from a few to about 100 nm can be obtained. The most often used block copolymer to obtain such templates is poly(styrene)-*block*-poly(methylmethacrylate) (PS-*b*-PMMA) (see Figure 1 G and H). *Russell* and coworkers have intensively investigated PS-*b*-PMMA. The porous films are usually generated by UV-initiated degradation of PMMA, accompanied by a partial cross-linking of the PS matrix, and subsequent selectively etching with acetic acid to dissolve the PMMA fragments.[111] To avoid a UV-initiated cross-linking of the PS, which complicates a removal of the PS template afterwards, *Lee* et al. recently used a mixture of PS-*b*-PMMA/PMMA, which allows to selectively remove the PMMA homopolymer in the cylindrical microdomains by treatment with acetic acid without prior UV exposure.[111] A thin film of randomly polymerized PS-*r*-PMMA has been used as a non-differentiating interface to control the interfacial contact with a block copolymer layer and thus, prepare oriented and aligned block copolymer thin films to yield nanoporous block copolymer templates with a thickness up to 100 nm on ITO/glass substrates.[4] Other block copolymer templates are based on poly(4-fluorostyrene)-*b*-poly(D,L-lactide) (PFS-*b*-PLA) and were used by *Crossland* et al. for patterning of semi-conducting titania. The micro domains were oriented by applying an electric field, and the minor polylactide block can be removed by hydrolytic degradation under mild conditions.[112, 113] For further information about block copolymer used as templates we refer to the following review.[114] Recently, several groups have reported on the use of cleavable linkers of PS-b-PEO block copolymers. The groups of *Gohy* and *Schubert* have demonstrated that metallo-supramolecular block copolymers on the basis of a *bis*-2,2',6',2''-terpyridine-ruthenium(II) complex form thin films with PEO cylinders oriented normal to the film surface.[115, 116] Addition of a competitive ligand caused the cleavage of the ruthenium complex and provides the possibility to dissolve the PEO block selectively. *Russell* and coworkers introduced an acid labile linker and prepared a PS-b-PEO block copolymer using a tritly linker between a PS and a PEO block.[117] The removal of PEO from PS-*b*-PEO thin films was carried out in a simple process using aqueous TFA. *Moon* and coworkers investigated also a PS-*b*-PEO block copolymer, but have used a photocleavable linker on the basis of an *o*-nitrobenzyl ester.[118] After irradiation with UV light, the PEO block could be removed with a methanol/H_2O mixture, resulting in a nanoporous PS thin film.

1.2 One-dimensional Nanostructures by Infiltrating Nanoporous Hard Templates

The template-assisted fabrication of tailored shape-anisotropic nanostructures, such as nanowires, nanorods and nanotubes, is intensively investigated and a commonly used technique and as such has been reviewed in several outstanding articles.[40, 119-121] Nanoporous hard templates can be used as shape-defining molds for numerous different materials, like metals[122, 123],carbon[124, 125], inorganic semiconductors[126], nanoparticles[127, 128], low-molecular organic materials[129], polymers[130-134] and metal-polymer amphiphiles.[135-137] There are relatively few limitations regarding the materials, which can by patterned by utilizing hard templates. This versatility is one of the major advantages of hard templates over the alternative patterning strategies like direct self-assembly of building blocks or surfactant-directed soft templating. For the later approaches the employed materials have to exhibit an intrinsic ability for self-assembly or their assembly has to be induced by the soft templates and therefore the number of materials, which can be patterned by these alternative routes, is limited.

For the hard template-assisted formation of monodisperse nanocylinders with precisely adjustable aspect ratios, the cavities of nanoporous templates, which were introduced in the previous chapter, can be filled with the desired material or their precursors. Depending on the infiltration technique these nanocylinders may be solid or hollow, which results in the formation of nanorods and nanotubes respectively. The most commonly employed methods for the pore infiltration are electrochemical deposition[138] and polymerization,[139, 140] sol-gel deposition,[141, 142] chemical vapour desposition and wetting of precursors and polymers.

In this thesis the method of choice for the patterning of a number of functional materials is the wetting of low molecular weight precursors and their subsequent polymerization inside of the porous AAO template. The wetting-assisted fabrication of polymeric one-dimensional nanoobjects was pioneered by *Wendorff* and coworker.[143-146] They reported that depending on the used material either nanorods or nanotubes can be obtained by the wetting of nanoporous templates. The wetting of nanoporous AAO is claimed to be driven by the different surface energies of the organic materials and the oxide surface. Polar inorganic oxide surfaces commonly exhibit high surface energies, whereas those of organic solutions or polymeric melts are one order of magnitude lower.[147] Consequently organic materials with a sufficient low viscosity spread on inorganic oxide surfaces since the system tends to minimize the overall interfacial energy.

Wendorff and coworkers proposed that the filling of the pores could be divided into two different stages. In the first state, the pore walls are covered with a thin film, in order to minimize the overall surface energy within seconds after the fluid is brought in contact with the template. For polymer melt and solutions the system is kinetically stable after the first state since the cohesive forces, which drives the thermodynamically stable complete filling of the pores, are weaker than the viscous forces of the polymeric liquid. Due to the higher mobility of low molecular weight materials, the cohesive forces could be sufficient to form a meniscus and finally a complete filling of the pore in the second stage.[145] The wetting technique was employed for various polymers in order to form polymeric nanotubes.[148-150]

In general the filling of the nanoporous templates initially yields hybrid materials based upon the template and the infiltrated material. If tubular structures are formed inside the pores, which decorate the surface of the template but still provide accessible nanochannels, these hybrid materials can be applied as sensors[151] and smart separating filters.[152, 153]
The release of the templated nanostructures is commonly achieved by the wet-chemical etching of the sacrificial template. Recently the mechanical release of the nanorods from the porous templates has also been demonstrated but still needs to be optimized for a versatile applicability.[154]

1.2.1 Formation of Well-Ordered Arrays of Nanorods

If the released nanostructures are attached to a supporting substrate, more or less-ordered arrays of nanostructures with high lateral densities can be obtained after the removal of the template. These arrays possess large and spatially distinct surface areas and a topography that is well separated from the under-lying substrate. They play an important role in wide field of applications, like superhydrophobic surfaces,[155-158] dry adhesives,[157-159] sensors,[160, 161] actuators,[162] tissue engineering,[163, 164] data storage,[165] efficient batteries[166] and enhanced heat transfer,[167] to just mention a few. One very challenging issue for the fabrication of nanorod arrays is to remain the physical integrity of the polymer structure and to prevent collapsing and aggregation of the rod after the removal of the hard template. Well-ordered arrays of nanorods composed of stiff inorganic materials, like silicon and metals, with aspect ratios (height to diameter ratio) greater than 10 have been reported. However the mechanical stability of organic and polymeric nanorods is commonly lower than that of inorganic nanorods and therefore bending and collapsing is more likely for arrays composed of organic materials. Not only for the patterning with hard nanoporous templates but also for other patterning techniques like photolithography and soft lithography, these collapsing phenomena are well-known and characterized.[168-170]
It is distinguished between the ground collapse and the lateral collapse (see Figure 11). Ground collapse refers to the complete collapse of the nanorods to the ground, which is caused by gravity[171] or surface adhesive forces (see Figure 11 B).[172]

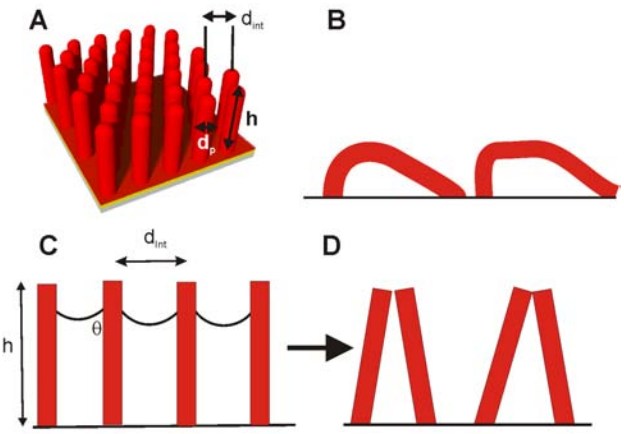

Figure 11. *(A) Schematic illustration of an array of free-standing nanorods with a diameter of d_p, a height h and a interpore distance of d_{Int}. (B) Ground collapse of nanorods; (C) Nanorods partially immersed in a liquid; (D) lateral collapse of nanorods after evaporation of the liquid.*

Lateral collapse yields the formation of bundles of nanorods and mainly refers to adhesive forces between nanorods.[171, 173] and capillary forces upon drying[173-175] Since nanorod arrays, which are fabricated by utilizing hard template, are commonly brought into contact with aqueous solutions during the wet-chemical removal of the template, the capillary forces during the drying process play an important role for the lateral collapsing.
The capillary interaction energy W_c of two cylinders, which are partially immersed in a liquid of a surface tension γ with a contact angle θ can be written as:[176]

$$W_C = -2\pi \left(\frac{d_p}{2} \right)^2 \gamma \cdot \cos^2 \theta \cdot \ln \left(\frac{l_c}{d_{Int} + \sqrt{{d_{Int}}^2 - 4\frac{d_p}{2}}} \right) \tag{7}$$

where d_p and d_{Int} is the radius and the interpore distance, respectively; $l_c=(\gamma/\rho)^{1/2}$ is the capillary length of the liquid (ρ: density and g: gravitational acceleration).

Consequently the capillary force F_C between the tow rods can be described by:[176]

$$F_C = \frac{\pi\gamma \left(\frac{d_p}{2} \right)^2 \cos^2 \theta}{\sqrt{\left(\frac{d_{Int}}{2} \right)^2 - \left(\frac{d_p}{2} \right)^2}} \tag{8}$$

Equation 8 shows that the capillary forces are proportional to the surface tension of the liquid and to the second power of cosine of the contact angle at the liquid/rod interface

To minimize these forces either the contact angle must be brought close to 90° or the surface tension must be reduced. Approaches to minimize lateral collapsing by replacing the aqueous media with low-surface tension solvents (e.g. methanol) or by employing supercritical and freeze drying techniques have been demonstrated.[175, 177]

1.3 Organic Photovoltaics

1.3.1 General Remarks

Solar cells based on organic or polymeric semiconductors are attracting increasing attention as an alternative renewable energy source. Compared to their inorganic counterparts organic photovoltaic devices (OPV) provide several advantages, such as low cost fabrication techniques (e.g. spin-coating,[178] roll-to-roll process[179] or inkjet-printing[180, 181]) and the potential for large area deposition on flexible, light-weight substrates.[182, 183] Furthermore, thin films made of organic semiconducting materials may exhibit high absorptions coefficients exceeding 10^5 cm^{-1} and thus are efficient chromophores. The optical bandgap of organic semiconductors could be varied by chemical modification and consequently their absorption range could be tuned in order to overlap with the terrestrial solar spectrum. The mentioned advantages and the recent success in organic light-emitting diodes (OLED) lead to the assumption that organic photovoltaic devices (OPV) will become competitive and will be vital alternatives to inorganic devices in the future.

This chapter will give a short overview about organic semiconducting materials and the working principle and characteristics of organic solar cells. The significance of the morphological control in organic solar cells will be discussed and template-based patterning methods for organic and polymeric semiconducting materials will be presented.

1.3.2 Semiconducting Polymers

Today conducting and semiconducting polymers and low molecular weight derivatives have found broad application in organic light-emitting devices (OLEDs), organic field-effect transistors (OFETs), organic photovoltaic devices (OPVs), optical switches and organic lasers. Most of the organic semiconducting materials are based on conjugated backbones, polymers that exhibit semiconducting side chains or low-molecular semiconducting derivatives. Figure 12 shows a small selection of organic semiconducting materials that are employed for the fabrication of organic photovoltaic devices.

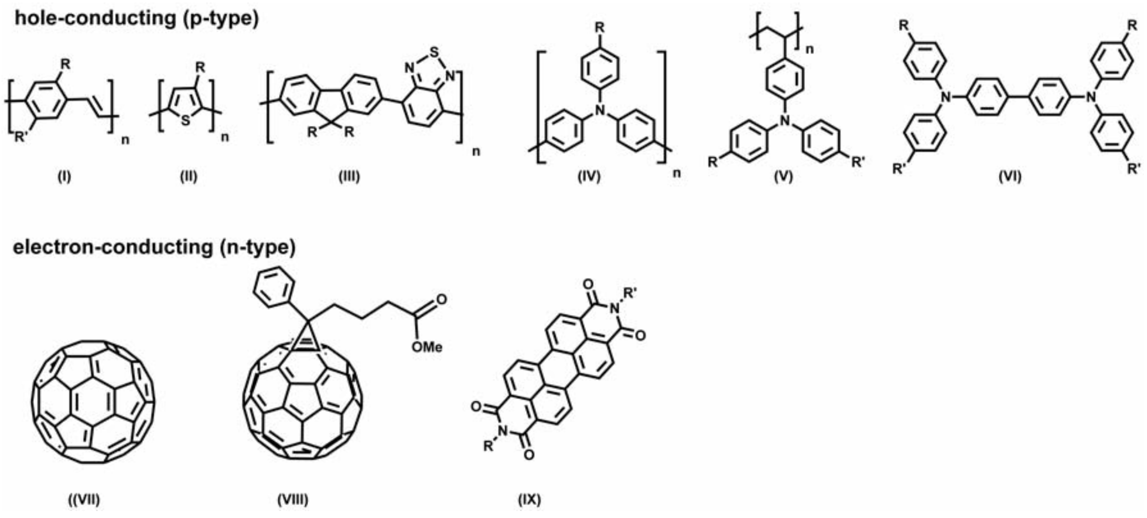

Figure 12. *Organic hole- (I-VI) and electron-conducting (VII) materials employed for the fabrication of OPVs: (I) poly(phenylenevinylene) poly[2-methoxy-5-(3,7-dimethyloctyloxy)]-1,4-phenylenevinylene) (MDMO-PPV): R':-OMe; R: 3,7-dimethyloctyloxy); (II) polythiophene (poly(3-hexylthiophene) (P3HT): R: hexyl); (III) poly(fluorene-co-benzothiadiazone) (poly(9,9'-dioctylfluorene-co-benzothiadiazole) (F8BT) R: octyl); (IV-V) poly(triphenylamine) (triphenylamine moiety (IV) integrated in the polymer backbone and (V) as side chain); (VI) tetraphenylbenzylidendiamine (TPD); (VII) buckminsterfullerene* C_{60}*; (VIII) 1-(3-methoxycarbonyl) propyl-1-phenyl[6,6]*C_{61} *(PCBM), (IX) disubstituted perylene diimide derivative.*

Depending on the energy level of their HOMO (highest occupied molecular orbital) and LUMO (lowest unoccupied molecular orbital) organic semiconductors are categorized into hole-conducting (p-type) and electron-conducting (n-type) materials. Noteworthy this distinction is artificial and the decision whether the material is a sufficient p- or n-type material in an OPV device also depends on the HOMO/LUMO levels of the second material and the work function of the electrode materials.

Prominent examples for organic p-type materials are conjugated polymers based on (i) derivatives of poly(phenylene vinylene) such as poly[2-methoxy-5-(3,7-dimethyloctyloxy)]-1,4-phenylenevinylene] (MDMO-PPV), (ii) alkyl substituted poly(thiophenes) like poly(3-hexylthiophene) (P3HT) and (iii) polyfluorene copolymers like poly(9,9′-dioctylfluorene-co-benzothiadiazole) (F8BT). All these conjuated polymers are solution-processible due to side-chain solubilization and exhibit broad absorption spectra. The charge carrier mobilities of the conjugated polymers strongly depend on the alignment of the polymers. The self-organization regioregular P3HT yield lamella structures of two-dimensional conjugated sheets.[184] Due to the formation of microcrystalline domains mobilities up to 0.1 $cm^2V^{-1}s^{-1}$ can be reached.[185, 186] However the charge carrier mobility is dramatically decreased by disturbing the formation of lamella sheets for example by using regio-random P3HT.

Another class of organic hole conducting materials is based on triphenylamine (TPA) and the corresponding dimer tetraphenylbenzylidendiamines (TPDs). Low molecular weight materials and polymers with TPA and TPD moieties integrated in the backbone and as side chains have found application as in organic solar cells,[187, 188] as hole-injecting layers in OLEDs[189, 190] and for data storage.[191] Due to the lack of long-range conjugation in low-molecular triarylamines and side chain polymers charges are transported by a reversible redox reaction of the moieties and a consecutive charge hopping between neighboring moieties.

Commonly used n-type (electron-conducting) materials in organic photovoltaic devices are based on derivates of the buckminsterfullerene C_{60}. C_{60} is an electron acceptor, which can be electrochemically reduced up to six electrons. However the solubility of simple C_{60} is limited. *Wudl et al.* have synthetized a soluble derivative of C_{60}, PCBM (1-(3-methoxycarbonyl) propyl-1-phenyl[6,6]C_{61}) that is widely used in polymer/fullerene photovoltaic devices.[192]

Low molecular weight perylene bisimide are also known to be good n-type materials with electron mobilities of up to 2.1 $cm^2\,V^{-1}\,s^{-1}$.[193-195] For polymers that contain perylene bisimide moieties as side chains electron mobilities of 10^{-2} $cm^2\,V^{-1}\,s^{-1}$ have been reported.[196] Due to strong π-π interactions perylene bisimides show discotic liquid crystalline properties and the formation of columnar aggregates favors the charge carrier transport.[197] Additionally perylene bisimides feature a good air stability and a high absorbance in the visible light.[198] Therefore they are suitable for the fabrication of n-type OFETs[196] and as electron-conducting materials in organic photovoltaic devices.[187, 199]

1.3.3 Working Principle of Organic Photovoltaic Devices

The conversion of light into electrical energy in an organic photovoltaic device is schematically illustrated in figure 13. In contrast to many inorganic semiconductors photon absorption in organic semiconductors does not directly generate free charge carriers. Instead, if incident light is absorbed within the photoactive layer of the device an electron from the HOMO level of the absorbing molecule is excited into the LUMO level and electron-hole pairs (so called excitons) are generated, which are often bound locally due to coulomb attractions at room temperature.[200-202] For an efficient dissociation of the exciton into free electron and holes, strong electrical fields are essential. These fields can be generated via applying external electrical fields as well as *via* gradients of the potential across a donor/acceptor interface. Photo induced charge transfer can occur when the exciton reaches such a donor /acceptor interface. The required driving force for the charge transfer is determined by the difference of the ionization potential of the excited donor and the electron affinity E_A of the acceptor minus the coulomb attractions of the exciton.[202] Consequently generated excitons have to diffuse to a near donor/acceptor interface in order to dissociate into separated charges. If a donor/acceptor interface is not within the range of the exciton diffusion length, which is usually limited to about 10-20 nm in organic and polymeric materials, the exciton is deactivated by photoluminescence or thermal dissipation and cannot contribute to the power conversion of the solar cell. After charge separation the hole and electron remain coulombically bound across the donor/acceptor interface and form a geminate polaron pair. The dissociation into completely separated charges is driven by an internal electrical field that is determined by the difference between the HOMO level of the donor and the LUMO level of the acceptor. Afterwards the charge need to be transported to the appropriate electrode, which can be supported by using electrode materials with different work functions. In common devices transparent indium tin oxide (ITO) with a work function of -4.8 eV matches to the HOMO level of the donor and is used as the anode material. For the cathode, evaporated aluminum that exhibits a work function of -4.3 eV and matches to the LUMO level of the acceptor is the material of choice in many devices.

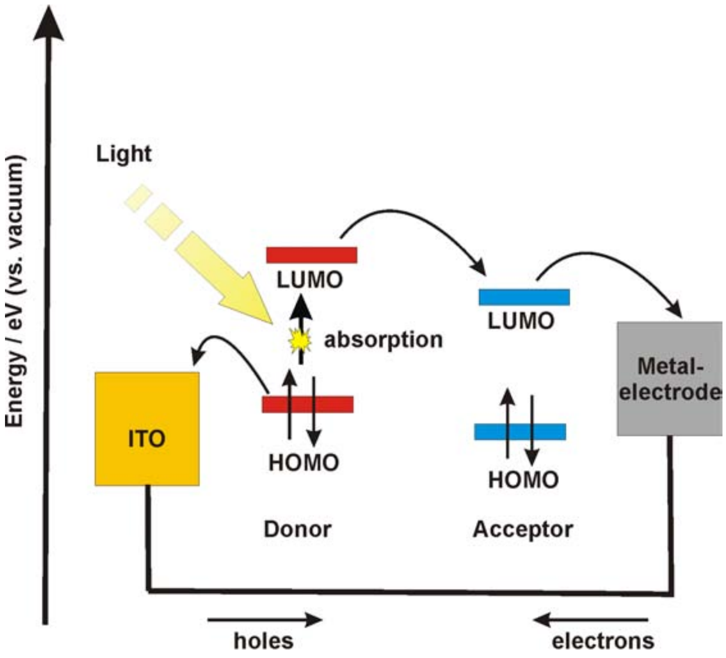

Figure 13. *Schematic diagram of the band structure of a heterojunction organic solar cell. The active layer in this type of device contains a donor and an acceptor.*

1.3.4 Characteristics of Organic Photovoltaic Devices

In order to characterize the physical properties of an organic photovoltaic device and to determine their characteristic parameters, the current/voltage (I-V) graph for the device is commonly recorded and evaluated. In figure 14 A an I-V graph for a P3HT/PCBM device in the dark (black line) and upon irradiation (red line) is illustrated. In the dark the curve passes through the origin and almost no current flows for applied voltages below the open circuit voltage (V_{OC}). Under illumination the device generates power and the I-V curve shifts down to the fourth quadrant of the graph. In order to guarantee a better comparability of I-V curves from different devices, solar simulators with a standardized intensity (100 mW cm^{-2}) and solar spectrum, which matches with the spectral intensity distribution that of the sun on the earths surface at an incident angle of 48.2° (air mass 1.5), are commonly used for the irradiation. Characteristic values of the I-V curve are the open-circuit voltage, V_{OC}, which is the maximum voltage difference attainable between the electrodes, and the short-circuit current I_{SC}, which is the maximum current that can ran through the device under short-cut conditions. The maximum power P_{max} that can be generated by the device is determined by the product of the I_{MPP} and V_{MPP} (see figure 14). The fill factor (FF)- an important value that is related to the quality of the device- is determined by the ratio of the actual maximum power output and the theoretical power output and can be written as:

$$FF = \frac{I_{MPP} V_{MMP}}{I_{SC} V_{OC}} \tag{9}$$

The ratio of the maximal output power and the incident light power yield the power conversion efficiency (η) of the device:

$$\eta = \frac{P_{Out}}{P_{In}} = \frac{I_{MPP} V_{MPP}}{P_{In}} = \frac{FF \cdot I_{SC} V_{OC}}{P_{In}} \tag{10}$$

In terms of a better understanding how the absorption of light with a particular wavelength results in the collections of charges at the electrodes, the IPCE (Incident Power to Current Efficiency) or also called the external quantum efficiency (EQE) is commonly recorded and determined as the following:

$$IPCE = \frac{1240 \cdot I_{SC}}{\lambda \cdot P_{In}} \tag{11}$$

where λ is expressed in nm, I_{SC} in amperes per meter squared and P_{In} in watts per meter squared.

Figure 14B illustrated the IPCE for a P3HT/fullerene-based OPV device. The peak between 450 and 650 nm correlates with the absorption spectrum of the P3HT and up to 50 % of the incident photons generate charges, which are transported to the electrodes.

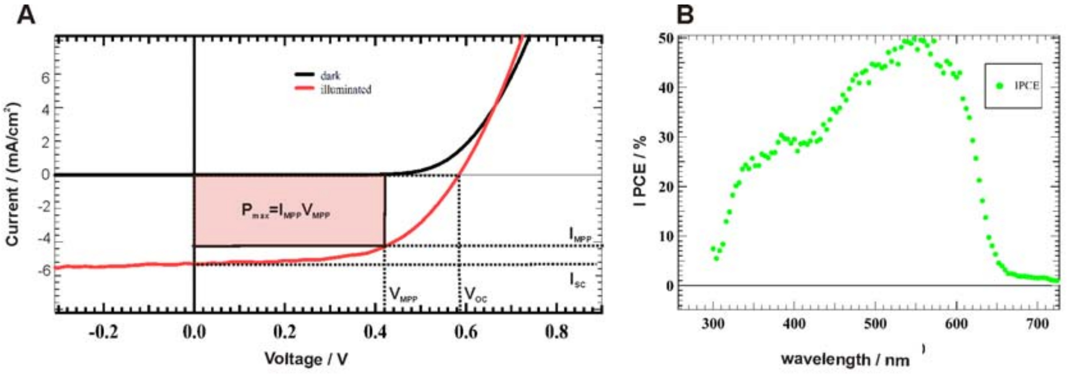

Figure 14. *(A) Typical I-V curve observed for an organic photovoltaic device. (B) Incident Power to Current Efficiency (IPCE) spectrum of a P3HT/PCBM solar cell.*

1.3.5 Device Architectures

Besides the synthesis of novel organic semiconductors with high charge carrier mobilities and well-tuned energy levels, the morphological control of the photoactive layer remains as one of the challenging issues for the fabrication of efficient photovoltaic devices. The importance of the morphology is due to the fact that the exciton diffusion length in organic semiconductors is limited to 10-20 nm. Therefore organic photovoltaic devices ideally require a bicontinuous and interpenetrating donor-acceptor network with an interfacial distance smaller than the exciton diffusion length to guarantee an efficient charge generation. Further, the donor/acceptor network must provide percolation pathways of both semiconductors to allow an efficient transport of the generated charges to their respective electrodes.

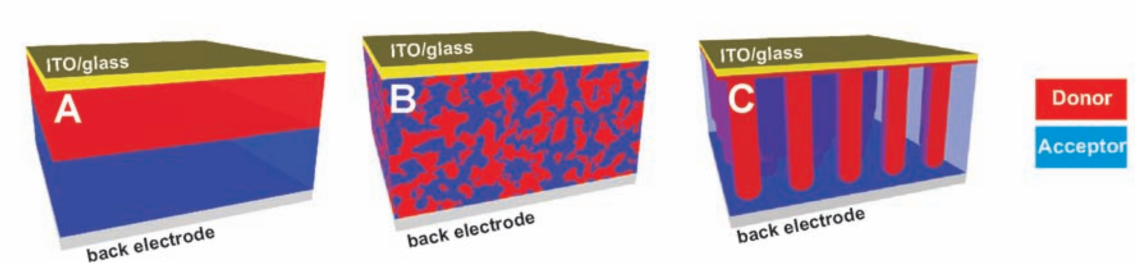

Figure 15. *Schematic diagram of different OPV architectures. (A) planar; (B) bulk-heterojunction and (C) well-ordered bulk-heterojunction morphology.*

The simplest morphology that features a donor-acceptor interface can be established by a conventional bilayer structure (see Figure 15 A).[203] However, this bilayer architecture only provides a small donor-acceptor interface and the two requirements for an efficient photoactive layer – a sufficient thickness for photon absorption and a donor/acceptor interface in the range of the exciton diffusion length – cannot be achieved in a simple bilayer architecture. In order to overcome these limitations bulk heterojunction morphologies have been introduced, in which the interfacial area is tremendously increased and the overall thicker photoactive layer provides a sufficient light absorption (see Figure 15 B).[204, 205] Current state-of-the-art bulk heterojunction photoactive layers are prepared by blending conjugated polymers, e.g. poly(3-hexylthiophene) (P3HT) or copolymers based on benzodithiophene as hole-conducting materials with electron-accepting fullerene derivatives. The resulting OPV cells can indeed reach power conversion efficiencies of more than 7 %.[206-209] However, it remains a challenge to precisely control bulk heterojunction morphologies composed of donor/acceptor mixtures and to increase their long-term stability. In these morphologies, phase separated donor and acceptor domains often do not exhibit the right length scale and are not morphologically stable. Furthermore, they can form 'isolated' domains, which are not connected to the respective electrode. Especially the 'isolated' domains result in a lack of pathways for the generated charges to the electrode. Accordingly, the fabrication of an idealized well-ordered bulk-heterojunction architecture that provides a large donor/acceptor interface as well as percolating pathways still remains a challenging issue by utilizing a phase separation approach (see Figure 15C).[210, 211]

1.4 Template-Assisted Patterning of Organic Semiconductors

Due to the importance of the morphological control of active layer in organic photovoltaics the patterning of organic semiconducting materials attracted increasing attention. In the following chapter the template-assisted patterning of organic and optoelectronic-relevant materials is described.

1.4.1 Templating in Track-Etched Membranes

The approach to use nanoporous membranes for such a patterning process was introduced by *Martin* and coworkers, who have done pioneering work in this area since the eighties of the last century.[212-215] By applying an *in-situ* oxidative polymerization of pyrroles, thiophenes or anilines, polymeric tubules and fibers consisting of conducting polymers, e.g. polypyrrole, poly(3-methylthiophene) and polyaniline, were synthesized in the nanoscopic confinement of porous membranes. The polymerization could be accomplished by either an electrochemical process[120, 216-220] or by using an oxidizing agent.[221, 222]
For example, porous track-etched membranes, which are opened on both sides, can be placed between a solution of a monomeric precursor and an oxidizing agent, such as $FeCl_3$,[223] or the template is simply immersed into a mixed solution of both materials,[224] resulting in the formation of respective polymers inside the pores. For the electrochemical process insulating porous track-etched membranes were first coated on one side with a conducting metal layer and then used as an anode for the electrochemical deposition process (see Fig 16 a).[225] *Demoustier-Champagne* and coworkers have used track-etched membranes, which were directly prepared on top of a conductive substrate, such as gold or ITO/glass, to electrochemically fabricate polypyrrole nanotubes.[225, 226]

For the template-based patterning of conductive polymers *Martin* and coworker found out that the oxidative polymerization is nucleated on the pore walls of the template and therefore short anodization times result in the formation of nanotubes.[227] This growing mechanism is probably caused by the positive charge of the formed polymer chains, which are absolutely insoluble in the aqueous solution, thus generating a solvophobic and electrostatic effect of the chains to the anionic sites of pore walls. Consequently, the wall thickness of the polymeric tubes can be controlled by the polymerization time and, as shown in the case of polypyrrole, can result in the formation of completely filled polymer fibers for longer polymerization times.[228]

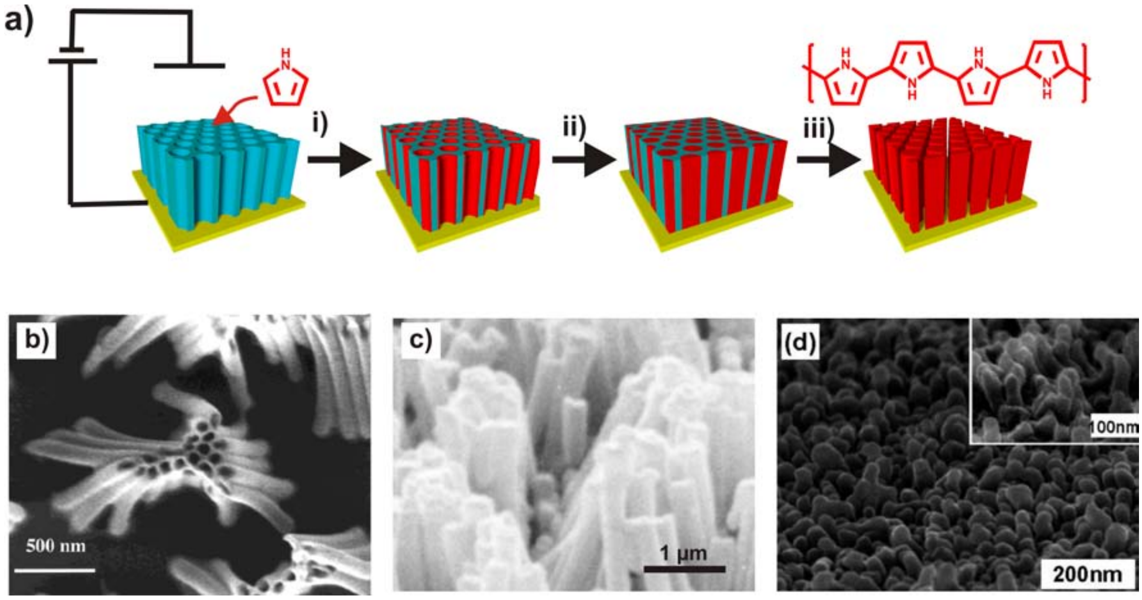

Figure 16. *a) General scheme about the template-based polymerization of polypyrrole: (i) For short anodization times nanotubes of polypyrrole can be generated (see also b); (ii) longer anodization time finally results in the formation of nanorods (see also c); (iii) after selective removal of the template free-standing nanotubes or nanorods can be obtained. b) top-view SEM micrograph of electropolymerized polypyrrole nanotubes fabricated in track-etched membranes. Reproduced from [225] c) SEM image of polypyrrole nanorods, which were electrochemically fabricated in AAO templates. Reproduced from [217] d) Polypyrrole nanorods on ITO/glass fabricated in block copolymer templates. Copied from [4].*

Further, *Demoustier-Champagne* et al. have investigated the influence of the pore size, surface modification of the pores and the nature and concentration of the electrolyte on the growing rate of polypyrrole tubes.[218, 219, 225] It has been shown that the thickness of the electropolymerized nanotubes does not vary with the concentration of the used electrolyte, although the filling of the pores is more rapid for increased concentrations of the electrolyte. Further investigations showed that the thickness of the nanotubules walls increased with the pore diameters of the template.[225] The group of *Demoustier-Champagne* also changed the hydrophilicity of hydrolyzed polycarbonate and poly(ethylene terephthalte) track etched membranes by adsorption of polyelectrolytes. By using these modified membranes as tempales much thicker polypyrrole tubules were obtained as in the non-modified templates.[225] In addition to the possibility to precisely control the dimensions of the fabricated conductive nanotubes by varying the pore dimension of the pores and the polymerization time, the templating process also results in an enhanced conductivity along the axis of the polymeric structure in comparison to bulk samples. *Martin* and coworker determined the conductivity of polypyrrole nanofibers with small diameters (~30 nm) to be over one order of magnitude higher than the conductivity of the bulk material.[223, 229] Comparable enhancements of the conductivity have also been observed for poly(3-methylthiophene)[216] and polyaniline[228], which have been patterned by a template-based synthesis. The effect of the conductivity enhancement depends also on the pore diameter of the template and it was found that the conductivity decreases for larger diameters. For example, films consisting of polyaniline nanotubes with a diameter of

100 nm provided a conductivity of approximately 50 S cm^{-1}, while the conductivity of nanotubes with a diameter of 400 nm dropped to ~9 S cm^{-1}.[228] It is proposed that a high orientation and an extended conjugation length of the polymer chains, which are deposited on the pore wall, cause the enhancement in conductivity. The extended conjugation length leads then to an increased conductivity. The orientation effect decreases for the deposition of polymer chains with a larger distance to the pore wall and as a consequence the conductivity drops for tubes with larger diameters.[217, 222, 223]

1.4.2 Anodic Aluminum Oxide and Macroporous Silicon Templates

Besides the template-based fabrication of conducting polymers using track-etched membranes, also AAO membranes and macroporous silicon have been used as sacrificial hard templates. *Berdichevsky* et al. have deposited pyrrole electrochemically in commercially available AAO templates.[230-232] The templates, which were open on both sides, were attached on one side onto a metal electrode for the following electropolymerization. The resulting doped polyprrole nanowires showed length variation of ~3% under applied voltages and were investigated as electrically controlled nanoactuators.

Park et al. fabricated electrochemically nanowires and nanotubes of poly(3-methylthiophene) with diameters of 100-200 nm and ~40 µm in length using AAO templates.[233] By lowering the temperature during the electrochemical polymerization, the resistance of the nanotubes could be reduced and consequently the photoluminescence became sharper, which was suggested to be the result of a better chain alignment. Raman spectroscopic studies of polythiophene tubes, which were also electrochemically polymerized in AAO templates (see Figure 17) also confirmed the aligned chain orientation.[234]

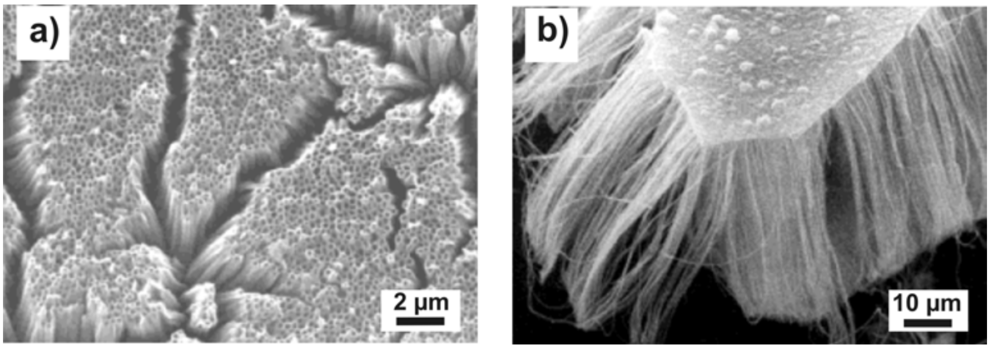

Figure 17. Scanning electron micrographs of aligned polythiophene microtubules after selective removal of the AAO template. Reproduced from [234].

Arrays of poly(3,4-ethylenedioxythiophene) (PEDOT) nanotubes fabricated by electrochemical polymerization of the corresponding monomer inside AAO membranes have been used by *Cho* et al. to prepare ultrafast elechrochromic displays.[235-238] In homogenous PEDOT films the rate of color switching, due to a reversible redox process, is limited by the diffusion rate of the counter ions during the switching process. However, due to the large surface of the fabricated nanotubes arrays, the diffusion distances of the counter ions are extremely short, which leads to ultrafast switching speeds

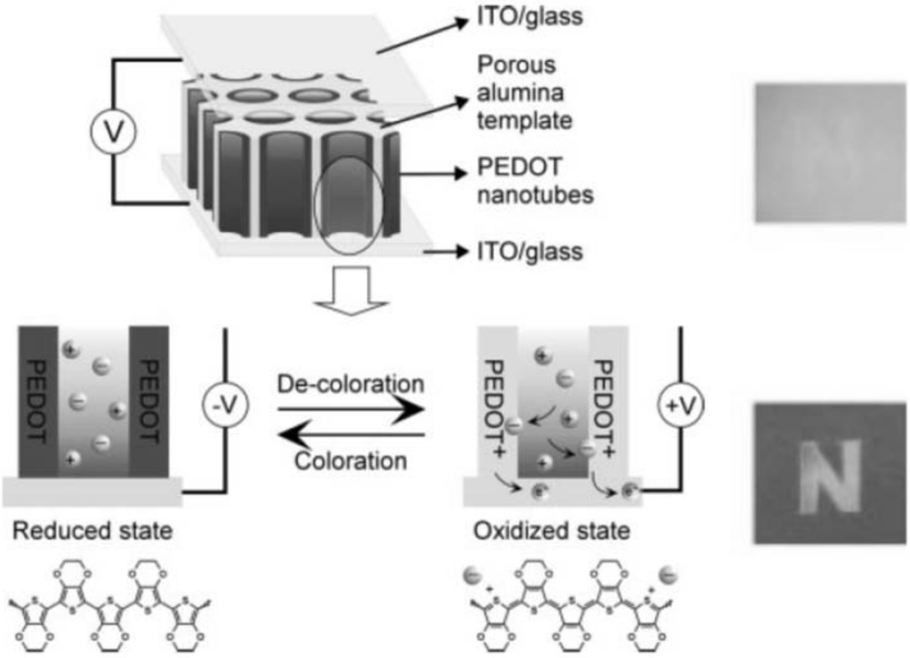

Figure 18. *Schematic representation of the ultrafast electrochromic device based on PEDOT nanotubes arrays. Copied from [236].*

An alternative approach to the infilling of the templates *via* an oxidation polymerization is a melt-assisted infiltration of polymeric material into the pores of a membrane. For example, microstructures of semiconducting poly(3-hexylthiophene) have been fabricated by wetting microporous silicon templates with the polymer melt at 250 °C for 30 min. After selective removal of the template, a freestanding array of microfibers and tubes was obtained, which has the potential to be used in OPVs as patterned *p*-type materials.[239]

1.4.3 Patterning using Block Copolymer Templates

The use of block copolymer templates for the patterning of organic semiconducting materials was shown by *Knoll* and coworkers, who fabricated polyaniline nanofibers using poly(styrene-*block*-2-vinylpyridine) block copolymer templates (Figure 19).[240] The nanoporous templates were prepared by spin coating a PS-*b*-P2VP micellar solution onto a substrate. The minor P2VP block, which formed a monolayer of micellar microdomains in a PS matrix, was selectively swollen with acetic acid. This process resulted in the migration of the P2VP chains to the surface of the PS matrix and after drying nanoporous polymer films were obtained, which were subsequently used as molds for the electrochemical deposition of polyaniline. The polyaniline nanofibers grew out of the template when longer deposition times were applied and intertwined into a porous film of polyaniline nanowires (Figure 19E)

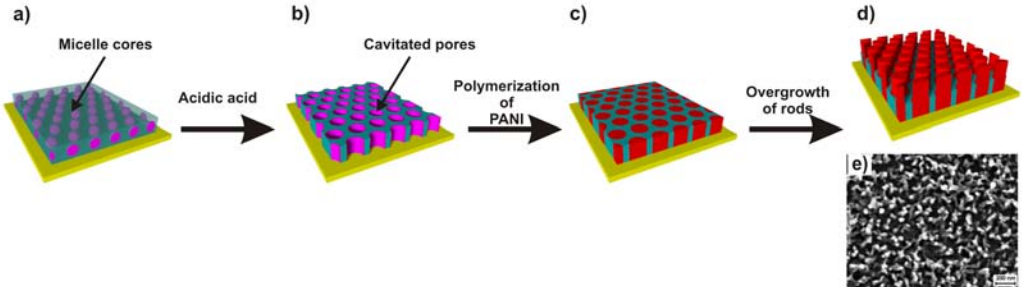

Figure 19. *Schematic illustration of the stepwise fabrication polyaniline nanofiber films. a) Preparation of aPS-b-P2VP monolayer micellar film on a gold substrate; b) Generation of vertically aligned pores in the film via treatment with acetic acid and subsequent removal of the solvent. c) Elcectrochemically induced formation of nanorods inside of the pores; d) Overgrowth of the nanofibers; e) Top-view SEM micrograph of overgrown polyaniline nanofibers. Reproduced from [240].*

Recently, *Russell* and coworkers showed the fabrication of conducting polypyrrole nanorods that were attached onto a conductive ITO/glass substrate by using nanoporous templates prepared from the block copolymer PS-*b*-PMMA after removal of the PMMA minority block.[4] The polymerization of pyrrole has been performed electrochemically within the nanopores and after the selective removal of the PS scaffold, free standing polypyrrole nanorods arrays on an ITO/glass have been obtained with diameters down to 25 nm, lengths of ~100 nm and areal densities of ~10^{11} rods/cm^2 (Figure 3 d) In analogy to the electrochemical deposition in track-etched membranes, the use of templates with larger pore diameters resulted in the formation of nanotubes instead of rods. The fabricated rods exhibited an enhanced conductivity comparable to that of a bulk sample, which was proposed to originate from the orientation of the polypyrrole along the axis of the rod as investigated by high resolution TEM and X-ray diffraction measurements. Besides the commonly used 2-point conductivity measurements the authors also presented the conductivity measurements of single nanorods *via* current-sensing atomic force microscopy.

Current research has demonstrated that it is possible to develop technologies on the basis of block copolymers. Ordered arrays of cylindrical microdomains with areal densities that reach 10 terabits per square inch have been prepared and are expected to revolutionize the microelectronic and storage industries.[241]

The template-based fabrication of nanorod arrays of organic semiconducting *n*-type materials, i.e. perylene diimide, was shown recently. An electrophoretic method was used to deposit the perylene derivative into porous silicon[242] and AAO templates.[243] The length of the *n*-type nanowires could be controlled by the deposition time, since the deposition of the material starts at the bottom of the pores and growth along the pore axis. Removal of the template afterwards results in arrays of nanofibers with photoconductivities that are one magnitude higher than the value of the bulk material and therefore can find potential application as photoconductive devices and also as nano-patterned *n*-tpye materials in organic photovoltaics. In addition, arrays of *n*-type fullerene nanofibers have been prepared by a solution wetting of the fullerene into AAO membranes, which were then used as photoreceptors showing an enhanced photosensitivity.[244]

Nanoporous templates cannot only be used for the fabrication of nanostructures materials to build up optoelectronic devices. Furthermore, their pores can also be used as molds for building up microcell devices. For example, *Kim* and coworker recently built and characterized photovoltaic microcells, by filling track-etched membranes with a mixture of a hole-conducting poly(3-octylthiophene) and electron-conducting fullerene material.[245] They envisioned that this cell configuration has the potential to fabricate flexible OPVs.

1.4.4 Discotic Organic Materials in Templates

Besides the templating of polymers, there has also been growing interest in the preparation of one-dimensional nanoobjects that consist of small discotic organic compounds. *Steinhart* et al. have used AAO membranes to fabricate nanowires of liquid crystalline (LC) 2-adamantanoyl-3,6,7,10,11-penta(1-butoxy)triphenylene, a discotic triphenylene derivative. Using XRD, they could show that the LC columns are oriented along the long axes of the AAO pores. However, strong LC/pore wall interactions promoted a thin layer of columns that have a homeotropic orientation with respect to the pore wall. Interestingly, if prepared in pores with larger pore diameter, the resulting LC nanowires had a higher degree of orientation and intrinsic columnar order.[129] Introducing PMMA together with the discotic triphenylene derivative into the AAO pores resulted in tubes consisting of a 30 nm thick PMMA layer outside and a 5 to 10 nm thick triphenylene derivative layer on the inside, if pores with a diameter of 400 nm were used, while pores with a diameter of 60 nm yielded solid rods instead of tubes.[246]

The group of *Müllen* has studied the self-assembly of hexa-*peri*-hexabenzocoronenes (HBCs)[247, 248] in porous templates. By melt processing the HBCs self-aligned inside the pores, which resulted in a high degree of long-range supramolecular orientation. Noteworthy, they did not observe any influence of the pore size of the template onto the orientation of the HBCs.[249] Carbonization of self-aligned HBCs inside a porous AAO template was induced by a three-step heat treatment up to 900 °C. As a result, carbon nanotubes with highly ordered graphene layers oriented perpendicularly to the pore axis were accomplished. Rapid heating to 900 °C resulted also in carbon nanotubes, however, the obtained graphene layers did not show a highly controlled orientation.[250] Similar, tetrakis(*tert*-butyl)-naphthalocyaninato nickel (Ni-BNc) could be organized inside a porous alumina template, leading to ordered columnar structures due to π-π interactions. Thermal treatment at 600 °C resulted in carbonized nanotubes.[251]

Hurt and coworkers have investigated the control of graphene layer orientation using LC surface anchoring.[252] They prepared orthogonal carbon nanofibers using a commercially available discotic mesophase pitch, which was first allowed to self-organize inside the pores of nanoporous AAO and glass membrane and then carbonized at 700 °C.[252, 253]

1.4.5 Opals as Templates

So far only templating of semiconducting materials inside two-dimensional porous structures has been described. However, also the templating using three-dimensional porous structures has been conducted. For example, several groups have used photonic crystals, which had been prepared by the self-assembly of polymer colloids, as templates for organic semiconductors. *Kramer* and coworkers have self-assembled monodisperse polystyrene colloidal particles in the presence of a polystyrene-*block*-poly(2-vinylpyridine) (PS-*b*-PVP) block copolymer and polyaniline-phenolsulfonate (PANI-PSA). During an annealing step the PS-*b*-PVP block copolymer segregated on the surface of the colloidal PS with the PVP chains stretching into the voids of the colloidal crystal. As a result, PVP and PANI-PSA produced a semiconducting polymer blend in a three-dimensionally continuous network around the PS colloids.[254]

Caruso and coworkers have described the preparation of a completely inverse opal that consists of a semiconducting polymer (see Figure 20). For this purpose, PS particles were sedimented out of suspension on an ITO-coated glass, which was then used as a working electrode for the electropolymerization of pyrrole or thiophene to infill the voids of the photonic crystal with polypyrrole or polythiophene, respectively. Afterwards the PS particles had been dissolved with THF, yielding freestanding inverse opal semiconducting polymer films.[255] In a similar fashion, they had also been able to prepare polyaniline inverse opals. First, aniline was infiltrated into the voids of a PS colloidal assembly, which was then exposed to potassium peroxodisulfate ($K_2S_2O_8$) to induce an oxidation polymerization of aniline. After removal of the PS colloids a polyaniline inverse opal was obtained.[256]

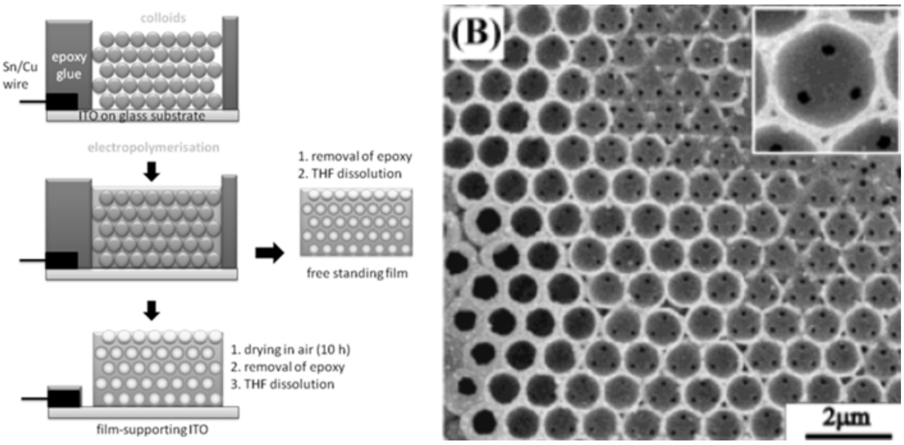

Figure 20. *a) General schematic illustration of the fabrication of a semi conducting inverse opal by electropolymerization of monomers, such as pyrrole or thiophene) within the interstices of a array of hexagonally packed polystryrol particles. Apapted from [255] b) SEM image of a free-standing inverse opal semiconducting film made of polythiophene. Copied from [255].*

Following this approach, also other materials, such as semicondutors (CdS, CdSe, ZnO), polymers (poly(3-methylthiophene), poly(bithiophene)) or metals (Au, Ni, Pt, Co), have been electrodeposited.[257] Yoshino et al. could show that the voids of SiO_2 opals can be infiltrated with poly(2,5-dioctyloxy-p-phenylenevinylene) (POOPPV) and poly(2-methoxy-5-dodecyloxy-p-phenylenevinylene) (PMDDOPP) and also fluorescent dyes from solution, leading to an amplified spontaneous emission and lasing.[258]

Besides the use of sacrificial block copolymer templates for the patterning of organic and inorganic semiconductors the self-assembly of block copolymers composed of one hole conducting and one electron conducting block can also be directly used to prepare well defined morphologies of the photoactive layer in OPVs. Although this approach is not based on a template-assisted method in a strict sense, it is worth to mention some recent work as a promising alternative route to the template-based approach. In 2000 the group of *Hadziioannou* showed the synthesis and microphase separation of a block copolymer consisting of a *p*-phenylenevinylene (PPV) and a partially fullerene containing block, which showed a strong quenching effect of photoluminescence of the PPV due to the efficient electron transfer to the fullerene.[259] *Zentel* and coworkers investigated the properties of a microphase separated block copolymer made of a triphenylamine and a non-linear optic (NLO) chromophore containing triphenylamine block.[260] Block copolymers based on hole conducting triarylamine and electron conducting perylene bisimide moieties have been intensively investigated and optimized for the application in bulk heterojunction solar cells by the group of *Thelakkat* in the last years.[261-264] Recently, *Thelakkat* and coworkers have also presented a crystalline-cyrstalline donor-acceptor block copolymer with P3HT as donor block an poly(perylene bisimide acrylate) as acceptor block.[265]

One of the crucial challenges for the fabrication of high effective OPVs via the self-assembly of donor/acceptor block copolymers is the controlled micro phase separation into an interpenetration network which is still a very delicate issue and therefore has not won the race versus the template-based approach so far.

1.5 References

1. Lück, H. B.; Matthes, H.; Gemende, B.; Heinrich, B.; Pfestorf, W.; Seidel, W.; Turuc, S., *Nucl. Instr. Meth. Phys. Res. B* **1990,** 50, 395-400.
2. Haberkorn, N.; Theato, P., *unpublished data*.
3. Paulose, M.; Shankar, K.; Varghese, O. K.; Mor, G. K.; Grimes, C. A., *J. Phys. D: Appl. Phys.* **2006,** 39, 2498-2503.
4. Lee, J.; Cho, S. H.; Park, S.-M.; Kim, J. K.; Kim, J. K.; Yu, J.-W.; Kim, Y. C.; Russell, T. P., *Nano Lett.* **2008**, 8, 2315-2320.
5. Diggle, J.; Downie, T.; Goulding, C., *Chem. Rev.* **1969,** *69*, 365.
6. *British Patent 223,994,* ***1923****.*
7. Thompson, G., *Thin Solid Films* **1997,** 297, 192-201.
8. Güntherschulze, A.; Betz, H., *Elektrolytkondensatoren*. M. Krayn Verlag: Berlin, **1937**.
9. Holleman A.; Wiberg, E.; *Lehrbuch der Anorganischen Chemie*, deGruyter **1995**.
10. Herrmann, E., Elektrolytisches Färben von Anodisiertem Aluminium. In *Galvanotechnik*, 1972; Vol. 63, pp 110-121.
11. Sheasby, P. G.; Cooke, W. E., The electrolytic colouring of anodized aluminum. In *Transactions of the Insitute of Metal Finishing*, **1974**; Vol. 52, pp 103-106.
12. Asada, T. US Patent 4, 022, 671. 1977.
13. Kawei, S.; Ishiguro, I., *J. Electrochem. Soc.* **1976,** *123*, 1047-1051.
14. Kawai, S.; Ueda, R., *J. Electrochem. Soc.* **1975,** *122*, 32-36.
15. URL: http://www.whatman.com/NucleporeTrackEtched-Membranes.aspx
16. Masuda, H.; Fukuda, K., *Science* **1995,** 268, 1466-1468.
17. Masuda, H.; Hasegwa, F.; Ono, S., *J. Electrochem. Soc.* **1997,** 144, L127-L130.
18. Masuda, H.; Yamada, H.; Satoh, M.; Asoh, H.; Nakao, M.; Tamamura, T., *Appl. Phys. Lett.* **1997,** 71, 2770-2772.
19. Lee, W.; Ji, R.; Ross, Caroline A.; Gösele, U.; Nielsch, K., *Small* **2006,** 2, 978-982.
20. Liu, C.; Datta, A.; Wang, Y., *Appl. Phys. Lett.* **2001,** 78, 120-122.
21. Sun, Z.; Kim, H., *Appl. Phys. Lett.* **2002,** 81, 3458-3460.
22. Fournier-Bidoz, S.; Kitaev, V.; Routkevitch, D.; Manners, I.; Ozin, G., *Adv. Mater.* **2004,** 16, 2193.
23. Choi, J.; Sauer, G.; Nielsch, K.; Wehrspohn, R.; Gösele, U., *Chem. Mater.* **2003,** 15, 776-779.
24. Kim, T.-Y.; Jeong, S.-H., *Korean J. Chem. Eng.* **2008,** 25, 609-611.
25. Jeong, S.-H.; Jung, S.-H.; Lee, K.-H., *J. Korean Ind. Eng. Chem.* **2005,** 16, 461.
26. Steinhart, M.; Shimazu, T.; Shimazu, T.; Steinhart, M., *Adv. Polym. Sci.* **2008,** 220, 123-187.
27. Zhang, F.; Liu, X.; Pan, C.; Zhu, J., *Nanotechnology* **2007,** 18, 345302.
28. Ono, S.; Saito, M.; Ishiguro, M.; Asoh, H., *J. Electrochem. Soc.* **2004,** 151, B473-B478.
29. Nielsch, K.; Choi, J.; Schwirn, K.; Wehrspohn, R.; Gösele, U., *Nano Lett.* **2002,** 2, 677-680.
30. Masuda, H.; Yada, K.; Osaka, A., *Jpn. J. Appl. Phys.* **1998,** 37, L1340-L1342.
31. Li, F.; Zhang, L.; Metzger, R., *Chem. Mater.* **1998,** 10, 2470-2480.
32. Li, A.; Muller, F.; Birner, A.; Nielsch, K.; Gösele, U., *J. Appl. Phys.* **1998,** 84, 6023-6026.

33. Jessensky, O.; Müller, F.; Gösele, U., *Appl. Phys. Lett.* **1998,** 72, 1173-1175.
34. Chen, W.; Wu, J.-S.; Xia, X.-H., *Acs Nano* **2008,** 2, 959-965.
35. Salerno, M.; Patra, N.; Cingolani, R., *Nanoscale Res Lett* **2009,** 4, 865-872.
36. Zaraska, L.; Sulka, G. D.; Jaskula, M., *Surf Coat Tech* **2010,** 204, 1729-1737.
37. Lee, W.; Nielsch, K.; Goesele, U., *Nanotechnology* **2007,** 18, 475713.
38. Lee, W.; Ji, R.; Gösele, U.; Nielsch, K., *Nature Materials* **2006,** 5, 741-747.
39. Meng, G.; Jung, Y.; Cao, A.; Vajtai, R.; Ajayan, P., *Proceedings of the National Academy of Sciences of the United States of America* **2005,** 102, 7074-7078.
40. Wade, T. L.; Wegrowe, J.-E., *The European Physical Journal Applied Physics* **2005,** 29, 3-22.
41. Lee, W., *Jom-Us* **2010,** 62, 57-63.
42. Thompson, G.; Wood, G., *Nature* **1981,** 290, 230-232.
43. O'Sullivan, J.; Wood, G., *Proceedings of the Royal Society of London. A. Mathematical and Physical Sciences* **1970,** 317, 511-543.
44. Hoar, T.; Mott, N., *J. Phys. Chem. Solids* **1959,** 9, 97-99.
45. Thompson, G.; Furneaux, R.; Wood, G.; Richardson, J.; Goode, J., *Nature* **1978,** 272, 433-435.
46. Patermarakis, G.; Lenas, P.; Karavassilis, C.; Papayiannis, G., *Electrochim. Acta* **1991,** 36, 709-725.
47. Patermarakis, G.; Tzouvelekis, D., *Electrochim. Acta* **1994,** 39, 2419-2429.
48. Thamida, S.; Chang, H., *Chaos* **2002,** 12, 240-251.
49. Wu, Z.; Richter, C.; Menon, L., *J. Electrochem. Soc.* **2007,** 154, E8-E12.
50. Singh, G.; Golovin, A.; Aranson, I., *Physical Review B (Condensed Matter and Materials Physics)* **2006,** 73, 205422.
51. Parkhutik, V.; Shershulsky, V., *J Phys D Appl Phys* **1992,** 25, 1258-1263.
52. Keller, F.; Hunter, M.; Robinson, D., *J. Electrochem. Soc.* **1953,** 100, 411.
53. Su, Z.; Hahner, G.; Zhou, W., *J. Mater. Chem.* **2008,** 18, 5787-5795.
54. Su, Z.; Zhou, W., *Adv. Mater.* **2008,** 20, 3663.
55. Valand, T.; Heusler, K., *J Electroanal Chem* **1983,** 149, 71-82.
56. Macdonald, D., *J. Electrochem. Soc.* **1992,** 139, 3434-3449.
57. Macdonald, D., *J. Electrochem. Soc.* **1993,** 140, L27-L30.
58. Wu, H.; Hebert, K.; Gessmann, T.; Lynn, K., *J. Electrochem. Soc.* **2002,** 149, B108-B116.
59. Hebert, K.; Wu, H.; Gessmann, T.; Lynn, K., *J. Electrochem. Soc.* **2001,** 148, B92-B100.
60. Huang, R.; Hebert, K.; Gessmann, T.; Lynn, K., *J. Electrochem. Soc.* **2004,** 151,B227-B232.
61. Jessensky, O.; Müller, F.; Gösele, U., *Appl. Phys. Lett.* **1998,** 72, 1173-1175.
62. Jessensky, O.; Müller, F.; Gösele, U., *J. Electrochem. Soc.* **1998,** 145, 3735-3740.
63. Paulose, M.; Varghese, O. K.; Mor, G. K.; Grimes, C. A.; Ong, K. G., *Nanotechnology* **2006,** 17, 398-402.
64. Grimes, C.; Ong, K.; Varghese, O.; Yang, X.; Mor, G.; Paulose, M.; Dickey, E.; Ruan, C.; Pishko, M.; Kendig, J.; Mason, A., *Sensors* **2003,** 3, 69-82.
65. Mor, G. K.; Shankar, K.; Paulose, M.; Varghese, O. K.; Grimes, C. A., *Nano Lett.* **2005,** 5, 191-195.

66. Allam, N. K.; Shankar, K.; Grimes, C. A., *J. Mater. Chem.* **2008,** 18, 2341-2348.
67. Mor, G. K.; Shankar, K.; Paulose, M.; Varghese, O. K.; Grimes, C. A., *Nano Lett.* **2006,** 6, 215-218.
68. Shin, Y.; Lee, S., *Nano Lett.* **2008,** 8, 3171-3173.
69. Grimes, C. A., *J. Mater. Chem.* **2007,** 17, 1451-1457.
70. Gong, D.; Grimes, C. A.; Varghese, O. K.; Chen, Z.; Hu, W.; Dickey, E. C., *J. Mater. Res.* **2001,** 16, 3331.
71. Taveira, L. V.; Macák, J. M.; Tsuchiya, H.; Dick, L. F. P.; Schmuki, P., *J. Electrochem. Soc.* **2005,** 152, B405-B410.
72. Zhao, J.; Wang, X.; Chen, R.; Li, L., *Solid State Commun.* **2005,** 134, 705-710.
73. Jaroenworaluck, A.; Regonini, D.; Bowen, C.; Stevens, R.; Allsopp, D., *J. Mater. Sci.* **2007,** 42, 6729-6734.
74. Macák, J. M.; Tsuchiya, H.; Schmuki, P., *Angew. Chem. Int. Ed.* **2005,** 44, 2100-2102.
75. Macak, J. M.; Tsuchiya, H.; Taveira, L.; Aldabergerova, S.; Schmuki, P., *Angew. Chem. Int. Ed.* **2005,** 44, 7463-7465.
76. Macak, J. M.; Sirotna, K.; Schmuki, P., *Electrochim. Acta* **2005,** 50, 3679-3684.
77. Paulose, M.; Shankar, K.; Yoriya, S.; Prakasam, H. E.; Varghese, O. K.; Mor, G. K.; Latempa, T. A.; Fitzgerald, A.; Grimes, C. A., *J. Phys. Chem. B* **2006,** 110, 16179-16184.
78. Shankar, K.; Mor, G. K.; Prakasam, H. E.; Yoriya, S.; Paulose, M.; Varghese, O. K.; Grimes, C. A., *Nanotechnology* **2007,** 18, 065707.
79. Allam, N. K.; Grimes, C. A., *Sol. Energy Mater. Sol. Cells* **2008,** 92, 1468-1475.
80. Bauer, S.; Kleber, S.; Schmuki, P., *Electrochem. Commun.* **2006,** 8, 1321-1325.
81. Sadek, A. Z.; Zheng, H.; Latham, K.; Wlodarski, W.; Kalantar-zadeh, K., *Langmuir* **2009,** 25, 509-514.
82. Lehmann, V.; Foll, H., *J. Electrochem. Soc.* **1990,** 137, 653-659.
83. Lehmann, V., *J. Electrochem. Soc.* **1993,** 140, 2836-2843.
84. Birner, A.; Grüning, U.; Ottow, S.; Schneider, A.; Müller, F.; Lehmann, V.; Föll, H.; Gösele, U., physica status solidi (a) **1998**, 165, 111-117.
85. Tao, Y.; Esashi, M., *J. Micromech. Microeng.* **2005,** 15, 764-770.
86. URL: http://www.whatman.com/NucleporeTrackEtched-Membranes.aspx
87. URL: http://www.osmolabstore.com/OsmoLabPage.dll?BuildPage&1&1&71.
88. Fleischer, R. L.; Price, P. B.; Walker, R. M., Nuclear tracks in solids. In University of California Press: Berkeley, **1975**.
89. Apel, P., *Radiat. Measur.* **2001,** 34, 559-566.
90. Apel, P. Y., *Radiat. Measur.* **1995,** 25, 667-674.
91. Shirkova, V. V.; Tretyakova, S. P., *Radiat. Measur.* **1997,** 28, 791-798.
92. Zhao, C.-D.; Vater, P.; Brandt, R., *Nucl. Tracks Radiat. Meas.* **1991,** 19, 829-834.
93. Trautmann, C.; Brüchle, W.; Spohr, R.; Vetter, J.; Angert, N., *Nucl. Instr. Meth. Phys. Res. B* **1996,** 111, 70-74.
94. Crawford, G. P.; Steele, L. M.; Ondris-Crawford, R.; Iannacchione, G. S.; Yeager, C. J.; Doane, J. W.; Finotello, D., *J. Chem. Phys.* **1992,** 96, 7788-7796.
95. Ferain, E.; Legras, R., *Nucl. Instr. Meth. Phys. Res. B* **2003,** 208, 115-122.
96. Wang, J.-Y.; Chen, W.; Russell, T. P., *Patterning with block copolymers*. Wiley: 2009.
97. Bates, F. S., *Science* **1991,** 251, 898-905.

98. Thurn-Albrecht, T.; DeRouchey, J.; Russell, T. P.; Jaeger, H. M., *Macromolecules* **2000,** 33, 3250-3253.
99. Boker, A.; Elbs, H.; Hansel, H.; Knoll, A.; Ludwigs, S.; Zettl, H.; Zvelindovsky, A. V.; Sevink, G. J. A.; Urban, V.; Abetz, V.; Muller, A. H. E.; Krausch, G., *Macromolecules* **2003,** 36, 8078-8087.
100. Thurn-Albrecht, T.; DeRouchey, J.; Russell, T. P.; Kolb, R., *Macromolecules* **2002,** 35, 8106-8110.
101. Thurn-Albrecht, T.; Schotter, J.; Kastle, G. A.; Emley, N.; Shibauchi, T.; Krusin-Elbaum, L.; Guarini, K.; Black, C. T.; Tuominen, M. T.; Russell, T. P., *Science* **2000,** 290, 2126-2129.
102. Thurn-Albrecht, T.; Steiner, R.; DeRouchey, J.; Stafford, C. M.; Huang, E.; Bal, M.; Tuominen, M.; Hawker, C. J.; T. P. Russell, *Adv. Mater.* **2000,** 12, 787-791.
103. Stoykovich, M. P.; Müller, M.; Kim, S. O.; Solak, H. H.; Edwards, E. W.; de Pablo, J. J.; Nealey, P. F., *Science* **2005,** 308, 1442-1446.
104. Ruiz, R.; Kang, H.; Detcheverry, F. A.; Dobisz, E.; Kercher, D. S.; Albrecht, T. R.; de Pablo, J. J.; Nealey, P. F., *Science* **2008,** 321, 936-939.
105. Ji, S.; Liu, C.-C.; Son, J. G.; Gotrik, K.; Craig, G. S. W.; Gopalan, P.; Himpsel, F. J.; Char, K.; Nealey, P. F., *Macromolecules* **2008,** 41, 9098-9103.
106. Son, J. G.; Bulliard, X.; Kang, H. M.; Nealey, P. E.; Char, K., *Adv. Mater.* **2008,** 20, 3643.
107. Kim, G.; Libera, M., *Macromolecules* **1998,** 31, 2569-2577.
108. Kim, S. H.; Misner, M. J.; Xu, T.; Kimura, M.; T. P. Russell, *Adv. Mater.* **2004,** 16, 226-231.
109. Bita, I.; Yang, J. K. W.; Jung, Y. S.; Ross, C. A.; Thomas, E. L.; Berggren, K. K., *Science* **2008,** 321, 939-943.
110. Mansky, P.; Liu, Y.; Huang, E.; Russell, T. P.; Hawker, C., *Science* **1997,** 275, 1458-1460.
111. Jeong, U.; Ryu, D. Y.; Kho, D. H.; Kim, J. K.; Goldbach, J. T.; Kim, D. H.; T. P. Russell, *Adv. Mater.* **2004,** 16, 533-536.
112. Crossland, E. J. W.; Ludwigs, S.; Hillmyer, M. A.; Steiner, U., *Soft Matter* **2007,** 3, 94-98.
113. Crossland, E. J. W.; Nedelcu, M.; Ducati, C.; Ludwigs, S.; Hillmyer, M. A.; Steiner, U.; Snaith, H. J., *Nano Lett.* **2009,** 9, 2813-2819.
114. Olson, D. A.; Chen, L.; Hillmyer, M. A., *Chem. Mater.* **2008,** 20, 869-890.
115. Fustin, C.-A.; Guillet, P.; Misner, M. J.; Russell, T. P.; Schubert, U. S.; Gohy, J.-F., *J. Polym. Sci., Part A: Polym. Chem.* **2008,** 46, 4719-4724.
116. Fustin, C.-A.; Guillet, P.; Schubert, U. S.; Gohy, J.-F., *Adv. Mater.* **2007,** 19, 1665-1673.
117. Zhang, M.; Yang, L.; Yurt, S.; Misner, M. J.; Chen, J.-T.; Coughlin, E. B.; Venkataraman, D.; T. P. Russell, *Adv. Mater.* **2007,** 19, 1571-1576.
118. Kang, M.; Moon, B., *Macromolecules* **2009,** 42, 455-458.
119. Huczko, A., *Appl. Phys. A* **2000,** 70, 365-376.
120. Martin, C. R., *Chem. Mater.* **1996,** 8, 1739-1746.
121. Hulteen, J. C.; Martin, C. R., *J. Mater. Chem.* **1997,** 7, 1075-1087.
122. Lee, W.; Scholz, R.; Nielsch, K.; Gösele, U., *Angew. Chem. Int. Ed.* **2005,** 44, 6050-6054.

123. Sapp, S. A.; Lakshmi, B. B.; Martin, C. R., *Adv. Mater.* **1999,** 11, 402-404.
124. Choi, W. B.; Chu, J. U.; Jeong, K. S.; Bae, E. J.; Lee, J.-W.; Kim, J.-J.; Lee, J.-O., *Appl. Phys. Lett.* **2001,** 79, 3696-3698.
125. Hu, W.; Gong, D.; Chen, Z.; Yuan, L.; Saito, K.; Grimes, C. A.; Kichambare, P., *Appl. Phys. Lett.* **2001,** 79, 3083-3085.
126. Klein, J. D.; Herrick, R. D.; Palmer, D.; Sailor, M. J.; Brumlik, C. J.; Martin, C. R., *Chem. Mater.* **1993,** 5, 902-904.
127. Misner, M. J.; Skaff, H.; Emrick, T.; Russell, T. P., *Adv. Mater.* **2003,** 15, 221-224.
128. Darling, S. B.; Yufa, N. A.; Cisse, A. L.; Bader, S. D.; Sibener, S. J., *Adv. Mater.* **2005,** 17, 2446-2450.
129. Steinhart, M.; Zimmermann, S.; Goring, P.; Schaper, A. K.; Gosele, U.; Weder, C.; Wendorff, J. H., *Nano Lett.* **2005,** 5, 429-434.
130. Steinhart, M.; Wendorff, J. H.; Greiner, A.; Wehrspohn, R. B.; Nielsch, K.; Schilling, J.; Choi, J.; Gösele, U., *Science* **2002,** 296, 1997-.
131. Cepak, V. M.; Martin, C. R., *Chem. Mater.* **1999,** 11, 1363-1367.
132. Steinhart, M.; H.Wendorff, J.; Ralf B. Wehrspohn, *Chem. Phys. Chem.* **2003,** 4, 1171-1176.
133. Steinhart, M.; Wehrspohn, R. B.; Gösele, U.; Wendorff, J. H., *Angew. Chem. Int. Ed.* **2004,** 43, 1334-1344.
134. Wang, Y.; Gösele, U.; Steinhart, M., *Chem. Mater.* **2008,** 20, 379-381.
135. Lim, J. K.; Ciszek, J. W.; Huo, F.; Jang, J.-W.; Hwang, S.; Mirkin, C. A., *Nano Lett.* **2008,** 8, 4441-4445.
136. Park, S.; Lim, J.-H.; Chung, S.-W.; Mirkin, C. A., *Science* **2004,** 303, 348-351.
137. Park, S.; Chung, S.-W.; Mirkin, C. A., *J. Am. Chem. Soc.* **2004,** 126, 11772-11773.
138. Liang, Y.; Zhen, C.; Zou, D.; Xu, D., *J Am Chem Soc* **2004,** 126, 16338-16339.
139. Xiao, R.; Cho, S.; Liu, R.; Lee, S., *J Am Chem Soc* **2007,** 129, 4483-4489.
140. Yang, S.; Chen, K.; Yang, Y., *Synth. Met.* **2005,** 152, 65-68.
141. Lakshmi, B.; Patrissi, C.; Martin, C., *Chem. Mater.* **1997,** 9, (11), 2544-2550.
142. Lakshmi, B.; Dorhout, P.; Martin, C., *Chem. Mater.* **1997,** 9, (3), 857-862.
143. Steinhart, M.; Wendorff, J.; Greiner, A.; Wehrspohn, R.; Nielsch, K.; Schilling, J.; Choi, J.; Gosele, U., *Science* **2002,** 296, 1997.
144. Steinhart, M.; H.Wendorff, J.; Wehrspohn, Ralf, *Chem. Phys. Chem.* **2003,** 4, 1171-1176.
145. Steinhart, M.; Wehrspohn, R.; Gösele, U.; Wendorff, J., *Angew. Chem. Int. Ed.* **2004,** 43, 1334-1344.
146. Schlitt, S.; Greiner, A.; Wendorff, J. H., *Macromolecules* **2008,** 41, 3228-3234.
147. Fox, H.; Hare, E.; Zisman, W., *J Phys Chem-Us* **1955,** 59, 1097-1106.
148. Steinhart, M., *Adv Polym Sci* **2008,** 220, 123-187.
149. Zhang, M.; Dobriyal, P.; Chen, J.-T.; Russell, T.; Olmo, J.; Merry, A., *Nano Lett.* **2006,** 6,1075-1079.
150. MartiÌn, J.; Mijangos, C., *Langmuir* **2009,** 25, 1181.
151. Alvarez, S. D.; Li, C.-P.; Chiang, C. E.; Schuller, I. K.; Sailor, M. J. *ACS Nano*, **2009**, 3, 3301-3307.
152. Lakshmi, B.; Martin, C., *Nature* **1997,** 388, 758-760.

153. Kohli, P.; Harrell, C.; Cao, Z.; Gasparac, R.; Tan, W.; Martin, C., *Science* **2004,** 305, 984-986.
154. Grimm, S.; Schwirn, K.; Göring, P.; Knoll, H.; Miclea, Paul T.; Greiner, A.; Wendorff, J.; Wehrspohn, R.; Gösele, U.; Steinhart, M., *Small* **2007,** 3, 993-1000.
155. Lee, Y.; Park, S.; Kim, K.; Lee, J., *Adv. Mater.* **2007,** 19, 2330-2335.
156. Lee, W.; Jin, M.; Yoo, W.; Lee, J., *Langmuir* **2004,** 20, 7665-7669.
157. Cho, W.; Choi, I., *Adv Funct Mater* **2008,** 18, 1089-1096.
158. Kustandi, T. S.; Samper, V. D.; Ng, W. S.; Chong, A. S.; Gao, H., *Journal of Micromechanics and Microengineering* **2007,** 17, N75-N81.
159. Lu, G.; Hong, W.; Tong, L.; Bai, H.; Wei, Y.; Shi, G., *Acs Nano* **2008,** 2, 2342-2348.
160. Martin, C., *Acc. Chem. Res.* **1995,** 28, 61-68.
161. Gitsas, A.; Yameen, B.; Lazzara, T. D.; Steinhart, M.; Duran, H.; Knoll, W., *Nano Lett.* **2010,** 10, 2173-2177.
162. Evans, B. A.; Shields, A. R.; Carroll, R. L.; Washburn, S.; Falvo, M. R.; Superfine, R., *Nano Lett.* **2007,** 7, 1428-1434.
163. du Roure, O.; Saez, A.; Buguin, A.; Austin, R.; Chavrier, P.; Silberzan, P.; Ladoux, B., *P Natl Acad Sci Usa* **2005,** 102, 2390-2395.
164. Tan, J.; Tien, J.; Pirone, D.; Gray, D.; Bhadriraju, K.; Chen, C., *P Natl Acad Sci Usa* **2003,** 100, 1484-1489.
165. Mallet, J.; Yu-Zhang, K.; Mátéfi-Tempfli, S.; Mátéfi-Tempfli, M.; Piraux, L., *J. Phys. D: Appl. Phys.* **2005,** 38, 909-914.
166. Kim, M. G.; Cho, J., *Adv Funct Mater* **2009,** 19, 1497-1514.
167. Chen, R.; Lu, M.-C.; Srinivasan, V.; Wang, Z.; Cho, H. H.; Majumdar, A., *Nano Lett.* **2009,** 9, 548-553.
168. Zhang, Y.; Lo, C.; Taylor, J.; Yang, S., *Langmuir* **2006,** 22, 8595-8601.
169. Kondo, T.; Juodkazis, S.; Misawa, H., *Applied Physics A: Materials Science & Processing* **2005,** 81,, 1583-1586.
170. Tanaka, T.; Morigami, M.; Atoda, N., *Japanese Journal of Applied Physics* 32, 6059.
171. Hui, C.; Jagota, A.; Lin, Y.; Kramer, E., *Langmuir* **2002,** 18, 1394-1407.
172. Roca-Cusachs, P.; Rico, F.; Martinez, E.; Toset, J.; Farre, R.; Navajas, D., *Langmuir* **2005,** 21, 5542-5548.
173. Chandra, D.; Taylor, J. A.; Yang, S., *Soft Matter* **2008,** 4, 979-984.
174. del Campo, A.; Greiner, C., *Journal of Micromechanics and Microengineering* **2007,** 17, R81.
175. Chen, G.; Soper, S. A.; McCarley, R. L., *Langmuir* **2007,** 23, 11777-11781.
176. Chandra, D.; Yang, S., *Langmuir* **2009,** 25, 10430-10434.
177. Tanaka, T.; Morigami, M.; Oizumi, H.; Ogawa, T., *Japanese Journal of Applied Physics* **1993,** 32, 5813-5814.
178. Krebs, F. C., *Sol. Energy Mater. Sol. Cells* **2009,** 93, 394-412.
179. Krebs, F. C.; Gevorgyan, S. A.; Alstrup, J., *J. Mater. Chem.* **2009,** 19, 5442-5451.
180. Hoth, C. N.; Choulis, S. A.; Schilinsky, P.; Brabec, C. J., *Adv. Mater.* **2007,** 19, 3973.
181. Aernouts, T.; Aleksandrov, T.; Girotto, C.; Genoe, J.; Poortmans, J., *Appl. Phys. Lett.* **2008,** 92, 033306.
182. Brabec, C.; Sariciftci, N.; Hummelen, J, *Adv Funct Mater* **2001,** 11, 15-26.

183. Gunes, S.; Neugebauer, H.; Sariciftci, N., *Chem. Rev.* **2007,** 107, 1324-1338.
184. Sirringhaus, H.; Brown, P.; FRIEND, R.; Nielsen, M.; Bechgaard, K.; Langeveld-Voss, B.; Spiering, A.; Janssen, R.; Meijer, E.; Herwig, P.; de Leeuw, D., *Nature* **1999,** 401, 685-688.
185. Bao, Z.; Dodabalapur, A.; Lovinger, A., *Appl. Phys. Lett.* **1996,** 69, 4108-4110.
186. Sirringhaus, H.; Tessler, N.; FRIEND, R., *Science* **1998,** 280, 1741-1744.
187. Sommer, M.; Lang, A. S.; Thelakkat, M., *Angew Chem Int Edit* **2008,** 47, 7901-7904.
188. Sommer, M.; Lindner, S.; Thelakkat, M., *Adv Funct Mater* **2007,** 17, 1493-1500.
189. Yan, H.; Lee, P.; Armstrong, N.; Graham, A.; Evmenenko, G.; Dutta, P.; Marks, T., *J Am Chem Soc* **2005,** 127, 3172-3183.
190. Huang, Q.; Evmenenko, G.; Dutta, P.; Marks, T., *J Am Chem Soc* **2003,** 12, 14704-14705.
191. Shang, Y.; Wen, Y.; Li, S.; Du, S.; He, X.; Cai, L.; Li, Y.; Yang, L.; Gao, H.; Song, Y., *J Am Chem Soc* **2007,** 129, 11674.
192. Sariciftci, N.; Smilowitz, L.; Heeger, A.; Wudl, F., *Science* **1992,** 258, 1474-1476.
193. Tatemichi, S.; Ichikawa, M.; Koyama, T.; Taniguchi, Y., *Appl. Phys. Lett.* **2006,** 89, 112108.
194. Chesterfield, R.; McKeen, J.; Newman, C.; Ewbank, P.; da Silva, D.; Bredas, J.; Miller, L.; Mann, K.; Frisbie, C., *J Phys Chem B* **2004,** 108, 19281-19292.
195. Jones, B. A.; Facchetti, A.; Wasielewski, M. R.; Marks, T. J., *J Am Chem Soc* **2007,** 129, 15259-15278.
196. Zhan, X.; Tan, Z. a.; Domercq, B.; An, Z.; Zhang, X.; Barlow, S.; Li, Y.; Zhu, D.; Kippelen, B.; Marder, S. R., *J Am Chem Soc* **2007,** 129, 7246.
197. Wicklein, A.; Lang, A.; Muth, M.; Thelakkat, M., *J Am Chem Soc* **2009,** 131, 14442-14453.
198. Huettner, S.; Sommer, M.; Thelakkat, M., *Appl. Phys. Lett.* **2008,** 92, 093302.
199. King, S.; Sommer, M.; Huettner, S.; Thelakkat, M.; Haque, S. A., *J. Mater. Chem.* **2009,** 19, 5436-5441.
200. Hill, I.; Kahn, A.; Soos, Z.; Pascal, R., *Chem. Phys. Lett.* **2000,** 327, 181-188.
201. Zhu, X.-Y.; Yang, Q.; Muntwiler, M., *Acc. Chem. Res.* **2009,** 42, 1779-1787.
202. Bredas, J.-L.; Norton, J. E.; Cornil, J.; Coropceanu, V., *Acc. Chem. Res.* **2009,** 42, 1691-1699.
203. Wohrle, D.; Meissner, D., *Adv. Mater.* **1991,** 3, 129-138.
204. Halls, J. J. M.; Walsh, C. A.; Greenham, N. C.; Marseglia, E. A.; Friend, R. H.; Moratti, S. C.; Holmes, A. B., *Nature* **1995,** 376, 498-500.
205. Yu, G.; Gao, J.; Hummelen, J.; Wudl, F.; Heeger, A., *Science* **1995,** 270, 1789.
206. Ma, W.; Yang, C.; Gong, X.; Lee, K.; Heeger, A., *Adv Funct Mater* **2005,** 15, 1617-1622.
207. Reyes-Reyes, M.; Kim, K.; Dewald, J.; Lopez-Sandoval, R.; Avadhanula, A.; Curran, S.; Carroll, D., *Org. Lett.* **2005,** 7, 5749-5752.
208. Liang, Y.; Xu, Z.; Xia, J.; Tsai, S.-T.; Wu, Y.; Li, G.; Ray, C.; Yu, L., *Adv. Mater.* **2010,** DOI: 10.1021/jp101925b.
209. Liang, Y.; Feng, D.; Wu, Y.; Tsai, S.-T.; Li, G.; Ray, C.; Yu, L., *J Am Chem Soc* **2009,** 131, 7792-7799.
210. Cai, W.; Gong, X.; Cao, Y., *Sol. Energy Mater. Sol. Cells* **2010,** 94, 114-127.
211. Hoppe, H.; Sariciftci, N. S., *Adv Polym Sci* **2008,** 214, 1-86.

212. Penner, R. M.; Martin, C. R., *J. Electrochem. Soc.* **1986,** 133, 2206-2207.
213. Penner, R. M.; Martin, C. R., *J. Electrochem. Soc.* **1986,** 133, 310-315.
214. Penner, R. M.; Martin, C. R., *J. Electrochem. Soc.* **1985,** 132, 514-515.
215. Martin, C. R., *Science* **1994,** 266, 1961-1966.
216. Cai, Z.; Martin, C. R., *J. Am. Chem. Soc.* **1989,** 111,, 4138-4139.
217. van Dyke, L. S.; Martin, C. R., *Langmuir* **1990,** 6, 1118-1123.
218. Demoustier-Champagne, S.; Stavaux, P.-Y., *Chem. Mater.* **1999,** 11, 829-834.
219. Demoustier-Champagne, S.; Ferain, E.; Jérôme, C.; Jérôme, R.; Legras, R., *Eur. Polym. J.* **1998,** 34, 1767-1774.
220. Cahalane, W.; Labes, M. M., *Chem. Mater.* **1989,** 1, 519-522.
221. Martin, C. R.; Van Dyke, L. S.; Cai, Z.; Liang, W., *J. Am. Chem. Soc.* **1990,** 112, 8976-8977.
222. Menon, V. P.; Lei, J.; Martin, C. R., *Chem. Mater.* **1996,** 8, 2382-2390.
223. Cai, Z.; Lei, J.; Liang, W.; Menon, V.; Martin, C. R., *Chem. Mater.* **1991,** 3, 960-967.
224. Martin, C. R.; Parthasarathy, R.; Menon, V., *Synth. Met.* **1993,** 55, 1165-1170.
225. Dauginet, L.; Duwez, A.-S.; Legras, R.; Demoustier-Champagne, S., *Langmuir* **2001,** 17, 3952-3957.
226. Dauginet-De Pra, L.; Ferain, E.; Legras, R.; Demoustier-Champagne, S., *Nucl. Instrum. Methods Phys. Res. B* **2002,** 196, 81-88.
227. Charles R. Martin, *Adv. Mater.* **1991,** 3, 457-459.
228. Parthasarathy, R. V.; Martin, C. R., *Chem. Mater.* **1994,** 6, 1627-1632.
229. Martin, C. R., *Acc. Chem. Res.* **1995,** 28, 61-68.
230. Berdichevsky, Y.; Lo, Y.-H., *Adv. Mater.* **2006,** 18, 122-125.
231. Berdichevsky, Y.; Lo, Y. H., *Mat. Res. Soc. Symp. Proc.* **2005**, 211-215.
232. Berdichevsky, Y.; Lo, Y.-H., *Proc. SPIE Int. Soc. Opt. Eng.* **2005**, 268-273.
233. Park, D. H.; Kim, B. H.; Jang, M. G.; Bae, K. Y.; Joo, J., *Appl. Phys. Lett.* **2005,** 86, 113116.
234. Fu, M.; Zhu, Y.; Tan, R.; Shi, G., *Adv. Mater.* **2001,** 13, 1874-1877.
235. Xiao, R.; Cho, S. I.; Liu, R.; Lee, S. B., *J. Am. Chem. Soc.* **2007,** 129, 4483-4489.
236. Cho, S. I.; Kwon, W. J.; Choi, S.-J.; Kim, P.; Park, S.-A.; Kim, J.; Son, S. J.; Xiao, R.; Kim, S.-H.; Lee, S. B., *Adv. Mater.* **2005,** 17, 171-175.
237. Cho, S.; Lee, S., *Acc. Chem. Res.* **2008,** 41,699-707.
238. Cho, S. I.; Choi, D. H.; Kim, S.-H.; Lee, S. B., *Chem. Mater.* **2005,** 17, 4564-4566.
239. Palacios, R.; Formentín, P.; Trifonov, T.; Estrada, M.; Alcubilla, R.; Pallarés, J.; Marsal, L. F., *Phys. Stat. Sol. (RRL)* **2008,** 2, 206-208.
240. Li, X.; Tian, S.; Ping, Y.; Kim, D. H.; Knoll, W., *Langmuir* **2005,** 21, 9393-9397.
241. Park, S.; Lee, D. H.; Xu, J.; Kim, B.; Hong, S. W.; Jeong, U.; Xu, T.; Russell, T. P., *Science* **2009,** 323, 1030-1033.
242. Liu, N.; Chen, H.-Z.; Wang, M., *Thin Solid Films* **2008,** 516, 4272-4276.
243. Bai, R.; Ouyang, M.; Zhou, R.-J.; Shi, M.-M.; Wang, M.; Chen, H.-Z., *Nanotechnology* **2008,** 19, 055604.
244. Bai, R.; Ouyang, M.; Li, Z.-Z.; Yang, L.-G.; Shi, M.-M.; Wu, G.; Wang, M.; Chen, H.-Z., *J. Mater. Chem.* **2008,** 18, 4318-4323.

245. Jeon, J.-H.; Keum, J.-H.; Song, J. H.; Kim, J. S., *Sol. Energy Mater. Sol. Cells* **2007,** 91, 645-651.

246. Steinhart, M.; Murano, S.; Schaper, A. K.; Ogawa, T.; Tsuji, M.; Gösele, U.; Weder, C.; Wendorff, J. H., *Adv. Funct. Mater.* **2005,** 15, 1656-1664.

247. Pisula, W.; Zeljko, T.; El Hamaoui, B.; Watson, M. D.; Pakula, T.; Müllen, K., *Adv. Funct. Mater.* **2005,** 15, 893-904.

248. Wu, J.; Pisula, W.; Müllen, K., *Chem. Rev.* **2007,** 107, 718-747.

249. Pisula, W.; Kastler, M.; Wasserfallen, D.; Davies, R. J.; Garcia-Gutierrez, M.-C.; Müllen, K., *J. Am. Chem. Soc.* **2006,** 128, 14424-14425.

250. Zhi, L.; Wu, J.; Li, J.; Kolb, U.; Müllen, K., *Angew. Chem. Int. Ed.* **2005,** 44, 2120-2123.

251. Zhi, L.; Gorelik, T.; Wu, J.; Kolb, U.; Müllen, K., *J. Am. Chem. Soc.* **2005,** 127, 12792-12793.

252. Jian, K. Q.; Shim, H.-S.; Schwartzman, A.; Crawford, G. P.; Hurt, R. H., *Adv. Mater.* **2003,** 15, 164-167.

253. Nancy, Y. C. Y.; Kengqing, J.; Indrek, K.; Gregory, P. C.; Robert, H. H., *J. Nanosci. Nanotech.* **2003,** 3, 386-391.

254. Mezzenga, R.; Ruokolainen, J.; Fredrickson, G. H.; Kramer, E. J.; Moses, D.; Heeger, A. J.; Ikkala, O., *Science* **2003,** 299, 1872-1874.

255. Cassagneau, T.; Caruso, F., *Adv. Mater.* **2002,** 14, 34-38.

256. Wang, D.; Caruso, F., *Adv. Mater.* **2001,** 13, 350-354.

257. Braun, P. V.; Wiltzius, P., *Curr. Op. Coll. Int. Sci.* **2002,** 7,116-123.

258. Yoshino, K.; Tatsuhara, S.; Kawagishi, Y.; Ozaki, M.; Zakhidov, A. A.; Vardeny, Z. V., *Appl. Phys. Lett.* **1999,** 74, 2590-2592.

259. Stalmach, U.; de Boer, B.; Videlot, C.; van Hutten, P. F.; Hadziioannou, G., *J. Am. Chem. Soc.* **2000,** 122, 5464-5472.

260. Behl, M.; Hattemer, E.; Brehmer, M.; Zentel, R., *Macromol. Chem. Phys.* **2002,** 203, 503-510.

261. Lindner, S. M.; Thelakkat, M., *Macromolecules* **2004,** 37, 8832-8835.

262. Sommer, M.; Lindner, S. M.; Thelakkat, M., *Adv. Funct. Mater.* **2007,** 17, 1493-1500.

263. Sommer, M.; Hüttner, S.; Wunder, S.; Thelakkat, M., *Adv. Mater.* **2008,** 20, 2523-2527.

264. Lindner, S. M.; Hüttner, S.; Chiche, A.; Thelakkat, M.; Krausch, G., *Angew. Chem. Int. Ed.* **2006,** 45, 3364-3368.

265. Sommer, M.; Lang, Andreas S.; Mukundan Thelakkat, *Angew. Chem. Int. Ed.* **2008,** 47, 7901-7904.

2 Scope and Objectives

The general aim of this thesis is to utilize nanoporous anodic aluminum oxide (AAO) membranes for the versatile and application-oriented fabrication of functional organic one-dimensional nanoobjects and their respective well-ordered arrays.

The main focus should be drawn on the development of a novel routine concept for the AAO template-based fabrication of well-ordered all-organic bulk heterojunctions. As shown in the introduction such well-ordered bulk heterojunctions, which basically consist of a nanometer-scale interpenetrating network of a donor and an acceptor phase, with an interfacial distance smaller than the exciton diffusion length would be highly advantageous for the application in organic photovoltaic devices.

These desirable interpenetrating donor/acceptor networks should be prepared by an AAO template-assisted fabrication of organic hole-conducting nanorod arrays and their subsequent embedding into an electron-conducting polymeric matrix *via* spin-coating.
For the successful feasibility of the described concept the hole-conducting nanorods arrays on a conductive substrate and their solution-based embedding into an electron-conducting matrix have to fulfill several requirements: (1) The aspect ratios of the rods and the process for the release from the template have to be optimized in a way to obtain free-standing nanorod arrays without any aggregation and collapsing. (2) In order to withstand the subsequent spin-coating process of the electron-conducting polymer, the nanorods have to exhibit a good solvent resistance. Consequently employing organic hole-conducting materials that can be cross-linked after the patterning step would be highly favorable. (3) The hole-conducting properties should be maintained during the templating process and the nanorod arrays should exhibit a sufficient mechanical and electrical contact to the conductive substrate. (4) The subsequent embedding procedure with an adequate electron-conducting polymer should be optimized in a way that the physical integrity of the rods is remained, that the space between the rods is completely filled and that the thickness of the homogeneous over standing layer is minimized. The morphology and the electrical properties of the nanorod arrays and the interpenetrating donor/acceptor networks should be investigated. To confirm the concept the photo physical properties and the characteristics of the resulting photovoltaic devices should be tested.

Furthermore, a novel route for the fabrication of functional nanowires *via* post-modification of reactive nanowires should be investigated. This route would facilitate the modification of the nanowires after the completed templating process and is therefore advantageous for the fabrication of polymeric nanowires with sensitive functional groups that may decompose during the templating process. Further, by starting from one batch of reactive nanorods, nanoobjects with identical aspect ratios and morphologies and various different functionalities would be directly accessible without optimizing the wetting parameters for each and every polymer.

For the successful feasibility of this route the reactive polymers and the experimental conditions for the templating process should be well chosen in order to completely remain the reactivity after the templating step. To reveal the variable applicability of the post-modification route, the post-modification into various functional nanowires should be presented. Further measurements that confirm quantitative conversion of the reactive moieties should be performed.

3 Results and Discussion

In the following the concept and the versatile applicability of the template-assisted fabrication of functional polymeric one-dimensional nanoobjects, like wires and rods, and the corresponding well-ordered arrays are presented.

Within this thesis the template-assisted approach was utilized as a patterning technique for several different objectives. The research work that will be presented can be categorized into four different projects and is schematically represented in Scheme 1.

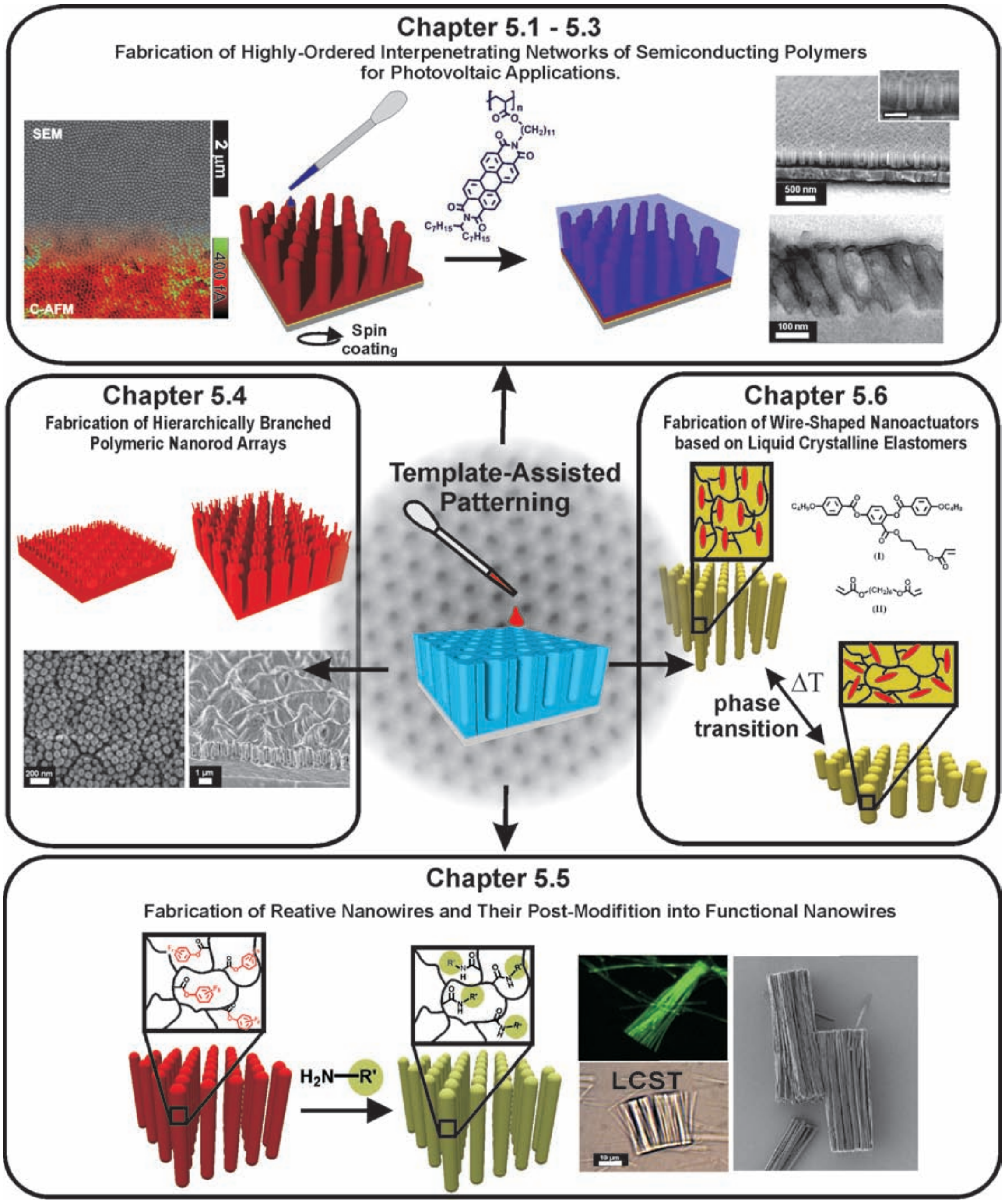

Scheme 1. *Schematic representation of the template-assisted patterning of various organic and polymeric materials for different objectives.*

Anodic aluminum oxide (AAO) membranes, which provide well-aligned mesoscopic pores and superb thermal and solvent resistance were used as hard templates throughout the present thesis. The two-step anodization process that is used for the fabrication of the template features the precise control of the pore dimensions, like length (few nanometer up to 100 µm), diameter (10-300 nm) and interpore distance (60-500 nm). Therefore the pore dimensions can be easily tuned to meet the requirements for the templating process.

The wetting of the templates with various functional precursor materials, followed by a thermal- or UV-initiated cross-linking and the subsequent selective removal of the inorganic template yield rod-like or wire-like replicas that are composed of functional polymers and whose dimensions match to those of the template pores.

In the following the individual projects that are represented in Scheme 1 are briefly introduced. The detailed procedures and extensive discussions are presented in the corresponding publications (see chapter 5).

3.1 Fabrication of Highly Ordered Interpenetrating Networks of Semiconducting Polymers for Photovoltaic Application

The template-assisted approach features the fabrication of well-ordered arrays of freestanding nanorods by attaching the semiconducting polymeric replicas to a substrate. These arrays attached to a conductive substrate are highly interesting in the field of organic optoelectronic. In chapter 5.1, 5.2 and 5.3 a novel template-based route for the fabrication of well-ordered bulk-heterojunction solar cells is presented. The general template-based concept, which is pursued for a routine solution-based fabrication of such well-ordered interpenetration networks composed of organic hole- and electron-conducting materials, as represented in Scheme 2, has been conducted for the very first time. As already mentioned in chapter 1 such donor/acceptor networks would be highly advantageous for an efficient charge separation and transport in organic photovoltaic devices.

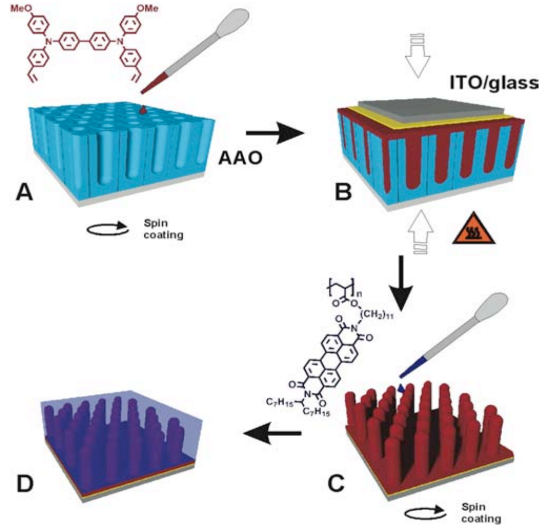

Scheme 2. *Schematic representation of the template-assisted fabrication of well-ordered bulk-heterojunction networks on transparent conductive ITO/glass substrates.*

Arrays of hole-conducting organic nanorods attached to a conductive indium tin oxide (ITO) coated glass substrate were prepared and used as a building block for the preparation of well-order interpenetrating networks. After selective removal of the AAO template, the nanorod arrays can be embedded into an electron-conductive polymer *via* spin-coating, which results in the formation of the desired well-ordered morphology.

Since it is essential for the presented concept that the fabricated nanorod arrays exhibit a good solvent resistance in order to remain their shape during the subsequent solvent-based infiltration into an electron-conducting matrix, thermally cross-linkable hole-conducting materials based on triphenylamine and tetraphenylbenzidine moieties are employed in the presented studies. An overview about the synthesis of the employed derivates is given in Scheme 3.

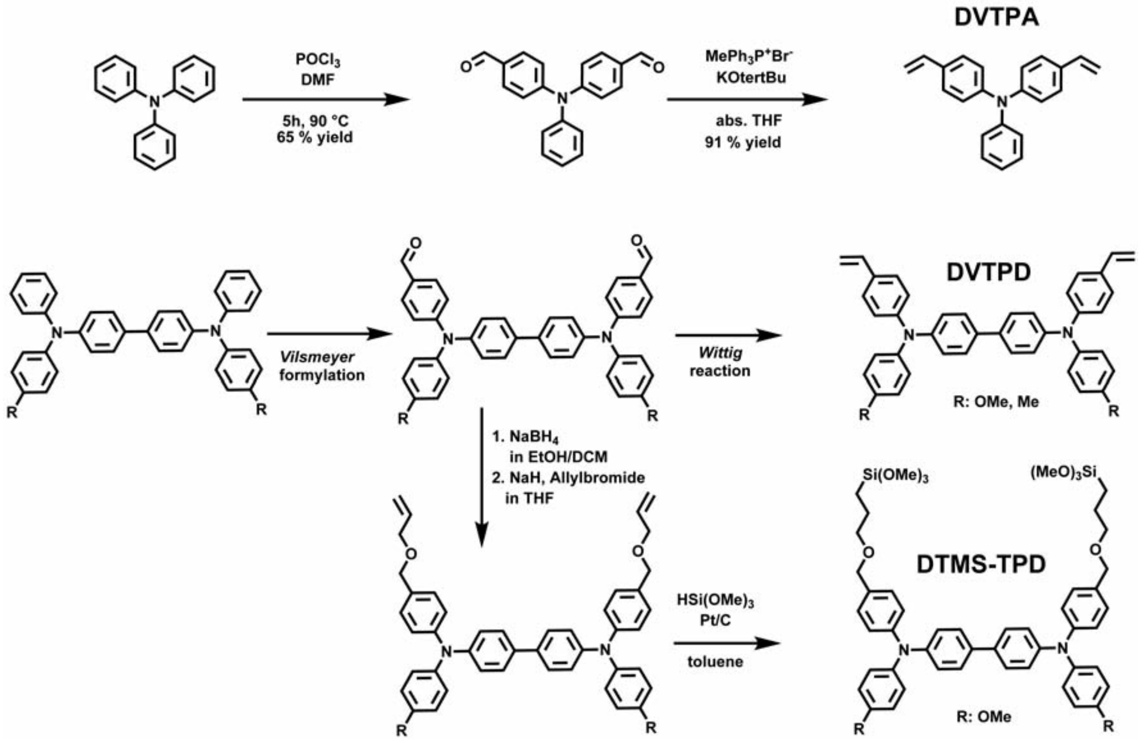

Scheme 3. *Synthetic route of cross-linkable hole-conducting triarylamine derivatives: 4,4'-divinyltriphenylamine (DVTPA), N,N'-bis(4-methoxyphenyl)-N,N'-bis(4-vinylphenyl- (1,1'-biphenyl)-4,4'-diamine) (DVTPD) and N,N'-bis(4-methoxyphenyl)-N,N'-bis(4-((3-(trimethoxysilyl) propoxy) methyl)-phenyl)- (1,1'-biphenyl)-4,4'-diamine (DTMS-TPD).*

In chapter 5.1 the route for the fabrication of free-standing hole-conducting nanorod arrays on ITO/glass substrates is introduced. AAO templates with pore-diameters of about 40 nm and lengths of several hundreds of nanometers were utilized for the patterning process. Noteworthy, in order to precisely adjust the pore length of the templates in the range below 1 µm the time-current transients were recorded during the anodic fabrication and the length was correlated with the total charge, that was applied during the fabrication step. Nanorods arrays attached to ITO/glass were successfully obtained after the transfer

of DVTPA-filled AAO templates onto a prefunctionalized ITO/glass, thermal annealing and subsequent removal of the template.
Further, chapter 5.1 focuses on the optimization of the rod's aspect ratio and on the use of a freeze-drying technique in order to prevent collapsing and aggregation of the arrays after removal of the mechanically stabilizing AAO template.

In order to optimize the adhesion of the patterned hole-conducting polymer film to the ITO/glass substrate and to avoid the prefunctionalization step of the substrate, that was essential for a covalent binding with the DVTPA film, the synthesis and characterization of a novel cross-linkable siloxane-derivatized tetraphenylbenzidine (DTMS-TPD) is reported in chapter 5.2. The trimethoxysilane moieties of DTMS-TPD feature a sufficient thermal cross-linking but also a simultaneous covalent binding to hydroxylated ITO/glass. Consequently, partial delamination of cross-linked DTMS-TPD films could be minimized and macroscopic arrays of perfectly free-standing nanorod arrays were obtained after freeze-drying. Besides the cyclovoltammetric measurements of thin DTMS-TPD films, the electrical properties of single nanorods were investigated with conductive scanning torsion mode microscopy (SCTMM). It revealed a good and homogeneous electrical connection of the DTMS-TPD nanostructures to the substrate. Detailed information about the SCTMM measurements and the electrical properties the DTMS-TPD nanorods were recently reported in another joint publication.[†]

The focus in chapter 5.3 is drawn on the fabrication and the morphological and photochemical characterization of the well-ordered interpenetrating donor/acceptor networks that are formed after embedding free-standing nanorod arrays into a electron-conducting poly(perylene bisimide acrylate) (PPerAcry) matrix by spin-coating. PPerAcry was chosen as an electron-conducting material since its energy levels match well to those of the employed triarylamines and it can be well processed via spin-coating. The embedding procedure was optimized in a way that (i) the physical integrity of the rods was remained, (ii) the space between the rods was completely filled and (iii) the thickness of the homogeneous overstanding PPerAcry layer was minimized. Transmission electron microscopy (TEM) investigation of the obtained morphologies confirmed the successful and complete embedding without causing aggregation and collapsing of the rods. Photoluminescence measurements revealed a more than threefold improvement in photoluminescence quenching relative to the planar bilayer architecture. The fundamental working principle of the templating approach for the fabrication of a solution-based all-polymer solar cell has also successfully been demonstrated for the first time.

[†]: S. A. L. Weber, N. Haberkorn, P. Theato, R. Berger, *Nano Lett.* **2010**, *10*, 1194.

3.2 Fabrication of hierarchically branched polymeric nanorod arrays

Besides the commonly used AAO templates, which provide cylindrically-shaped pores with a uniform size distribution, AAO templates with hierarchically branched pores are accessible. In chapter 5.4 these hierarchically branched templates were utilized for the fabrication of hierarchically branched polymeric nanorod arrays. To this end, AAO templates with hierarchical branched nanopores were fabricated by an asymmetric two-step anodization process, which facilitates the independent length variation of each hierarchical substructure. The polymeric replicas that were obtained after solution-based infiltration, thermal cross-linking and selective removal of the template were characterized *via* Scanning Electron Microscopy. They show remarkable similarities to various interesting biostructures such as the leaf surface of Lotus or the feet of a gecko and may find application in the fabrication of superhydrophobic surfaces or dry adhesives.

3.3 Fabrication of Reactive Nanowires and Their Post-Modification into Functional Nanowires

In chapter 5.5 a novel and versatile route for the preparation of polymeric functional nanowires *via* post-modification of reactive nanowires is demonstrated. Reactive nanowires with defined and tunable dimensions were fabricated by utilizing AAO templates. The reactive nanowires were based on pentafluorophenyl esters, which feature the quantitative post-modification with amines under mild reaction conditions yielding the corresponding functionalized amide. The post-modification with fluorescent dyes such as piperazinyl-4-chloro-7-nitrobenzofurane (Pip-NBD) and sulforhodamine 101 cadervarine (S101C) was demonstrated. Confocal laser scanning microscopy (CLSM) images of the corresponding wires revealed the successful modification. Further the conversion of nanowires composed of cross-linked pentafluorophenyl acrylates into wire-shaped poly(*N*-isopropylacrylamide) (PNIPAM) hydrogels, which exhibits a thermal-responsive phase transition, is demonstrated for the first time.

3.4 Fabrication of wire-shaped nanoactuators based on liquid crystalline elastomers

In chapter 5.6 the results of a project that was conducted in collaboration with Christian Ohm is presented. The objective of this project was to use the pores of AAO templates not only as shape-defining molds for liquid crystalline elastomers but also to utilized the confined geometry and the large surface interface of the pores to uniformly align the mesogens during the preparation step of the liquid crystalline elastomeric wires. To this end AAO templates with pore diameters of about 200 nm and variable length were filled with a mixture of a calamitic three-core mesogen (chemical structure is shown in Scheme 1), a cross-linking agent and a photoinitiator. By UV-irradiation the liquid crystalline material was polymerized and cross-linked within the supercooled nematic phase inside of the pores. After the selective removal of the AAO template nanowires with a uniform size-distribution were obtained. Polarized optical microscopy revealed the uniform alignment of the mesogenic moieties in the material parallel to the nanowires long axis. Due to this permanent internal orientation the thermal-induced phase transition between the liquid crystalline and the isotropic phase features a macroscopic change of the sample's dimensions. It was found that during the transition from the nematic to the isotropic phase the rod's length shortened by roughly 40 percent. The ability to reversibly change their shape on a micrometer-level *via* applying an external stimulus, combined with their uniformity in size, makes these liquid crystalline elastomeric wires very appealing for applications in interdisciplinary science.

4 Summary

In this thesis, anodic aluminum oxide (AAO) membranes, which provide well-aligned uniform mesoscopic pores with precisely adjustable pore parameters, were fabricated process and successfully utilized as templates for the fabrication of functional organic nanowires, nanorods and the respective well-ordered arrays. Rod-like or wire-like replicas, which are composed of functional cross-linked polymers and whose dimensions matches to that of the template pores were feasible by wetting of the templates with various functional precursor materials, followed by a thermal- or UV-initiated cross-linking and a subsequent selective removal of the inorganic template. The template-assisted patterning technique was successfully applied for the realization of different objectives:

High-density and well-ordered arrays of hole-conducting nanorods composed of cross-linked triphenylamine (TPA) and tetraphenylbenzidine (TPD) derivatives on conductive substrates like ITO/glass have been successfully fabricated. By applying a freeze-drying technique to remove the aqueous medium after the wet-chemical etching of the template, aggregation and collapsing of the rods was prevented and macroscopic areas of perfectly free standing nanorods with aspect ratios above 3 and a lengths of up to 250 nm were feasible. Exemplary the electrical properties of nanorod arrays composed of a siloxane-derivatized TPD derivative were investigated with conductive scanning torsion mode microscopy (SCTMM). The measurements revealed a good electrical contact of the rods to the conductive substrate.

Based on the hole-conducting nanorod arrays and their subsequent embedding into an electron-conducting polymer matrix *via* spin-coating, a novel routine concept for the fabrication of well-ordered all-organic bulk heterojunction for organic photovoltaic applications was successfully demonstrated. To this end, free-standing nanorod arrays composed of an cross-linked tetraphenylbenzidine derivate with an aspect ratio of 3.8 were successfully embedded into electron-conducting poly(perylene bisimide acrylate) matrix without causing aggregation of the rods. The increased donor/acceptor interface of the fabricated devices resulted in a remarkable increase of the photoluminescence quenching compared to a planar bilayer morphology. Further, the fundamental working principle of the templating approach for the solution-based all-organic photovoltaic device was demonstrated for the first time.

Furthermore, in order to broaden the applicability of patterned surfaces, which are feasible *via* the template-based patterning of functional materials, AAO with hierarchically branched pores were fabricated and utilized as templates. By pursuing the common templating process hierarchically polymeric replicas, which show remarkable similarities with interesting biostructures, like the surface of the lotus leaf and the feet of a gecko, were successfully prepared.

In contrast to the direct infiltration of organic functional materials, a novel route for the fabrication of functional nanowires *via* post-modification of reactive nanowires was established. Therefore, reactive nanowires based on cross-linked pentafluorophenylesters were fabricated by utilizing AAO templates. The post-modification with fluorescent dyes such as piperazinyl-4-chloro-7-nitrobenzofurane (Pip-NBD) and sulforhodamine 101 cadervarine (S101C) was demonstrated and the successful modification was revealed by confocal laser scanning micrography (CLSM). Furthermore, reactive wires were converted into well-dispersed poly(*N*-isopropylacrylamide) (PNIPAM) hydrogels, which exhibit a thermal-responsive reversible phase transition. The reversible thermal-responsible swelling of the PNIPAM nanowires exhibited a more than 50 % extended length than in the collapsed PNIPAM state.

Last but not least, the shape-anisotropic pores of AAO were utilized to uniformly align the mesogens of a nematic liquid crystalline elastomer. Liquid crystalline nanowires with uniformly aligned mesogens and a narrow size distribution were fabricated. It was shown that during the transition from the nematic to the isotropic phase the rod's length shortened by roughly 40 percent. As such these liquid crystalline elastomeric nanowires may find application as wire-shaped nanoactuators in various fields of research, like lab-on-chip systems, micro fluidics and biomimetics.

5 Publications

In the following the publications that contribute to this thesis are given:

5.1 "*Template-Assisted Fabrication of Free-Standing Nanorod Arrays of a Hole-Conducting Cross Linked Triphenylamine Derivative: Toward Ordered Bulk-Heterojunction Solar Cells.",*
Niko Haberkorn, Jochen S. Gutmann, Patrick Theato, *ACS Nano* **2009**, *3*, 1415.

5.2 *"Template-Based Preparation of Free-Standing Semiconducting Polymeric Nanorod Arrays on Conductive Substrates",*
Niko Haberkorn, Stefan A. L. Weber, Rüdiger Berger, Patrick Theato, *ACS Appl. Mater. Interfaces*, **2010,** 2, 1573-1580.

5.3 *"Template-Assisted Fabrication of Highly-Ordered Interpenetration Networks of Semi-Conducting Polymers for Photovoltaic Applications",*
Niko Haberkorn, Sehee Kim, Ki-Se Kim, Michael Sommer, Mukudun Thelakkat, Byeong-Hyeok Sohn, Patrick Theato, submitted.

5.4 "Fabrication of Hierarchically Branched Polymeric Nanorod Arrays by Utilizing Branched Alumina Templates"
Niko Haberkorn, Patrick Theato, in preparation.

5.5 *"Reactive Nanowires Based on Activated Ester Polymers: A Versatile Template-Assisted Approach for the Fabrication of Functional Nanowires "*
Niko Haberkorn, Katja Nilles, Philipp Schattling, Patrick Theato, submitted.

5.6 *"Template-Based Fabrication of Nanometer-Scaled Actuators from Liquid Crystalline Elastomers"*
Christian Ohm‡, Niko Haberkorn‡, Patrick Theato, Rudolf Zentel, in preparation.
‡: C.O. and N.H. have contributed equally.

5.1 Template-Assisted Fabrication of Free-Standing Nanorod Arrays of a Hole-Conducting Cross-linked Triphenylamine Derivative: Towards Ordered Bulk-Heterojunction Solar Cells

*Niko Haberkorn[1], Jochen S. Gutmann[2,3] and Patrick Theato[1]**

[1] Institute of Organic Chemistry, University of Mainz, Duesbergweg 10-14, 55099 Mainz, Germany
[2] Institute of Physical Chemistry, University of Mainz, Welderweg 11, 55099, Mainz, Germany
[3] Max-Planck-Institut für Polymerforschung, Ackermannweg 10, 55128 Mainz, German

Reproduced with permission from ACS Nano, **2009**, *3*, 1415-1422, *Copyright 2009 American Chemical Society.*

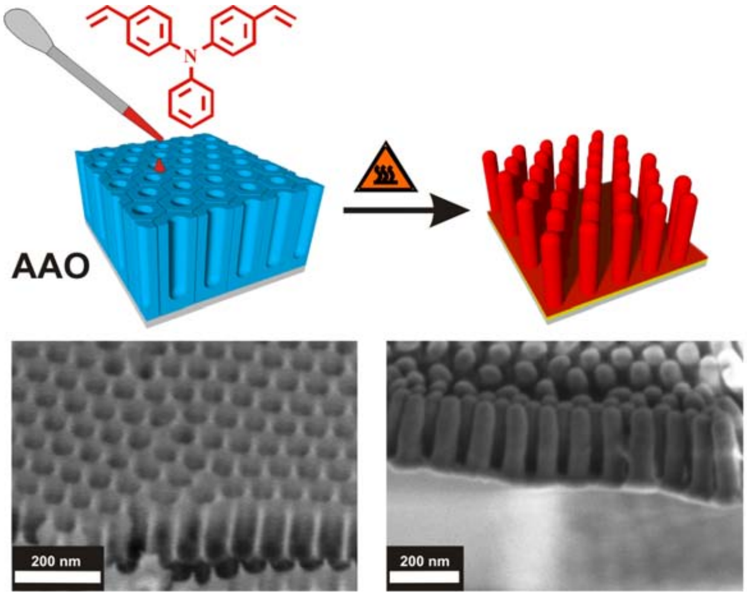

Summary

Template-Assisted Fabrication of Free-Standing Nanorod Arrays of a Hole-Conducting Cross-Linked Triphenylamine Derivative: Towards Ordered Bulk-Heterojunction Solar Cells.Arrays of free-standing nanorod arrays attached to an ITO/glass substrate were fabricated via an anodic aluminum oxide (AAO) template-assisted approach. Aggregation of the nanorod arrays after removal of the template was prevented by applying a freeze drying technique. Due to the large surface area and the electrochemical properties these highly-ordered polymeric replicas have potential application in the field of organic photovoltaics.

Keywords

triarylamine; semiconductive polymer(s); template-assisted patterning; anodic aluminum oxide; nanorod(s); organic photovoltaic.

Abstract

Free-standing nanorod arrays of a thermally cross-linked semi-conducting triphenylamine were fabricated on conductive ITO/glass substrates via an anodic aluminum oxide (AAO) template-assisted approach. By using a solution wetting method combined with a subsequent thermal imprinting step to fill the nanoporous structure of the template with a cross-linkable triphenylamine derivative, a polymeric replication of the AAO was obtained after thermal curing and selective removal of the template. To obtain well-aligned and free-standing nanorod arrays aggregation and collapse of the nanorods was prevented by optimizing their aspect ratio and applying a freeze-drying technique to remove the aqueous medium after the etching step. Due to their electrochemical properties and their resistance against organic solvents after curing, these high-density nanorod arrays have potential application in organic photovoltaics.

Introduction

Arrays of nanometer-scale structures such as nanorods, nanowires and nanotubes have attracted increasing attention, mainly due to the potential application in many fields of research like data storage [1-3],artificial actuators [4,5], surfaces exhibiting special wetting probabilities[6-8], sensing[9] and optoelectronics.[10-12] For example, one crucial and still very challenging part of the fabrication of high-efficient organic solar cells is to produce a nanometer-scale inter-penetrating network of a donor and an acceptor phase, with an interfacial distance smaller than the exciton diffusion length (~10-20 nm) in the organic material.[13] An ideal morphology that has been proposed for these cells consists of an array of vertically aligned hole-conducting polymeric nanorods attached to an electrode and surrounded by an electron-conducting material connected to a cathode or *vice versa*.[14, 15]

Polymeric nanorods and nanowires can be fabricated by sub-micro lithography[16], electro-spinning[17], mechanical drawing[18] and template-based methods.[19] For the production of highly-ordered nanorod arrays the template-based approach seems to be the most suitable. Track-etched polymer membranes or block-copolymer thin films as well as anodic aluminum oxide (AAO) membranes are widely used as templates to prepare nanowires. The former usually are made by bombarding a polycarbonate sheet with nuclear fission fragments to create damage tracks and then chemically etch these track into pores.[20] The membranes were used to fabricate arrays of conducting polymer rods but their pores are only randomly distributed and their areal density of ~10^9 pores/cm^2 is relatively low compared to other template-based methods.[21, 22]

By using thin films of diblock copolymers with cylindrically aligned micro domains, porous templates with areal densities in excess of 10^{11} pores/cm^2 can be obtained after selective removal of the minor component of the block copolymer.[23-27] For example, *Russell* and coworkers recently showed the fabrication of nanorods of electropolymerized polypyrrole by using diblock copolymers templates of polystyrene-*block*-poly(methylmethacrylate).[28]

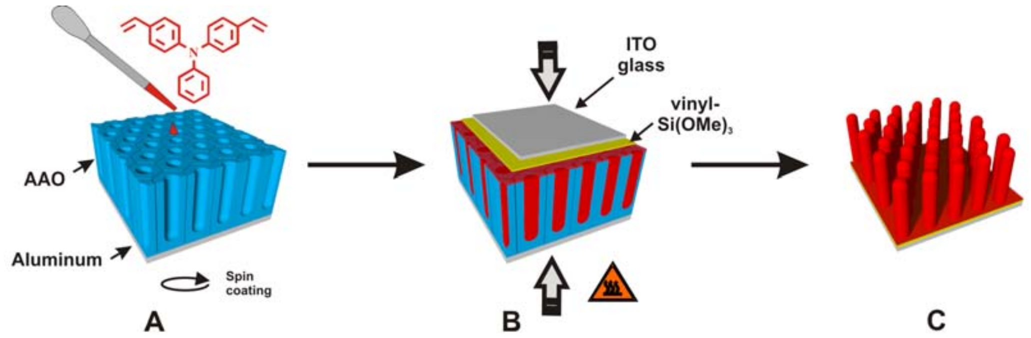

Scheme 1. *Schematic diagram of the template-assisted fabrication of cross-linked free-standing nanorod arrays.*

AAO membranes provide lateral pore densities comparable to that of block copolymer templates but they also allow a greater range of pore sizes (pore diameter and pore length) and offer a higher thermal and mechanical stability. They can easily be fabricated by a controlled anodization process and have been well characterized in the last decades.[7, 29-32] Polymeric nanorods and nanotubes have been fabricated by either wetting of the porous alumina template with (i) a polymer solution or (ii) a melt or by direct polymerization of a monomer inside of the template.[33] For example, the latter case has been used to prepare nanowires and nanotubes of polypyrrole, poly (3-methylthiophene) and poly(3,4-ethylenedioxythiophene) (PEDOT) by electropolymerization.[34-36]

One very challenging step for the template-based fabrication of arrays of free-standing nanorods is the retention of the integrity of the polymeric structure after the selective removal of the template. The nanorods tend to collapse and lose their well-aligned orientation during the wet-chemical etching of the template in acidic or alkaline solutions. These collapsing and aggregation is mainly caused by capillary forces between the rods upon drying. Approaches to overcome aggregation mainly avoid the occurrence of liquid/solid interfaces during the removal of the template, for example by supercritical drying or non wet-chemical mechanical release from the template.[37-39]

In this work, we describe the fabrication of arrays of high density free-standing nanorods composed of a cross-linked triphenylamine derivative on ITO/glass substrate by using AAO templates. Due to the limited usability of aggregated arrays in photovoltaic devices, one of the key issues is to overcome aggregation and collapsing of the semi-conducting nanorods after removal of the template Therefore, the aspect ratio of the rods was varied by using AAO templates, whose pore length and diameter can be precisely controlled during their fabrication. We also demonstrate that the tendency of forming aggregates of nanorods can be significantly decreased by applying a freeze drying step after wet-chemical etching of the porous alumina.

Results and Discussion

The template-assisted fabrication of arrays of hole-conducting nanorods seems to be an appropriate approach for building up polymer/polymer solar cells with a well-defined photoactive layer consisting of nanorods embedded into an electron-conducting matrix. For the application in such photovoltaic devices the arrays of nanorods have to fulfill a number of requirements. First, the dimension of the rods needs to be adapted to the needs in organic photovoltaics. Due to the relatively low exciton diffusion length in polymeric materials, the diameter and the space between the rods needs to be in the order of several nanometers to provide a large donor/acceptor interface, which is within the accessible exciton diffusion range.

Furthermore the nanorods need to be contacted to a conducting electrode and have to be aligned perpendicular to the substrate. To provide the maximal interfacial area and to permit a subsequent complete filling of the space between the rods with an electron-conducting material, it is crucial that the nanorods are free-standing and do not show any sign of aggregation and collapses. In addition, a high chemical resistance of the nanorod array against organic solvents is required for a subsequent spin-coating of the second polymer layer. We present a template-assisted approach, which allows the fabrication of large-area and high density arrays of nanorods fulfilling the criteria mentioned above. Scheme 1 illustrates the stepwise production of these arrays.

For the template-assisted patterning of the semi-conducting triphenylamine derivative DVTPA, the use of AAO templates seemed to be promising since the parameters of their pores, such as diameter, pore-inter-distance and length, can independently be varied during the fabrication process. As a consequence, this offers the possibility to exactly tune the structural properties of the nanorods replicating the structure of the AAO.

The templates were fabricated by a well established two step anodization process in oxalic acid yielding templates with an interpore distance of ~100 nm and pore diameters down to 40 nm. Pore lengths of only several hundreds of nanometers are desired for potential application in photovoltaics. These thin templates were fabricated by performing a short second anodization step for less than 10 min. The obtained thickness of AAO membranes usually correlates linearly with the anodization time when micrometer thick membranes are produced.[40] However, we observed that for thin templates a correlation between the pore length and the total charge used for the anodization seems to be a more suitable correlation parameter rather than the anodization time because of the typical variation of current density at the beginning of the pore formation. Furthermore, determination of the thickness by measuring the total charge instead of the time minimized the influences from experimental variations like temperature fluctuations.

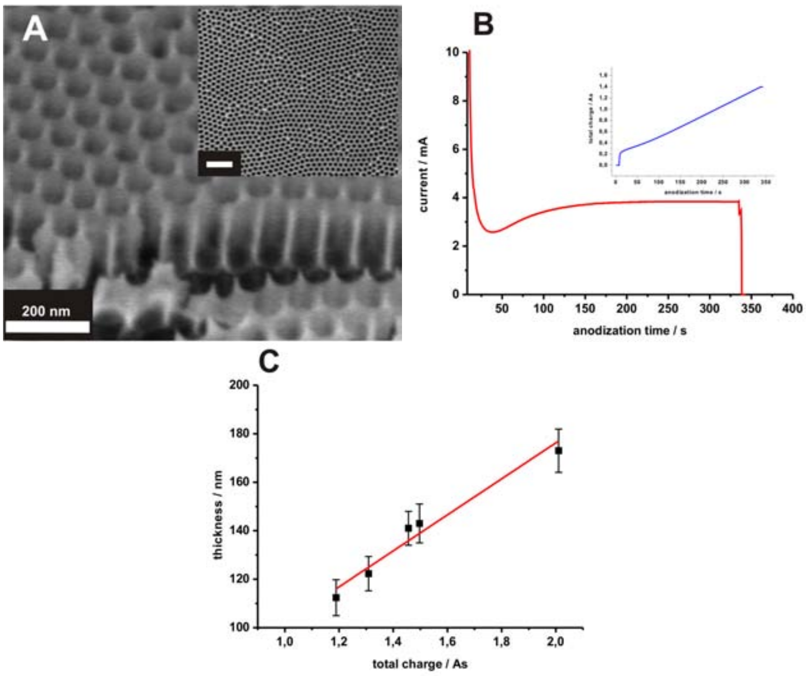

Figure 1. *(A) Cross-sectional scanning electron microscopy (SEM) micrographs of a AAO template fabricated in 0.3 M oxalic acid of 2 °C at 40 V for 5.5 min. Pore widening was carried out in 5 wt % phosphoric acid at 30 °C for 35 min (Inlet: top view of the AAO; scale bar: 500 nm), (B) Corresponding current–time transient during the second anodization step of the aluminum substrate (Inlet: Charge used for the anodization as a function of time), (C) Film thickness as a function of total charge used during the anodization step in 0.3 M oxalic acid of 2 °C at 40 V.*

Fig. 1A shows a cross-sectional and a top view SEM micrograph of one of the AAO template anodized for 5.5 min at 40 V, demonstrating the determination of the pore lengths. Noteworthy, even after very short anodization times the pores are well-ordered and have a narrow size distribution. The total charge was determined by integration of the corresponding time/current transient, which is shown in Figure 1B exemplary for one of the anodization steps. A correlation curve (see figure 1C) can be created by plotting the pore length of several AAO templates that have been anodized for different periods of time, ranging from 3 to 6 min, versus the total charge. With this correlation plot, it was possible to fabricate templates with very well adjusted pore lengths without checking every template by cross-sectional SEM, which usually requires the destruction of at least a small part of the template. To obtain a complete filling of the fabricated AAO templates with the cross-linkable divinyltriphenylamine (DVTPA) and to attach this nanostructured material to an ITO/glass substrate, a solution wetting process combined with a subsequent thermal imprinting step was applied. In contrast to the wetting of hard templates with polymeric solutions, which usually results in the formation of hollow nanowires,[2] the wetting with solutions of small organic

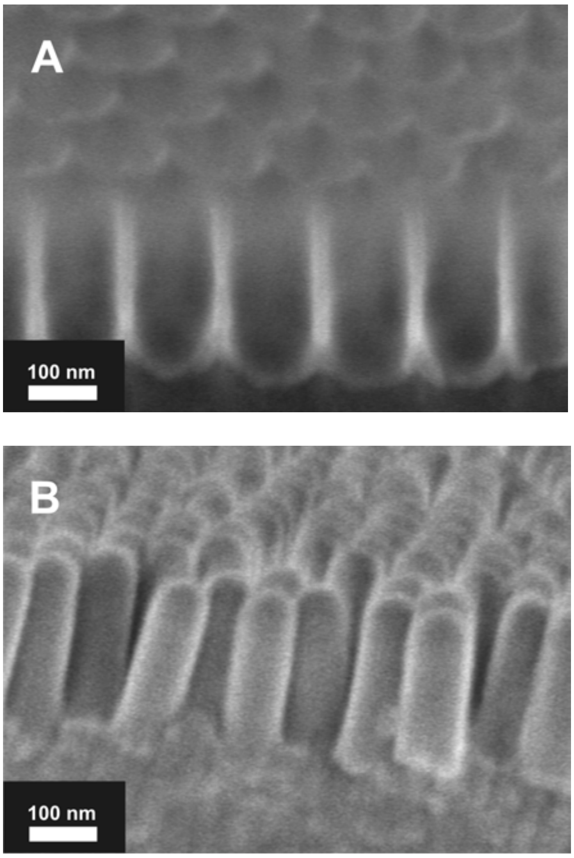

Figure 2. *SEM images,(A) Side view of an empty AAO template, Cross-sectional (B) of the corresponding cross-linked DVTPA replica after removal of the AAO by treatment with a 0.9 M KOH solution (30 min, room temperature).*

molecules, i.e. DVTPA monomer, leads to formation of mechanically more stable, completely filled rods. To minimize the thickness of the remaining DVTPA layer on top of the template after the solution wetting process, the solution was spin-coated on the AAO instead of drop casted. After drying, an ITO/glass substrate that has been pre-functionalized with vinyltrimethoxysilane was pressed on the top of the filled AAO template and clamped together. The sample was initially heated up *in vacuo* above the melting temperature of DVTPA (mp= 60°C) to remove any air inclusions between the DVTPA film and the ITO/glass as well to improve the complete filling of the nanopores. Subsequently, the samples were thermally annealed at 150 °C for 180 minutes. Prior experiments have shown that using ITO substrates without any pre-functionalization resulted in a relatively low adhesion of the ITO substrate to the cured DVTPA film, which made it difficult to selectively remove the AAO and its supporting aluminum layer without causing any delamination of the patterned DVTPA film from the ITO/glass.

The adhesion was dramatically increased by using ITO/glass that has been functionalized with vinyltrimethoxysilane as it provides a covalent attachment of the DVTPA film to the ITO via incorporating the vinyl group of the silane into the polymer network during thermal annealing procedure. Nevertheless, the layered construct was very fragile and delamination can occur during the removal of the template, in particular during wet chemical etching of the supporting aluminum because of the heat release during the exothermic reaction. Accordingly, the samples were ice-cooled during the chemical etching process and the concentration of the $CuCl_2$ solution, which was used to oxidatively etch the aluminum away, was lowered to 0.2 mol L^{-1} to slow down the exothermic reaction. As a result, pattered DVTPA films on ITO substrates could routinely be obtained.

Arrays of the polymeric nanorods (see Figure 2B) that match to the contours of the used AAO template (Figure 2A) can be obtained after subsequent removal of the AAO by treatment with KOH solution. To check if the fabricated nanorods were completely solid without any embedded gas bubbles or hollow canals, cross-sectional transmission electron microscopy (TEM) measurements were performed. The TEM images (see Figure 3) show a homogenous filling of the rods, which ensures that they have a maximal mechanical stability and their conductivity is not degraded by any voids inside the material.

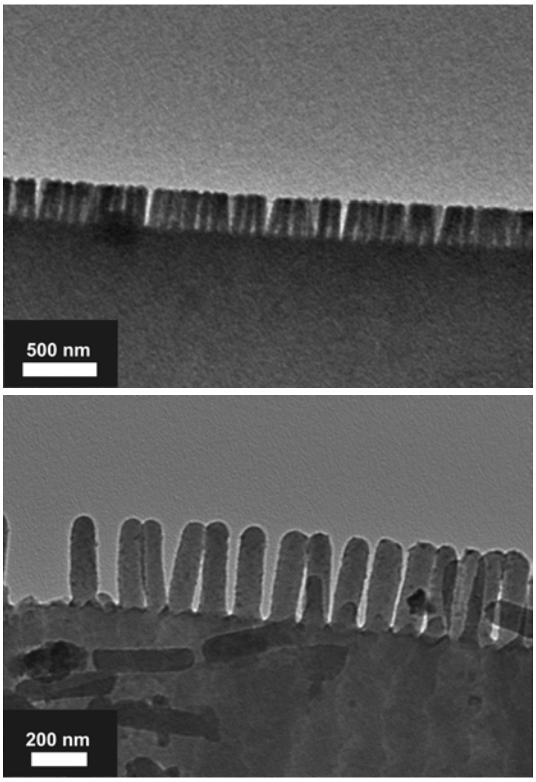

Figure 3. *TEM cross sections of a cross-linked DVTPA replica after removal of the template. The patterned DVTPA film was detached from the ITO glass by dipping into liquid nitrogen and the mechanical stability was increased by coating of an epoxy film on the backside. After curing the sample was ultra-microtomed into 60 nm thick sections at room temperature.*

For the fabrication of free-standing nanorod arrays it is very important to overcome the collapsing and aggregation of the replica after removal of the template. Due to their polymer nature, nanorods generally show a certain tendency to bend and thus arrays of nanorods easily aggregate into bundles, which are mainly caused due to capillary forces acting on the rods during evaporation of the solvent after the wet-chemical etching step.[41, 42] To investigate the degree of aggregation as a function of the aspect ratio of the nanorods, arrays of cured DVTPA nanorods with aspect ratios ranging from 3.1 to 6.3 and lengths of 240-375 nm with a constant distance of 100 nm between the rods were fabricated. After wet-chemical removal of the AAO with KOH solution, the samples were conventionally air dried. The top-view SEM micrographs of the samples are shown in the upper row of Figure 4. Even though highly cross-linked poly(DVTPA) provides an improved mechanical stability, it can be seen that the regular patterns of the rods were distorted and bundles of rods have formed after the drying step. In the case of nanorods with an aspect ratio of 5.2 and higher (see Figure 4A and C) bundles consisting of more than 20 rods in average have formed. By reducing the aspect ratio down to 3.1, the degree of aggregation was decreased to an average of 6 rods per bundle but still the physical integrity of the arrays was distorted due to the capillary forces during the drying process.
Besides the influence of the aspect ratio and the mechanical stability of the rods the degree of aggregation also depends on the properties of the liquid that is used during the drying process.

The capillary forces are proportional to the surface tension of the liquid and to the cosine of the contact angle at the liquid/rod interface. To minimize these forces either the contact angle must be

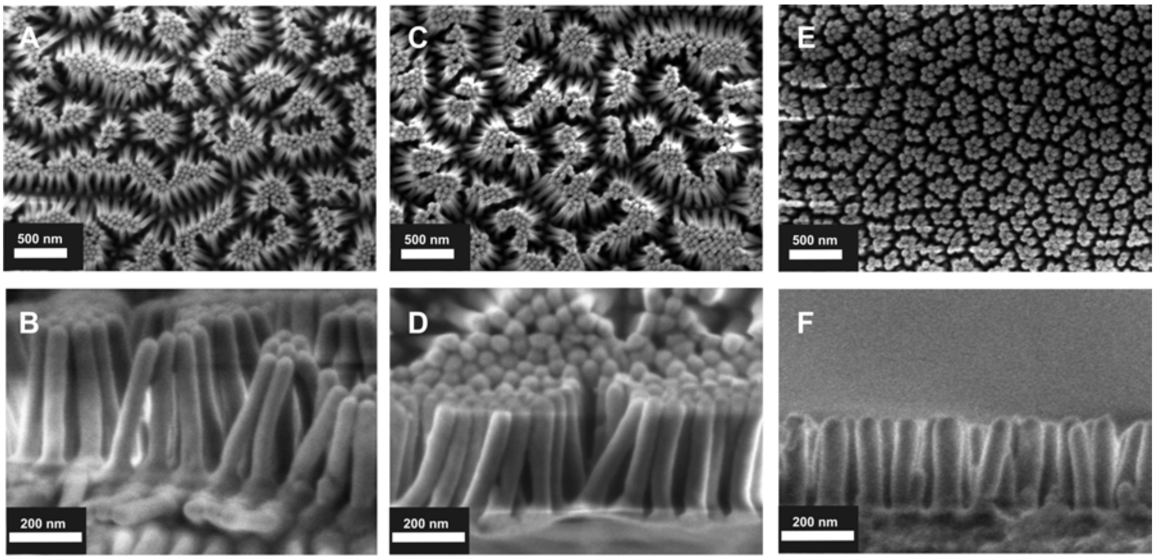

Figure 4. *SEM images showing top and cross-sectional view of thermally cured DVTPA nanorod arrays after removal of the AAO template by treatment with a 4.5 M KOH solution (30 min, room temperature) followed by a conventional drying step: (A) and (B): Nanorods with a length of 375 nm and a diameter of 60 nm (aspect ratio = 6.3, average inter-pore distance of the template 100 nm), (C) and (D) 310-nm long and 60-nm diameter nanorods (aspect ratio 5.2, average inter-pore distance of AAO:100 nm), (E) and (F) Nanopillars with an aspect ratio of 3.1 (length: 240 nm, diameter: 77 nm).*

brought close to 90° or the surface tension must be reduced. This can be achieved by either supercritical drying, which is an expensive process and demands special equipments, or by freeze drying, a technique that has already be proven to be very useful in the area of lithography to prevent collapses of the resists by nullifying the surface tension.[43]

It turned out that the freeze-drying technique is indeed an appropriate and cost-effective method to minimize the aggregation of the cured DVTPA nanorods during the drying step. To remove residual water that remained on the top of the polymeric replica after the removal of the AAO by wet-chemical means, the samples were cooled down to -60 °C and dried *in vacuo*. Arrays of nanorods with an aspect ratio of up to 4.0 and a total length of 200 nm showed only a small degree of aggregation after the freeze drying step (see Figure 5A). The majority of the rods were totally free-standing and non-aggregated. Applying the freeze drying step to samples with an aspect ratio of the rods of 3.1 and a length of 200 nm proved that it was possible to totally suppress the aggregation and to obtain large areas of non-aggregated, free-standing nanorod arrays (Figure 5C). Thus, the preparation of nano-patterned films, which provide a large internal surface necessary for photovoltaic devices, has been achieved.

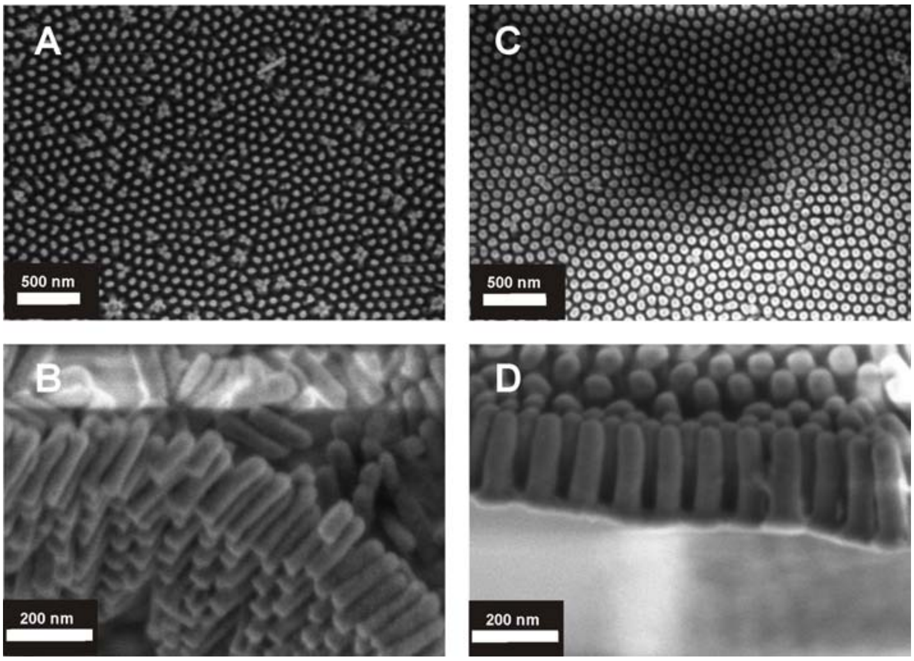

Figure 5. *SEM micrographs of free-standing cross-linked DVTPA nanorod arrays after removal of the AAO template followed by a lyophilization step. Top (A) and cross-sectional (B) view of nanopillars with an aspect ratio of 4.0 (length: 200 nm, diameter: 50 nm). (C) and (D) Ensemble of non-aggregated nanorods with an aspect ratio of 3.1 (length: 200nm, diameter: 65 nm).*

The thermally-cured poly(DVTPA) films also showed a sufficient resistance against organic solvents, which would allow a subsequent polymer solution coating step. The thermal properties of monomeric DVTPA were studied by differential scanning calorimetry (DSC) measurements (see supporting information, Fig S1). The DSC measurement showed a broad exothermic transition in the range between 120 and 160 °C, corresponding to the heat released during of the cross-linking process. After an isothermal heating of DVTPA at 150 °C for 1 h and slowly cooling to room temperature, which are the same thermal conditions used for the curing step of the patterned DVTPA films, the re-scan did not show any exothermic transition up to 180 °C, indicating that the cross-linking was completed during the first heating at 150 °C. Further, the films on ITO/glass, which were thermally cured at 150 °C for 1 h under inert atmosphere, were washed thoroughly with dichloromethane, which is excellent solvent for the non-cross-linked DVTPA, and the UV/vis spectra of the thin films before and after washing were investigated. After rinsing with dichloromethane, the absorption of the cured film slightly decreased (see Figure 6A). But even after dipping the film in dichloromethane for 10 min the absorption did not decrease further, which indicated that the cured films showed a sufficient resistance against organic solvents.

In the end, the HOMO and LUMO energy levels of poly(DVTPA) were determined using cyclic voltammetry measurements along with UV/vis absorption spectroscopy. The HOMO level was determined from the oxidation peak of the cyclic voltammetry curve.

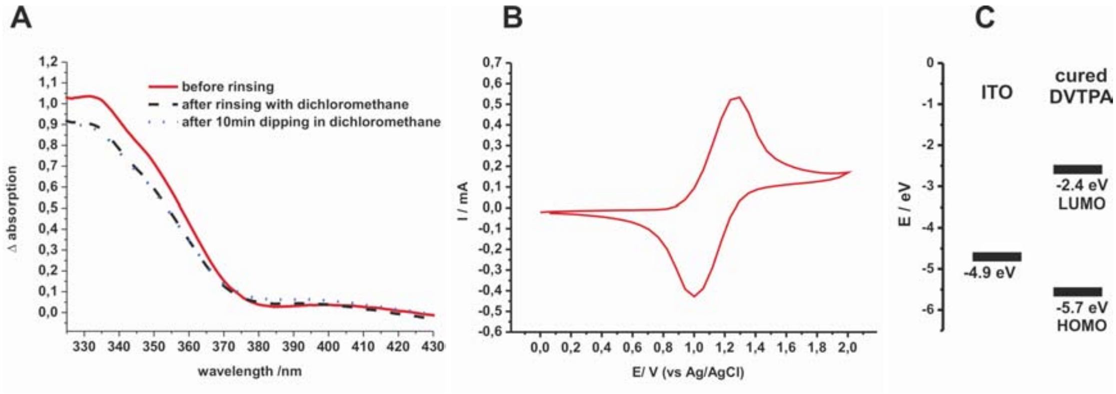

Figure 6. *(A) Difference UV/vis absorption spectra of a spin-coated DVTPA film (10 wt% in dichloromethane, 3000 min^{-1}) on ITO glass cured at 150 °C for 1 h, before rinsing (solid line), after rinsing for 3 times with dichloromethane (dashed line) and after dipping for 10 min in dichloromethane (dotted line) (B) Cyclic voltammogram of a cured (2 h at 150 °C) patterned DVTPA film on ITO glass in a solution of n-Bu_4NPF_6 in acetonitrile (0.1 mol L^{-1}) at a scan rate of 0.1 Vs^{-1}. (C) Energy level diagram for thermally crosslinked DVTPA (HOMO level was converted from the measured oxidation potentials assuming the absolute energy level of ferrocene to be -4.8 eV. LUMO level was estimated from the HOMO level and energy gap, which was calculated from the onset of the UV/vis absorption spectrum).*

Using *E*(Ferrocene/Ferrocene+) = -4.8 eV below the vacuum level, the HOMO level was determined to be -5.7 eV for poly(DVTPA).

The optical band gap value of 3.3 eV, obtained from the lower energy onset of the absorption spectra, was then used to calculate the LUMO level as -2.4 eV. Accordingly, the position of the energy levels and the totally reversible cyclic voltammetry of the arrays of the free-standing nanorods of poly(DVTPA) proved that the nano-patterned poly(DVTPA) films fulfill the required properties in order to be used as hole-conducting materials in an organic photovoltaic devices.

Experimental Section

Materials. ITO-coated glass substrates (with sheet resistance of <10 Ohm/sq obtained from Präzisions Glas & Optik GmbH) were cleaned by ultrasonication in detergent, isopropanol and acetone. They were then dried with a stream of pressurized N_2 and subjected to O_2 plasma cleaning for 10 min. For the silanization of ITO/glass substrates the O2-plasma treated substrates were dipped into a 1 wt% solution of vinyltrimethoxysilane in tetrahydrofurane for 48 h at 40 °C.

Synthesis. Divinyltriphenylamine (DVTPA) was synthesized via a *Vilsmeyer* and a subsequent *Wittig* reaction starting from triphenylamine by modification of the procedure described in the literature.[44] The detailed synthetic procedure and characterization data are given in the supporting information.

Fabrication of AAO templates. AAO templates were fabricated by a two-step anodization process developed by Masuda and Fukuda.[29, 30] High purity aluminum

(99.997 %, 0.1 mm thick) purchased from Alfa Aesar was cleaned by sonification treatment in isopropanol and acetone respectively followed by an electropolishing step in a mixture of ethanol and perchloric acid (v/v 4:1) at a current density of 300-350 mA/cm^{-1} for 1 min at 0 °C. Subsequently the samples were rinsed with deionized water, isopropanol and acetone. The anodization steps were performed in a self-build apparatus, similar to those described in the literature. Briefly, the aluminum sheets were mounted on a copper plate serving as the anode. A radial area of 2.27 cm^2 was exposed to an aqueous acidic solution. A platinum wire was used as the cathode. The apparatus was surrounded by a cryostatic bath to control the temperature during anodization and the electrolyte solution was rigorously stirred during anodization. The anodization current as a function of time was measured using a multimeter and recorded with an attached computer.

Anodization was performed in an aqueous solution of oxalic acid (c = 0.3 mol/L) at 40.0 V and 2±1 °C. In the first step, aluminum was anodized for 6 h, followed by an etching step in aqueous solution of chromic acid (1.8 wt%) and phosphoric acid (6.0 wt%) at 60 °C for 12 h. The second anodization was performed for different time intervals ranging from 3 min to 10 min. Pore widening was carried out in aqueous phosphoric acid (5 wt%) at 25 °C for a defined time.

Fabrication of arrays of free-standing nanorods. The template-assisted fabrication of arrays of free-standing nanorods is schematically shown in SCHEME 1.

The AAO templates consisted of an aluminum substrate with a thin porous anodized alumina layer with nanopores opened on one side. A solution of 4,4'divinyltriphenylamine (DVTPA) in dichloromethane (20 wt%) was degassed by two freeze-pump-thaw cycles and subsequently spin-coated on the top of the AAO template (2000 rpm, 1 min). The samples were vacuum-treated for 30 min at room temperature. An ITO/glass substrate, which had been treated with O_2-plasma and silanized with vinyltrimethoxysilane, was pressed on the top of the spin-coated film and clamped together with the template. Under vacuum conditions the sample was heated up to 80 °C for 1 h and then cured for 3 h at 150 °C. Subsequently, the supporting aluminum layer was removed by treatment with a solution of $CuCl_2$ (c = 0.2 mol/L) at room temperature. By treatment with a solution of potassium hydroxide (5 wt%) for 1 h the porous alumina template was removed. The patterned polymer film attached to ITO/glass was rinsed with deionized water (Milliopore 18MΩ) for several times and then stored in deionized water for 30 min to remove residual potassium and aluminum hydroxide. For samples that were not dried via freeze drying technique, the water was removed under reduced pressure at room temperature. In the case of applying the freeze drying technique, the wetted samples were first cooled down to -60 °C and then dried by subliming the ice under high vacuum conditions.

Characterization.

The morphologies of the fabricated nanoporous AAO templates and their polymeric replicas were investigated by low voltage field emission scanning electron microscopy (FE-SEM, Zeiss LEO 1530) at 3 kV and 0.7 kV, respectively, without using any conductive coating. For cross-sectional TEM measurements a sample with a relative thick (> 1µm) polymeric layer was fabricated in a similar way to the procedure described above by using drop-casting instead of spin-coating. Dipping the patterned polymer film into liquid nitrogen resulted in a delamination from the ITO/glass. The delaminated film was cut by ultramicrotomy and TEM measurements were performed using a Philipps EM-420 at 120 kV. Cyclovoltametric measurements were performed using an Autolab PGSTAT30 (Eco Chemie) Potentiosat/Galvanostat. Pt wire and Ag/AgCl were used as the counter and reference electrode, respectivlely. The patterned hole-conducting polymer film on ITO/glass was used as the working electrode and 0.1 M tetrabutylammonium tetrafluoroborate ($TBABF_4$) in acetonitrile was used as electrode.

Conclusion.

In this contribution, we reported on the fabrication of large arrays of semi-conducting, polymeric nanorods attached to an ITO/glass electrode via an anodic aluminum oxide (AAO) template-assisted approach. The use of AAO templates with a dimensionally controllable, highly ordered porous structure allowed the production of polymeric nanorods with tunable aspect ratios. By filling the templates with a triphenylamine derivative via a template-wetting step combined with a subsequent imprinting, a good polymeric replication, which matches to the contours of the pores and does not show any voids, was obtained. The thermally initiated cross-linking of the triphenylamine derivative while pressing on an ITO/glass electrode, which was pre-functionalized with vinyl-trimethoxysilane, resulted in good resistance against organic solvents and a sufficient adhesion between the substrate and the replica. Arrays of perfectly free-standing and non-aggregated nanorods with a length of 200 nm and an aspect ratio larger than 3 have been fabricated by applying a freeze-drying technique to remove the aqueous medium after the etching of the template. Due to the electrochemical properties and the highly-ordered two-dimensional nanostructure, which provides a larger interface, these nanorod arrays have a potential application to build up ordered bulk-heterojunction solar cells.

Acknowledgment.

N. H. gratefully acknowledges support of the international research and training group (IRTG 1404) funded by the DFG. The authors thank the department of Electron Microscopy at the Max-Planck Institute for Polymer Research in Mainz, in particular G. Glasser, providing support for SEM measurements.

References.

[1] C. R. Martin, *Science* **1994,** *266*, 1961-1966.

[2] M. Steinhart; Wehrspohn, R. B.; Gösele, U.; Wendorff, J. H., *Angew. Chem. Int. Ed.* **2004,** *43*, 1334-1344.

[3] J. Mallet; Yu-Zhang, K.; Mátéfi-Tempfli, S.; Mátéfi-Tempfli, M.; Piraux, L., *J. Phys. D: Appl. Phys.* **2005,** *38*, 909-914.

[4] Y. Berdichevsky; Lo, Y.-H., *Adv. Mater.* **2006,** *18*, 122-125.

[5] Y. Shirota; Kageyama, H., *Chem. Rev.* **2007,** *107*, 953-1010.

[6] Y. Lee; Park, S.-H.; Kim, K.-B.; Lee, J.-K., *Adv. Mater.* **2007,** *19*, 2330-2335.

[7] W. Lee; Jin, M.-K.; Yoo, W.-C.; Lee, J.-K., *Langmuir* **2004,** *20*, 7665-7669.

[8] I. S. C. Woo Kyung Cho, *Adv. Funct. Mater.* **2008,** *18*, 1089-1096.

[9] C. R. Martin, *Acc. Chem. Res.* **1995,** *28*, 61-68.

[10] R. Bai; Ouyang, M.; Zhou, R.-J.; Shi, M.-M.; Wang, M.; Chen, H.-Z., *Nanotechnology* **2008,** *19*, 055604.

[11] Y. Xia; Yang, P.; Sun, Y.; Wu, Y.; Mayers, B.; Gates, B.; Yin; Y.; Kim, F.; Yan, H., *Adv. Mater.* **2003,** *15*, 353-389.

[12] K. P. Musselman; Mulholland, G. J.; Robinson, A. P.; Schmidt-Mende, L.; MacManus-Driscoll, J. L., *Adv. Mater.* **2008,** *20*, 4470-4475.

[13] X. Yang; Loos, J., *Macromolecules* **2007,** *40*, 1353-1362.

[14] A. C. Mayer; Scully, S. R.; Hardin, B. E.; Rowell, M. W.; McGehee, M. D., *Mater. Today* **2007,** *10*, 28-33.

[15] S. Gunes; Neugebauer, H.; Sariciftci, N. S., *Chem. Rev.* **2007,** *107*, 1324-1338.

[16] A. del Campo; Arzt, E., *Chem. Rev.* **2008,** *108*, 911-945.

[17] A. Greiner; Wendorff, Joachim H., *Angew. Chem. Int. Ed.* **2007,** *46*, 5670-5703.

[18] S. A. Harfenist; Cambron, S. D.; Nelson, E. W.; Berry, S. M.; Isham, A. W.; Crain, M. M.; Walsh, K. M.; Keynton, R. S.; Cohn, R. W., *Nano Lett.* **2004,** *4*, 1931-1937.

[19] G. Cao; Liu, D., *Adv. Colloid Interface Sci.* **2008,** *136*, 45-64.

[20] P. Apel, *Radiation Measurements* **2001,** *34*, 559-566.

[21] C. R. Martin, *Chem. Mater.* **1996,** *8*, 1739-1746.

[22] R. V. Parthasarathy; Martin, C. R., *Chem. Mater.* **1994,** *6*, 1627-1632.

[23] C. Park; Yoon, J.; Thomas, E. L., *Polymer* **2003,** *44*, 6725-6760.

[24] T. Thurn-Albrecht; Schotter, J.; Kastle, G. A.; Emley, N.; Shibauchi, T.; Krusin-Elbaum, L.; Guarini, K.; Black, C. T.; Tuominen, M. T.; Russell, T. P., *Science* **2000,** *290*, 2126-2129.

[25] E. J. W. Crossland; Sabine Ludwigs Hillmyer, M. A.; Steiner, U., *Soft Matter* **2007,** *3*, 94-98.

[26] M. Park; Harrison, C.; Chaikin, P. M.; Register, R. A.; Adamson, D. H., *Science* **1997,** *276*, 1401-1404.

[27] C. Tang; Lennon, E. M.; Fredrickson, G. H.; Kramer, E. J.;

Hawker, C. J., *Science* **2008,** *322*, 429-432.

[28] J. Lee; Cho, S. H.; Park, S.-M.; Kim, J. K.; Kim, J. K.; Yu, J.-W.; Kim, Y. C.; Russell, T. P., *Nano Lett.* **2008**.

[29] H. Masuda; Fukuda, K., *Science* **1995,** *268*, 1466-1468.

[30] H. Masuda; Yamada, H.; Satoh, M.; Asoh, H.; Nakao, M.; Tamamura, T., *Appl. Phys. Lett.* **1997,** *71*, 2770-2772.

[31] H. Masuda; Hasegwa, F.; Ono, S., *J. Electrochem. Soc.* **1997,** *144*, L127-L130.

[32] K. Nielsch; Choi, J.; Schwirn, K.; Wehrspohn, R. B.; Gosele, U., *Nano Lett.* **2002,** *2*, 677-680.

[33] M. Steinhart; Wendorff, J. H.; Greiner, A.; Wehrspohn, R. B.; Nielsch, K.; Schilling, J.; Choi, J.; Gosele, U., *Science* **2002,** *296*, 1997-.

[34] S. Demoustier-Champagne; Stavaux, P.-Y., *Chem. Mater.* **1999,** *11*, 829-834.

[35] D. H. Park; Kim, B. H.; Jang, M. G.; Bae, K. Y.; Joo, J., *Appl. Phys. Lett.* **2005,** *86*, 113116.

[36] S. I. Cho; Kwon, W. J.; Choi, S.-J.; Kim, P.; Park, S.-A.; Kim, J.; Son, S. J.; R., X.; Kim, S.-H.; Lee, S. B., *Adv. Mater.* **2005,** *17*, 171-175.

[37] Y. Liang; Zhen, C.; Zou, D.; Xu, D., *J. Am. Chem. Soc.* **2004,** *126*, 16338-16339.

[38] S. Grimm; Schwirn, K.; Göring, P.; Knoll, H.; Miclea, Paul T.; Greiner, A.; Wendorff, Joachim H.; Wehrspohn, Ralf B.; Gösele, U.; Steinhart, M., *Small* **2007,** *3*, 993-1000.

[39] Y. Zhang; Lo, C.-W.; Taylor, J. A.; Yang, S., *Langmuir* **2006,** *22*, 8595-8601.

[40] M. Steinhart, Supramolecular Organization of PolymericMaterials in Nanoporous Hard Templates- Self-Assembled Nanomaterials II: Nanotubes. In *Adv. Polym. Sci.*, Shimazu, T., Ed. Springer: Berlin, Heidelberg, 2008; Vol. 220, pp 123-187.

[41] T. Kondo; Juodkazis, S.; Misawa, H., *Appl. Phys. A* **2005,** *81*, 1583-1586.

[42] T. Tanaka; Morigami, M.; Atoda, N., *Japanese Journal of Applied Physics 32*, 6059.

[43] T. Tanaka; Morigami, M.; Oizumi, H.; Ogawa, T., *Japanese Journal of Applied Physics* **1993,** *32*, 5813-5814.

[44] M. Behl; Hattemer, E.; Brehmer, M.; Zentel, R., *Macromol. Chem. Phys.* **2002,** *203*, 503-510.

Supporting Information

Synthesis of 4,4'-Divinyltriphenylamine (DVTPA)

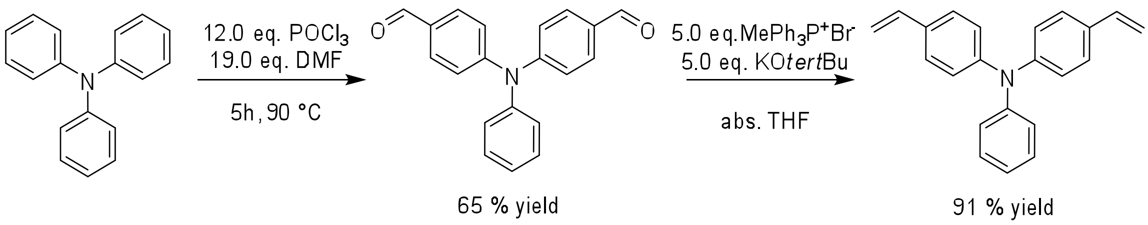

Scheme S1. *Reaction scheme for the synthesis of 4,4'-Divinyltriphenylamine (DVTPA).*

4,4'-Diformyltriphenylamine. The reaction was performed under inert atmosphere using Schlenck technique. 10.0 g of triphenylamine (40.8 mmol) were dissolved in 60 mL of dry *N,N*-dimethylformamide (775mmol, 19 eq.). The solution was cooled down to 0 °C and 44.8 mL of phosphoroxychloride (490 mmol, 12 eq.) were added dropwise. The reaction mixture was heated up to 90 °C and stirred for 5 h. After cooling down to room temperature the mixture was poured on 50 g of ice. The mixture was neutralized with 5 N sodium hydroxide solution. The formed precipitation was filtered off, washed with water, dried under reduced pressure at 50 °C and purified by flash column chromatography (silica gel, petrol ether/ethyl acetate 1:1) to give 7.86 g (26.1 mmol, 64 % yield)

^{1}H-NMR (300 Mhz, $CDCl_3$): δ/ppm = 9.87 (s, 2H), 7.75 (d, 4H), 7.38 (t, 2H), 7.24 (t, 1H), 7.16 (d, 4H), 7.15 (d, 2H).

4,4'-Divinyltriphenylamine (DVTPA). 9.3 g of potassium *tert*-butanolate (83.0 mmol, 5.0 eq.) were added slowly to an ice-cooled suspension of 29.6 g of methyltriphosphoniumbromide (83.0 mmol, 5.0 eq.) in 60 mL of dry tetrahydrofuran (THF). 5.0 g of **2** (16.6 mmol, 1.0 eq.) dissolved in 50 mL of dry THF were added dropewise to the mixture at 0 °C. The mixture was warmed up to room temperature and stirred for 6 h. Subsequently the solvent was removed under reduced pressure, the residue was redissolved in 200 mL of dichloromethane, filtered off over celite. The filtrate was concentrated under reduced pressure and purified by flash column chromatography (silica gel, petrol ether/ethyl acetate 24:1). 4.50 g of the 4,4'-Divinyltriphenylamine **(3)** were isolated as a yellow solid material.

^{1}H-NMR (300 MHz, THF-d8): δ/ppm = 7.28 (d, 4H); 7.21 (t, 2H); 7.06 (d, 2H);6.99 (m, 5H); 6.65 (dd, 2H); 5.63 (d, 2H); 5.12 (d,2H).

Differential scanning calorimetry (DSC) data

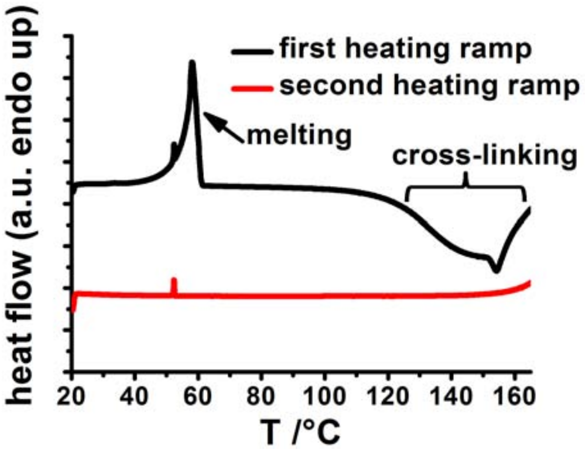

Figure S1. *The plot illustrates the heating curves of the DSC measurement of DVTPA. It shows that the exothermic cross-linking starts around 120 °C and peaks at 155 °C. After cooling to room temperature, the second heating curve did not show any melting and further cross-linking. The ramp scan was 10 K min*$^{-1}$.

5.2 Template-based Preparation of Free-Standing Semiconducting Polymeric Nanorod Arrays on Conductive Substrates

*Niko Haberkorn[1,2], Stefan A. L. Weber[2], Rüdiger Berger[2] and Patrick Theato[1,3] **

[1]*Institute of Organic Chemistry, University of Mainz, Duesbergweg 10-14, 55099 Mainz, Germany.*

[2]Max Planck Institute for Polymer Research, Ackermannweg 10, 55128 Mainz, Germany.

[3]School of Chemical and Biological Engineering, WCU Program of Chemical Convergence for Energy & Environment (C2E2), College of Engineering, Seoul National University, 151-744 Seoul, Korea.

Reproduced with permission from ACS Appl. Mater. Interfaces, **2010**, *2*, 1573-1580 *Copyright 2010 American Chemical Society.*
Coverpage *ACS Appl. Mater. Interfaces*, **2010**, *2 (6).*

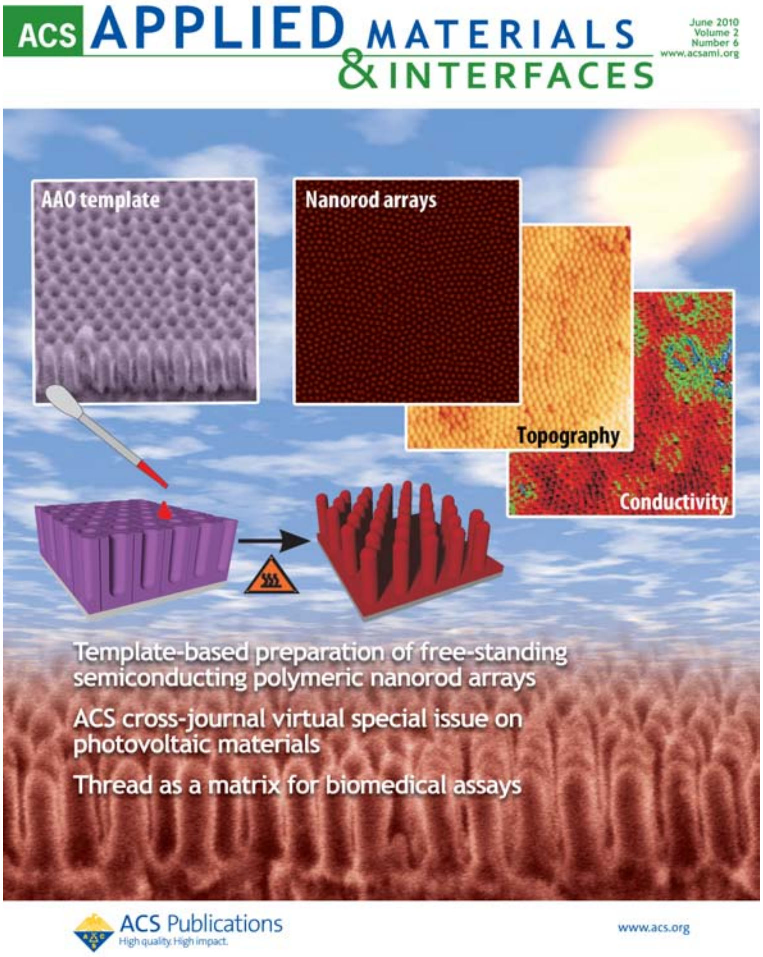

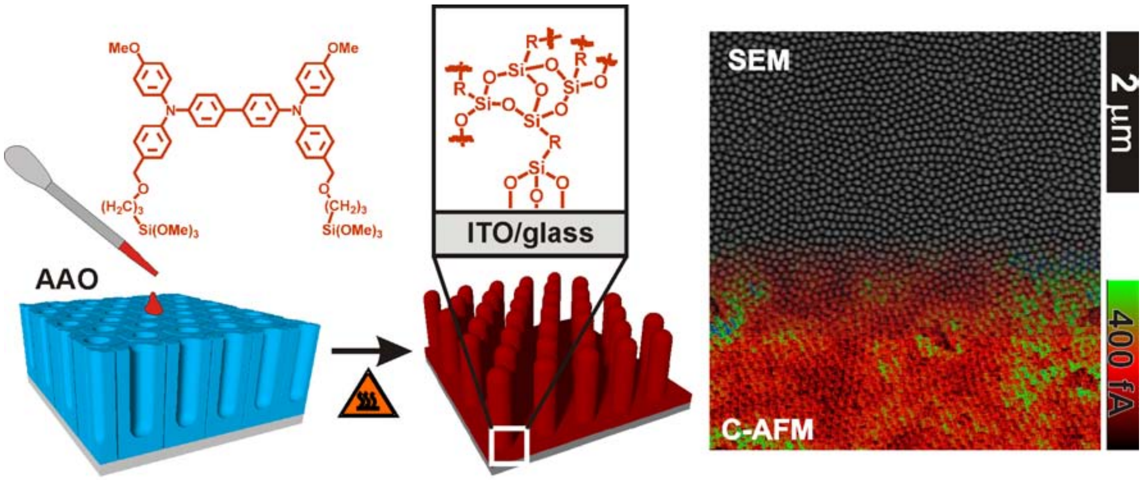

Abstract

We described the synthesis and characterization of a cross-linkable siloxane-derivatized tetraphenylbenzidine (DTMS-TPD), which was used for the fabrication of semi-conducting highly-ordered nanorod arrays on conductive indium tin oxide or Pt-coated substrates. The stepwise process allowed fabricating of macroscopic areas of well-ordered free-standing nanorod arrays, which feature a high resistance against organic solvents, semiconducting properties and a good adhesion to the substrate. Thin films of the TPD derivate with good hole-conducting properties could be prepared by cross-linking and covalently attachment to hydroxylated substrates utilizing an initiator-free thermal curing at 160 °C. The nanorod arrays composed of cross-linked DTMS-TPD were fabricated by an anodic aluminum oxide (AAO) template approach. Furthermore, the nanorod arrays were investigated by a recently introduced method allowing to probe local conductivity on fragile structures. It revealed that more than 98% of the nanorods exhibit electrical conductance and consequently features a good electrical contact to the substrate. The prepared nanorod arrays have the potential to find application in the fabrication of multilayered device architectures for building up well-ordered bulk-heterojunction solar cells.

Keywords

Nanorod arrays; anodic aluminum oxide (AAO), tetraphenylbenzidine; organic photovoltaics, conductive scanning force microscopy.

Introduction

In recent years, there has been a remarkable progress in patterning of conducting organic and polymeric materials for electronic and optoelectronic applications.[1, 2] Besides commonly used techniques like photolithography[3, 4] and inkjet printing,[5, 6] the use of nanoporous templates has gained increasing attention for nanoscopic patterning of inorganic[7-10] as well as organic materials. As such, nanoporous templates have proven to be a versatile tool for the fabrication of well-ordered arrays of nanorods and tubes.[11]

In particular, it has been widely proposed that such nanorod arrays composed of semiconducting materials -- which are attached to a conductive substrate and can subsequently be embedded into a semiconducting matrix -- are the ideal morphological architecture for organic solar cell devices with high performances.[12-14] Such morphologies would provide not only a nanoscopic interpenetrating donor/acceptor network with an interfacial distance in the range of the exciton diffusion length (approx. 10-20 nm) but also percolated pathways to guarantee charge transport to the electrodes. Nanoporous templates, *e.g.* anodic aluminum oxide (AAO) membranes[15-19] and block copolymer templates,[20-22] provide uniform and well-ordered nanopores with large lateral pore densities up to 10^{11} cm^{-2}.[23, 24] The templates can be filled with the semi-conducting materials by electro-deposition,[25] electropoly-merization[26-28] or by wetting of polymer melts or solutions (in the case of AAO).[29-31] Accordingly, arrays of nanorods composed of several conducting and semiconducting polymers have been fabricated by applying such a template-assisted approach.[32-36] However, one of the crucial issues especially for polymeric nanorods is to prevent the rods from collapsing and aggregating after selective removal of the template.[37] Furthermore, the patterned semi-conducting material should provide a good adhesion to the conductive substrate and a good chemical resistance against organic solvents in order to enable subsequent spin-coating steps, which are required for a solution-based preparation of organic photovoltaic cells.

In this paper we present the fabrication of large arrays of free-standing nanorods composed of a cross-linked siloxane-derivatized tetraphenylbenzidine (TPD) on conductive substrates by applying an AAO-assisted templating technique, following a procedure that had been published recently.[38] Siloxane-derivatized TPDs -- first pioneered by *Marks* and coworkers as self-assembled hole-injecting layers on ITO surfaces to improve the device performance of organic light emitting diodes[39-43] -- were used as a class of hole-conducting TPDs, which is also highly suitable for the fabrication of nanorod arrays on conducting substrates since it provides both the hole-conducting properties of the TPD mojeties and the organosilanol groups that can covalently bind to a substrate and cross-link. As a consequence, delamination of the nanorod arrays during the fabrication can be drastically decreased and large areas of free-standing nanorods can be obtained, which show a high resistance against organic solvents.

Experimental Section

Instrumentation. All ^1H- and ^{13}C-NMR spectra were recorded on a Bruker 300 MHz FT-NMR spectrometer. ^{29}Si-MAS NMR spectra were measured on a Bruker DSX 400MHz FT NMR spectrometer (rotation: 5000 Hz, 4mm rotor). Chemical shifts (d) were given in parts per million (ppm) relative to TMS. Thermogravimetric analysis (TGA) was performed using a Perkin-Elmer Pyris 6 TGA in nitrogen atmosphere (10 mg of the compound in an aluminum pan). Cyclovoltametric measurements were performed using an Autolab PGSTAT30 (Eco Chemie) Potentiosat/Galvanostat. Pt wire and Ag/AgCl were used as the counter and reference electrode, respectively. The hole-conducting polymer film on ITO/glass was used as the working electrode and 0.1 M tetrabutylammonium tetrafluoroborate ($TBABF_4$) in acetonitrile was used as electrolyte. HOMO values were determined relative to ferrocene.

SEM images were recorded using a Zeiss Leo 1530 at an acceleration voltage of 3.0 kV for AAO membranes and 0.7 kV for polymeric samples. For detection an Inlens detector was used. Conductive scanning torsion mode microscopy (SCTMM) measurements were performed with a Veeco MultiMode (NanoScope IIIa Controller with Quadrex-extender and current amplifier TUNA, sensitivity 1 pA/V) using rectangular PtIr-coated cantilevers (Nanosensors PPP-EFM, Switzerland) with a vertical and a torsional resonance frequency of 50 - 80 kHz and 700 - 900 kHz, respectively. The typical amplitude of the lateral tip movement at resonance was in the range of 2 - 5 nm. All experiments were performed at ambient conditions (21°C, relative humidity 30 - 50%).

Materials. All reagents were purchased from Aldrich, Fluka and Acros and were used without further purification unless otherwise stated. Toluene and tetrahydrofuran (THF) were distilled from sodium/potassium. The syntheses were carried out under argon atmosphere using standard Schlenk techniques. ITO-coated glass substrates with sheet resistance of <10 Ohm/sq were purchased from Präzisions Glas & Optik GmbH, Germany, and were cleaned by ultrasonication in aqueous Helmanex (1 wt%), isopropyl alcohol, and acetone. Prior measurements, they were dried with a stream of pressurized N_2 and subjected to O_2 plasma cleaning for 10 min.

Synthesis

General procedure for *Buchwald-Hartwig* arylation. Tris(di-benzylidene-acetone)dipalladium(0) (Pd_2dba_3) (2 mol% according to the amine reagent) and 1,1'-bis(diphenylphosphino)-ferrocene (DPPF) (4 mol% according to the amine reagent) were dissolved in toluene under argon and degassed by two freeze-pump-thaw cycles. This activated catalyst was then added to a degassed mixture of the bromoaryl compound (1.0 eq of bromo units), the aromatic amine (1.0 eq) and sodium-*tert*-butylate (2.8 eq) in toluene. The mixture was stirred for 15 h at 90 °C. After cooling down to room temperature the reaction was quenched by adding 5 mL of methanol, diluted with diethylether and washed twice with brine and water, respectively.

The combined aqueous phase was extracted twice with diethylether. The combined organic phase was then dried with $MgSO_4$, filtered and the solvent was evaporated under reduced pressure. The residue was purified by column chromatography on silica gel with petrol ether/ethyl acetate (9:1 v/v).

Synthesis of *N*-(4-methoxyphenyl)-*N*-phenyl-amine (1). *N*-(4-methoxyphenyl)-*N*-phenyl-amine was synthesized according to the general procedure for *Buchwald-Hartwig* arylation described above starting from 4-bromoanisol and aniline (yield 86 %).

^{1}H NMR (300 MHz, $CDCl_3$): δ= 3.79 (s, 3H, -OMe), 5.50 (s, br, 1H, NH), 6.80-6.91 (m, 4H, Ar-H), 7.02 -7.12 (m, 2H, Ar-H), 7.21 (t, 2H, $^3J_{H-H}$= 8.5 Hz, Ar-H).

^{13}C-NMR (75 MHz, $CDCl_3$): *δ*/ppm= 55.6, 114.7, 115.7, 119.6, 122.2, 129.3.

Synthesis of *N,N′*-bis(4-methoxyphenyl)-*N,N′*-bisphenyl-1,1′-bisphenyl-4,4′-diamine (2). *N,N′*-bis(4-methoxyphenyl)-*N,N*-bisphenyl-1,1'-bisphenyl-4,4'-diamine was synthesized according to the general procedure for *Buchwald-Hartwig* arylation described above starting from *N*-(4-methoxyphenyl)-*N*-phenyl-amine and 4,4'-dibromodiphenyl (yield 92%).

^{1}H NMR (300 MHz, $CDCl_3$): *δ*/ ppm= 3.80 (s, 6H, -OMe), 6.85 (d, 4H, $^3J_{H-H}$= 8.7 Hz, Ar-H), 6.96 (t, 2H, $^3J_{H-H}$= 8.5 Hz, Ar-H_{para}), 7.04-7.13 (m, 12H, Ar-H), 7.22 (t, 4H, $^3J_{H-H}$= 8.5 Hz, Ar-H), 7.40 (d, 4H, $^3J_{H-H}$= 8.5 Hz, Ar-H).

Synthesis of *N,N′*-bis(4-methoxyphenyl)-*N,N′*-bis(4-formylphenyl)-(1,1′-biphenyl)-4,4′-diamine (3). 10.0 g (18.23 mmol) of 2 were dissolved in 120 mL of dry *N,N*-dimethylformamide. The solution was cooled down to 0 °C and 24.95 mL (273.0 mmol, 15.0 eq.) of phosphoroxychloride were added dropwise. The mixture was stirred at 90 °C for 15 h. After cooling to room temperature the mixture was poured on 500 g of ice and neutralized with 5 N sodium hydroxide solution. The precipitate was filtered off, washed with water and dried at 50 °C *in vacuo*. The crude product was purified by flash column chromatography (silica gel, petrol ether/ethyl acetate 9:1) to yield 6.64 g (11.0 mmol, 60% yield) of **3** as a yellow crystalline powder.

^{1}H NMR (300 MHz, $CDCl_3$): *δ*/ppm= 3.81 (s, 6H, -OMe), 6.90 (d, 4H, $^3J_{H-H}$= 8.5 Hz, Ar-H), 6.99 (d, 2H, $^3J_{H-H}$= 8.5 Hz, Ar-H), 7.13 (d, 4H, Ar-H), 7.20 (d, 4H, $^3J_{H-H}$= 8.5 Hz, Ar-H), 7.49 (d, 4H, $^3J_{H-H}$= 8.5 Hz, Ar-H), 7.66 (d, 4H, $^3J_{H-H}$= 8.5 Hz, Ar-H), 9.77 (s, 2H, Ar-C(=O)H).

^{13}C-NMR (75 MHz, $CDCl_3$): *δ*/ppm= 55.5, 115.2, 118.6, 125.7, 127.9, 128.5, 128.7, 131.4, 136.4, 136.7, 145.4, 153.4, 157.6, 190.4.

Synthesis of *N,N′*-bis(4-methoxyphenyl)-*N,N′*-bis(4-(hydroxymethyl)-phenyl)- (1,1′-biphenyl)-4,4′-diamine (4). 6.64 g (11.0 mmol) of 3 were dissolved in a mixture of 150 mL of dry ethanol and 60 mL of dry dichloromethane. 3.20 g (84.6 mmol) of sodium borohydrid was added stepwise and the mixture was stirred 2for 20 h at room temperature. The reaction was quenched by slowly adding water. The solvent was then evaporated, the residue redissolved in 150 mL dichloromethane and washed twice with brine and water, respectively. The combined aqueous phases were extracted with dichloromethane and the organic phases were then dried over magnesium sulfate and the solvent was evaporated *in vacuo*. Purification of the residue by flash column chromatography (silica gel, petrol ether/ethyl acetate 1:4) yielded 6.40 g (10.5 mmol, 96% yield) of **4** as a green crystalline powder.

^{1}H NMR (300 MHz, CDCl$_3$): δ/ppm= 3.79 (s, 6H, -OMe), 4.59 (s, 4H, Ar-C$\underline{H}_2$-OH), 6.84 (d, 4H, $^{3}J_{H\text{-}H}$= 8.5 Hz, Ar-$\underline{H}$), 7.01-7.10 (m, 12H, Ar-$\underline{H}$), 7.21 (d, 4H, $^{3}J_{H\text{-}H}$= 8.5 Hz, Ar-$\underline{H}$), 7.38 (d, 4H, $^{3}J_{H\text{-}H}$= 8.8 Hz, Ar-$\underline{H}$).

^{13}C-NMR (75 MHz, CDCl$_3$): δ/ppm= 55.5, 65.1, 114.8, 122.9, 127.2, 127.3, 128.3, 129.1, 131.7, 134.0, 134.1, 134.2, 134.3, 146.9, 147.6, 156.3.

Synthesis of *N,N′*-bis(4-methoxy-phenyl)-*N,N′*-bis(4-(allyloxy-methyl)-phenyl)- (1,1′-biphenyl)-4,4′-diamine (5). 3.00 g (4.93 mmol) of 4 were dissolved in 100 mL of dry tetrahydrofuran, cooled down to 0 °C and 0.75 g (31.25 mmol) of sodium hydride were added in small portions. After stirring for 1 h at room temperature, 1.79 g (14.8 mmol) of allyl bromide were added dropwise at 0 °C and the mixture was stirred at 50 °C for 5 h. Residues of sodium hydride were removed by slowly adding water. The solvent was then evaporated *in vacuo*, the residue was dissolved in diethyl ether and washed with brine and water twice. The organic phase was dried over magnesium sulfate and the solvent was removed under reduced pressure. The residue was purified by flash column chromatography on silica gel (petrol ether/ethyl acetate 4:1) to yield 2.30 g (3.34 mmol, 68 % yield) of **5** as a slightly yellow solid.

^{1}H NMR (300 MHz, CDCl$_3$): δ/ppm= 3.79 (s, 6H, -OMe), 4.04 (d, 4H, $^{3}J_{H\text{-}H}$= 5.6 Hz, OC$\underline{H}_2$-CH=CH$_2$), 4.44 (s, 4H, Ar-C$\underline{H}_2$-O), 5.20 (dd, 2H, $^{3}J_{H\text{-}H}$= 10.3 Hz, $^{2}J_{H\text{-}H}$= 1.5 Hz, O-CH$_2$-CH=CH$_{cis}\underline{H}_{trans}$), 5.31 (dd, 2H, $^{3}J_{H\text{-}H}$= 17.2 Hz, $^{2}J_{H\text{-}H}$= 1.5 Hz, O-CH$_2$-CH=C$\underline{H}_{cis}$H$_{trans}$), 5.96 (ddd, 2H, $^{3}J_{H\text{-}H}$= 17.2 Hz, $^{3}J_{H\text{-}H}$= 10.3 Hz, $^{3}J_{H\text{-}H}$= 5.5 Hz, O-CH$_2$-C$\underline{H}$=CH$_{cis}$H$_{trans}$), 6.84 (d, 4H, $^{3}J_{H\text{-}H}$= 8.7 Hz, Ar-$\underline{H}$), 7.03 (d, 4H, $^{3}J_{H\text{-}H}$= 8.5 Hz, Ar-$\underline{H}$), 7.05 (d, 4H, $^{3}J_{H\text{-}H}$= 8.7 Hz, Ar-$\underline{H}$), 7.08 (d, 4H, $^{3}J_{H\text{-}H}$= 8.8 Hz, Ar-$\underline{H}$), 7.20 (d, 4H, $^{3}J_{H\text{-}H}$= 8.5 Hz, Ar-$\underline{H}$), 7.39 (d, 4H, $^{3}J_{H\text{-}H}$= 8.8 Hz, Ar-$\underline{H}$).

Synthesis of *N,N′*-bis(4-methoxy-phenyl)-*N,N′*-bis(4-((3-(trimethoxy-silyl)propoxy) methyl)-phenyl)- (1,1′-biphenyl)-4,4′-diamine (DTMS-TPD). With the use of standard Schlenk technique, 20 mg of platinum on carbon (5 wt% loading) was added to a solution of 5 (2.3 g, 3.34 mmol) in dry toluene (50 mL). 1.50 mL (11.78 mmol) of trimethoxysilane were added dropwise at room temperature and the mixture was heated to 90 °C for 24 h. After cooling to room temperature the mixture was filtrated twice over celite under inert atmosphere to remove the catalyst. The solvent was evaporated under reduced pressure and the residue was purified by column chromatography on silica gel (chloroform, under inert atmosphere). 1.62 g (1.73 mmol, 52 %) of **6** were obtained as a yellow viscous oil and was stored at -20 °C under inert atmosphere.

^{1}H NMR (300 MHz, CDCl$_3$): δ/ppm= 0.70 (m, 4H, -CH$_2$-Si(OMe)$_3$), 1.66-1.78 (m, 4H, O-CH$_2$-C$\underline{H}_2$), 3.46 (t, 4H, $^{3}J_{H\text{-}H}$= 7.0 Hz, O-C$\underline{H}_2$-CH$_2$), 3.55 (s, Si(OCH$_3$)$_3$), 3.79 (s, 6H, -OMe), 4.41 (s, 4H, Ar-C$\underline{H}_2$-O), 6.83 (d, 4H, $^{3}J_{H\text{-}H}$= 8.7 Hz, Ar-$\underline{H}$), 7.00-7.11 (m, 12H, Ar-$\underline{H}$), 7.18 (d, 4H, $^{3}J_{H\text{-}H}$= 8.5 Hz, Ar-$\underline{H}$), 7.38 (d, 4H, $^{3}J_{H\text{-}H}$= 8.8 Hz, Ar-$\underline{H}$). FD mass spectra (m/z): 931.8 (calcd mass: 932.4 g/mol)

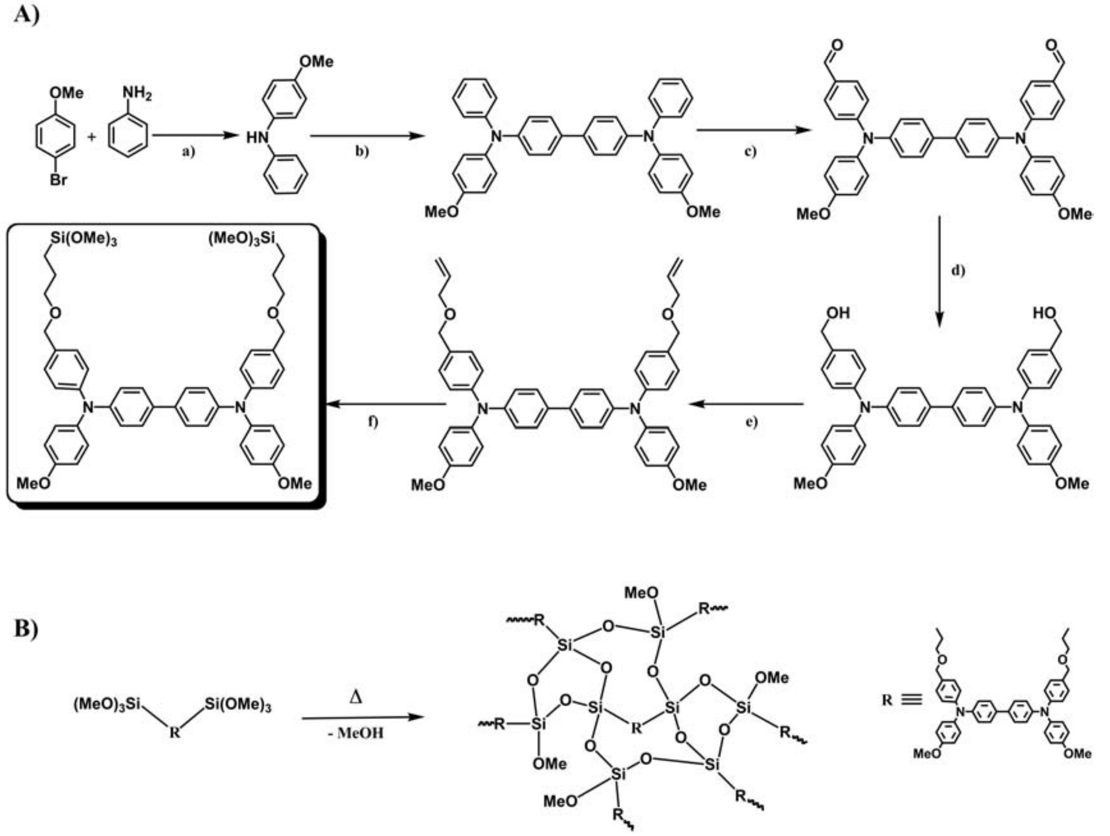

Scheme 1. *A) Synthetic route of DTMS-TPD. a) and b) Pd_2dba_3 (2 mmol%), DPPF (4 mmol%), NaOtertBu (2.8 eq.), toluene, 15 h at 90 °C (86% yield (a) and 92% yield (b)); c) $POCl_3$, DMF, 0°C → 90°C, 15 h (60% yield); d) $NaBH_4$, EtOH/dichloromethane, 20 h, room temperature (96 % yield); e) NaH, allyl bromide, dry THF, 0 °C → 5 h at 50 °C (68% yield); f) Pt/C, $HSi(OMe)_3$, toluene, 24 h at 90 °C (52% yield). B) Formation of a cross-linked siloxane-network of DTMS-TPD via thermally induced condensation.*

Following the concept of well organized interpenetrating phases of organic hole- and electron-conductors that might find application for all-organic based photovoltaics, we recently reported on the thermal cross-linking of divinyltriphenylamine, which was used to fabricate successfully free standing nanorod arrays. However, in order to obtain a suitable adhesion and covalent binding of triphenylamine derivatives on ITO/glass, the substrate had to be pre-functionalized with an organosiloxane. But still the templating of large areas remained a delicate issue due to partial delamination. To abandon the pre-functionalization step of the substrate and to optimize the large-area patterning process avoiding delamination, we designed a siloxane-derivatized TPD.

Synthesis. The bifunctional organo-siloxane-derivatized tetraphenylbenzide *N,N′*-bis(4-methoxyphenyl)-*N,N′*-bis(4-((3-(trimethoxysilyl)propoxy)methyl)-phenyl)-(1,1′biphenyl)4,4′-diamine (TMS-TPD) was synthesized in a six step reaction (see scheme 1A). TPD-based materials are known to be suitable hole conductors and the trimethoxysilane groups allow for covalently binding to hydroxyl functionalities of an ITO surface and for formation of cross-linked siloxane-based networks by thermally induced condensation.

Preparation of nanorod arrays. A thin AAO template, which was fabricated by a two step anodization process and still mechanically stabilized on the remaining aluminum layer, was spin-coated with a diluted, pre-condensed DTMS-TPD solution (6 wt% in toluene, 60 min stirring at atmospheric conditions before coating, 2000 rpm). The complete coated templates were then dried *in vacuo* and cut into several parts with a razor blade to prepare several samples. The cleaned substrates, like ITO/glass, Pt-coated silicon and quartz, were pressed on the coated template and clamped together. Air inclusions between substrate and TPD films were removed by vacuum treatment. A PDMS layer between the aluminum and the pressing plate was used to homogenize the imprinting pressure all over the sample. The samples were heated to 50 °C for 1 h and then thermally cross-linked at 160 °C for 4 h. The aluminum and the AAO were selectively etched away by treatment with aqueous $CuCl_2$ ($c = 0.2$ mol L^{-1}) and aqueous phosphoric acid (10 wt%, 90 min). After repeated rinsing and dipping cycles with deionized water, the samples were dried by freeze-drying.

Results and Discussion

In a sequential palladium-catalyzed *Buchwald-Hartwig* arylation, aniline was allowed to react with *para*-bromoanisole to afford the secondary amine **1**, which was then coupled with 4,4'-dibromodiphenyl to yield the dimethoxy substituted TPD **2**. In a double *Vilsmeyer-Haack* formylation using phosphoroxychloride and *N,N*-dimethylformamine compound **3** was obtained, which was subsequently converted to the dimethylenehydroxy substituted TPD **4** by reduction with sodium borohydride in quantitative yields. Etherfication with allyl bromide using sodium hydride as a base, afforded the tethered divinyl substituted TPD **5**. Compound **5** was coupled with trimethoxysilane to yield the corresponding disiloxane derivatized TPD (DTMS-TPD) *via* platinum catalyzed hydrosilylation. The compound DTMS-TPD was successfully identified and characterized by NMR and mass spectroscopy.

Characterization and thin film preparation. The thermogravimetric analysis (TGA) (see supporting information S2) of DTMS-TPD showed a slight weight loss (approximately 7%) starting at 100 °C, which indicates the thermally induced condensation of the two trimethoxysilane groups (see Scheme 1B). The thermal-induced decomposition of the cross-linked material started above 250 °C and therefore the compound provides a suitable thermal stability for the cross-linking step. To study the cross-linking characteristics in more detail, we performed solid state ^{29}Si-MAS-NMR spectroscopy. The ^{29}Si chemical shift values of the organosiloxane units allowed to clearly distinguish between T_0, T_1, T_2 and T_3 branches, which indicate the degree of self-condensation.[44, 45] The T_0 corresponds to the non-condensed $R\text{-}Si(OMe)_3$ unit and the T_3 branch indicates the fully condensed $R\text{-}Si(OSi\text{-}R)_3$ unit (T_x:$R\text{-}Si(OSi)_x(OMe)_{3-x}$).

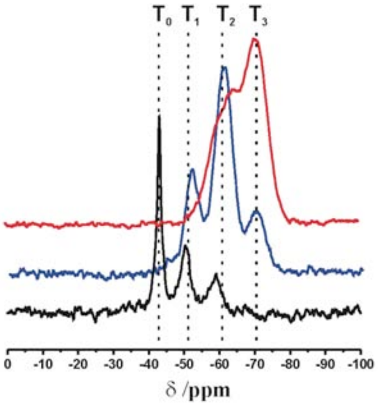

Figure 1. *^{29}Si-MAS-NMR spectra of DTMS-TPD before thermal curing (black line), after exposure to air moisture for 18 h (blue line) and after thermal curing for 4 h at 160°C (red line).*

Before thermal treatment of DTMS-TPD the ^{29}Si-MAS-NMR spectrum showed signals at d= -43.1 ppm (51 %), -50.7 ppm (32 %) and -59.0 ppm (17 %) corresponding to the T_0, T_1, and T_2 branch (see Figure 1). The observation of T_1 and T_2 branches is due to fact that moisture exposure during the sample preparation was not specifically avoided and the material had already undergone partially self-condensation before the actually measurement. But most of the siloxane was not condensed and the material was still completely soluble in toluene, dichlorobenzene and tetrahydrofurane. Noteworthy, the partially condensed material actually showed better casting properties, *e.g.* no partially dewetting effects after spin-coating when compared to the freshly synthesized and non-condensed one material were observed. It turned out that stirring all solutions of DTMS-TPD under air atmosphere for 60 min before spin-coating was most beneficial for the spin-coating process.

Further exposure of the material to air moisture resulted in a further cross-linking of the bulk material, which was indicated by the most intensive T_2 signal in the ^{29}Si-MAS-NMR spectrum. The T_0 signal completely disappeared and the sample was not completely soluble in THF anymore. After thermal treatment for 4 h at 160 °C the ^{29}Si-MAS-NMR spectrum showed only the T_2 and the T_3 signals, which indicated the formation of a highly cross-linked siloxane network showing good solvent resistance against tetahydrofurane and toluene. The reason for the minor amount of the remaining double condensed siloxane units indicated by the T_2 is probably due to steric hindrance of the remaining methoxy group in the rigid siloxane network and could not be further converted even after longer thermal treatment.

Next, spin-coated and thermally-cured films of DTMS-TPD on quartz with a film thickness of 100-150 nm, were washed thoroughly with toluene, which is good solvent for the non-cross-linked TPD monomer, and the UV/Vis spectra of the thin films before and after washing were measured to estimate the amount of non-cross-linked monomer/polymer after the thermal treatment process. After rinsing with toluene the absorption of the cured film showed only a slight decrease of less than 5%, which indicates a sufficient resistance against organic solvents as well as a satisfactory cross-linking reaction (see Supporting Information figure S3).

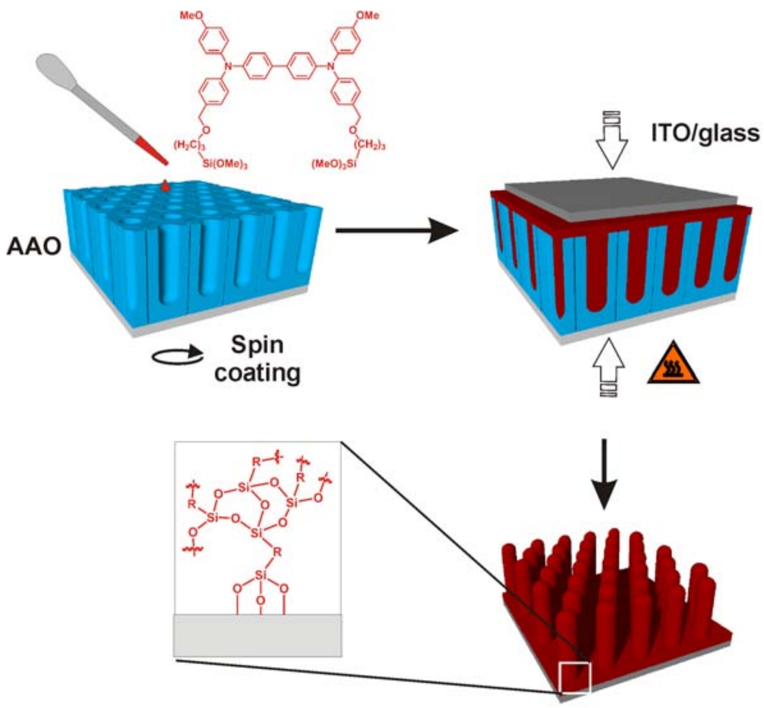

Figure 2. *Schematic diagram of the template-assisted fabrication of cross-linked free-standing nanorod arrays.*

The electrochemical properties of DTMS-TPD thin films were investigated by cyclic voltammetry (CV). As such, the CV curves of both the non-cross linked and the cross-linked films on ITO/glass were measured. Both showed the characteristic two oxidative peaks of the TPD moiety (see figure 4). The cross-linking did not result in a shift of the redox potentials. Furthermore, the oxidation and reduction current, which is detected at the ITO electrode, indicated that the charge transport through the polymer film was not inhibited by the formation of the siloxane network. The highest occupied molecular orbital (HOMO) energy level was determined from the first oxidation peak to be -5.03 eV by using ferrocene/ferrocene$^+$ as a standard (E= -4.8 eV). Due to the two electron rich methoxy substituents, the HOMO of DTMS-TPD exhibits a higher value and thus, a smaller band gap to the work function of ITO (E= -4.7 eV) compared to other reported alkyl substituted TPD derivates (E_{Homo}= ~ -5.3 eV)[40] was calculated.

This shows promise for an enhanced hole injection efficiency from ITO to DTMS-TPD. The lowest unoccupied molecular orbital (LUMO) was estimated to be E= -2.27 eV, which was determined from the difference of the HOMO value and the optical band gap value of 2.76 eV, obtained from the lower energy onset of the absorption spectrum.

Template-assisted patterning. Well-ordered nanoporous AAO templates were used for the templating process of the TPD derivative. The AAO templates were fabricated in a two step anodization process as published recently.[38] Detailed experimental information about the fabrication of the templates is given in the Supporting Information. The dimensional parameters, such as the interpore distance, length and diameter of the pores could be varied and tailored to particular needs for the patterning by controlling the experimental parameters during the anodization process and by using an optional post pore widening process. To fulfill the morphological demands for the potential application in organic photovoltaics, only templates with a pore length in the range of 100-200 nm were used (see supporting information S1).

The stepwise templating procedure is schematically illustrated in Figure 2. Since the thin AAO template is very fragile and can not be manipulated itself, the aluminum foil, which remains on the backside of the AAO after the anodization, was not directly removed and was used to mechanically stabilize the porous aluminum oxide during the patterning process.

The pores of the AAO membrane were filled by wetting the topside of the membrane with the DTMS-TPD solution, followed by a subsequent imprinting step. The wetting *via* spin-coating of a diluted solution on top of the template resulted in a homogenous coating and allowed to control the thickness of the DTMS-TPD layer on top of the template. Afterwards the coated template was imprinted on a conductive substrate, i.e. ITO/glass or Pt-coated silicon.

For this purpose, the coated template was first pressed onto the substrate at 50 °C. Applied vacuum and the use of a PDMS layer between the sample and the pressing plates assured the removal of air inclusions and guaranteed a homogenous imprinting pressure all over the sample. To increase the adhesion between the substrate and the TPD layer, the surface of the substrates was hydroxylated by a short O_2-plasma treatment prior the imprinting process. As a result, the trimethoxysilane groups could react with the hydroxy groups and covalently bind to the surface. After imprinting at 50°C, the DTMS-TPD was thermally cured *in vacuo* at 160°C for 3 h.

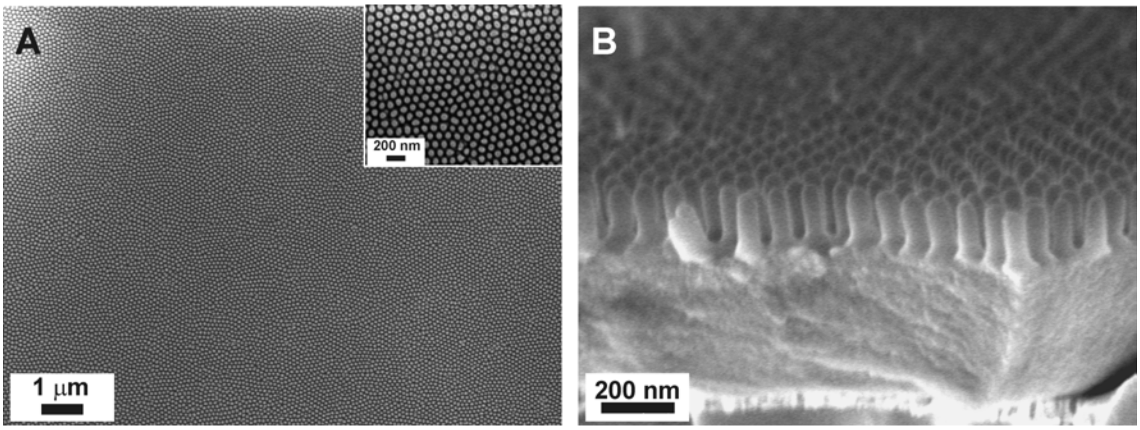

Figure 3. *SEM images of free-standing cross-linked DTMS-TPD nanorod arrays with a length and diameter of 165 ± 5 nm and 64 ± 2 nm respectively.* ***(A)*** *Low magnification top view of nanorod arrays on ITO/glass. (Inlet: higher magnified image, scale bar: 200 nm);* ***(B)*** *Cross-section of nanorod arrays on Pt-coated silicon substrate.*

Then, the aluminum layer was removed by treatment with a diluted $CuCl_2$ solution. Due to the instability of the cross-linking siloxane units against strong bases, the AAO template itself could not be removed by the commonly used treatment with aqueous KOH. Instead the template was selectively removed by treatment with diluted phosphoric acid. In explorative experiments we have found that nanorods based upon cross-linked DTMS-TPD with a length below 300 nm and an aspect ratio up to 5 exhibit a sufficient stiffness to prevent ground collapse after removal of the AAO scaffold. However, the nanorods tend to aggregate and form bundles after conventional drying. The capillary force upon drying is considered to be one of the main causes of aggregation.[46-50] By applying a freeze-drying technique, following a procedure recently published,[38] these capillary forces and consequently the formation of nanorod bundles was prevented and aggregation-free arrays were obtained.

Since the cured DTMS-TPD is covalently attached to the substrate, delamination effects, which were observed for different other cross-linkable materials without siloxane units, were drastically decreased and large macroscopic arrays of perfectly free-standing nanorods, which were all vertically aligned, had successfully been prepared by our method.

For example, figure 3 shows a top-view and cross-sectional SEM image of an aggregation-free array of DTMS-TPD nanorods on ITO/glass (figure 3A) and Pt-coated silicon (figure 3B). The lengths of the rods (170 nm) are in the appropriate range for photovoltaic application and the arrays provide a large surface that would allow the creation of a large well-ordered donor/acceptor interface.

To show that the thermal curing conditions are sufficient for a complete cross-linking and that the aqueous etching steps of the template do not affect the solvent resistance of the patterned DTMS -TPD, the UV/Vis absorption of a patterned DTMS-TPD layer on a quartz substrate was measured before and after rinsing the substrate with toluene (see figure 4A). In agreement with the results for the spin coated DTMS-TPD films the absorption spectra only showed a slightly decrease of the absorption (< 4 %) after rinsing, which indicated a very good solvent resistance of the nanorod arrays even after the patterning procedure and the etching of the template under acidic conditions.

Cyclovoltammetric measurements of the patterned film on ITO/glass showed no significant change of the electrochemical properties compared to the spin-coated and non cross-linked thin films (see figure 4B). The CV curve still showed a reversible shape and the detectable oxidation and reduction current indicated a sufficient charge transport to the electrode.

The above described results elucidate the macroscopic characteristics of the entire sample. However for the application of such structures the homogeneity on a microscopic scale is of major interest. In order to investigate the properties of individual nanorods, we performed conductive scanning force microscopy (C-SFM).

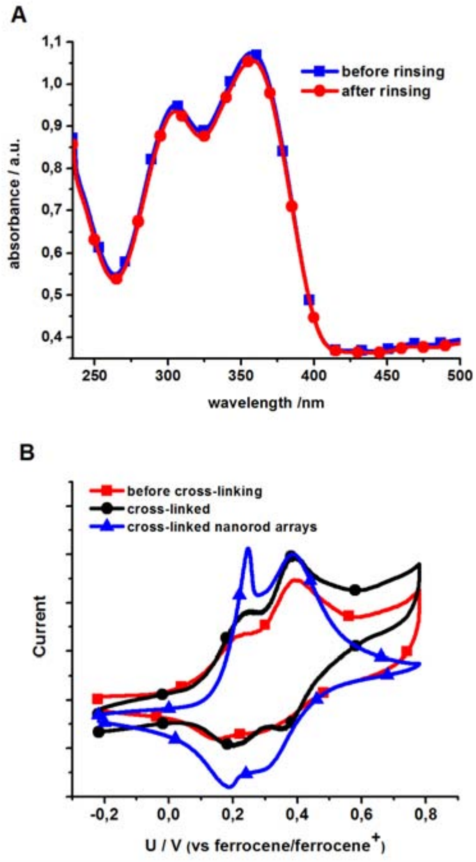

Figure 4. *(A) Absorption spectra of an AAO-templated DTMS-TPD film on quartz (cured at 160 °C for 4 h) before (red line) and after rinsing (blue line) by toluene. (B) Cyclic voltammogram of a non-cured (red line), cured (160 °C, 4 h) and cured AAO-templated (blue line) DTMS-TPD film on an ITO/glass substrate in a solution of n-Bu$_4$NPF$_6$ in acetonitrile (0.1 mol L^{-1}) at a scan rate of 0.1 Vs^{-1}. The second scans are illustrated, respectively.*

Here, an electrically conductive tip is scanned over a surface at a constant normal force and bias voltage. Simultaneously to the topography, variations in the current through the tip are recorded. However, tip sample interactions and lateral forces are hard to control in this operation mode. This can lead to bending and the complete destruction of fragile structures. The latter effect can be avoided by performing the C-SFM study in on a sample with stabilized nanorods. This can be achieved by only removing the supporting template on the topside and thus the nanorods are still stabilized by the template during the measurement.[51, 52] Only a few C-SFM studies were reported on organic free-standing nanorod arrays. Recently, *Lee et al.* reported on local conductivity measurements (without simultaneous topography mapping) of polyprrole nanopillars.[32] *Wang* and coworker presented C-SFM studies on the charge carrier generation in illuminated low aspect ratio core/shell nanorods composed of polythiophene/fullerene.[53]

To avoid the destruction of individual nanorods the charge transport through the nanorods to the Pt-electrode of the substrate were investigated by a recently introduced C-SFM technique named scanning conductive torsion mode microscopy (SCTMM).[54] Since it is a non-contact mode, tip sample interactions and lateral forces are minimized. For this study nanorod arrays were fabricated on Pt coated Si wafers in order to minimize the surface roughness on the electrode. In the topographic image (Figure 5 A), the well aligned nanorod array could be clearly resolved with an average nanorod distance of 100 nm in consistence with the SEM studies (see Figure 3B). Due to its geometry, the tip could not completely penetrate into the voids between the rods and therefore the image showed a depth between the rods of only 30-40 nm. In the simultaneously recorded current map (Figure 5B) individual

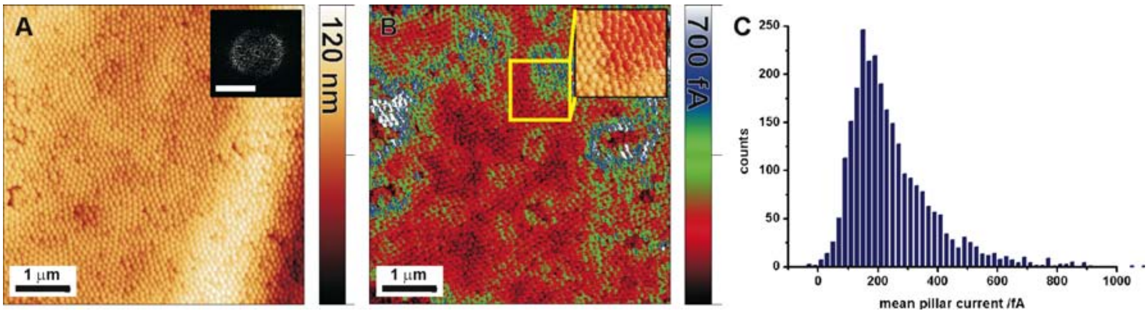

***Figure 5. (A)** Topography of a thermally cured DTMS-TPD nanorod array on a Si/Pt substrate. The inset shows a FFT analysis of the image (scale bar: 20 μm^{-1}). The halo at ~11 μm^{-1} corresponds to a mean nanorod distance of 90 nm. **(B)** Electrical current at V_{bias}= 12 V. The inset shows an overlay of the topography and the areas carrying currents higher than the mean current value of 250 fA (marked in red), which shows the good correlation of current and topography. **(C)** Histogram of the mean pillar currents of the 2660 nanorods visualized in (A) and (B).*

structures of the same average size and distance were observed. Each of these structures can be associated with the top part of an individual nanorod.

By marking the positions of the 2660 nanorods in the topography image in Figure 5A and transferring them as a mask to the current map, the average current through each nanorod can be determined. Taking the average currents from all nanorods that were measured in one image, a current distribution was obtained (Figure 5 C). From this histogram we find that more than 98% of the nanorods carry a current higher than 50 fA, i.e. higher than the noise level of the current measurement. The observation that almost every nanorod can conduct an electrical current of 250 ± 140 fA on average demonstrates that the electrical contact to the substrate is uniform and that there are no larger areas without contact to the substrate. Topographic features, such as the ridge in the lower right corner of figure 5 A, do not have an observable influence on the electrical conductance of the sample. Moreover, we found that height differences between adjacent nanorods, which would indicate differences in the nanorod length, cannot be correlated with the current variations. Thus, the origin of the fluctuations is assigned to intrinsic conductivity variations in the rod material. Such fluctuations might be caused by variations in the alignment of the TPD moieties in the siloxane network.

Conclusion

The results shown in this contribution demonstrate that the AAO template-based fabrication of macroscopic arrays of well-ordered nanorods, which are vertically aligned and non-collapsed on conductive substrates and composed of a hole-conducting trimethoxysilane-substituted tetraphenylbenzydine derivative (DTMS-TPD), is very feasible. Non-aggregated nanorod arrays were replicated on the substrate by solution wetting and imprinting of the AAO template. The DTMS-TPD could thermally be cross-linked at 160 °C and showed high resistance against organic solvents in bulk, within thin films and also within nanorod arrays. Due to covalent attachment onto the substrate during the thermal curing, the films also exhibited a good mechanical adhesion to the substrate. The local electrical properties were investigated with conductive scanning torsion mode microscopy (SCTMM). It revealed a good and homogeneous electrical connection of the DTMS-TPD nanostructures to the substrate. Furthermore, 98% of the nanorods were carrying a current significantly above the noise level. Finally, samples were investigated by cyclovoltammetry, which indicated good hole-conducting behavior of the DTMS-TPD. Therefore, these nanorod arrays are highly interesting for the fabrication of multilayered device architectures to be used in organic photovoltaics.

Acknowledgment. The authors thank B. Mathiasch for their help of solid state NMR measurements. The Electron Microscopy at the Max-Planck Institute for Polymer Research in Mainz, in particular G. Glasser, is acknowledged for access to SEM measurements. This research was supported by the DFG (IRTG 1404) and by the WCU (World Class University) program through the National Research Foundation of Korea funded by the Ministry of Education, Science and Technology (R31-10013).

References

[1] Menard, E.; Meitl, M.; Sun, Y.; Park, J.; Shir, D.; Nam, Y.; Jeon, S.; Rogers, J., *Chem. Rev.* **2007,** *107*, 1117-1160.

[2] Hohnholz, D.; Okuzaki, H.; MacDiarmid, A., *Adv. Funct. Mater.* **2005,** *15*, 51-56.

[3] Wallraff, G.; Hinsberg, W., *Chem. Rev.* **1999,** *99*, 1801-1822.

[4] Gather, M. C.; Köhnen, A.; Falcou, A.; Becker, H.; Meerholz, K., *Adv. Funct. Mater.* **2007,** *17*, 191-200.

[5] de Gans, B.-J.; Duineveld, P. C.; Schubert, U. S., *Adv. Mater.* **2004,** *16*, 203-213.

[6] Sirringhaus, H.; Kawase, T.; Friend, R.; Shimoda, T.; Inbasekaran, M.; Wu, W.; Woo, E., *Science* **2000,** *290*, 2123-2126.

[7] Xia, Y.; Yang, P.; Sun, Y.; Wu, Y.; Mayers, B.; Gates, B.; Yin; Y.; Kim, F.; Yan, H., *Adv. Mater.* **2003,** *15*, 353-389.

[8] Lee, W.; Scholz, R.; Nielsch, K.; Gösele, U., *Angew. Chem. Int. Ed.* **2005,** *44*., 6050-6054.

[9] Choi, J.; Sauer, G.; Nielsch, K.; Wehrspohn, R.; Gösele, U., *Chem. Mater.* **2003,** *15*, 776-779.

[10] Hu, W.; Gong, D.; Chen, Z.; Yuan, L.; Saito, K.; Grimes, C.; Kichambare, P., *Appl. Phys. Lett.* **2001,** *79*, 3083-3085.

[11] Haberkorn, N.; Lechmann, M. C.; Sohn, B. H.; Char, K.; Gutmann, J. S.; Theato, P., *Macromol. Rapid Comm.* **2009,** *30*, 1146-1166.

[12] Coakley, K.; McGehee, M., *Chem. Mater.* **2004,** *16*, 4533-4542.

[13] Gunes, S.; Neugebauer, H.; Sariciftci, N., *Chem. Rev.* **2007,** *107*, 1324-1338.

[14] Yang, X.; Loos, J., *Macromolecules* **2007,** *40*, 1353-1362.

[15] Masuda, H.; Fukuda, K., *Science* **1995,** *268*, 1466-1468.

[16] Li, A.; Muller, F.; Birner, A.; Nielsch, K.; Gösele, U., *J. Appl. Phys.* **1998,** *84*, 6023-6026.

[17] Nielsch, K.; Choi, J.; Schwirn, K.; Wehrspohn, R.; Gösele, U., *Nano Lett.* **2002,** *2*, 677-680.

[18] Masuda, H.; Yamada, H.; Satoh, M.; Asoh, H.; Nakao, M.; Tamamura, T., *Appl. Phys. Lett.* **1997,** *71*, 2770-2772.

[19] Li, F.; Zhang, L.; Metzger, R., *Chem. Mater.* **1998,** *10*, 2470-2480.

[20] Park, S.; Wang, J.-Y.; Kim, B.; Xu, J.; Russell, T., *ACS Nano* **2008,** *2*, 766-772.

[21] Thurn-Albrecht, T.; Schotter, J.; Kastle, G.; Emley, N.; Shibauchi, T.; Krusin-Elbaum, L.; Guarini, K.; Black, C.; Tuominen, M.; Russell, T., *Science* **2000,** *290*, 2126-2129.

[22] Thurn-Albrecht, T.; Steiner, R.; DeRouchey, J.; Stafford, C.; Huang, E.; Bal, M.; Tuominen, M.; Hawker, C.; Russell, T, *Adv. Mater.* **2000,** *12*, 787-791.

[23] Kim, T.-Y.; Jeong, S.-H., *Korean J. Chem. Eng.* **2008,** *25*, 609-611.

[24] Park, S.; Lee, D.; Xu, J.; Kim, B.; Hong, S.; Jeong, U.; Xu, T.; Russell, T., *Science* **2009,** *323*, 1030-1033.

[25] Liang, Y.; Zhen, C.; Zou, D.; Xu, D., *J. Am. Chem. Soc.* **2004,** *126*, 16338-16339.

[26] Demoustier-Champagne, S.; Stavaux, P., *Chem. Mater.* **1999,** *11*, 829-834.

[27] Yang, S.; Chen, K.; Yang, Y., *Synth. Met.* **2005,** *152*, 65-68.

[28] Xiao, R.; Cho, S.; Liu, R.; Lee, S., *J. Am. Chem. Soc.* **2007,** *129*, 4483-4489.

[29] Steinhart, M.; Shimazu, T.; Shimazu, T.; Steinhart, M., *Adv. Polym. Sci.* **2008,** *220*, 123-187.

[30] Steinhart, M.; Wendorff, J.; Greiner, A.; Wehrspohn, R.; Nielsch, K.; Schilling, J.; Choi, J.; Gösele, U., *Science* **2002,** *296*, 1997.

[31] Steinhart, M.; H.Wendorff, J.; Wehrspohn, Ralf, *Chem. Phys. Chem.* **2003,** *4*, 1171-1176.

[32] Lee, J. I.; Cho, S. H.; Park, S.-M.; Kim, J. K.; Kim, J. K.; Yu, J.-W.; Kim, Y. C.; Russell, T. P., *Nano Lett.* **2008,** *8*, 2315-2320.

[33] Berdichevsky, Y.; Lo, Y., *Adv. Mater.* **2006,** *18*, 122-125.

[34] Park, D.; Kim, B.; Jang, M.; Bae, K.; Joo, J., *Appl. Phys. Lett.* **2005,** *86*, 113116.

[35] Bai, R.; Ouyang, M.; Zhou, R.-J.; Shi, M.-M.; Wang, M.; Chen, H.-Z., *Nanotechnology* **2008,** *19*, 055604.

[36] Li, X.; Tian, S.; Ping, Y.; Kim, D.; Knoll, W., *Langmuir* **2005,** *21*, 9393-9397.

[37] Goh, C.; Coakley, K.; McGehee, M., *Nano Lett.* **2005,** *5*, 1545.

[38] Haberkorn, N.; Gutmann, J. S.; Theato, P., *ACS Nano* **2009,** *3*, 1415-1422.

[39] Cui, J.; Huang, Q.; Wang, Q.; Marks, T., *Langmuir* **2001,** *17*, 2051-2054.

[40] Li, J.; Marks, T. J., *Chem. Mater.* **2008,** *20*, 4873-4882.

[41] Yan, H.; Huang, Q.; Cui, J.; Veinot, J.; Kern, M.; Marks, T., *Adv. Mater.* **2003,** *15*, 835.

[42] Yan, H.; Lee, P.; Armstrong, N.; Graham, A.; Evmenenko, G.; Dutta, P.; Marks, T., *J. Am. Chem. Soc.* **2005,** *127*, 3172-3183.

[43] Veinot, J.; Marks, T., *Acc. Chem. Res.* **2005,** *38*, 632-643.

[44] Kessler, D.; Theato, P., *Macromolecules* **2008,** *41*, 5237-5244.

[45] Sakamoto, S.; Shimojima, A.; Miyasaka, K.; Ruan, J.; Terasaki, O.; Kuroda, K., *J. Am. Chem. Soc.* **2009,** *131*, 9634-9635.

[46] Fan, J.; Dyer, D.; Zhang, G.; Zhao, Y., *Nano Letters* **2004,** *4*, 2133-2138.

[47] Chandra, D.; Taylor, J. A.; Yang, S., *Soft Matter* **2008,** *4*, 979-984.

[48] Chandra, D.; Yang, S.; Soshinsky, A. A.; Gambogi, R. J., *ACS Appl. Mater. Interfaces* **2009,** *1*, 1698-1704.

[49] Chen, G.; Soper, S.; McCarley, R., *Langmuir* **2007,** *23*, 11777-11781.

[50] Tanaka, T.; Morigami, M.; Oizumi, H.; Ogawa, T., *Jap. J. Appl. Phys.* **1993,** *32*, 5813-5814.

[51] Wang, K.; Birjukovs, P.; Erts, D.; Phelan, R.; Morris, M. A.; Zhou, H.; Holmes, J. D., *J. Mater. Chem.* **2009,** *19*, 1331-1338.

[52] Erts, D.; Polyakov, B.; Dalyt, B.; Morris, M.; Ellingboe, S.; Boland, J.; Holmes, J., *J Phys Chem B* **2006,** *110*, 820-826.

[53] Wang, H.-S.; Lin, L.-H.; Chen, S.-Y.; Wang, Y.-L.; Wei, K.-H., *Nanotechnology* **2009,** *20*, 075201.

[54] Berger, R.; Butt, H.-J.; Retschke, M. B.; Weber, S. A. L., *Macromol. Rapid Comm.* **2009,** *30*, 1167-1178.

Supporting Information

Fabrication of AAO templates. High purity aluminum (99.997 %, 0.1 mm thick) purchased from Alfa Aesar was cleaned by sonification treatment in isopropanol and acetone respectively followed by an electropolishing step in a mixture of ethanol and perchloric acid (v/v 4:1) at a current density of 300-350 mA/cm^{-1} for 1 min at 0 °C. Subsequently the samples were rinsed with deionized water, isopropanol and acetone. To obtain well-ordered porous templates, the anodization was performed in a two step process, which was developed by Masuda and Fukuda.The anodization.[S1]

The anodization steps were performed in a self-build apparatus, similar to those described in the literature. Briefly, the aluminum sheets were mounted on a copper plate serving as the anode. A radial area of 2.27 cm^2 was exposed to an aqueous acidic solution. A platinum wire was used as the cathode. The apparatus was surrounded by a cryostatic bath to control the temperature during anodization and the electrolyte solution was rigorously stirred during anodization. The anodization current as a function of time was measured using a multimeter and recorded with an attached computer. Anodization was performed in an aqueous solution of oxalic acid (c = 0.3 mol/L) at 40.0 V and 2±1 °C. In the first step, aluminum was anodized for 6 h, followed by an etching step in aqueous solution of chromic acid (1.8 wt%) and phosphoric acid (6.0 wt%) at 60 °C for 12 h. To obtain AAO templates with a thickness below 500 nm, the second anodization was performed for a short period under the same conditions like the first anodization step. Due to temperature fluctuations, it is more precisely to control the resulting thickness of the template by controlling the total charge, which is used for the anodization. Therefore the current density is monitored by a multimeter during the anodization.

The AAO templates are cleaned by rinsing with deionized water, isopropanol and acetone and were stored in an acetone bath. Pore widening was performed in aqueous phosphoric acid (5 wt%) at 25 °C.

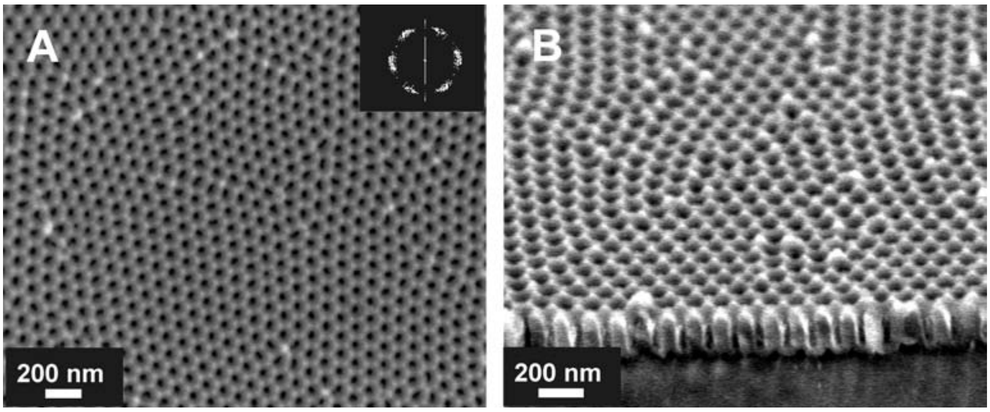

Figure S1. *Top-view (A) and cross-sectional (B) SEM micrograph of a AAO template fabricated in 0.3 M oxalic acid of 2 °C at 40 V for 3.5 min (integrated total charge for anodization: 1.75 As). Pore widening was carried out in 5 wt % phosphoric acid at 25 °C for 10 min (Inlet in A: Fast Fourier Transformation (FFT) of A showing the hexagonal order of the pores).*

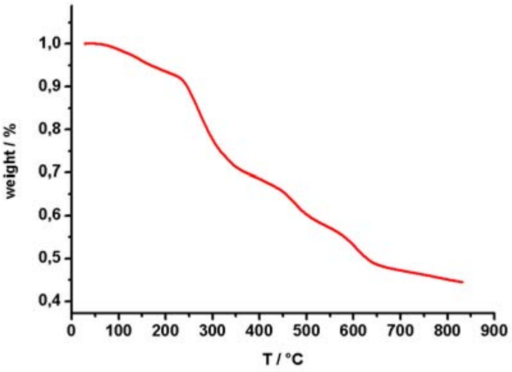

Figure S2. *Thermogravimetric analysis (TGA) diagram of DTMS-TPD (10 Kmin^{-1}, nitrogen atmosphere).*

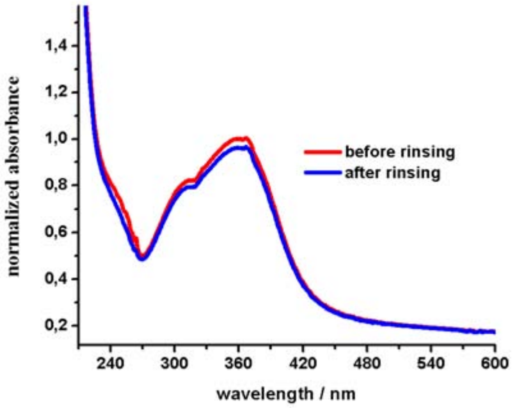

Figure S3. *Absorption spectra of a DTMS-TPD film on quartz (cured at 160 °C for 4 h) before, (red line) and after rinsing (blue line) by toluene.*

5.3 Template-Assisted Fabrication of Highly-Ordered Interpenetrating Networks of Semiconducting Polymers with Enhanced Photoluminescence Properties

*By Niko Haberkorn, Sehee Kim, Ki-Se Kim, Michael Sommer, Mukundan Thelakkat, Byeong-Hyeok Sohn and Patrick Theato**

[*] Dr. Patrick Theato, Niko Haberkorn
Institute of Organic Chemistry, University of Mainz
Duesbergweg 10-14, 55099 Mainz, Germany
E-mail: theato@uni-mainz.de

Sehee Kim, Ki-Se Kim, Prof. Byeong-Hyeok Sohn
Department of Chemistry
Seoul National University, Seoul, Korea

Dr. Michael Sommer[#], Prof. Mukundan Thelakkat
Applied Functional Polymers, Macromolecular Chemistry I, Universität Bayreuth
Universitätstr-30, 95440 Bayreuth, Germany
[#]: Present address: Melville Laboratory for Polymer Synthesis, Department of Chemistry, Lensfield Road, University of Cambridge, Cambridge CB2 1EW, UK

Niko Haberkorn
Max Planck Institute for Polymer Research
Ackermannweg 10, 55128 Mainz, Germany

Dr. Patrick Theato
School of Chemical and Biological Engineering, WCU Program of Chemical Convergence for Energy & Environment (C2E2), College of Engineering, Seoul National University, Seoul, Korea.

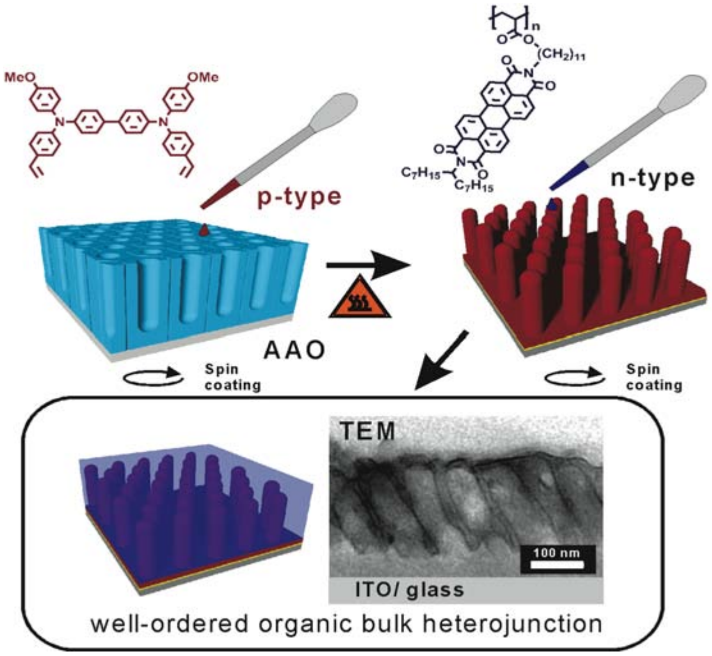

Abstract

We report on the template-assisted fabrication of well-ordered interpenetrating donor/acceptor networks based on polymeric semiconductors on conductive substrates. For that purpose arrays of free-standing nanorods composed of a cross-linked tetraphenylbenzidine derivative (N,N′-bis(4-methoxyphenyl)-N,N′-bis(4-vinylphenyl-(1,1′-biphenyl)-4,4′-diamine, DVTPD) were fabricated on indium tin oxide (ITO) substrates by utilizing anodic aluminum oxide (AAO) templates. The nanorod arrays were embedded into a poly(perylene bisimide acrylate) (PPerAcry) matrix by spin-coating. Transmission electron microscopy (TEM) investigation of the obtained morphologies confirm the successful and complete embedding without causing aggregation and collapsing of the rods. Photoluminescence measurements reveal a more than threefold improvement in photoluminescence quenching relative to the planar bilayer architecture. The presented approach describes a versatile all solution-based technique for the fabrication of well-ordered bulk heterojunction films with a large donor/acceptor interface for the application in polymer/polymer photovoltaic devices.

Introduction

Solar cells based on organic or polymeric semiconductors are attracting increasing attention as an alternative renewable energy source. Compared to their inorganic counterparts organic photovoltaic devices (OPV) provide several advantages, such as low cost fabrication techniques (e.g. spin-coating*[1]*, roll-to-roll process*[2]* or inkjet-printing*[3, 4]*) and the potential for large area deposition on flexible, light-weight substrates.*[5, 6]*

Besides the synthesis of novel organic semiconductors with high charge carrier mobilities and well-tuned energy levels, the morphological control of the photoactive layer remains as one of the challenging issues for the fabrication of efficient photovoltaic devices.*[7-10]* The importance of the morphology is due to the fact that photon absorption in organic semiconductors does not directly generate free charge carries, as it is the case in many inorganic semiconductors. Instead electron-hole pairs (so called excitons) are generated, which are often bound locally due to coulomb attractions at room temperature.*[11-13]* However, for an efficient charge generation these excitons have to dissociate into free electrons and holes, which can then be separated at the interface of electron-donating / electron-accepting organic semiconductors in order to migrate to the respective electrodes. As the exciton diffusion length in organic semiconductors is limited to 10-20 nm,*[6]* organic photovoltaic cells require a bicontinuous and interpenetrating donor-acceptor network with an interfacial distance smaller than the exciton diffusion length to guarantee an efficient charge generation. Further, the donor/acceptor network must provide percolation pathways of both semiconductors to allow an efficient transport of the generated charges to their respective electrodes.

The simplest morphology that features a donor-acceptor interface can be established by a conventional bilayer structure.*[14]* However, this bilayer architecture only provides a small donor-acceptor interface and the two requirements for an efficient photoactive layer – a sufficient thickness for photon absorption and a donor/acceptor interface in the range of the exciton diffusion length – cannot be achieved in a simple bilayer architecture. In order to overcome these limitations bulk heterojunction morphologies have been introduced, in which the interfacial area is tremendously increased and the overall thicker photoactive layer provides a sufficient light absorption.*[15, 16]* Current state-of-the-art bulk heterojunction photoactive layers are prepared by blending conjugated polymers, e.g. poly(3-hexylthiophene) (P3HT) or copolymers based on benzodithiophene as hole-conducting materials with electron-accepting fullerene derivatives. The resulting OPV cells can indeed reach power conversion efficiencies of more than 7 %. *[17-20]* However, it remains a challenge to precisely control bulk heterojunction morphologies composed of donor/acceptor mixtures as well as to increase their long-term stability. In these morphologies, phase separated donor and acceptor domains often do not exhibit the right length scale and are not morphologically stable. Furthermore, they can form 'isolated' domains, which are not connected to the respective electrode. Especially the 'isolated' domains result in a lack of pathways for the generated charges to the electrode. Accordingly, the fabrication of an idealized well-ordered bulk-heterojunction architecture that provides a large donor/acceptor interface as well as percolating pathways still remains a challenging issue by utilizing a phase separation approach.*[21, 22]*

In this paper we present a template-assisted approach for fabricating such well-ordered bulk heterojunction morphologies on conducting substrates. The morphologies consist of vertically aligned hole-conducting nanorods connected to an electrode that are surrounded by an electron-conducting polymer (see Figure 1). Hole-conducting nanorod arrays are prepared by thermally cross-linking a tetraphenylbenzidine derivative inside the pores of anodic aluminum oxide (AAO) templates. Subsequent transfer to a conductive indium tin oxide substrate and dissolution of the template yields highly ordered, free-standing and stable nanorod arrays. Completion of the donor-acceptor heterojunction is achieved by spin coating a perylene bisimide side chain polymer on top.

Up to now only few template-assisted approaches for building up well-ordered donor/acceptor morphologies have been reported and these mainly focus on inorganic/organic hybrid*[23-31]* or on polymer/C_{60} systems.*[32, 33]* To the best of our knowledge, all-organic well-ordered bulk heterojunctions fabricated *via* an AAO template-based approach have not been described and characterized so far.

Results and Discussion

The fabrication of nanorods and -tubes based on conducting and semiconducting polymers, e.g. polypyrrole, polythiophene or polyaniline, via replication of nanoporous templates has been described by several research groups.*[23, 34-37]* However, in order to be used as a versatile method for the solution-based preparation of all-polymer well-ordered

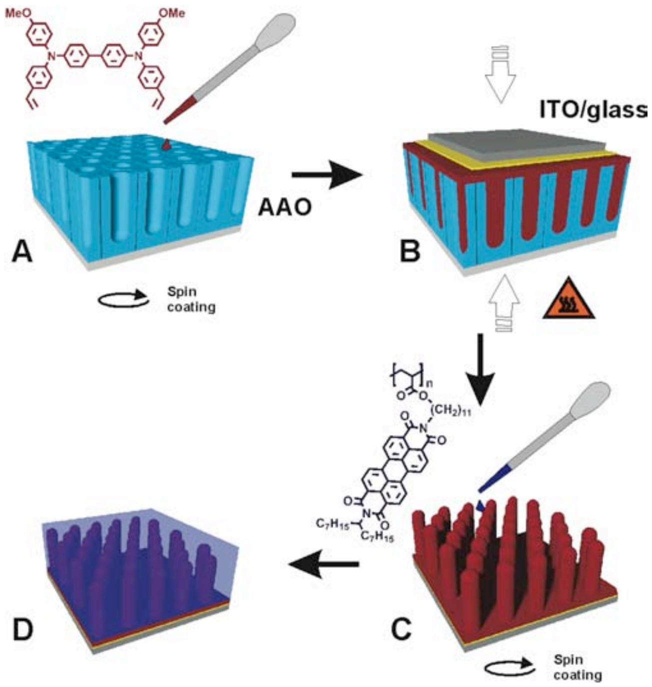

Scheme 1. *Schematic representation of the template-assisted fabrication of well-ordered bulk-heterojunction networks on transparent conductive ITO/glass substrates. (A) AAO template is filled via spin-coating of a* ***DVTPD*** *solution in toluene (3 wt%, 2000 rpm). (B) A prefunctionalized ITO substrate is pressed on the top of the filled template and DVTPD is thermally cross-linked in vacuo at 190 °C for 30 min. (C) Free standing nanorod arrays after selective removal of the supporting AAO template. Back-filling of the voids between the nanorod arrays with electron transporting PPerAcry via spin-coating. (D) Well-ordered bulk heterojunction morphology of non-aggregated cross-linked* ***DVTPD*** *nanorod array on ITO/glass substrates embedded into* ***PPerArcy*** *matrix.*

donor/acceptor morphologies, nanorod arrays have to fulfill several additional requirements besides the successful replication onto a conductive substrate: (i) the electrochemical properties of the donor and acceptor should match, (ii) aggregation and collapsing phenomena of the nanorods should be avoided after the removal of the supporting template to provide a maximal interface and allow a complete embedding and (iii) the nanorods should provide a good resistance against common organic solvents to allow their embedding into an electron-conducting matrix via a solution-based deposition technique. The latter point is important since solution based fabrication methods are though, versatile and inexpensive alternatives to vapor deposition techniques.

We anticipate to use a templating approach to develop routine solution-based preparation methods yielding all-polymer based well-ordered donor/acceptor morphologies. To meet the requirements mentioned above, we used a nanoporous anodic anodized oxide (AAO) template and filled the pores with a thermally cross-linkable donor material based on tetraphenylen-benzidine (TPD). In general TPD moieties are preferred in materials that are used as organic hole-conductors since they provide a better electrochemical stability and charge carrier mobility compared to the simpler triphenylamines.*[38]* As such, TPD based polmyers should provide reasonable properties to justify a the development of a new route towards all-polymer based well-ordered donor/acceptor morph-ologies. Once the templating, the embedding with an electron-conducting material and its thorough characterization of the internal morphology has been achieve, further developments to adopt this approach to the best hole-conducting and electron-conducting materials available have to be initiated. The thermally cross-linkable TPD derivative (**DVTPD**, see **Fig. 1A**) was synthesized in a four-step reaction. Briefly, the dimethoxy substituted TPD moiety was synthesized via two consecutive palladium-catalyzed Buchwald-Hartwig reactions. The two vinyl substituents were introduced by a double Vilsmeier formylation and a subsequent double Wittig reaction (see Supporting Information). The introduction of the two methoxy functionalities in *para* position increases the solubility and the electrochemical stability of the material.*[39]* The functionalization with two vinyl groups allows an efficient initiator-free thermal cross-linking of the material, which was characterized by differential scanning calorimetry (DSC) analysis (see Supporting Information S1). An endothermic peak at 180 °C (i.e. melting point of **DVTPD**) was observed during the first heating curve, which directly led over to an exothermic peak after 180°C indicating the thermally initiated polymerization. In the second heating curve, the absence of the melting peak as well as the polymerization peak demonstrated efficient cross-linking of the **DVTPD**.

For this purpose, a diluted **DVTPD** solution was spin-coated onto the AAO template to minimize the thickness of the **DVTPD** film on top of the AAO membrane. The filled template was pressed onto an ITO/glass substrate, which was pre-functionalized with a monolayer of vinyltrimethoxysilane. The use of this monolayer was crucial in avoiding delamination of the **DVTPD** film from the ITO substrate during all subsequent fabrication steps. Cross-linking via thermal curing at 180°C *in vacuo* for 30 min resulted in the covalent attachement of the **DVTPD** film to the ITO/glass substrate. Freestanding nanorod arrays composed of cross-linked **DVTPD** on ITO were obtained after selective chemical etching of the supporting Al layer and the AAO template using $CuCl_2$ solution and 10 wt% phosphoric acid. To prevent aggregation and collapsing of the rods caused by capillary effects the samples were dried by freeze drying process as reported recently.*[38]* The SEM pictures in **Fig. 1** exemplarily show cross-sections of an empty AAO template (**Fig. 1A**) and the corresponding **DVTPD** replication on ITO/glass (**Fig. 1B**). It can be seen that the polymeric replication nicely fits to the contours of the template. Further, no collapsing of the rods occurred, which is essential for the preparation of well-ordered donor/acceptor morphologies. Noteworthy, the homogenous **DVTPD** film between the rods and the ITO layer can be adjusted and decreased to several nanometers by the spin-coating assisted filling to optimize the surface to volume ratio of the **DVTPD** film. Compared to a smooth spin-coated thin film, the surface area of the nanorod array is increased at least by a factor of 7.

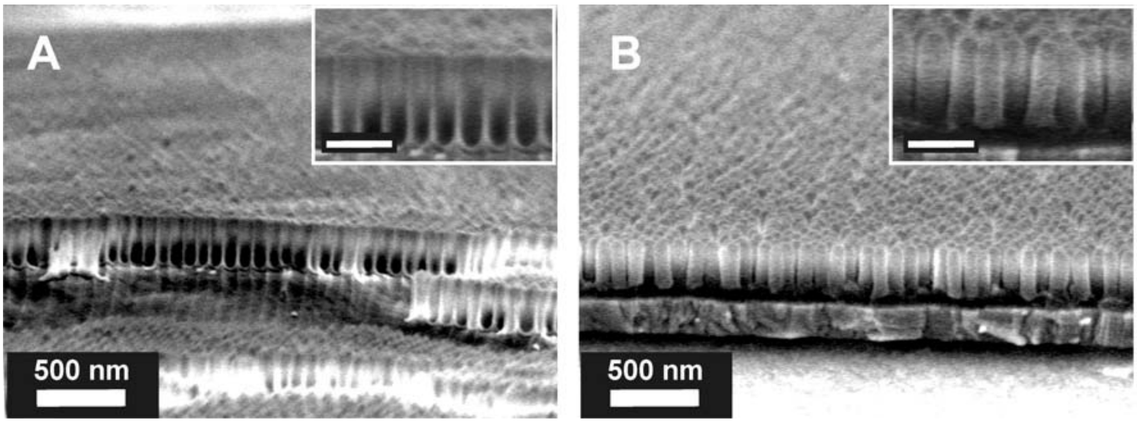

Figure 1. *Cross-sectional SEM images. (A) unfilled AAO template fabricated in 0.3 M oxalic acid of 2 °C at 40 V. (B) Cross-linked DVTPD nanorod arrays on ITO/glass substrate after selective etching of the supporting AAO template. The scale bars of the insets indicate 200 nm.*

For further processing it was essential that the **DVTPD** nanorod arrays are resistant towards organic solvents. As such, the patterned film was shown to withstand rinsing with toluene, which is a good solvent for the **DVTPD** monomer. The UV/vis absorption of the film before and after rinsing with toluene showed no significant change, demonstrating excellent structural integrity of the nanorods as well as quantitative polymerization of the **DVTPD** monomer (**Fig. 2A**). In addition, the electrochemical properties of the patterned DVTPD film on ITO/glass were investigated via cyclovoltammetry analysis. The HOMO and LUMO levels were determined to be -5.2 eV and -2.2 eV, respectively. Because of the more electron-rich TPD moiety, the HOMO and LUMO levels are slightly increased in comparison with those reported for the cross-linked triphenylamine and therefore promises a better electrochemical stability. Also, the energy levels of **DVTPD** match better with the employed electron-conducting poly(perylene bisimide acrylate) (**PPerAcry)** when compared to triphenylamine.*[39]* The reversible shape of the cyclovoltammogram in combination with the determined HOMO and LUMO values, that are in agreement with other TPD derivatives,*[40]* indicate that the good hole-conducting properties of **DVTPD** are maintained after the cross-linking and patterning step.

In order to embed the nanorod arrays into an organic electron-conductor, poly(perylene bisimide acrylate) (**PPerAcry**) introduced by *Thelakkat* and coworkers was selected as the material of choice.*[41]* Unsymmetrical functionalized perylene-bisimide (PBI) derivatives have often been used as electron-conducting materials in organic photovoltaics, owing to their high electron mobilities as well as their high extinction coefficients between 400 and 600 nm.*[39],[42-44]* Furthermore, the swallow-tail substituents ensure excellent solubility in organic solvents. These favorable electronic properties can be combined with good film forming properties when PBIs are attached to a polyacrylate backbone.*[45]* Therefore, the unsymmetrical perylene-3,4:9,10-tetracarboxylic bisimide monomer (**PerAcry**) was synthesized and polymerized. Briefly, the condensation of perylene-3,4:9,10-tetracarboxylic dianhydride with a primary amine yielded the symmetrically swallow-tail *N*-functionalized peylene bisimide, which was converted to an unsymmetrically functionalized PBI following the procedure of partial saponification and conversion with ammonia described by *Langhals.[46]*

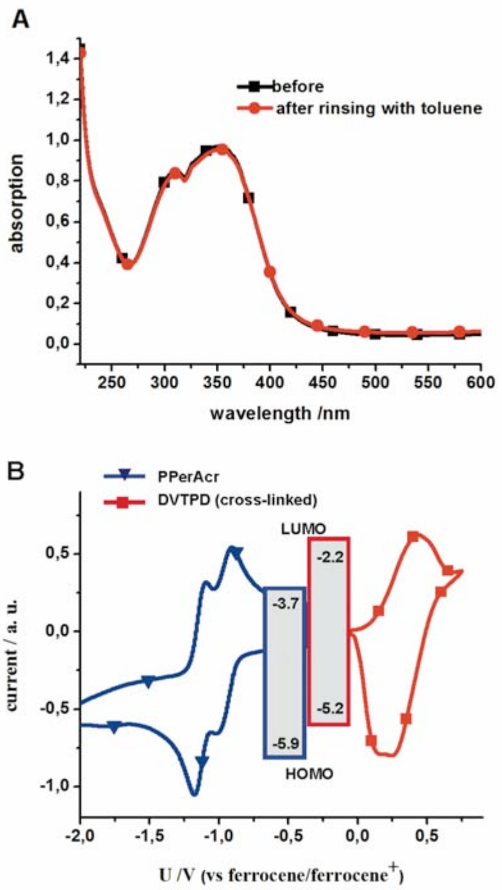

Figure 2. *(A) UV/vis absorption spectra of thermal cross-linked DVTPD nanorod arrays on quartz substrate before and after rinsing with toluene. (B) Cyclic voltammogram of PPerAcry dissolved in 1,2-dichlorbenzene with 0.1 M n-Bu4NPF6 as conducting electrolyte (blue) and cross-linked DVTPD film on ITO in a solution of n-Bu$_4$NPF$_6$ in acetonitrile (0.1 mol L^{-1}).*

Introduction of a hydroxy functionalized alkyl chain at the second imide *via* nucleophilic substitution with the corresponding hydoxylated alkylhalide and a subsequent esterification with acrylic chloride yielded the monomer **PerAcry**. **PerAcry** was then polymerized under free-radical conditions to yield **PPerAcry** with a molecular weight of M_n = 17300 g/mol. Further information about the synthesis and characterization of **PerAcry** and its polymerization can be found in the Supporting Information.

To fill the voids between the nanorods with **PPerAcry**, diluted toluene solutions of **PPerAcry** with varying concentrations were used for spin coating. The procedure was optimized in a way that the physical integrity of the rods was remained, that the space between the rods was completely filled and that the thickness of the homogeneous overstanding **PPerAcry** layer was minimized. Using nanorod arrays that were not subjected to freeze drying already collapsed into bundles before the embedding. This resulted in an inhomogeneous filling and disordered morphologies were formed after spin-coating of **PPerAcry**. SEM images of the obtained morphologies (see Supporting Information) still showed domains of nanorod bundles several hundred nanometers in size that were surrounded by the **PPerAcry** matrix. The images clearly indicated that **PPerAcry** was not infiltrated between the nanorods. Accordingly, these films showed a drastically decreased donor/acceptor interface, highlighting the importance of utilizing non-collapsed freeze-dried nanorod arrays.

In addition, we used transition electron microscopy to investigate nanorod filling and the thickness of the overstanding of **PPerAcry**. The cross-sectional TEM images shown in **Fig. 3** illustrate the

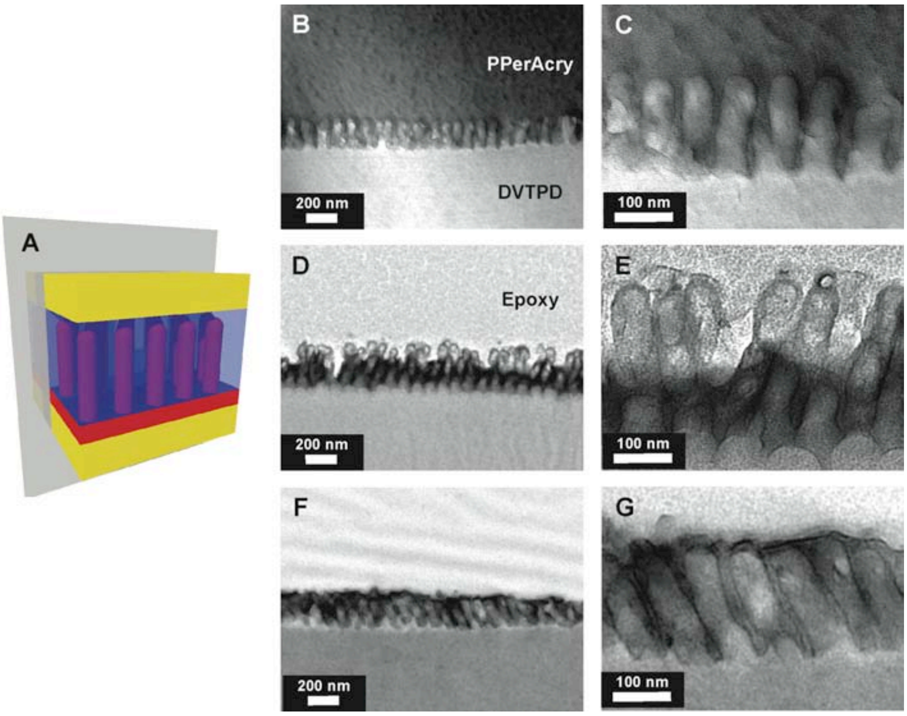

Figure 3. *Schematic representation (A) and cross-sectional TEM micrographs (B-G) of DVTPD nanorods (grey domains) embedded into PPerArcy (black domains) after detaching from ITO substrate, embedding in epoxy resin (white), cutting (thickness of microtomed cuts: 80 nm) and staining with RuO4 for 10 min.*

morphology of freeze-dried **DVTPD** nanorods after **PPerAcry** coating. The samples were detached from the ITO/glass substrate, embedded into epoxy resin and cut prior to TEM measurements. **PPerAcry** domains appear darker than the **DVTPD** rods, which is due to the preferential staining with ruthenium tetroxide.*[39]* **Fig. 3B** show nanorod arrays (length: 175±3 nm, diameter: 53±3, interpore distance: 100±3 nm) after drop casting of a 2.0 wt% **PPerAcry** solution. After evaporation of the solvent *in vacuo* the rods are perfectly embedded in the perylene matrix without aggregating or collapsing into bundles. Further, **PPerAcry** completely infiltrated into the voids of the rods and no air inclusions were observed. Notably, due to the high solvent resistance of the **DVTPD** nanorod layer, no damages were caused by partial dissolving of the rods. However, the thickness of the overstanding **PPerAcry** layer after drop casting was too thick, which is disadvantageous for photovoltaic applications. Therefore, the film thickness of the overstanding layer was optimized by using spin-coating assisted infiltration. Spin-coating (2000 rpm, 1.2 wt% solution) on nanorods arrays (length: 320±5 nm, interpor-distance: 100±3, diameter: 60±2 nm) resulted in a **PPerAcry** layer (~115 nm) thinner than the film thickness provided by the nanorods (**Fig. 3D**). The voids between the nanorods is filled only up to half the length of the nanorods. Noteworthy, the TEM images suggest that the voids of the nanorod arrays are filled from the bottom up and the upper half of the rods is not covered with **PPerAcry**.

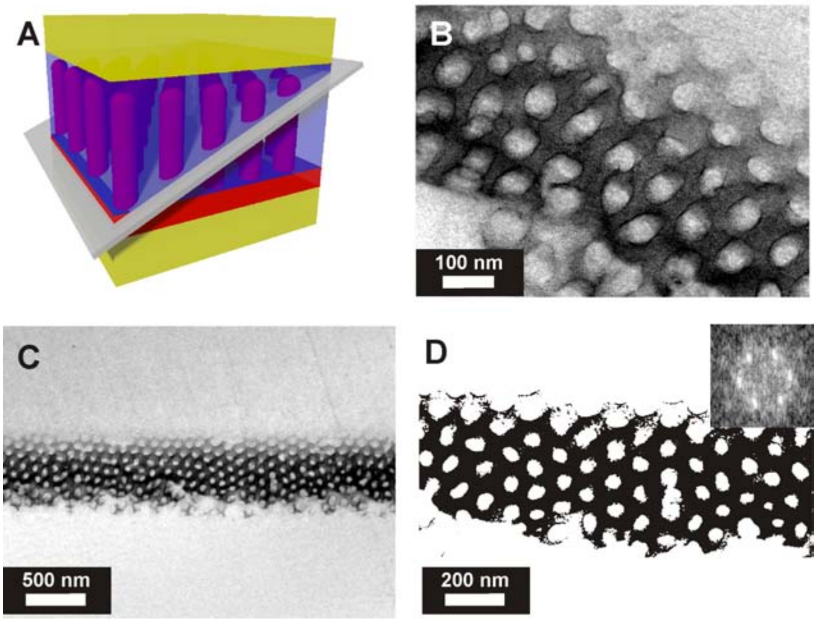

Figure 4. *(A) Schematic diagram (plane of microtomed cuts is visualized in grey) and (B-C) TEM images of patterned DVTPD/PPerAcry morphology. (D) Corresponding binary image showing the nanorods (white) embedded in PPerAcry (black). The inset shows a 2D-FFT analysis of the image.*

This would potentially allow for a regioselective coating of the nanorods with two different materials by two subsequent deposition steps. A complete infiltration with a thin overstanding **PPerAcry** layer was obtained by spin coating slightly thicker solutions (2000 rpm, 1.8 wt% solution) on nanorods with a length of 210±5 nm, diameter of 55±2 nm (**Fig. 3F**). The TEM images visualize the well-ordered and aggregation-free interpenetrating net-work, which exhibits a 9 fold donor/acceptor interface compared to a bilayer structure. In addition to the cross-sectional view (**Fig. 3**), the interpenetrating network was also visualized perpendicular to the axis of the nanorods by TEM of microtomed sections (see **Fig. 4**). The images clearly show the bright **DVTPD** rods embedded in a dark **PPerAcry** matrix. In agreement with the cross-sectional view shown in **Fig. 3F**, the rods are well-aligned perpendicular to the substrate and show no evidence for aggregation. The average center-to-center distance of the embedded rods was determined to be 100±2 nm, which corresponds to the interpore distance of the originally used AAO template. Analysis of the morphology by Fourier-transformation (see **Fig. 4C**) still indicates a hexagonally distribution of the rods, that originates from the hexagonal pore alignment of AAO.

The improved charge separation in the patterned **DVTPD/PPerAcry** layer compared to that of the planar bilayer was confirmed by the photoluminescence (PL) results. The PL intensity of a single **PPerAcry** layer (thickness 50 nm), a planar bilayer and a patterned **DVTPD/PPerAcry** nanorod film on quartz substrates were measured (Figure 4B). The samples were excited at 540 nm, i.e. at a wavelength at which the **PPerAcry** absorbs light due to the electronic S_0-S_1 transition of the PBI

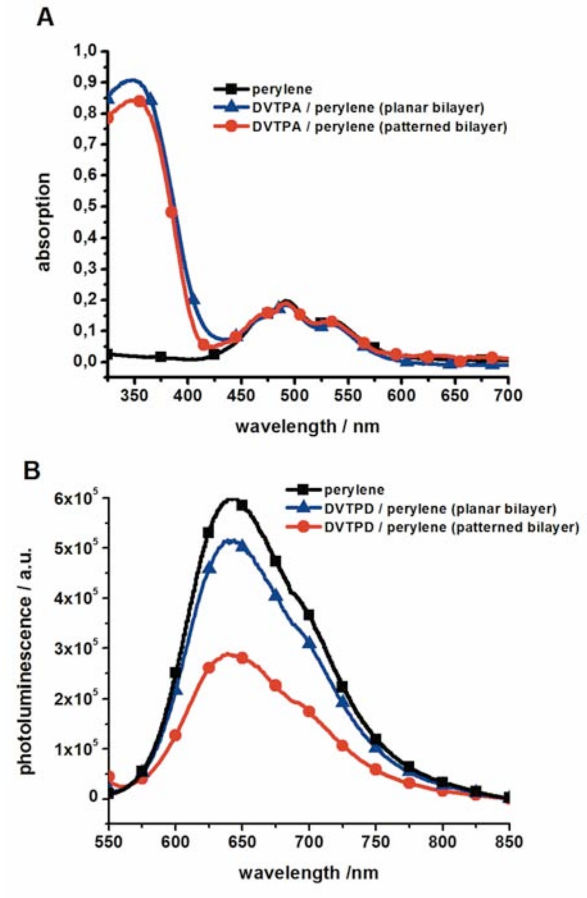

Figure 5. *UV/vis absorption (A) and photoluminescence (B) spectra of thin films on quartz. The photoluminescence was measured at excitation wavelength of λ_{ex} = 540 nm.*

moieties. At this wavelength the **DVTPD** does not show any absorption (see Figure 4A). The PL of **PPerAcry** was quenched by 17 % in the planar bilayer architechture and by remarkable 57 % in the patterned nanorod device, when compared to the pristine **PPerAcry** layer. Since the ratio of the two vibronic transitions of **PPerAcry** at 492 nm and 530 nm is the same in all samples, we exclude effects that influence the PL intensity due to different π-π stacking of the PBI moieties.*[47]* As expected, the PL intensity is only slightly quenched in the planar bilayer device, since most excitons are not generated within the diffusion length to the interface. Due to the increased donor/acceptor interface in the patterned nanorod film, this device showed a more efficient PL quenching, which is indicative for an enhanced charge separation.

We could further show that the presented template-based consecutive multi-coating approach facilitates the fabrication of all-polymer photovoltaic devices. A first demonstrative photovoltaic device whose active layer exhibits a well-ordered morphology, as shown in **Fig. 3F**, was prepared by additional evaporation of a thin LiF and Al layer onto the ordered DVTPD/PPerAcry layer. As such, a demonstrative solar cell array with an active area of six times 1.96 mm^2 was prepared on an indium tin oxide (ITO) covered glass substrate onto which a thin layer of MoO_3 as hole-injection layer was evaporated. The current–voltage curves (see supporting information) were measured under illumination (AM 1.5 illumination intensity of 100 mW cm^{-2}) and in the dark. While no current could be measured in the dark, typical current–voltage characteristics could be recorded under illumination. Even though the performance of the fabricated photovoltaic device was relatively poor (power conversion efficiency = 1.2*10^{-3} %), the fundamental working principle of the templating approach for a solution-based all-polymer solar cell could successfully be demonstrated for the first time. Optimization of hole- and electron-conducting materials, as well as development of a better solar cell preparation provide confidence in reaching improved power conversion efficiency in the near future.

Conclusion

In conclusion, we have shown that the fabrication of well-ordered bulk heterojunction morphologies based on polymeric semiconductors is very feasible by combining an AAO template-based patterning with a solution-based multilayer coating. Free-standing nanorod arrays composed of cross-linked tetraphenylbenzidines (**DVTPD**) were prepared on ITO/glass and were successfully embedded into a poly(perylene bisimide acrylate) matrix by a solution-based coating step. Cross sectional transmission electron microscopy of the interpenetrating donor/acceptor nanorod morphology confirmed that the PPerAcry could be successfully infiltrated into the voids of the fragile nanorod arrays by solution-based spin-coating without causing collapsing effects or destruction of the order of the rods. The increased donor/acceptor interface of the fabricated devices resulted in a remarkable photoluminescence quenching compared to a planar bilayer morphology. Further, the nanorod morphologies ensure continuous pathways for charge extraction, are easily scalable within the range of the exciton diffusion length and promise morphological long-term stability.

The presented template-assisted approach describes a versatile route for the solution-based fabrication of well-ordered polymer/polymer bulk heterojunctions composed of various solution-processable semiconducting polymers. The utilization of shape-defining AAO templates with tailored pore parameters features the precise control of the nanoscopic dimensions of the formed heterojunctions. After presenting a detailed morphological characterization and preliminary characteristics of such fabricated photovoltaic devices based on the model compounds DVTPD and PPerAcry, a thorough study of the photovoltaic characteristics of such fabricated devices by varying the semiconducting polymers and the interfacial area to not only optimize the performance of organic/organic photovoltaic devices but also to provide a detailed understanding of the influence of the interfacial area is anticipated.

Experimental

Instrumentation. All ^{1}H- and ^{13}C-NMR spectra were recorded on a Bruker 300 MHz FT-NMR spectrometer. Chemical shifts (d) were given in parts per million (ppm) relative to TMS. Thermogravimetric analysis (TGA) was performed using a Perkin-Elmer Pyris 6 TGA in nitrogen atmosphere (10 mg of the compound in an aluminum pan). Cyclovoltammetric measurements were performed using an Autolab PGSTAT30 (Eco Chemie) Potentiosat/Galvanostat. Pt wire and Ag/AgCl were used as the counter and reference electrode, respectively. The energy levels for cross-linked **DVTPD** and **PPerAcry** were determined by using the measured oxidation (for the HOMO of **DVTPD**) and reduction (for the LUMO of **PPerAcry**) potentials and assuming the absolute level of ferrocene to be E = -4.8 eV. The energy gaps and the corresponding LUMO (for **DVTPD**) and HOMO (for **PPerAcry**) were determined by using the onset of the absorption spectra. FD mass spectra were measured using a Finnigan MAT 95 mass spectrometer. Gel permeation chromatography (GPC) was used to determine molecular weights and molecular weight distributions, Mw/Mn, of polymer samples. (THF used as solvent; polymer concentration, 2 mg/mL; column setup, MZ-Gel-SDplus 10^2, 10^4 and 10^6 $Å^2$; used detectors, refractive index, UV, and light scattering). SEM images were recorded using a Zeiss Leo 1530 at an acceleration voltage of 3.0 kV for AAO membranes and 0.7 kV for polymeric samples. For detection an Inlens detector was used. UV-Vis spectra were recorded on a Sinco-3100 spectrophotometer. Photoluminescence measurements were performed on an Acton Spectra Pro with a 500 W Xenon light source. TEM measurements were recorded on a Hitachi H-7600 at an acceleration voltage of 100 kV. For the microtoming a MODEL MT-X Ultramicrotome from Boeckeler Instruments, Inc. was used.

Materials. All reagents were purchased from Aldrich, Fluka and Acros and were used without further purification unless otherwise stated. Toluene and tetrahydrofuran (THF) were distilled from sodium/potassium. The syntheses were carried out under argon atmosphere using standard Schlenk techniques. ITO-coated glass substrates with sheet resistance of <10 Ohm/sq were purchased from Präzisions Glas & Optik GmbH, Germany, and were cleaned by ultrasonication in aqueous Helmanex (1.0 wt%), isopropyl alcohol, and acetone. Prior measurements, they were dried with a stream of pressurized N_2 and subjected to O_2 plasma cleaning for 10 min.

Synthesis. The synthetic procedure and characterization of **DVTPD** and **PPerAcry** are given in the Supporting Information.

*Preparation of well-ordered **DVTPD/ PPerAcry** bulk heterojunctions*. AAO membranes were fabricated by a two step anodic oxidation*[48, 49]* of an aluminum sheet in 0.3 M oxalic acid at 40 V. Further information about the AAO fabrication are given in the Supporting Information. The thin AAO templates that are mechanically stabilized by an aluminum layer on the backside were spin-coated with a diluted **DVTPD** solution (3 wt% in toluene, 2000 rpm, 60 s). A 10 wt% **DVTPD** solution in toluene was used for the preparation of samples, which were used for the preparation of ultrathin sections, in order to increase the thickness of the homogenous **DVTPD** layer between nanorods and substrate. This interlayer assured that the morphology of the embedded nanorods is not damaged during the preparation of ultrathin sections later on. The spin-coated templates were carefully stamped onto the substrate (ITO/glass or quartz prefunctionalized with a 1 wt% vinyltrimethoxysilane in THF for 24 h) and subsequently thermally annealed *in vacuo* at 190 °C for 30 min. The aluminum and the AAO were selectively etched away by treatment with aqueous $CuCl_2$ ($c = 0.2$ mol L^{-1}) and aqueous phosphoric acid (10 wt%) respectively. After repeated rinsing and dipping cycles with deionized water, the samples were freeze-dried. The nanorod arrays were embedded into PPerAcry by drop coating or spin-coating of a **PPerAcry** solution in toluene (1-5 wt%) and drying *in vacuo*.

For the preparation of ultra-thin sections for TEM investigations the patterned **DVTPD/PPerAcry** films on ITO/glass substrates were first coated with a thin carbon layer (< 1nm) to prevent swelling and structural damage of the active layer while embedding into epoxy resin.

Subsequently the samples were coated with epoxy resin and thermally cured at 60°C. The active layer was detached form the ITO/glass substrate by dipping into liquid nitrogen. The detached films were carbon-coated, completely embedded into epoxy resin and microtomed to ultra-thin sections (thickness 80 nm). The sections were stained with RuO_4 for 10 min. RuO_4 was produced *in situ* by adding RuO_2 to an aqueous $NaIO_4$ solution.

Acknowledgements

We thank the department of Electron Microscopy at the Max-Planck Institute for Polymer Research providing support for SEM measurements. Prof. Chang-Hee Lee and Seoung-Uk Noh are acknowledged for the fabrication and characterization of photovoltaic devices. The support by the DFG (IRTG 1404) and by the WCU (World Class University) program through the National Research Foundation of Korea funded by the Ministry of Education, Science and Technology (400-2008-0230) are acknowledged. M. S. and M. T. acknowledge funding from the Deutsche Forschungsgemeinschaft (SFB 481) and the European Science Foundation (EUROCORES SOHYDS).

References

[1] F. C. Krebs, *Sol. Energy Mater. Sol. Cells* **2009**, *93*, 394.

[2] F. C. Krebs, S. A. Gevorgyan, J. Alstrup, *J. Mater. Chem.* **2009**, *19*, 5442.

[3] C. N. Hoth, S. A. Choulis, P. Schilinsky, C. J. Brabec, *Adv. Mater.* **2007**, *19*, 3973.

[4] T. Aernouts, T. Aleksandrov, C. Girotto, J. Genoe, J. Poortmans, *Appl. Phys. Lett.* **2008**, *92*, 033306.

[5] C. Brabec, N. Sariciftci, Hummelen, J, *Adv Funct Mater* **2001**, *11*, 15.

[6] S. Gunes, H. Neugebauer, N. Sariciftci, *Chem. Rev.* **2007**, *107*, 1324.

[7] T. Benanti, D. Venkataraman, *Photosynth Res* **2006**, *87*, 73.

[8] X. Yang, J. Loos, *Macromolecules* **2007**, *40*, 1353.

[9] K. Coakley, M. McGehee, *Chem. Mater.* **2004**, *16*, 4533.

[10] A. C. Mayer, S. R. Scully, B. E. Hardin, M. W. Rowell, M. D. McGehee, *Mater. Today* **2007**, *10*, 28.

[11] I. Hill, A. Kahn, Z. Soos, R. Pascal, *Chem. Phys. Lett.* **2000**, *327*, 181.

[12] X.-Y. Zhu, Q. Yang, M. Muntwiler, *Acc. Chem. Res.* **2009**, *42*, 1779.

[13] J.-L. Bredas, J. E. Norton, J. Cornil, V. Coropceanu, *Acc. Chem. Res.* **2009**, *42*, 1691.

[14] D. Wohrle, D. Meissner, *Adv. Mater.* **1991**, *3*, 129.

[15] J. J. M. Halls, C. A. Walsh, N. C. Greenham, E. A. Marseglia, R. H. Friend, S. C. Moratti, A. B. Holmes, *Nature* **1995**, *376*, 498.

[16] G. Yu, J. Gao, J. Hummelen, F. Wudl, A. Heeger, *Science* **1995**, *270*, 1789.

[17] W. Ma, C. Yang, X. Gong, K. Lee, A. Heeger, *Adv Funct Mater* **2005**, *15*, 1617.

[18] M. Reyes-Reyes, K. Kim, J. Dewald, R. Lopez-Sandoval, A. Avadhanula, S. Curran, D. Carroll, *Org. Lett.* **2005**, *7*, 5749.

[19] Y. Liang, D. Feng, Y. Wu, S.-T. Tsai, G. Li, C. Ray, L. Yu, *J Am Chem Soc* **2009**, *131*, 7792.

[20] Y. Liang, Z. Xu, J. Xia, S.-T. Tsai, Y. Wu, G. Li, C. Ray, L. Yu, *Adv. Mater.* **2010**, *9999*.

[21] W. Cai, X. Gong, Y. Cao, *Sol. Energy Mater. Sol. Cells* **2010**, *94*, 114.

[22] H. Hoppe, N. S. Sariciftci, *Adv Polym Sci* **2008**, *214*, 1.

[23] N. Haberkorn, M. C. Lechmann, B. H. Sohn, K. Char, J. S. Gutmann, P. Theato, *Macromol Rapid Comm* **2009**, *30*, 1146.

[24] K. Coakley, Y. Liu, M. McGehee, K. Frindell, G. Stucky, *Adv Funct Mater* **2003**, *13*, 301.

[25] S. S. Williams, M. J. Hampton, V. Gowrishankar, I.-K. Ding, J. L. Templeton, E. T. Samulski, J. M. DeSimone, M. D. McGehee, *Chem. Mater.* **2008**, *20*, 5229.

[26] E. Crossland, M. Nedelcu, C. Ducati, S. Ludwigs, M. Hillmyer, U. Steiner, H. Snaith, *Nano Lett.* **2009**, *9*, 2813.

[27] K. Shankar, J. Bandara, M. Paulose, H. Wietasch, O. Varghese, G. Mor, T. LaTempa, M. Thelakkat, C. Grimes, *Nano Lett.* **2008**, *8*, 1654.

[28] G. Mor, K. Shankar, M. Paulose, O. Varghese, C. Grimes, *Nano Lett.* **2006**, *6*, 215.

[29] M. Paulose, K. Shankar, O. Varghese, G. Mor, C. Grimes, *J. Phys. D: Appl. Phys.* **2006**, *39*, 2498.

[30] G. K. Mor, S. Kim, M. Paulose, O. K. Varghese, K. Shankar, J. Basham, C. A. Grimes, *Nano Lett.* **2009**, *9*, 4250.

[31] E. Crossland, M. Kamperman, M. Nedelcu, C. Ducati, U. Wiesner, D. Smilgies, G. Toombes, M. Hillmyer, S. Ludwigs, U. Steiner, H. Snaith, *Nano Lett.* **2008**, *9*, 2807.

[32] I. Botiz, S. B. Darling, *Macromolecules* **2009**, *42*, 8211.

[33] J. S. Kim, Y. Park, D. Y. Lee, J. H. Lee, J. H. Park, J. K. Kim, K. Cho, *Adv Funct Mater* **2010**, *20*, 540.

[34] J. I. Lee, S. H. Cho, S.-M. Park, J. K. Kim, J. K. Kim, J.-W. Yu, Y. C. Kim, T.Russell, *Nano Lett.***2008**,*8*, 2315.

[35] M. Fu, Y. Zhu, R. Tan, G. Shi, *Adv. Mater.* **2001**, *13*, 1874.

[36] D. Park, B. Kim, M. Jang, K. Bae, J. Joo, *Appl. Phys. Lett.* **2005**, *86*, 113116.

[37] M. Aryal, K. Trivedi, W. W. Hu, *Acs Nano* **2009**, *3,* 3085.

[38] N. Haberkorn, J. S. Gutmann, P. Theato, *Acs Nano* **2009**, *3*, 1415.

[39] M. Sommer, S. Lindner, M. Thelakkat, *Adv Funct Mater* **2007**, *17*, 1493.

[40] Y. Shirota, H. Kageyama, *Chem. Rev.* **2007**, *107*, 953.

[41] S. Lindner, M. Thelakkat, *Macromolecules* **2004**, *37*, 8832.

[42] M. Sommer, Andreas S. Lang, Thelakkat, Mukundan, *Angew. Chem. Int. Ed.* **2008**, *47*, 7901.

[43] M. Sommer, S. Hüttner, S. Wunder, M. Thelakkat, *Adv. Mater.* **2008**, *20*, 2523.

[44] Q. Zhang, A. Cirpan, T. Russell, T. Emrick, *Macromolecules* **2009**, *42*, 1079.

[45] S. Huettner, M. Sommer, M. Thelakkat, *Appl. Phys. Lett.* **2008**, *92*, 093302.

[46] H. Kaiser, J. Lindner, H. Langhals, *Chem. Ber.* **1991**, *124*, 529.

[47] S. Huettner, M. Sommer, A. Chiche, G. Krausch, U. Steiner, M. Thelakkat, *Soft Matter* **2009**, *5*, 4206.

[48] H. Masuda, K. Fukuda, *Science* **1995**, *268*, 1466.

[49] H. Masuda, K. Yada, A. Osaka, *Jpn. J. Appl. Phys.* **1998**, *37*, L1340.

Supporting Information

Fabrication of AAO templates. High purity aluminum (99.997 %, 0.1 mm thick) purchased from Alfa Aesar was cleaned by sonification treatment in isopropanol and acetone respectively followed by an electropolishing step in a mixture of ethanol and perchloric acid (v/v 4:1) at a current density of 300-350 mA/cm^{-1} for 1 min at 0 °C. Subsequently the samples were rinsed with deionized water, isopropanol and acetone. To obtain well-ordered porous templates, the anodization was performed in a two-step process. The anodization steps were performed in a self-build apparatus. Briefly, the aluminum sheets were mounted on a copper plate serving as the anode. A radial area of 2.27 cm^2 was exposed to an aqueous acidic solution. A platinum wire was used as the cathode. The apparatus was surrounded by a cryostatic bath to control the temperature during anodization and the electrolyte solution was rigorously stirred during anodization. The anodization voltage is controlled by a power supply unit with an integrated USB interface (model: EA-PS 8360-10 DT; manufacturer: EA Elektro-Automatik, Germany). Anodization transients were measured using a multimeter and recorded with an attached computer. Anodization was performed in an aqueous solution of oxalic acid (c = 0.3 mol/L) at 40.0 V and 2±1 °C. In the first step, aluminum was anodized for 6 h, followed by an etching step in aqueous solution of chromic acid (1.8 wt%) and phosphoric acid (6.0 wt%) at 60 °C for 12 h. To obtain AAO templates with a thickness below 500 nm, the second anodization was performed for a short period under the same conditions like the first anodization step. Due to temperature fluctuations, it is more precisely to control the resulting thickness of the template by controlling the total charge, which is used for the anodization. The AAO templates are cleaned by rinsing with deionized water, isopropanol and acetone and were stored in an acetone bath. Pore widening was performed in aqueous phosphoric acid (5 wt%) at 25 °C.

Synthesis of N,N′-bis(4-methoxy-phenyl)-N,N′-bis(4-vinylphenyl- (1,1′-biphenyl)-4,4′-diamine) (DVTPD).

General procedure for *Buchwald-Hartwig* arylation. Tris(di-benzylideneacetone) dipalladium(0) (Pd_2dba_3) (2 mol% according to the amine reagent) and 1,1'-bis(diphenylphosphino)-ferrocene (4 mol% according to the amine reagent) were dissolved in toluene under argon and degassed by two freeze-pump-thaw cycles. This activated catalyst was then added to a degassed mixture of the bromoaryl compound (1.0 eq of bromo units), the aromatic amine (1.0 eq) and sodium-*tert*-butylate (2.8 eq) in toluene. The mixture was stirred for 15 h at 90 °C. After cooling down to room temperature the reaction was quenched by adding 5 mL of methanol, diluted with diethylether and washed twice with brine and water respectively. The combined aqueous phase was extracted with diethylether twice. The combined organic phase was dried with $MgSO_4$, filtered and the solvent was evaporated under reduced pressure. The residue was purified by column chromatography on silica gel with petrol ether/ethyl acetate (9:1 v/v).

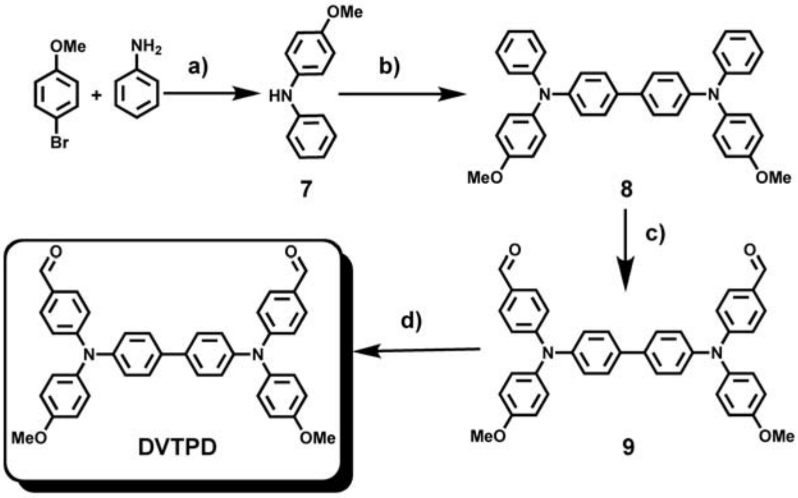

Scheme S1. *Synthetic route of N,N′-bis(4-methoxyphenyl)-N,N′-bis(4-vinylphenyl- (1,1′-biphenyl)-4,4′-diamine) (**DVTPD**). (a) and (b) 0.02 eq. Pd$_2$dba$_3$, 0.04 eq. DPPF, 2.8 eq. sodium-tert-butylate, toulene, 15 h, 90 °C, (c) 12.0 eq. POCl$_3$, 19 eq. DMF, 5 h, 90°C, (d) 5.0 eq. MePh$_3$P$^+$Br$^-$, 5.0 eq. KOtertBu, abs. THF.*

Synthesis of *N*-(4-methoxyphenyl)-*N*-phenyl-amine (7). *N*-(4-methoxy-phenyl)-*N*-phenyl-amine was synthesized according to the general procedure described above starting from 4-bromoanisol and aniline (yield 86 %).

^{1}H NMR (300 MHz, CDCl$_3$): δ= 3.79 (s, 3H, -OMe), 5.50 (s, br, 1H, NH), 6.80-6.91 (m, 4H, Ar-H), 7.02 -7.12 (m, 2H, Ar-H), 7.21 (t, 2H, $^{3}J_{H\text{-}H}$= 8.5 Hz, Ar-H).

^{13}C-NMR (75 MHz, CDCl$_3$): δ/ppm= 55.6, 114.7, 115.7, 119.6, 122.2, 129.3.

Synthesis of *N,N′*-bis(4-methoxy-phenyl)-*N,N*-bisphenyl-1,1′-bisphenyl-4,4′-diamine (8). *N,N′*-bis(4-methoxyphenyl)-*N,N*-bisphenyl-1,1′-bis-phenyl-4,4′-diamine was synthesized according to the general procedure for *Buchwald-Hartwig* arylation described above starting from *N*-(4-methoxyphenyl)-*N*-phenyl-amine and 4,4′-dibromodiphenyl (yield 92%).

^{1}H NMR (300 MHz, CDCl$_3$): δ/ ppm= 3.80 (s, 6H, -OMe), 6.85 (d, 4H, $^{3}J_{H\text{-}H}$= 8.7 Hz, Ar-H), 6.96 (t, 2H, $^{3}J_{H\text{-}H}$= 8.5 Hz, Ar-H$_{para}$), 7.04-7.13 (m, 12H, Ar-H), 7.22 (t, 4H, $^{3}J_{H\text{-}H}$= 8.5 Hz, Ar-H), 7.40 (d, 4H, $^{3}J_{H\text{-}H}$= 8.5 Hz, Ar-H).

^{13}C-NMR (75 MHz, CDCl$_3$): δ/ppm= 55.6, 114.7, 115.7, 119.6, 122.2, 129.3.

Synthesis of *N,N′*-bis(4-methoxyphenyl)-*N,N′*-bis(4-formyl-phenyl-(1,1′-biphenyl)-4,4′-diamine) (9). According to the general procedure previously described for DVTPA.[3] *N,N′*-bis(4-methoxyphenyl)-*N,N′*-bis(4-formylphenyl-(1,1′-biphenyl)-4,4′-diamine) was synthesized *via* a *Vilsmeier-Haack* formylation starting from *N,N′*-bis(4-methoxyphenyl)-*N,N*-bisphenyl-1,1′-bisphenyl-4,4′-diamine (**8**). The product was obtained as a yellow crystalline powder (yield 61%).

^{1}H NMR (300 MHz, CDCl$_3$): δ/ppm= 3.81 (s, 6H, -OMe), 6.90 (d, 4H, $^{3}J_{H\text{-}H}$= 8.5 Hz, Ar-H), 6.99 (d, 2H, $^{3}J_{H\text{-}H}$= 8.5 Hz, Ar-H), 7.13 (d, 4H, Ar-H), 7.20 (d, 4H, $^{3}J_{H\text{-}H}$= 8.5 Hz, Ar-H), 7.49 (d, 4H, $^{3}J_{H\text{-}H}$= 8.5 Hz, Ar-H), 7.66 (d, 4H, $^{3}J_{H\text{-}H}$= 8.5 Hz, Ar-H), 9.77 (s, 2H, Ar-C(=O)H).

^{13}C-NMR (75 MHz, CDCl$_3$): δ/ppm= 55.5, 115.2, 118.6, 125.7, 127.9, 128.5, 128.7, 131.4, 136.4, 136.7, 145.4, 153.4, 157.6, 190.4.

Synthesis of *N,N′*-bis(4-methoxyphenyl)-*N,N′*-bis(4-vinylphenyl-(1,1′-biphenyl)-4,4′-diamine) (DVTPD). DVTPD was synthesized via a *Wittig* reaction[3] starting from *N,N′*-bis(4-methoxyphenyl)-*N,N′*-bis(4-formyl-phenyl-(1,1′-biphenyl)-4,4′-diamine) (**9**). After purification by column chromatography and recrystallization from acetone **DVTPD** was obtained as a yellow solid in a yield of 81%.

^{1}H NMR (300 MHz, CDCl$_3$): δ/ppm= 3.79 (s, 6H, -OMe), 5.12 (d, 2H, $^3J_{H\text{-}H}$= 10.8 Hz, (Ar)CH=C$\underline{\text{H}}_{\text{cis}}H_{\text{trans}}$, 5.61 (d, 2H, $^3J_{H\text{-}H}$= 17.7 Hz, (Ar)CH=CH$_{\text{cis}}\underline{\text{H}}_{\text{trans}}$), 6.64 (dd, 2H, $^3J_{H\text{-}H}$= 17.7 Hz, $^3J_{H\text{-}H}$= 10.8 Hz (Ar)C$\underline{\text{H}}$=CH$_{\text{cis}}$H$_{\text{trans}}$), 6.84 (d, 4H, $^3J_{H\text{-}H}$= 8.5 Hz, Ar-$\underline{\text{H}}$), 7.00 (d, 4H, $^3J_{H\text{-}H}$= 8.5 Hz, Ar-H), 7.06 (d, 4H, $^3J_{H\text{-}H}$= 8.5 Hz, Ar-$\underline{\text{H}}$), 7.09 (d, 4H, $^3J_{H\text{-}H}$= 8.5 Hz, Ar-$\underline{\text{H}}$), 7.27 (d, 4H, $^3J_{H\text{-}H}$= 8.5 Hz, Ar-$\underline{\text{H}}$), 7.40 (d, 4H, $^3J_{H\text{-}H}$= 8.5 Hz, Ar-$\underline{\text{H}}$).

^{13}C-NMR (75 MHz, CDCl$_3$): *δ*/ppm= 55.5, 11.8, 114.8, 122.5, 123.2, 127.0, 127.2, 127.4, 131.2, 134.3, 136.2, 140.4, 146.7, 147.7, 156.3.

***Synthesis of poly(perylene diimide acrylate)* (PPerAcry).**

Synthesis of *N,N'*-Di(1-Hepyloctyl)-perylene-3,4,9,10-tetracarboxylic bisimide (2). A mixture of 28.2 g (71.7 mmol) of perylene-3,4,9,10-tetracarboxylic dianhydride (**1**), 35.9 g (157.8 mmol, 2.2 eq.) of 8-aminopentadecane, 97.6 g (1.43 mol, 20 eq.) of imidazole and 12.6 g (57.4 mmol, 0.8 eq.) of zinc acetate were stirred under argon for 4 h at 170 °C. The mixture was cooled to room temperature, dissolved in isopropanol (500 mL) and precipitated in 2 N HCl (500 mL). The precipitation was filtered off, washed with diionized water and dried in vacuo. The crude product was purified by coluum chromatography (CHCl$_3$/PE 3:7) to yield 47.6 g (82 %) of a red solid.

^{1}H NMR (300 MHz, CDCl$_3$): δ/ppm = 0.79 (t, ^{3}J = 6.8 Hz, 12H), 1.19-1.28 (m, 40H), 1.84 (m, 4H), 2.22 (m, 4H), 5.16 (m, 2H), 8.57-8.64 (m, 8H). MS (m/z, FD): [M+H]$^+$ = 811.5 (100%). Analy. calcd. for $C_{54}H_{70}N_2O_4$; C: 79.96, H: 8.70; N: 3.45; found: C: 76.90; H: 8.85, N: 3.46.

Synthesis of *N*-(1-Heptyloctyl)-perylene-3,4,9,10-tetracarboxylic-3,4-anhydride-9,10-imide (**3**). 2.0 g (2.47 mmol) of *N,N'*-Di(1-Hepyloctyl)perylene-3,4,9,10-tetracarboxylic bisimide (**2**) were dissolved in *tert*-butanol (30 mL) and heated up to 110 °C. 0.42 g (74 mmol, 30 eq.) of KOH powder were added to the solution and vigorously stirred for 12 min. The reaction was quenched by pouring into acidic acid. The mixture was extracted with chloroform, dried over MgSO$_4$ and the solvent was removed *in vacuo*. Purification *via* coluum chromatography (CHCl$_3$) yielded 0.53 g (36 %) of **3** as a red solid.

^{1}H NMR (300 MHz, CDCl$_3$): δ/ppm = 0.80 (t, ^{3}J = 6.8 Hz, 6H), 1.19-1.30 (m, 20H), 1.85 (m, 2H), 2.19 (m, 2H), 5.16 (m, 1H), 8.58-8.66 (m, 8H). MS (m/z, FD): [M]$^+$ = 601.9 (100%).

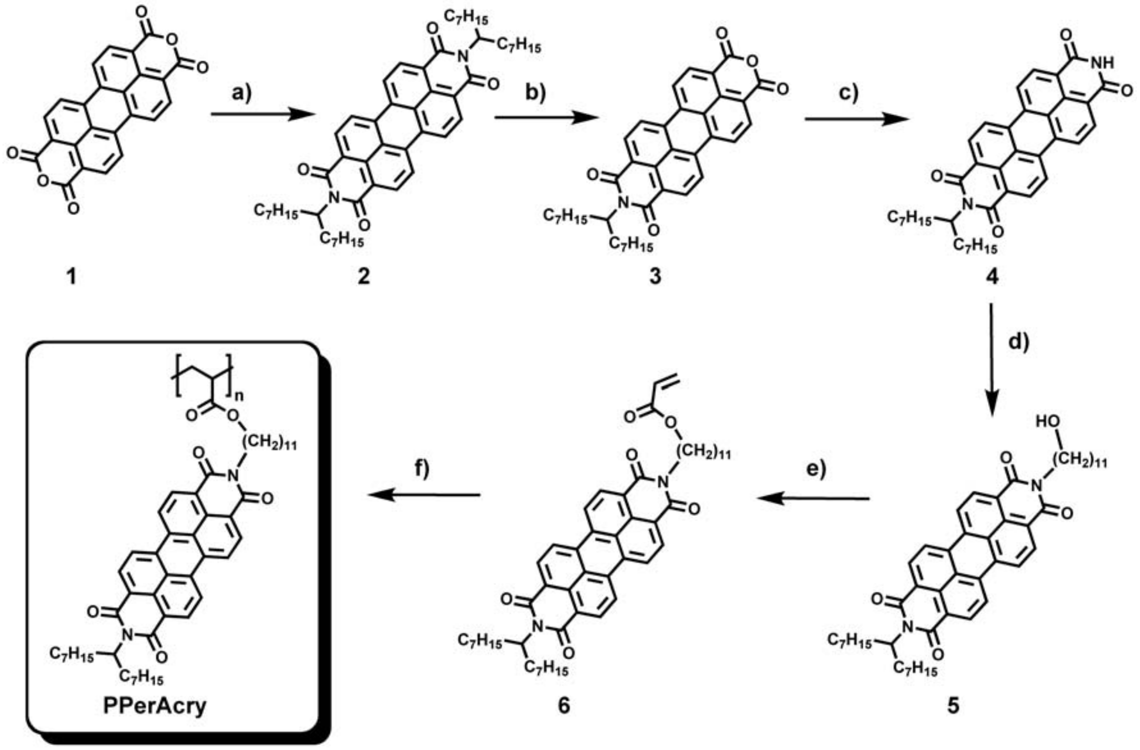

Scheme S2. *Synthetic route of poly(perylene diimide acylate) (**PPerAcry**). a) 2.2 eq. 8-amino-pentadecane, 20 eq. imidazole, 0.8 eq. zinc acetate, 4h, 170 °C, (b) 30 eq. KOH, tert-butanol, 12 min, 110 °C, (c) NH_4OH, K_2CO_3, 90 °C, (d) 33 eq. 1-bromo-11-hydroxy-undecane, 28 eq. K_2CO_3, DMF, 24 h, 100 °C, (e) 1.3 eq. triethylamine, 1.2 eq. acryl chloride, diethyl ether, room temperature, 12 h, (f) AIBN, 1,2-dichlorobenzene, 14 h, 85 °C.*

Synthesis of *N*-(1-Heptyloctyl)-perylene-3,4,9,10-tetracarboxylic-bisimide (**4**). 3.5 g (5.82 mmol) *N*-(1-Heptyloctyl)-perylene-3,4,9,10-tetra-carboxylic-3,4-anhydride-9,10-imide (**3**) were axdded to aqueous NH_4OH solution (3 wt%, 160 mL) and stirred at 90°C for 1 h. 1.2 g of K_2CO_3 were added and the mixture was stirred for another 2 h at 90°C. After cooling to room temperature the red solid was collected by vacuum filtration and washed with aqueous K_2CO_3 (2wt%). The solid residue was suspended in deionized water and 1N HCl, filtered off again and dried under reduced pressure. The crude product was purified by column chromatography ($CHCl_3$/EtOH 20:1). 2.2 g (3.6 mmol, 62 %) of the unsymmetrical bisimide **4** were obtained as a red solid.

^{1}H NMR (300 MHz, $CDCl_3$): δ/ppm = 0.68 (t, ^{3}J = 6.8 Hz, 6H), 1.08-1.18 (m, 20H), 1.71-1.76 (m, 2H), 2.08-2.13 (m, 2H), 5.04 (m, 1H), 8.37-8.47 (m, 8H). MS (m/z, FD): $[M]^+$ = 601.0 (100%).

Synthesis of *N*-(1-Heptyloctyl)-N'-(11-hydroxyundecan)-perylene-3,4,9,10-tetracarboxylic-bisimide (**5**). 0.9 g (1.5 mmol) of **4**, 12.4 g (49.4 mmol, 33 eq.) of 1-bromo-11-hydroxy-undecane and 5.73 g (41.5 mmol, 28 eq.) K_2CO_3 were dissolved in 50 mL of dry DMF and stirred at 100 °C for 24 h. After cooling to room temperatur the mixture was poured into deionized water and 400 mL of 1N HCl were slowly added. The precipitation was collected by vacuum filtration, washed with water (3x50 mL) and dried *in vacuo*. The crude product was purified by column chromatography (CH_2Cl_2 pure) to yield 0.68 g (0.89 mmol, 57 %) of **5**.

^1H NMR (300 MHz, $CDCl_3$): δ/ppm = 0.80 (t, ^3J = 6.8 Hz, 6H), 1.08-1.18 (m, 26H), 1.52-1.66 (m, 8H), 1.81-1.86 (m, 2H), 2.20-2.24 (m, 2H), 3.61 (t, 2H), 4.12 (m, 6H), 5.04 (m, 1H), 8.51-8.65 (m, 8H). MS (m/z, FD): $[M]^+$ = 771.5.

Synthesis of *N*-(1-Heptyloctyl)-N'-(11-acryloyloxyundecan)-perylene-3,4,9,10-tetracarboxylic-bisimide (**6**). 0.68 g (0.88 mmol) of **5** and 0.2 mL (1.47 mmol, 1.3 eq.) triethylamine were dissolved in 30 mL of anhydrous diethyl ether under schlenk conditions. 0.1 mL (1.06 mmol, 1.2 eq.) of acryl chloride were slowly added while vigorously stirring. The mixture was stirred at room temperature overnight. After diluting with diethyl ether the suspension was filtered over celite and the filtrate was dried under reduced pressure. Column chromatographic purification (petrol ether/dioxane 5:1) afforded 0.54 g of the perylene diimide acrylate **6**.

^1H NMR (300 MHz, $CDCl_3$): δ/ppm = 0.80 (t, ^3J = 6.8 Hz, 6H), 1.18-1.26 (m, 26H), 1.52-1.66 (m, 8H), 1.81-1.86 (m, 2H), 2.21-2.28 (m, 2H), 4.12 (m, 8H), 5.04 (m, 1H), 5.79 (d, J= 10.7 Hz, 1H), 6.09 (dd, J= 10.7 Hz, J= 17.8 Hz, 1H), 6.37 (d, J= 17.8 Hz, 1H), 8.51-8.65 (m, 8H). MS (m/z, FD): $[M]^+$ = 824.7.

Synthesis of poly(perylene bisimide acrylate) (PPerAcry). 400 mg of perylene bisimide acrylate (*6*) and 2.63 mg of AIBN were dissolved in 600 µL of 1,2-dichlorbenzene. The mixture was degassed by two freeze/thaw cycles and stirred under argon atmosphere for 14 h at 85°C.

The mixture was cooled down to room temperature, diluted with THF and precipitated in acetone (3 times). After centrifugation and drying at 50 °C *in vacuo* 280 mg of poly(perylene acrylate) were obtained (70 % yield, M_n = 17300 g/mol, PDI = 1.5 (GPC).

^1H NMR (300 MHz, $CDCl_3$): δ/ppm = 8.01 (m, br, 8H), 5.08 (s, 1H), 4.06 (s, br, 6H), 2.86 (m, 1H), 2.20 (m, br, 2H), 1.90 (m, br, 2H), 1.62 (m, 10H), 1.10-1.48 (m, 28H), 0.81 (m, br, 6H).

Solar cell Preparation and Characterization. A pre-etched ITO substrate was cleaned by sonication in isopropanol, methanol, acetone and DI water respectively and a thin layer of MoO_3 as hole-injection layer was evaporated on the substrate by chemical vapor deposition. For the template-based fabrication of a well-ordered active layer an AAO template (length: 175±3 nm, diameter: 53±3, interpore distance: 100±3 nm) was spin-coated with a diluted **DVTPD** solution (3 wt% in toluene, 2000 rpm, 60 s). The spin-coated templates were carefully stamped onto the substrate and subsequently thermally annealed *in vacuo* at 190 °C for 30 min. The aluminum and the AAO were selectively etched away by treatment with aqueous $CuCl_2$ (c = 0.2 mol L^{-1}) and aqueous phosphoric acid (10 wt%) respectively. After repeated rinsing and dipping cycles with deionized water, the samples were freeze-dried. The nanorod arrays were embedded into **PPerAcry** by spin-coating of a **PPerAcry** solution in toluene (1.8 wt%, 2000 rpm) and drying *in vacuo*. Then, a thin LiF layer, which served as an electron injection layer (EIL), was evaporated.

Finally, a 100-nm-thick Al layer was deposited onto the LiF layer. The current–voltage measurements for the devices were performed on a Keithley 237 instrument.

The device performances were characterized under uniform illumination (AM 1.5G illumination intensity of 100 mW cm^{-2}) using a solar simulator (Newport, 91160A). The I-V curve is shown in **Figure S4.**

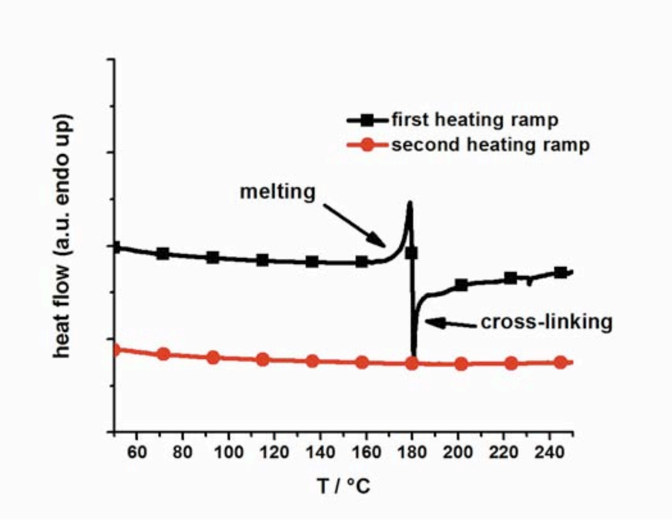

Figure S1. *Differential Scanning Calorimetry (DSC) heating curves of* ***DVTPD***. *The first heating curve (black) illustrates the endothermic melting at 175 °C and the exothermic cross-linking peak at 180 °C. The second heating curve did not show any peak indicating the complete cross-linking of the material. The ramp scan was 10 K min*$^{-1}$.

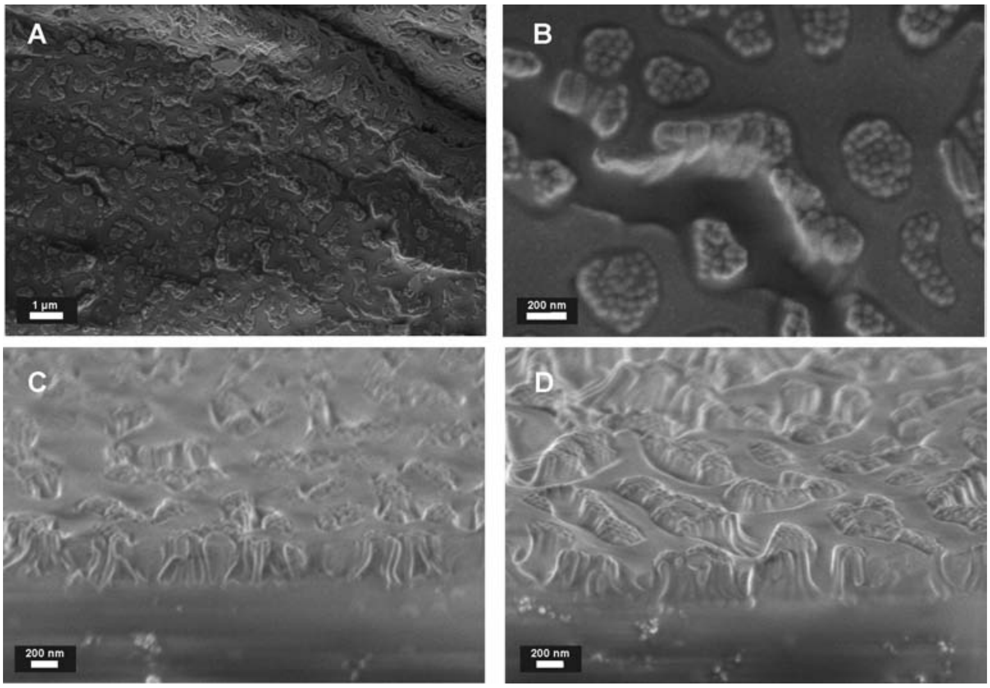

Figure S2. *SEM images of non-freeze dried* ***DVTPD*** *nanorod bundles after spin-coating of* ***PPerAcry****.*

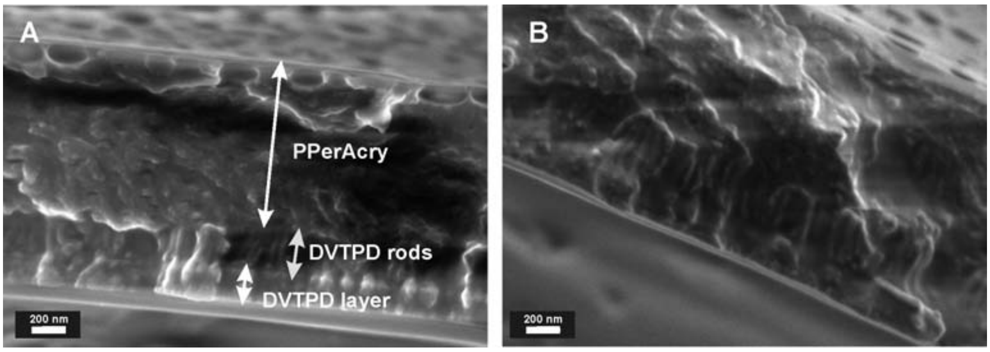

Figure S3. *Cross-sectional SEM images of* ***DVTPD*** *nanorods that were embedded into a PPerAcry matrix by drop-casting. Visualization by SEM without staining only resulted in a low contrast between* ***DVTPD*** *and* ***PPerAcry*** *and therefore makes a precise characterization of the resulting morphology difficult. A better contrast was obtained after staining and performing TEM for visualization (see Figure 3 and 4).*

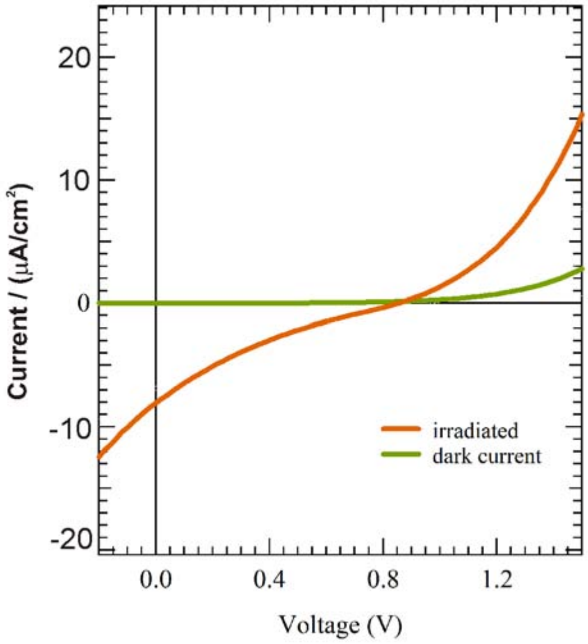

Figure S4. *I-V-characteristics of a nanostructured ITO/MoO_3/cross-linked DVTPD/PPerAcry/LiF/Al device. The measurements were carried out under white light illumination (100 mW cm^{-2}) in a N_2 atmosphere.*

5.4 Fabrication of Hierarchically Branched Polymeric Nanorod Arrays by Utilizing Branched Alumina Templates

*By Niko Haberkorn, Patrick Theato**

[*] Patrick Theato, Niko Haberkorn
Institute of Organic Chemistry, University of Mainz
Duesbergweg 10-14, 55099 Mainz, Germany
E-mail: theato@uni-mainz.de

Niko Haberkorn
Max Planck Institute for Polymer Research
Ackermannweg 10, 55128 Mainz, Germany

Patrick Theato
School of Chemical and Biological Engineering, WCU Program of Chemical Convergence for Energy & Environment (C2E2), College of Engineering, Seoul National University, Seoul, Korea

Abstract.
In this paper we demonstrate a template-assisted method for the fabrication of well-ordered arrays of hierarchical branched mesoscopic structures composed of a thermally cross-linkable 4,4'-divinyltriphenylamine. Anodic aluminum oxide (AAO) membranes with hierarchical branched nanopores are fabricated by an asymmetric two-step anodization process that facilitates the independent length variation of each hierarchical substructure. The polymeric replicas that were obtained after solution-based infiltration, thermal cross-linking and selective removal of the template, show remarkable similarities with interesting biostructures such as the leaf surface of Lotus or the feet of a gecko. Further the mesoscopic structures composed of the semiconducting triphenylamine derivative provide a large surface and may find application in sensors or as building blocks in organic photovoltaic.

The fabrication of two-dimensional periodic arrays of polymeric shape-anisotropic nanostructures, like nanorods and nanotube, has attracted a lot of research interest in the past few years. Due to their extraordinary properties and the development and improvement of patterning techniques with a high lateral resolution, such periodic arrays of polymeric nanostructures have found application in various research fields like superhydrophobic surfaces,*[1-4]* dry adhesives,*[3-5]* sensors,*[6, 7]* actuators,*[8]* tissue engineering,*[9, 10]* data storage,*[11]* and efficient batteries.*[12]* In addition to photolithographic*[13]* and soft lithographic*[14]* techniques hard nanoporous templates like anodic aluminum oxide (AAO), whose pores can be used as molds for organic and polymeric materials, are a versatile toolbox for the fabrication of such well-ordered nanorod arrays with tunable dimensions. AAO templates provide well-aligned pores with a narrow size distribution and can be fabricated by a two-step anodization process.*[15, 16]* Their pore parameters can be tuned by varying the experimental parameters for the anodization step, resulting in adjustable pore lengths (several nanometer up to 100 µm), pore diameters (10 nm to 300 nm) and inter-pore distances (60 nm to 500 nm).*[17]* In addition, the fabrication of AAO templates is cost-effective, allows a high-throughput patterning of organic materials and features a superb thermal- and solvent-resistance.

Besides conventional arrays of nanostructures, which consist of rods or tubes with a homogeneous shape along their axis, arrays of hierarchically branched nanostructure are gaining more and more importance in order to broaden the applicability of nanostructured arrays.*[4, 18, 19]* In particular the fabrication of multibranched nanorod arrays was inspired in order to mimic the topography of biological surfaces. For instance, the lotus leaf (*Nelumbo nucifera*) exhibits a rough surface in the form of cilium-like nanopillars superimposed on micrometer-scale papillae.*[20]* This hierarchically branched topography protects the leaf from contaminations and yield superhydrophobic properties ("lotus effect").*[21]* The gecko also utilizes hierarchically patterned surfaces on his

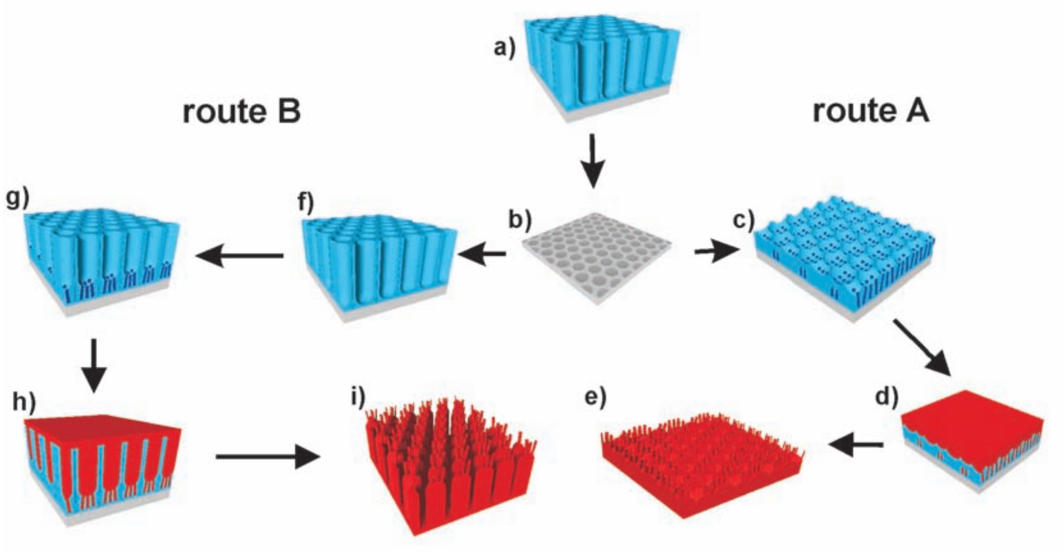

Scheme 1. *Schematical representation of the fabrication of branched nanorod arrays. Route A yield in the fabrication of hierarchical structures based on mesoscopic hemispheres decorated with thin nanopillars. Route B describes the fabrication of two-tiered branched rod arrays.*

feet in order to generate large adhesive forces, which enables the gecko to climb on smooth vertical substrates. Further, the increased surface area of such biomimetic hierarchically-branched arrays makes them highly desirable for applications, which require large interfaces such as drug delivery, catalysis and sensing.*[22, 23]*

In this work we report on the template-assisted patterning of hierarchically branched polymeric nanorod arrays *via* utilization of branched nanoporous AAO templates, which were fabricated *via* a modified two-step anodization process (see Scheme 1). *Masuda* and *Fukuda* invented in 1995 a two-step anodization process to obtain well-ordered nanopores.*[15, 24]* Briefly, they conducted a first anodization step and a subsequent etching step of the formed alumina in acidic chromic acid yielding in the formation of hexagonally ordered mesoscopic indentions on the aluminum surface. These indentions act as seeds for the pore growth in the second anodization step and a hexagonally ordered pore alignment is obtained after the two-step anodization, if the experimental parameters of both anodization steps are identical.

However, we found that if one varies the experimental parameters like the applied voltage and the employed electrolyte in the second anodization step hierarchically ordered porous morphologies could be obtained (see Scheme 1). Figure 1A shows a top-view scanning electron micrograph of the hexagonal indentions on an aluminum surface, which are left behind after anodization in aqueous phosphoric acid (1 wt%) at 195 V and subsequent etching. The average diameter was determined to be ~500 nm. A subsequent second anodization step in oxalic acid (c = 0.3 mol L^{-1}) at 40.0 V results in the formation of pores with considerably

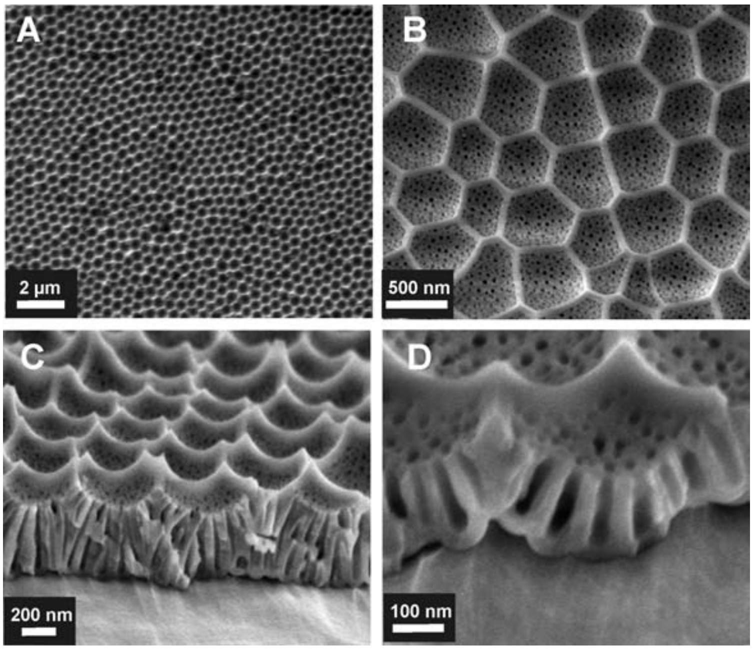

Figure 1. *Scanning electron micrographs: (A) Mesoscopic hexagonal indentions on the aluminum surface after anodization in aqueous phosphoric acid (1 wt%) at 195 V and subsequent etching in acidic chromic acid (average diameter of the indentions: 500 nm); (B) Top view and (C) corresponding cross-sectional view of a hierarchically patterned AAO template. 500-nm-diameter indentions are connected with 40-nm pores. (D) Cross-sectional view of a hierarchically patterned AAO template with a shorter length of the small pores and after pore widening by treatment with phosphoric acid.*

smaller pore diameters of about 35 nm. The hemispherical shape of the indentions on the aluminum surface was replicated to the surface of the formed porous alumina. As usual, the length of the fine pores was controlled by variation the anodization time. By measuring the length of pores that have formed after anodization times in the range of 5 to 20 min the growth rate was determined to be 15±2 nm min^{-1}. Noteworthy, due to the curvature of the hemispherical indentions, the small pores exhibit a restriction at their opening after the anodization step (see Figure 1C). These restrictions of the pores could be widened by post-treatment with phosphor acid (5 wt%).

In addition to the hemispherical shaped substructure a cylindrical pore with a tunable length is desirable as a substructure in the hierarchal-branched template. This would consequently result in a two-tiered porous morphology, which features an independently variation in length of both substructures. For this purpose another route is pursued, which is schematically represented in Scheme 1 (route B).

For that reason, the second anodization was initially performed at identical experimental conditions like the first step, which resulted in the growth of pores with relatively large diameters (see Scheme 1F). Performing the anodization in phosphoric acid (1 wt%) at 195 V yielded pores with a diameter of about 180 nm and an interpore distance of 500 nm. During the anodization an oxidic barrier layer, whose thickness is

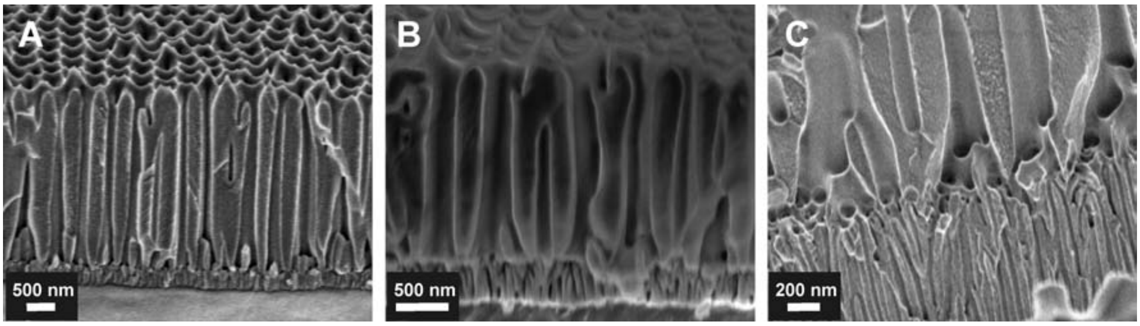

Figure 2. *Cross-sectional scanning electron micrographs of two-tiered branched AAO templates with cylindrical substructures of 500 nm and 40 nm in diameter.*

proportional to the applied voltage, is formed at the origin of the pores.*[25]* The thick insulating barrier layer that is formed at high voltages is an obstacle the formation of two-tiered pores if one would simply performing a subsequent anodization in oxalic acid (c = 0.3 mol L^{-1}) at 40 V. Consequently, a thinning process of the barrier layer is essential in order to facilitate the subsequent growth of smaller pores in oxalic acid. *Gösele* and coworker recently reported on a thinning process for the barrier layer *via* a consecutive reduction of the applied voltage.*[26, 27]* Following this reported thinning procedure, the anodization was performed at 195 V for a certain period and after that the applied voltage was stepwise reduced by 2 V every 3 minutes down to 80 V. Thereafter, the thinning was continued in oxalic acid from 80 V down to 5 V by applying a consecutive exponentially decay of the voltage. After this electro chemical thinning procedure, the barrier layer was further thinned by an isotropic wet chemical etching step in phosphoric acid (10 wt%) for 1 h. A cross-sectional SEM image of the templates before and after the thinning of the barrier layer is shown in the Supporting Information. For the fabrication of branched pores a subsequent anodization step at 40 V in oxalic acid could successfully be accomplished after the thinning of the barrier layer. Figure 2 shows cross-sectional scanning electron micrographs of two-tiered branched templates with hierarchically ordered pores of 200 nm and 40 nm in diameter, respectively. The advantage of this procedure is that the pore length of both hierarchical substructures can be varied independently by the corresponding anodization time.

Branched AAO templates have so far been utilized for the fabrication of carbon nanotubes and metallic nanowires.*[27-30]* In the present study, we used branched AAOs to fabricate hierarchically patterned polymeric surfaces. The filling of polymeric materials into the porous templates can be accomplished either by wetting of polymer melts or polymer solutions or by infiltration of a precursor material that can be subsequently polymerized inside the template.[30-33] Since the infiltration of polymeric materials usually results in the formation of nanotubes that are mechanically less stable than completely filled rods, the replica tends to collapse after the selective removal of the template. In order to prevent a complete ground

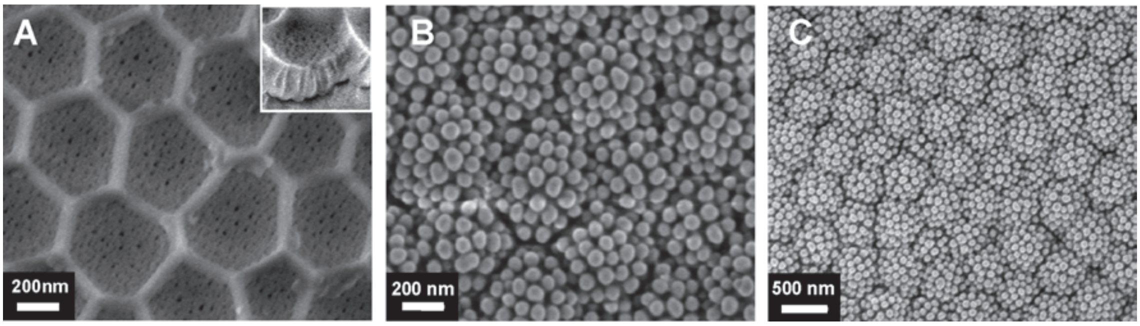

Figure 3. *Top-view SEM images of hierarchical mesoscopic structures based on hexagonally arranged hemispheres decorated with nanopillars. (A) AAO template (inset: cross-sectional view of one hemispherical unit) and (B and C) the corresponding raspberry-like polymeric DVTPA replication.*

collapse of the polymeric replication after removal of the template and to obtain polymeric replications whose contours match those of the pores, we used a cross-linkable triphenylamine derivative (4,4'-divinyltriphenylamine (DVTPA)) for the infiltration since the cross-linked DVTPA exhibits a good mechanical stability and collapsing phenomina of the polymeric replication could be reduced. The solution wetting of low molecular weight derivates tends to result in a complete infiltration of the porous template and the subsequent thermal cross-linking of the material leads in a high mechanical stability of the polymeric replica. Noteworthy, DVTPA was used as a model compound for the infiltration, because it exhibits not only a high mechanical stability but also semiconducting properties, which could be advantageous for potential applications of the polymeric replica in the field of optoelectronics, sensing or electro-wetting.

The infiltration of DVTPA into the porous AAO templates was conducted by spin-coating of a DVTPA solution in dichlormethane (20 wt%) onto the template. For the cross-linking of DVTPA, the templates were pressed between two glass slides and the sample was heated to 150 °C for 4 h. To perform SEM measurements of the resulting polymeric morphologies, the DVTPA support film on the top of the AAO was attached to a carbon tape pad and the aluminum and the aluminum oxide layer was selectively removed by wet chemical treatment with aqueous $CuCl_2$ and aqueous phosphoric acid, respectively. Figure 3 B and C show the SEM images of the cross-linked DVTPA replica of a hierarchical branched AAO with a hemispherical substructure (see Figure 3A). A well-ordered raspberry-like topography was obtained. The topography consisted of hexagonally-ordered hemispheres with a diameter of 500 nm which were decorated with approximately 25-30 nanopillars in average (40 nm in diameter). In contrast, tree-like replicas were obtained for the templates with two-tiered cylindrical pores (see Figure 2), as illustrated in Figure 4. The images reveal that the mechanical stability of the cross-linked DVTPA was sufficient to prevent the ground collapse after the removal of the mechanical stabilizing AAO scaffold. The "trunks" of the hierarchical structure were perfectly free-standing and separated form each other. Due to their high aspect ratio, the thinner branches on the top of the "trunks" (see Figure 4 A

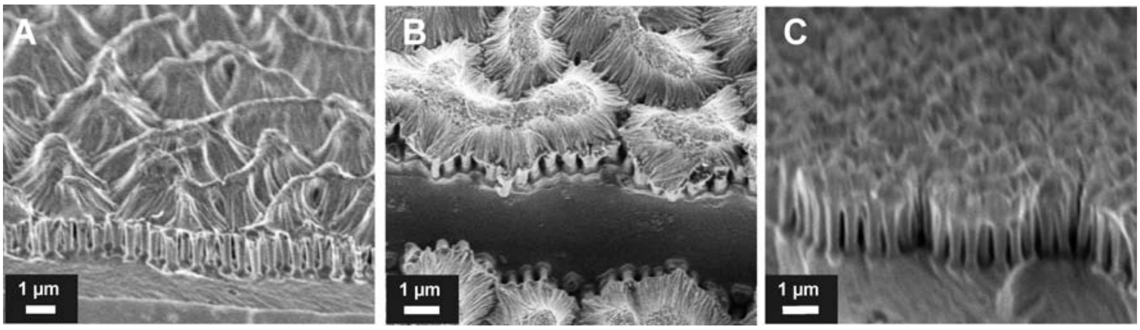

Figure 4. *SEM images of cross-linked DVTPA replicas of two-tiered branched AAOs with cylindrical substructures of 180 nm and 40 nm in diameter, respectively.*

and B) however tended to assemble into bundles. By decreasing the aspect ratio of the thinner branches (see Figure 4 C), the degree of aggregation could be minimized and hierarchical brush-like structures form.

In summary, we have presented a method to fabricate well-ordered arrays of hierarchically branched mesoscopic polymer rods by utilizing branched AAO templates. The stepwise fabrication of the porous templates *via* a modified two-step anodization process facilitated the independent variation of the pore length of both hierarchical substructures by controlling the anodization time. The wetting-based infiltration of divinyl triphenylamine, thermal cross-linking and subsequent removal of the template resulted in well-ordered arrays of polymeric, hierarchical mesoscopic structures. The cross-linked polymer provided a sufficient mechanical stability in order to prevent ground collapse of the replica after removal of the template. Due to the large surface area of the two-tiered branched replicas and the semiconducting properties of the cross-linked triphenylamine, these replicas will be further explored for the potential application as building blocks in optoelectronic applications, sensing or electro-wetting. Further, the presented versatile concept is expected to be easily extended to the hierarchical patterning of other organic materials enabling the preparation of bio-inspired functional surfaces with superhydrophobic properties or superb adhesions.

Experimental Section.

Materials. 4,4’-Divinyltriphenylamine (DVTPA) was synthesized via a *Vilsmeyer* and a subsequent *Wittig* reaction starting from triphenylamine by the procedure described in the literature.*[31]*

Fabrication of AAO templates. High purity aluminum (99.997 %, 0.1 mm thick) purchased from Alfa Aesar was cleaned by sonification treatment in isopropanol and acetone respectively followed by an electropolishing step in a mixture of ethanol and perchloric acid (v/v 4:1) at a current density of 300-350 mA/cm^{-1} for 1 min at 0 °C. Subsequently the samples were rinsed with deionized water, isopropanol and acetone. To obtain well-ordered porous templates, the anodization was performed in a two-step process. The anodization steps were performed in a self-build apparatus. Briefly, the aluminum sheets were mounted on a copper plate serving as the anode. A radial area of 2.27 cm^2 was exposed to an aqueous acidic solution. A platinum wire was used as the cathode.

The apparatus was surrounded by a cryostatic bath to control the temperature during anodization and the electrolyte solution was rigorously stirred during anodization. The anodization voltage is controlled by a power supply unit with an integrated USB interface (model: EA-PS 8360-10 DT; manufacturer: EA Elektro-Automatik, Germany). Anodization transients were measured using a multimeter and recorded with an attached computer. For the hierarchical branched AAO templates an asymmetric two-step anodization was applied. In the first step aluminum was anodized in an aqueous solution of phosphoric acid (1.0 wt%) at 195 V for 12 h, followed by an etching step in aqueous solution of chromic acid (1.8 wt%) and phosphoric acid (6.0 wt%) at 60 °C for 24 h. In order to pursue route A (see Scheme 1) the second anodization step was performed in oxalic acid ($c = 0.3$ mol L^{-1}) at 40.0 V. The rate of pore growth was determined to be 15±2 nm min^{-1}. Pore widening was performed in aqueous phosphoric acid (5 wt%) at 25 °C.

For pursuing route B (see Scheme 1), the second anodization step was initially performed in aqueous solution of phosphoric acid (1.0 wt%) at 195 V for a certain period. The barrier layer was subsequently thinned by consecutive reduction of the applied voltage down to 80 V (reduction of 2V every 3 min). After exchanging the electrolyte to oxalic acid ($c = 0.3$ mol L^{-1}) the reduction of the applied voltage was continued down to 5 V (exponential decay of the applied voltage). For further thinning of the barrier layer the template was treated with phosphoric acide (10 wt%) for 1 h at room temperature. A subsequent anodization in oxalic acid ($c = 0.3$ mol L^{-1}) at 40.0 V resulted in the formation of branched pores. Pore widening was performed in aqueous phosphoric acid (10 wt%) at 25 °C for 15 min.

Polymeric replication. A solution of 4,4'-divinyltriphenylamine (DVTPA) in dichloromethane (20 wt%) was spin-coated on the top of the AAO template (3000 rpm, 1 min). The samples were vacuum-treated for 30 min at room temperature and subsequently pressed between two glass plates and thermally cured at 150 °C for 2 h. The supporting aluminum and the AAO layer was removed by treatment with a solution of $CuCl_2$ and phosphoric acid respectively The patterned polymer film attached to an carbon pad rinsed with deionized water (Milliopore 18MΩ) and dried.

Characterization. The topographies of the fabricated nanoporous AAO templates and their polymeric replicas were investigated by low voltage field emission scanning electron microscopy (FE-SEM, Zeiss LEO 1530) at 3 kV and 0.7 kV, respectively, without using any conductive coating.

References.

[1] Y. Lee, S. Park, K. Kim, J. Lee, *Adv. Mater.* **2007**, *19*, 2330.

[2] W. Lee, M. Jin, W. Yoo, J. Lee, *Langmuir* **2004**, *20*, 7665.

[3] W. Cho, I. Choi, *Adv Funct Mater* **2008**, *18*, 1089.

[4] T. S. Kustandi, V. D. Samper, W. S. Ng, A. S. Chong, H. Gao, *Journal of Micromechanics and Micro-engineering* **2007**, *17*, N75.

[5] G. Lu, W. Hong, L. Tong, H. Bai, Y. Wei, G. Shi, *Acs Nano* **2008**, *2*, 2342.

[6] C. Martin, *Acc. Chem. Res.* **1995**, *28*, 61.

[7] A. Gitsas, B. Yameen, T. D. Lazzara, M. Steinhart, H. Duran, W. Knoll, *Nano Lett.* **2010**, *10*, 2173.

[8] B. A. Evans, A. R. Shields, R. L. Carroll, S. Washburn, M. R. Falvo, R. Superfine, *Nano Lett.* **2007**, *7*, 1428.

[9] O. du Roure, A. Saez, A. Buguin, R. Austin, P. Chavrier, P. Silberzan, B. Ladoux, *P Natl Acad Sci Usa* **2005**, *102*, 2390.

[10] J. Tan, J. Tien, D. Pirone, D. Gray, K. Bhadriraju, C. Chen, *P Natl Acad Sci Usa* **2003**, *100*, 1484.

[11] J. Mallet, K. Yu-Zhang, S. Mátéfi-Tempfli, M. Mátéfi-Tempfli, L. Piraux, *J. Phys. D: Appl. Phys.* **2005**, *38*, 909.

[12] M. G. Kim, J. Cho, *Adv Funct Mater* **2009**, *19*, 1497.

[13] A. del Campo, E. Arzt, *Chem. Rev.* **2008**, *108*, 911.

[14] G. Younan Xia, *Angew. Chem. Int. Ed.* **1998**, *37*, 550.

[15] H. Masuda, K. Fukuda, *Science* **1995**, *268*, 1466.

[16] H. Masuda, H. Yamada, M. Satoh, H. Asoh, M. Nakao, T. Tamamura, *Appl. Phys. Lett.* **1997**, *71*, 2770.

[17] N. Haberkorn, M. C. Lechmann, B. H. Sohn, K. Char, J. S. Gutmann, P. Theato, *Macromol Rapid Comm* **2009**, *30*, 1146.

[18] B. Zhao, M. M. Collinson.

[19] C. Shuoshuo, L. Zhiyuan, H. Xing, Y. Hui, L. Yi, *J. Mater. Chem.* **2010**, *20*, 1794.

[20] M. K. Kwak, H.-E. Jeong, T.-I. Kim, H. Yoon, K. Y. Suh, *Soft Matter* **2010**, *6*, 1849.

[21] C. R. Crick, I. P. Parkin, *Chem-Eur J* **2010**, *16*, 3568.

[22] A. Stein, F. Li, N. R. Denny, *Chem. Mater.* **2008**, *20*, 649.

[23] M. Tiemann, *Chem. Mater.* **2008**, *20*, 961.

[24] H. Masuda, K. Yada, A. Osaka, *Jpn. J. Appl. Phys.* **1998**, *37*, L1340.

[25] F. KELLER, M. HUNTER, D. ROBINSON, *J. Electrochem. Soc.* **1953**, *100*, 411.

[26] K. Nielsch, F. Muller, A. Li, U. Gosele, *Adv. Mater.* **2000**, *12*, 582.

[27] W. Lee, M. Alexe, K. Nielsch, U. Gosele, *Chem. Mater.* **2005**, *17*, 3325.

[28] G. Meng, Y. Jung, A. Cao, R. Vajtai, P. Ajayan, *Proceedings of the National Academy of Sciences of the United States of America* **2005**, *102*, 7074.

[29] C. Papadopoulos, A. Rakitin, J. Li, A. Vedeneev, J. Xu, *Phys Rev Lett* **2000**, *85*, 3476.

[30] J. Li, C. Papadopoulos, J. Xu, *Nature* **1999**, *402*, 253.

[31] N. Haberkorn, J. S. Gutmann, P. Theato, *ACS Nano* **2009**, *3*, 1415.

Supporting Information.

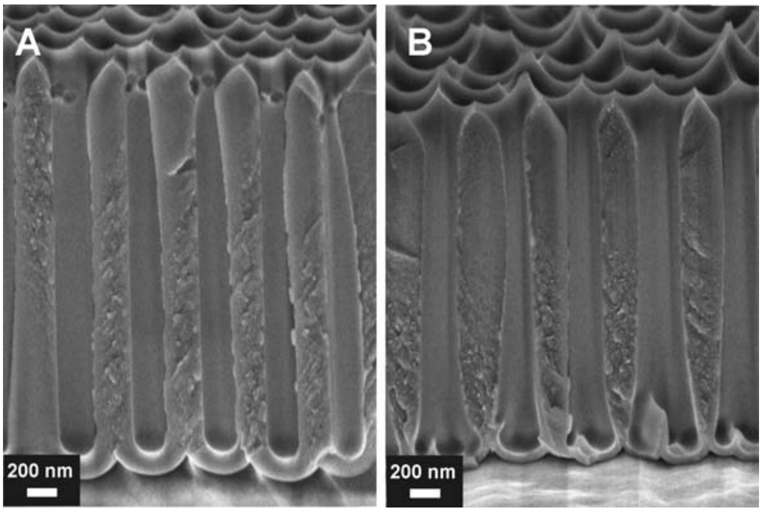

Figure S1. Cross-sections of AAO templates before (A) and after (B) thinning procedure.

5.5 Reactive Nanowires Based on Activated Ester Polymers: A Versatile Template-Assisted Approach for the Fabrication of Functional Nanowires

*By Niko Haberkorn, Katja Nilles, Philipp Schattling, Patrick Theato**

[*] Patrick Theato, Niko Haberkorn, Katja Nilles, Philipp Schattling
Institute of Organic Chemistry, University of Mainz
Duesbergweg 10-14, 55099 Mainz, Germany
E-mail: theato@uni-mainz.de

Niko Haberkorn
Max Planck Institute for Polymer Research
Ackermannweg 10, 55128 Mainz, Germany

Patrick Theato
School of Chemical and Biological Engineering, WCU Program of Chemical Convergence for Energy & Environment (C2E2), College of Engineering, Seoul National University, Seoul, Korea

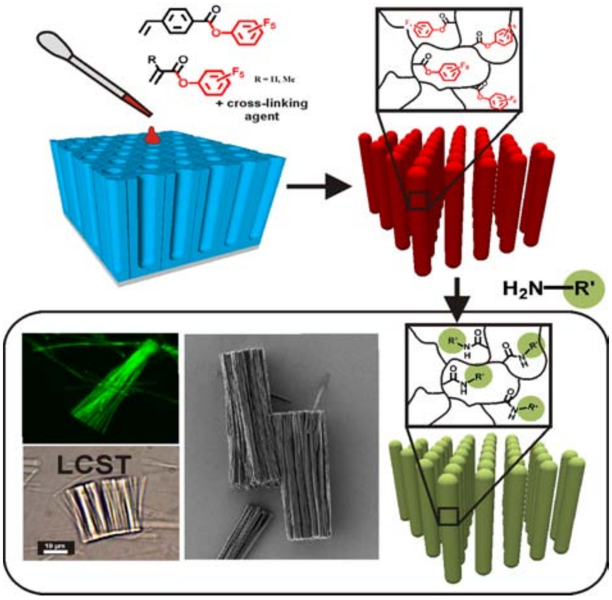

Keywords.
Anodic aluminum oxide templates; template-assisted patterning; activated ester polymers, reactive nanowires, PNIPAM nanowires.

Abstract

In this paper we describe a new route for the fabrication of polymeric nanowires with functional moieties *via* post-modifiaction of reactive nanowires. To this end reactive nanowires with a homogenous and narrow size distribution were fabricated by utilizing an anodic aluminum oxide (AAO) templates-assisted approach. The nanowires are based on activated pentafluorphenylesters, which feature the quantitative post-modification with amines under very mild reaction conditions yielding the corresponding functionalized amide. We demonstrate the post-modification with fluorescent dyes as well as the conversion into well-dispersed wired-shaped PNIPAM hydrogels that exhibit a thermal-responsive phase transition. The platform of reactive nanowires features the fabrication of various functional nanoobjects and may find application in research fields like drug delivery.

One-dimensional organic nanometer-scaled objects such as rods, tubes and wires have attracted increasingly attention as a result of their interesting properties*[1]* and their potential application in different research areas like optoelectronic*[2]*, sensors*[3, 4]*, catalysis*[5]* and drug delivery*[6, 7]*. The replication by using porous templates like macroporous silicon and anodic aluminium oxide (AAO) templates has become a well-established and versatile technique for the fabrication of such one-dimensional organic nanostructures.*[8-12]* In contrast to other techniques, such as electrospinning*[13]* and direct drawing*[14]*, the template-based approach facilitates the fabrication of nanoobjects with very defined aspect ratios. Nanoporous AAO templates, which are used as shape-defining molds, can be fabricated by a controlled electrochemical two-step anodization of aluminum.*[15, 16]* They provide hexagonally well-ordered pores with tunable pore diameters in the range of 10 to 200 nm and pore densities up to 10^{11} cm^{-2}.*[8, 17]* The infiltration of low molecular organic materials or polymers into porous templates can be accomplished by template wetting with melts or solutions of the corresponding material or precursor. The template wetting technique was first demonstrated by *Martin* and coworkers and has since then been intensively investigated and extended to prepare functional nanoobjects.*[18-23]* Based on the template wetting of functional precursor or polymeric materials, nanotubes and rods with ferroelectric,*[24]* biodegradable*[25]* and semiconducting*[26-28]* properties - to just mention a few - have been reported.

The scope of this communication is to describe a new versatile route for the template-based fabrication of polymeric functional nanorods via post-functionalization of reactive rods (**see Scheme 1**). The functionalization after the completed templating process is advantageous since sensitive functional groups may decompose during direct melt wetting step or during the removal of the template, which usually requires the treatment with strong acids or bases. Further, by starting from one batch of reactive nanorods, nanoobjects with identical aspect ratios and morphologies and various different functionalities are

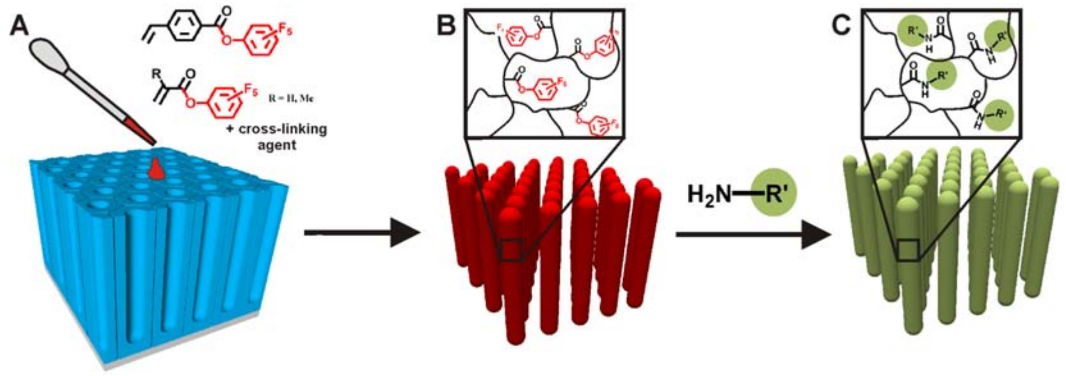

Scheme 1. Schematic diagram of the template-assisted fabrication of reactive nanowires and their post-functionalization. (A) Infiltration of a mixture of an activated ester monomer, cross-linking agent and initiator into nanoporous AAO templates via solution-wetting. (B) Thermal or UV-initiated polymerization and subsequent removal of the template yield cross-linked polymeric nanowires containing activated ester moieties. (C) Post-functionalization of the reactive rods via conversion with amine-functionalized reagents.

directly accessible without optimizing the wetting parameters for each and every polymer.

Several reactive groups that facilitate a functionalization after the templating procedure may in principle be used, however, due to our established experience with activated pentafluorophenyl esters, we haven chosen those for the present study.*[29]* Polymeric activated esters based on pentafluorophenyl esters of acrylic, methacrylic and 4-vinyl benzoic acids have found broad application for the synthesis of reactive polymers.*[29, 30]* They feature quantitative post-polymerization modification with amines under very mild reaction conditions yielding the corresponding functionalized amide.*[31, 32]* So far activated ester based polymers have been used as reactive building blocks in copolymers as well as for the preparation of reactive thin polymer films.*[32, 33, 34]*

In this communication, we will show that polymeric activated esters are also highly suitable for the fabrication of reactive nanowires that facilitate a post-funtionalization with functional amines.

For the preparation of reactive nanowires a replication technique using AAO templates was chosen. A two-step anodization process in either oxalic or phosphoric acid was used for the fabrication of AAO templates with nanometer sized pore diameters – tunable between 30 nm to 300 nm – and narrow pore size distributions. The length of the pores could precisely be varied by controlling the anodization time. Since a versatile post-modification requires the treatment with amines that are dissolved in organic solvents, the nanowires need to be resistant against the exposure of organic solvents. Furthermore, in order to enable a complete conversion of all activated ester moieties and not only of those located at the surface, a certain swelling ability of the material during the conversion step is favorable. To match the mentioned requirements the polymerization of the activated ester monomers was conducted inside the pores in the presence of a small amount of crosslinking agent.

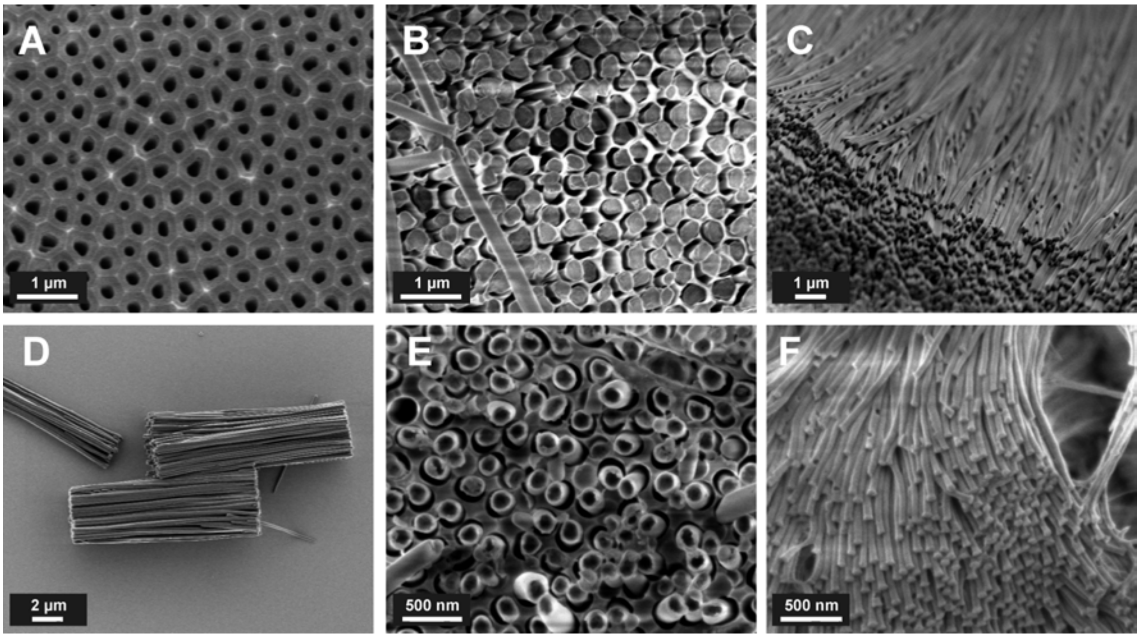

Figure 1. *Scanning electron micrographs. (**A**) Top view of an unfilled AAO template; Cross-linked PPFPMA nanowires after partial (**B**) and complete (**C**) etching of the AAO template; (**D**) Bundles of cross-linked PPFPVB nanowires; (**E**) Top view of PPFPVB nanotubes after partial etching of the AAO template; (**F**) Array of PPFPVB nanowires with an average diameter of 40 nm.*

It turned out that in the case of pentafluorphenyl-acrylate (PFPA) and methacrylate (PFPMA) the bifunctional hexamethylenediacrylate was the most efficient crosslinker, while for the polymerization of 4-vinyl benzoate (PFPVB) divinylbenzene worked best. The cross-linking polymerization could successfully be initiated thermally or photochemically through the addition of azobisisobutyronitrile (AIBN) or Lucirin TPO, respectively. The AAO pores were filled by either solution wetting of highly concentrated solutions of the monomer mixture or bulk wetting of the monomer mixture. **Fig. 1** and **Fig. S1** show a selection of scanning electron micrographs of AAO templates and the corresponding nanoobjects after partial and complete etching of the sacrificial AAO template. The length and also the diameter of the wires correspond to those of the porous molds, even for templates with very small diameters. After the complete etching of the AAO templates, arrays of well-aligned reactive nanowires were obtained. The nanowire arrays could be fragmented into bundles (see Figure 2D) and even into single dispersed wires (see Figure S3) by moderate sonication treatment. Independent of the infiltration technique used, completely filled nanowires were always obtained. Noteworthy, when the solution wetting was performed with diluted solutions (3 wt%) nanotubes could be prepared (see Figure 2E). However, it turned out that the tubular objects tended to collapse during subsequent centrifugation and sonication steps and we therefore focus in the following on the post-modification of the mechanically more stable nanowires.

One aspect that is crucial for any post-functionalization is the preservation of the activated ester groups during the wet chemical etching step of the sacrificial AAO template.

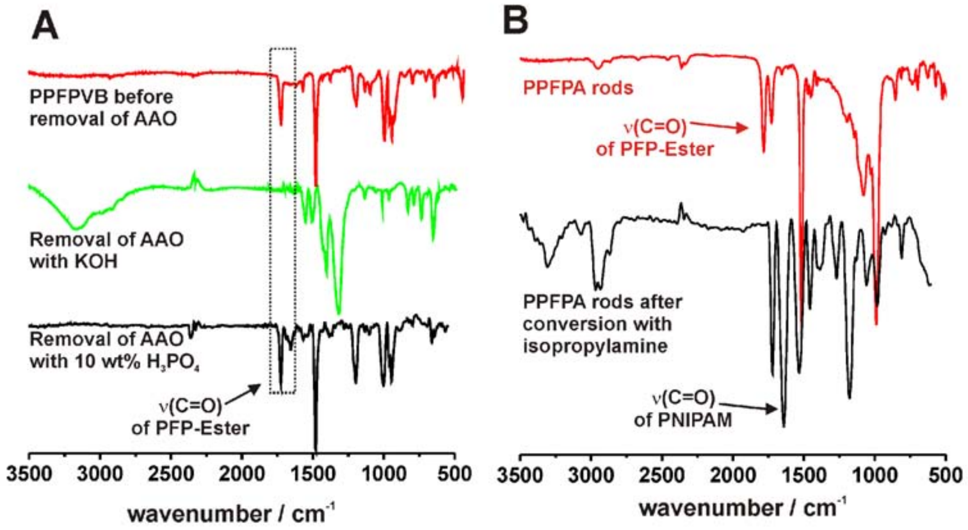

Figure 2. *(A) ATR-FTIR spectra of a thin film of poly(pentafluorophenyl 4-vinylbenzoate) (PPFPVB) (red line), PPFPVB nanowires after etching of the template with potassium hydroxide (green line) and phosphoric acid (black line) respectively. (B) ATR-FTIR spectra of crosslinked PPFPA nanowires (15 wt% crosslinker) after removal of the template (red line) and conversion with isopropylamine (black line).*

Usually AAO templates are selectively etched away by treatment with aqueous solutions of strong bases such as potassium hydroxide. However, the FT-IR spectrum of crosslinked poly(pentafluorophenyl 4-vinylbenzoate) (PPFPVB) nanowires recorded after the template removal under basic conditions did not show the characteristic band of the PFP-ester at 1763 cm^{-1} anymore (**Fig. 2A**). This indicated the complete saponification of the ester groups, confirming that the etching under basic condition is not feasible. In contrast, the removal of the amphoteric aluminum oxide mold by treatment with phosphoric acid did not saponify the activated ester, as shown by FT-IR, and the reactive groups of the obtained nanowires was retained . Similarly, PPFPA and PPFPMA nanowires could be treated with phosphoric acid without any hydrolysis of the activated ester groups.

The feasibility of the post-modification of the reactive wires is first demonstrated by the conversion of poly (pentafluorophenylacrylate) (PPFPA) nanowires with isopropylamine. For that purpose the nanowires were dispersed in a 25 wt% solution of isopropylamine in tetrahydrofuran (THF) for 6 h and subsequently purified by repeating cycles of centrifugation and sonication-assisted redispersion in water. Besides a good solubility of the amine and the formed pentafluorophenol in THF, the reaction medium should provide a suitable swelling of the crosslinked nanowires to allow an access to all reactive groups. The conversion of the reactive groups was recorded by FT-IR measurements (**Fig. 2B**). In the IR spectrum of the nanowires after treatment with isopropylamine the characteristic band of the PFP ester at 1783 cm^{-1} completely disappeared. The appearance of two amide bands at 1640 cm^{-1} and 1533 cm^{-1} as well as the NH valence vibration band at 3306 cm^{-1} in the infrared spectrum indicated the

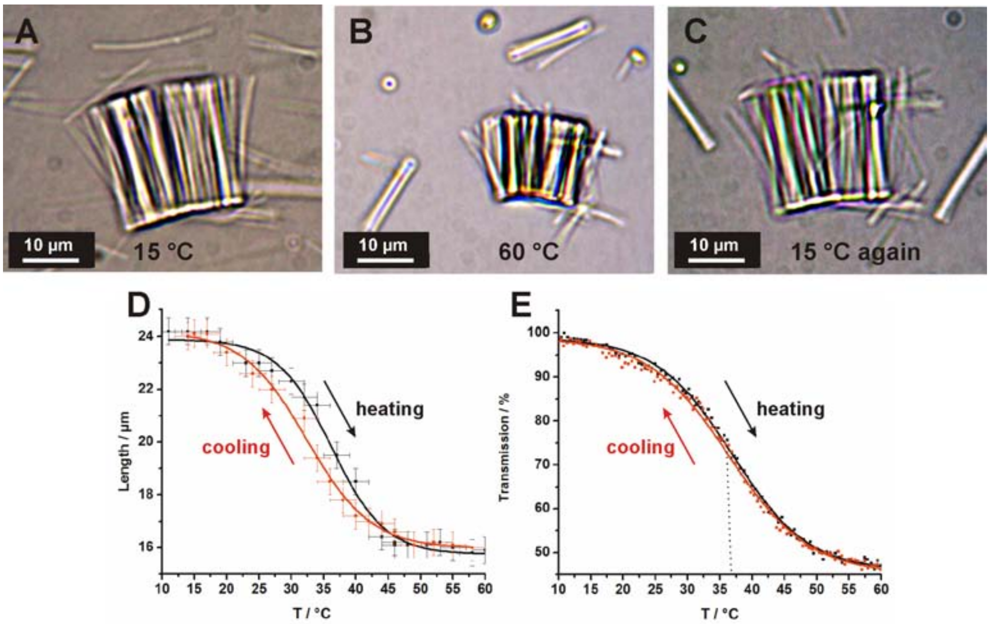

Figure 3. *(A-C) Optical micrographs of a bundle of cross-linked poly(pentafluorphyenylacrylate) nanowires after conversion into PNIPMA nanowires via post-functionalization with isopropylamine. The heating experiments that were performed in an aqueous media visualize the reversible collapsing and swelling of the nanowires due to the lower critical solution temperature (LCST) of the cross-linked PNIPMA nanowires. (D) Plot of the length variation (along the axis of the wires) of PNIPAM nanowires dispersed in water versus the temperature (heating rate 10°C min^{-1}). The slight hysteresis is probably caused by a limited heat transfer of the heating set-up (E) Temperature-dependent turbidity measurement curve of an aqueous dispersion of PNIPAM nanowires.*

quantitative conversion yielding crosslinked poly(*N*-isopropylacrylamide) (PNIPAM) nanowires. Optical micrographs confirmed that the wires still remained their shape and their dispersibility after the post-functionalization step. Further investigations that proved the successful preparation of cross-linked PNIPAM nanowires were based on the fact that PNIPAM is a temperature-responsive polymer, which features a lower critical solution temperature (LCST) in water. When solutions of PNIPAM are heated above the LCST, a reversible phase transition from a swollen hydrated state into a collapsed dehydrated form occurs.*[35, 36]* The responsive behavior of crosslinked PNIPAM hydrogels is accompanied by deswelling and swelling, which results in a shrinkage or expansion of the hydrogel. Therefore, the temperature-responsive behavior of water dispersed PNIPAM nanowires with a crosslinker content of 2 wt% was investigated by optical microscopy and turbidity measurements. For better visualization and size analysis, a whole bundle of post-functionalized PNIPAM nanowires was selected for optical microscopy measurements. **Fig. 3A** to **3C** clearly visualize the reversible temperature-dependent shape variation of the nanowire bundle. At 15 °C -- which is below the LCST -- the nanopatterned PNIPAM hydrogel is swollen in water and exhibited a more than 50 % extended length (and also diameter) in comparison

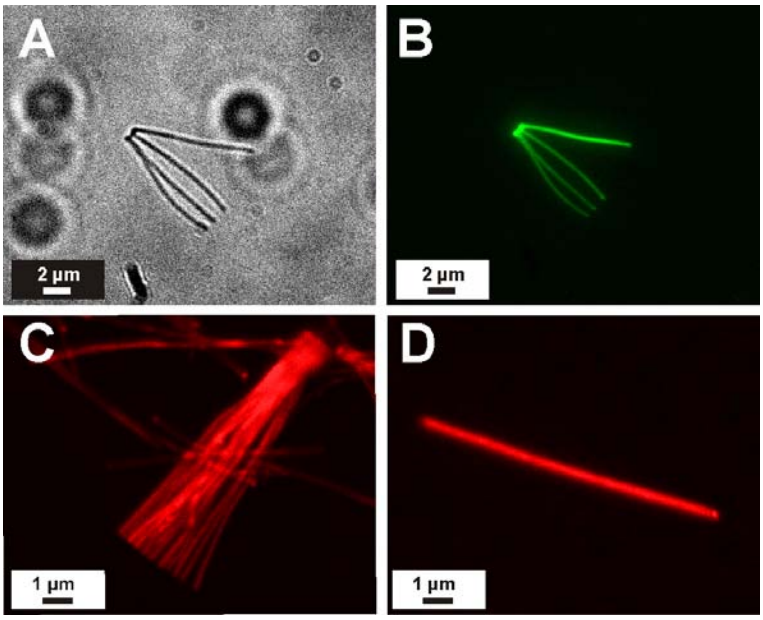

Figure 4. *Optical micrograph (A) and corresponding fluorescence microscopy (confocal, LSM) image (B) of post-functionalized PPFPVB nanowires with Pip-NBD (excitation wavelength λ_{ex} = 488 nm). Fluorescence microscope images of a bundle of PPFPVB nanowires (C) and an individual nanowire (D) after functionalization with sulforhodamine 101 cadervarine (excitation wavelength λ_{ex} = 543 nm).*

to the dried nanowires. By heating up to 60 °C the nanowires considerable shrunk, which indicated the phase-transition into the deswollen hydrophobic state. Noteworthy, when the nanowires were prepared with an increased amount of cross-linker (> 15 wt%), no significant thermal responsive shape change could be observed. The swelling and subsequent shrinking is completely reversible and can be repeated for numerous cycles. The curve of the temperature-dependent length variation is illustrated in **Fig. 3 D**. Due to its small size and large surface, the nanowires exhibited a rapid response rate compared to macroscopic PNIPAM hydrogels, which may require up to several hours for complete swelling. The shape of curve in Fig. 3A has a turning point at about 35 °C, which is in agreement with the turbidity measurements of water-dispersed PNIPMA nanowires (**see Fig. 3E**). Due to deswelling of the water-dispersed nanowires above the LCST, the optical transmittance decreased to 50%. Compared to the sharp LCST behavior of non-cross linked PNIPAM the thermal responsive transition is significantly broadened, which has, however, also been reported for other PNIPAM microgels.*[37]* Noteworthy, even though there are numerous reports about thermo responsive PNIPAM microgels*[38]* not a lot of work has been devoted to wire-shaped PNIPAM microgels. These mesoscopic shape-anisotropic particles exhibit a very large surface to volume ratio and may thus be of interest for drug release applications.

In further experiments the post-modification of reactive PPFPVB nanowires with amine-functionalized fluorescence dyes, such as Piperazinyl-4-chloro-7-nitrobenzofurane (Pip-NBD) and sulforhodamine 101 cadervarine

(S101C) was demonstrated. For this purpose, the PPFPVB wires were dispersed in a dilute solution of pip-NBD in THF or S101C in a THF/DMSO mixture, respectively. The residual non-covalently attached fluorescent dye molecules were removed by several cycles of centrifugation and redispersion in THF and water.

Figure 4 shows the optical micrograph image (**Fig. 4A**) and the corresponding confocal laser scanning micrography (CLSM) images (**Fig. 4B**) of an array of four nanowires after the post-functionalization with pip-NBD. **Fig. 4C** and **4D** illustrates the CLSM images of a bundle and a single isolated PPFPVB nanowire after their modification with S101C. Even though it is difficult to comment on the radial distribution of immobilized dye molecules because it is beyond the resolution limit of the CLSM, the images reveal that the reactive nanowires can be successfully functionalized with fluorescence dyes with a homogenous distribution along the their axis.

Conclusion

In conclusion, it could be demonstrated that preparation of reactive nanowires via a templating approach provides a new versatile platform for the fabrication of functional wires via post-modification with various amines. The modification of reactive nanowires with fluorescent dyes as well the conversion into well-dispersed wired-shaped PNIPAM hydrogels, which exhibit a thermal-responsive phase transition, could be demonstrated for the very first time. As such, future experiments utilizing this reactive platform for the preparation of very well-defined functional nanoobjects are expected to have an impact an different research areas, including drug delivery applications.

Experimental

Materials. All reagents were purchased from Aldrich, Fluka and Acros and were used without further purification unless otherwise stated. The synthesis of the activated ester monomers pentafluorophenyl-acrylate (PFPA), –methacrylate (PFPMA) and pentafluorophenyl *4-vinyl-benzoicacid ester (PFPVB) were synthesized according to the reported procedure.[30, 31] Piperazinyl-4-chloro-7-nitrobenzofurane (*pip-NBD) was synthesized as reported.[39]

Instrumentation. An Oriel Instruments mercury lamp (500 W) with a 365 nm line filter was used for UV-irradiation. IR spectra were recorded at a Bruker Vector 22 FT-IR spectrometer using an ATR unit. Temperature-dependent turbidity measurements of an aqueous dispersion of nanowires were performed with a Jasco V-630 photo-spectrometer and a Jasco ETC-717 peltier element at a concentration of 3 mg/mL and continuous stirring. The cloud point curves were recorded by optical transmittance at 632 nm. The heating rate was 1°C min^{-1}. SEM images were recorded using a Zeiss Leo 1530 at an acceleration voltage of 3.0 kV for AAO membranes and 0.7 kV for polymeric samples. For detection an Inlens detector was used. For the transmission electron microscopy a Philips EM420 120 kV was used.

Fluorescence measurements were performed by using an inverted laser scanning microscope (Leica TCS SL, Leica Microsystems, Bensheim, Germany). A drop of the nanowire dispersion was dropped onto a glass plate and dried. An immersion objective (40x) was used for the imaging. An argon laser with an excitation wavelength of λ_{ex} = 488 nm was used for the excitation of pipNBD. The sulforhodamine 101 cadaverine (S101C) was imaged by excitation with the 543 nm line of a He/Ne laser.

Fabrication of AAO. The templates were prepared by a two-step anodization process. Experimental details are given in the Supporting Information section.

Fabrication of reactive wires. AAO templates were filled by solution wetting at room temperature with mixtures of PFPA and PFPMA respectively, hexamethylenediacrylate (2-15 wt %) and an initiator. In the case of the solid PFPVB, a highly concentrated mixture with divinylbenzene (10 wt%) in dichlormethane was prepared. After solution wetting, most of the solution that was not infiltrated and remained on the surface of the template was removed via spin-coating. For the thermal-initiated polymerization with AIBN (1.0 wt%), the samples were pressed between to glass plates and heated to 80 °C for 12 h. UV-initiated polymerization with Lucerin TPO (5 wt%) was performed by UV-irradiation for 20 min. Subsequently, the remaining homogenous polymer film on top of the template was mechanically removed with a razor blade and the template was selectively etched away in an aqueous solution of phosphoric acid (10 wt%). The wires were purified by three cycles of centrifugation and sonication-assisted redispersion in deionized (DI) water.

Post-functionalization of reactive wires. Centrifuged cross-linked PPFPA wires were redispered in a solution of isopropylamine in tetrahydrofuran (50 wt%) and stirred for 8 h. After the reaction, the nanowires were isolated by centrifugation/redisperison cycles in DI water. For the post-functionalization with fluorescent dyes centrifuged PPFPVB wires were redispersed in a solution of pip-NBD in THF (w/v 0.5%) and sulforhodamine 101 cadervarine in a mixture of DMSO/THF (v/v 1:1, w/v 0.05%), respectively, and stirred for 18 h. Non-covalently attached residual dyes was removed by subsequent centrifugation/redisperison cycles in the same solvent that was used for the functionalization. Finally, the wires were redispersed in DI water.

Acknowledgements

The Electron Microscopy center at the Max-Planck Institute for Polymer Research in Mainz, in particular G. Glasser, is acknowledged for access to SEM measurements. Dr. H. Götz is acknowledged for the help with CLSM measurements. This research was supported by the DFG (IRTG 1404) and by the WCU (World Class University) program through the National Research Foundation of Korea funded by the Ministry of Education, Science and Technology (R31-10013).

References

[1] M. Aryal, K. Trivedi, W. W. Hu, Acs Nano **2009**, 3, 3085.

[2] N. Haberkorn, M. C. Lechmann, B. H. Sohn, K. Char, J. S. Gutmann, P. Theato, Macromol Rapid Comm **2009**, 30, 1146.

[3] C. Martin, Acc. Chem. Res. **1995**, 28, 61.

[4] A. Gitsas, B. Yameen, T. D. Lazzara, M. Steinhart, H. Duran, W. Knoll, Nano Lett. **2010**, 10, 2173.

[5] M. Steinhart, Z. Jia, A. Schaper, R. Wehrspohn, U. Gosele, J. Wendorff, Adv. Mater. **2003**, 15, 706.

[6] R. Dersch, M. Steinhart, U. Boudriot, A. Greiner, J. Wendorff, Polym. Adv. Technol. **2005**, 16, 276.

[7] A. Greiner, J. H. Wendorff, A. L. Yarin, E. Zussman, Appl Microbiol Biot **2006**, 71, 387.

[8] M. Steinhart, T. Shimazu, T. Shimazu, M. Steinhart, Adv. Polym. Sci. **2008**, 220, 123.

[9] J. Hulteen, C. Martin, J. Mater. Chem. **1997**, 7, 1075.

[10] A. Huczko, Appl. Phys. A **2000**, 70, 365.

[11] A. Li, F. Muller, A. Birner, K. Nielsch, U. Gösele, J. Appl. Phys. **1998**, 84, 6023.

[12] S. Ono, M. Saito, M. Ishiguro, H. Asoh, J. Electrochem. Soc. **2004**, 151, B473.

[13] A. Greiner, J. Wendorff, Angew. Chem. Int. Ed. **2007**, 46, 5670.

[14] S. Harfenist, S. Cambron, E. Nelson, S. Berry, A. Isham, M. Crain, K. Walsh, R. Keynton, R. Cohn, Nano Lett. **2004**, 4, 1931.

[15] H. Masuda, K. Fukuda, Science **1995**, 268, 1466.

[16] H. Masuda, H. Yamada, M. Satoh, H. Asoh, M. Nakao, T. Tamamura, Appl. Phys. Lett. **1997**, 71, 2770.

[17] T.-Y. Kim, S.-H. Jeong, Korean J. Chem. Eng. **2008**, 25, 609.

[18] V. Cepak, C. Martin, Chem. Mater. **1999**, 11, 1363.

[19] M. Steinhart, R. Wehrspohn, U. Gösele, J. Wendorff, Angew. Chem. Int. Ed. **2004**, 43, 1334.

[20] M. Steinhart, J. H.Wendorff, Wehrspohn, Ralf, Chem. Phys. Chem. **2003**, 4, 1171.

[21] S. Schlitt, A. Greiner, J. H. Wendorff, Macromolecules **2008**, 41, 3228.

[22] R. O. Al-Kaysi, T. H. Ghaddar, G. Guirado, J Nanomater **2009**, 1.

[23] M. Zhang, P. Dobriyal, J. Chen, T. Russell, J. Olmo, A. Merry, Nano Lett. **2006**, 6, 1075.

[24] C.-C. Wang, Q.-D. Shen, S.-C. Tang, Q. Wu, H.-M. Bao, C.-Z. Yang, X.-Q. Jiang, Macromol Rapid Comm **2008**, 29, 724.

[25] S. L. Bechara, A. Judson, K. C. Popat, Biomaterials **2010**, 31, 3492.

[26] N. Haberkorn, J. S. Gutmann, P. Theato, ACS Nano **2009**, 3, 1415.

[27] R. Palacios, P. Formentín, T. Trifonov, M. Estrada, R. Alcubilla, J. Pallarés, L. Marsal, Phys. Stat. Sol. (RRL) **2008**, 2, 206.

[28] H.-S. Wang, L.-H. Lin, S.-Y. Chen, Y.-L. Wang, K.-H. Wei, Nanotechnology **2009**, 20, 075201.

[29] P. Theato, J Polym Sci Pol Chem **2008**, 46, 6677.

[30] M. Eberhardt, R. Mruk, R. Zentel, P. Théato, Eur. Polym. J. **2005**, 41, 1569.

[31] K. Nilles, P. Theato, Eur. Polym. J. **2007**, 43, 2901.

[32] M. I. Gibson, E. Froehlich, H.-A. Klok, J Polym Sci Pol Chem **2009**, 47, 4332.

[33] F. D. Jochum, P. Theato, Macromolecules **2009**, 42, 5941.

[34] D. Kessler, P. Theato, Macromolecules **2008**, 41, 5237.

[35] D. Kuckling, Colloid Polym Sci **2009**, 287, 881.

[36] H. Schild, Prog Polym Sci **1992**, 17, 163.

[37] J. Rubio-Retama, N. E. Zafeiropoulos, C. Serafinelli, R. Rojas-Reyna, B. Voit, E. L. Cabarcos, M. Stamm, Langmuir **2007**, 23, 10280.

[38] D. Kuckling, J. Hoffmann, M. Plotner, D. Ferse, K. Kretschmer, H. Adler, K. Arndt, R. Reichelt, Polymer **2003**, 44, 4455.

[39] R. Nudelman, O. Ardon, Y. Hadar, Y. Chen, J. Libman, A. Shanzer, J Med Chem **1998**, 41, 1671.

Supporting Information

Fabrication of AAO templates. High purity aluminum (99.997 %, 0.5 mm thick) for the template fabrication was purchased from Alfa Aesar. Aluminum plates were cleaned by sonication treatment in isopropanol and acetone respectively followed by an electropolishing step in a mixture of ethanol and perchloric acid (v/v 4:1) at 0 °C. The anodization steps were performed in a self-build apparatus. Briefly, the aluminum sheets were mounted on a copper plate serving as the anode. A radial area of 2.27 cm^2 was exposed to an aqueous acidic solution. A platinum wire was used as the cathode. The apparatus was surrounded by a cryostatic bath and the electrolyte solution was rigorously stirred during anodization. The anodization voltage was controlled by a power supply unit with an integrated USB interface. Anodization was performed in an aqueous solution of phosphoric acid (c =1.0 wt%) at 195 V (for pore diameters of 180 nm) and oxalic acid (c = 0.3 mol/L) at 40.0 V (for pore diameters of 40 nm) respectively. The first anodization step was carried out for 12 h, followed by an etching step in aqueous solution of chromic acid (1.8 wt%) and phosphoric acid (6.0 wt%) at 60 °C for 18 h. The second anodization was performed under the some conditions like the first step. The length of the templates was controlled by the anodization time. A subsequent pore widening was carried out in aqueous phosphoric acid (5 wt%) at 25 °C.

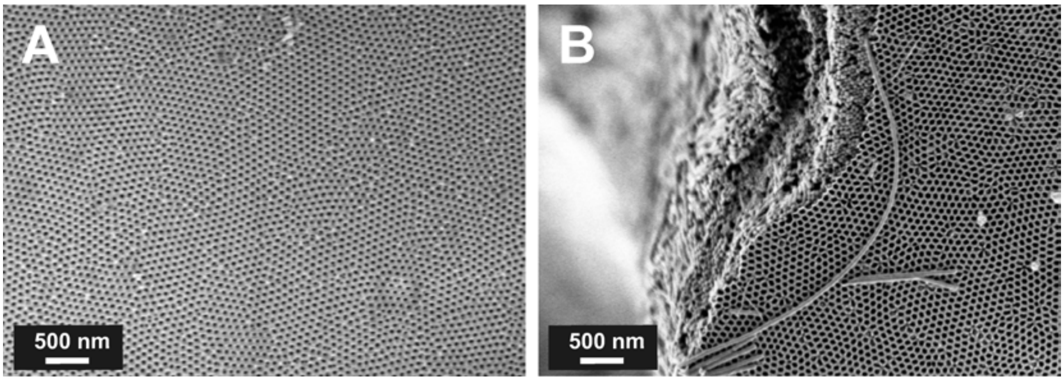

Figure S1. *Scanning electron micrographs. (A) Unfilled AAO template fabricated in oxalic acid (c = 0.3 mol/L) at 40.0 V. (B) Partial etching of the AAO template images exposed arrays of PPFPVB nanowires with a diameter of 40 nm (on the left side).*

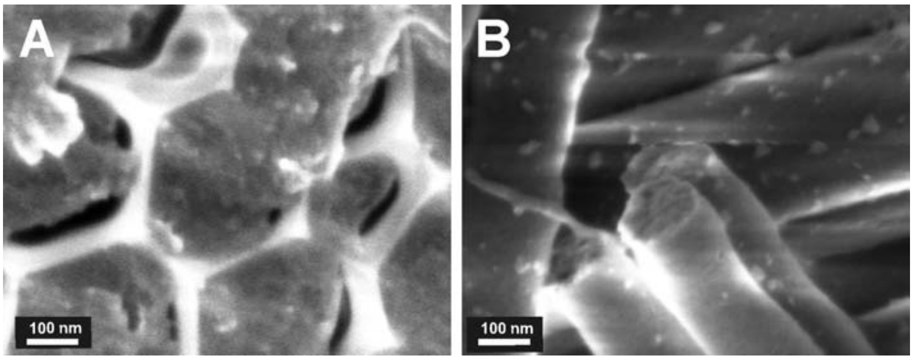

Figure S2. *SEM images of PPFPVB wires after thermal-initiated polymerization. The visualization of the wires inside of the AAO after partial mechanical scratching of the AAO (A) and after removal for the template (B) reveal the complete filling.*

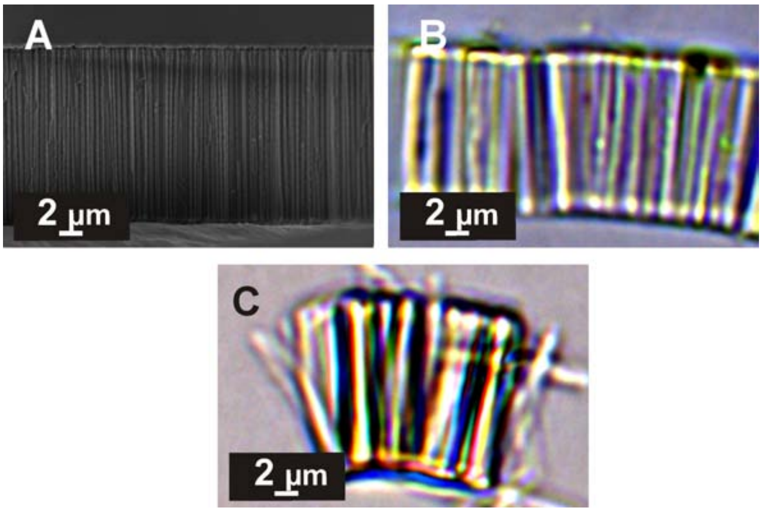

Figure S3. (A) Cross-sectional scanning electron micrograph of an unfilled AAO template. Optical microscope image of the corresponding cross-linked poly(pentafluorophenylacrylate) replication after removal of the AAO template (B) and after conversion into cross-linked PNIPAM wires (C, image was taken above the LCST temperature of the wires). The length of the wires in (B) as well in (C) matched well to the pore length of the AAO template.

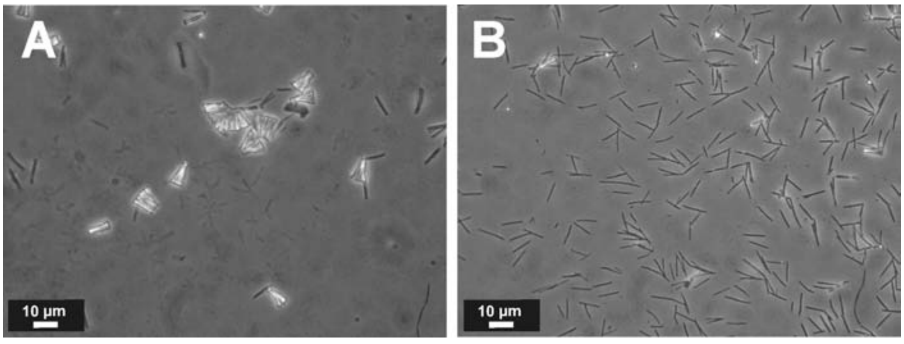

Figure S4. *Phase contrast micrographs of an aqueous dispersion of nanowires before (A) and after (B) sonication treatment.*

5.6 Template-Based Fabrication of Nanometer-Scaled Actuators from Liquid Crystalline Elastomers

Christian Ohm‡, Niko Haberkorn‡, Patrick Theato and Rudolf Zentel**

‡: C.O. and N.H. have contributed equally

[*] Rudolf Zentel, Christian Ohm, Niko Haberkorn, Patrick Theato
Institute of Organic Chemistry, University of Mainz
Duesbergweg 10-14, 55099 Mainz, Germany
E-mail: theato@uni-mainz.de ; zentel@uni-mainz.de

Niko Haberkorn
Max Planck Institute for Polymer Research
Ackermannweg 10, 55128 Mainz, Germany

Patrick Theato
School of Chemical and Biological Engineering, WCU Program of Chemical Convergence for Energy & Environment (C2E2), College of Engineering, Seoul National University, Seoul, Korea.

Keywords.

Liquid crystalline elastomers, nanoactuators, Anodic Aluminum Oxide, template

Liquid crystalline elastomers (LCEs) *[1-3]* are an interesting class of functional materials that combine the ability of self-organization from liquid crystals with the superior mechanical properties of elastomers. They consist of weakly cross-linked polymer chains that are covalently linked to stiff, shape-anisotropic molecules (mesogens). Depending on the ambient conditions, these mesogens can either be in an unordered state (isotropic phase) or self-organize into ordered liquid crystalline phases. In the isotropic phase, the polymer chains can adopt the energetically favored random coil conformation. On the other hand, if the mesogens align into a liquid crystalline phase, the polymer chains have to respond to the resulting anisotropic environment and adapt a stretched conformation. A phase transition between the liquid crystalline and the isotropic phase thus allows to switch the polymer backbone between these two conformations. This conformational change comes along with a macroscopic change of the sample's dimensions,*[4]* which enables the utilization of LCEs as materials for actuator applications.*[5, 6]* Every stimulus that leads to a phase transition in the liquid crystalline material (heat, UV-light, presence of a solvent) can be used to trigger the actuation process. As a result of the reversibility of liquid crystalline phase transitions, the change in shape is reversible as well. It has to be mentioned, that these shape-changing effects can only be observed in samples with a uniform alignment of the director field. To prepare such oriented samples, the mesogens have to be aligned in a uniform direction, followed by crosslinking to permanently fix the orientation. Suitable methods for orientation are for example mechanical stretching *[7]*, electric *[8]* or magnetic *[9]* fields, surface alignment *[10]* or a flow field.*[11]* Using these methods, a variety of different actuating systems based on LCEs could be realized.*[5]* Recently, there has been a growing interest in the fabrication of LCE actuators on a micrometer size scale. Examples are pillars on a surface that can change their height *[12-14]*, cantilevers that can bend upon UV-irradiation *[15]* and particles with the ability to change from a spherical to a rod-like shape.*[11]* In the present publication we present a method to prepare even smaller, structurally defined and oriented objects from liquid crystalline elastomers that can deform reversibly during a liquid crystalline phase transition. To this end, we used porous anodized aluminum oxide (AAO) as templates to prepare nanowires from an LCE material. AAO templates provide uniform and well-ordered nanopores with pore sizes ranging from several nanometers to 300 nm in diameter and up to 100 μm in length.*[16-18]* They can be fabricated by a controlled two-step anodization of aluminum in aqueous electrolytes under acidic conditions.*[19, 20]* AAO templates have been utilized as porous molds for the preparation of shape anisotropic nanoobjects composed of a number of different materials, e.g. metals, carbon, inorganic semiconductors and polymers.*[21-26]* Polymeric nanowires and nanotubes whose contours matches to the shape of the pores can be fabricated in a replicating process by either wetting of the porous alumina template with polymer solutions or melts or by direct polymerization of a monomer inside of the template.*[26, 27]*

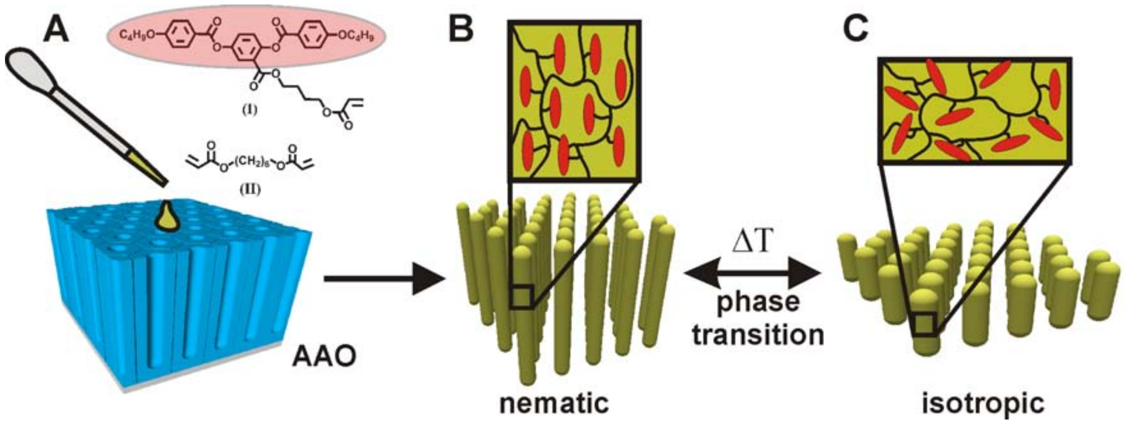

Scheme 1. *Schematical diagram. (A) Nanoporous AAO templates were used as molds for patterning of liquid crystalline elastomers. A mixture of the LC monomer (I), cross-linker (II) and UV initiator were infiltrated via solution wetting. Heating up to the LC phase of the monomer, simultaneous UV-initiated polymerization inside the template and subsequent selective removal of the template yielded arrays of liquid crystalline nanowires with uniformly aligned mesogens (B). By thermal-induced phase transition into the isotropic phase the nanowires undergo a macroscopic contraction along their axis (C).*

Besides the feasibility to control the shape of the replicated nanoobjects, the one-dimensional confined geometry of the pores has also been used to induce a molecular long-range orientation in the replicated material. The template-induced ordering can be obtained after infiltration of crystalline or liquid crystalline materials *via* solution or melt wetting and by subsequent crystallization or formation of mesophases inside the porous template.*[28, 29]* For instance, the nano-confinement induced crystallization of poly(3-hexylthiophene) (P3HT) inside AAO templates was recently used to enhance the electrical conductivity of P3HT nanorods.*[30]* For liquid crystalline materials the confinement-induced orientation was investigated particularly for disc-like molecules that self-organize into columnar stacks, so-called discotics. *Wendorff* and coworker utilized AAO templates to prepare nanowires composed of discotic triphenylene derivative with highly oriented LC columns along their axis.*[31, 32]* Further *Pisula et al.* presented the spontaneous self-alignment of discotic hexa-*peri*-hexabenzocoronene with a long-range supramolecular orientation.*[33-35]*

In our case, the material used to prepare nanowires is a polymerizable, calamitic three-core mesogen (chemical structure (1) shown in scheme 1), which exhibits a nematic phase between 72 and 98°C.*[36]* It was mixed with 20 mol% of the crosslinking-agent hexanedioldiacrylate and 2 wt% of the photoinitiator Lucirin TPO. The resulting mixture showed no crystallization and had a monotropic nematic phase with a clearing temperature of 80°C. The AAO templates were fabricated by a two-step anodization process in phosphoric acid at 195 V and had an average pore diameter of 180 nm and pore lengths of 10 and 30 μm respectively. The monomer mixture described above was dissolved in dichloromethane (20 wt%) and infiltrated into the porous template via

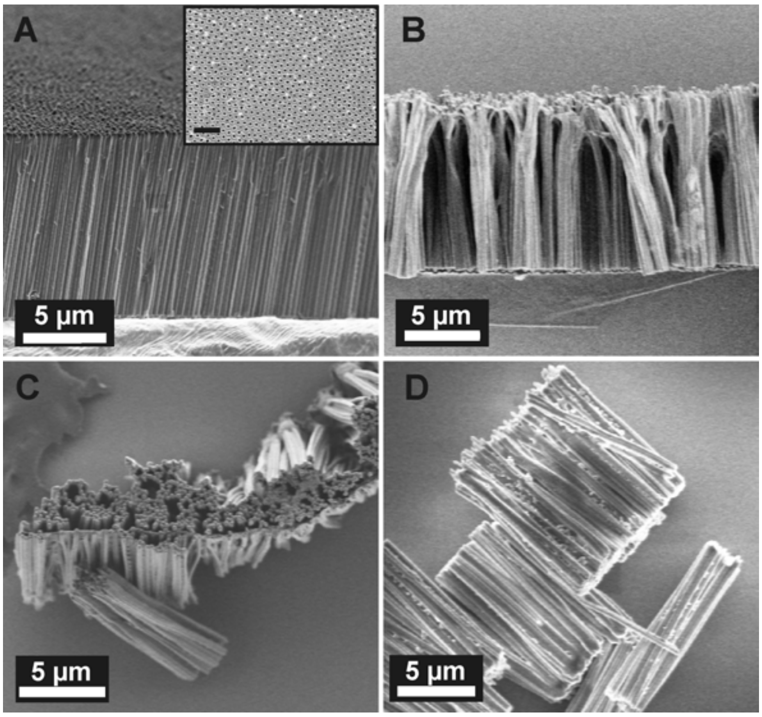

Figure 1. *Scanning electron micrographs. (A) Cross-sectional view of an unfilled AAO template fabricated in an aqueous solution of phosphoric acid (1.0 wt%) at 195 V. Post pore widening was carried out in 10 wt% phosphoric acid for 45 min (The inlet shows the top view of the template. The scale bar indicates 2 µm). Cross-sectional (B) and top-view (C) of the corresponding wire-shaped elastomers after the templating process and the selective removal of the AAO. (D) Bundles of the corresponding nanowires after short sonication treatment.*

solution wetting (see Scheme 1). To achieve a regular filling, the templates were annealed above the melting temperature of the monomer at 100°C. Subsequently, the residual LC material on top of the templates was removed mechanically with a razor blade. To polymerize the material, it was first heated to the isotropic phase at 100°C and was afterwards slowly cooled to the supercooled nematic phase at 65°C. Polymerization and crosslinking within the nematic phase was initiated by irradiation with UV light at 365 nm for 20 minutes. After selective removal of the AAO templates by treatment with diluted phosphoric acid, assemblies of parallel ordered LCE nanowires were obtained. The scanning electron micrographs in Figure 1 reveal that the length of the obtained wires was uniform and matched with the thickness of the porous AAO template. The AAO templating process features the fabrication of LCE nanowires with precise and adjustable dimensions. Due the hydrophobic nature of the cross-linked LC material the nanowires directly form ladder-like or bundle-like assemblies right after the removal of the template. However, the scanning electron micrographs indicated that the assemblies consisted of single wires. By sonication treatment the ladder-like assemblies could be separated into smaller bundles and even into single wires.

The characterization of the mesogen alignment in the nanowires was performed by optical microscopy. The results are presented in figure 2. The images with a dark background were taken with crossed polarizer and

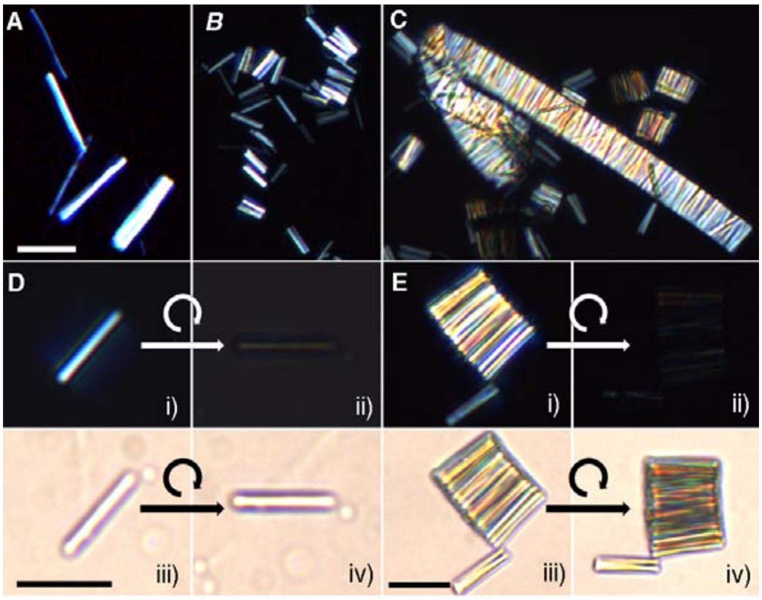

Figure 2. *Polarizing microscopy images of the polymerized liquid crystalline nanowires. Polarizer and analyzer were crossed in the first two rows of images (dark background, POM), while the analyzer was removed in the third row (bright background, OM). A and B show two samples of mostly separated rods with a length of roughly 30 and 10 µm respectively. The sample presented in C consists mainly of agglomerated rods, which form a regular ladder-like structure. D and E show the rotation of a single rod (D) and a "ladder" (E) under the microscope in order to determine their internal orientation. In figures i) the rod's long axis of both samples have an angle of 45° to the polarizer, while they are parallel to it in ii). Figures iii) and iv) show the rotation process in the OM mode. We find that the rods become completely dark in POM during the rotation. This demonstrates the high degree of internal order in these structures. The mesogens must be aligned uniformly either parallel or perpendicular to the rod's long axis.*

analyzer. Using this technique, only birefringent objects (like liquid crystals) are imaged as bright spots with a very high contrast. Figure 2A and 2B show two samples of nanowires prepared in templates with a different length of the cavitations. The resulting rods had a length of approximately 30 and 10 micrometers, respectively, and possessed a narrow length distribution. They appear as lines on the images, because their thickness is way below the resolution limit of conventional optical microscopy. However, some of the rods in figure 2A and 2B appear brighter than others. We assume, that the brighter ones consist of several assembled nanowires that were not separated after the templating and sonication process. Figure 2C shows a sample that had not been sonicated during the workup procedure. Here, ladder like assemblies are present, similar to the onses observed by SEM. To analyze the orientation of the mesogens in the nanowires we rotated the samples between crossed polarizers under the microscope. The results for a single rod and a larger aggregate are presented in figure 2D and 2E. We found, that both structures became completely dark when

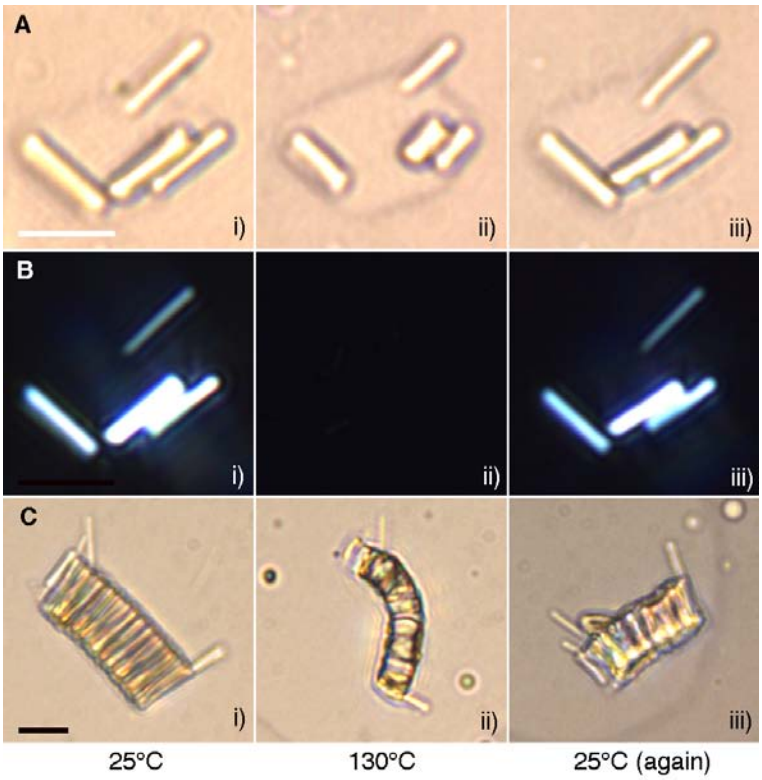

Figure 3. *Shape changing behavior of our nano-actuators during heating experiments. Part A shows several nanowires at temperatures of 25°C (i), 130°C (ii) and after cooling back to 25°C (iii). When heated from the nematic phase at room temperature to the isotropic phase at 130°C, the rods exhibit a significant change in length of roughly 40%. After cooling back to ambient conditions they completely recover their primal shape. Part B presents the heating process between crossed polarizers. It shows, that the change in shape comes along with a change between nematic and isotropic phase. In the nematic phase the rods posses a strong birefringence, which vanishes completely at 130°C and is regained upon cooling. Part C shows the actuation process of a ladder-like structure. Due to an increase of the rod's diameters during the actuation, the ladder becomes longer. The observed bending deformation of the whole structure is probably caused by adhesion to the substrate. Also in this case the deformation is reversible.*

the rod's long axes were situated parallel or perpendicular to the polarizer. This is a very typical behavior for samples with a liquid crystalline monodomain *[37]*. We therefore conclude, that the mesogens in our nanowires are oriented uniformly with the director situated either parallel or perpendicular to the rod's long axes. From this permanent internal orientation, actuation properties should arise. The actuation properties were tested by heating the nanowires under the microscope to a temperature above the clearing point of the LCE. The results are summarized in figure 3. Row A in figure 3 shows three images of some rods in the nematic phase at 25°C, (i) in the isotropic phase at 130°C (ii) and after cooling back to 25°C (iii). We found, that during the transition from the nematic to the isotropic phase the rod's length shortened by roughly 40 percent from 10 to approximately 6 micrometers. Upon cooling, they fully regained their initial length. Row B in figure 3 shows that the actuation goes along with a loss and regain of birefringence. At 25°C all rods were birefringent, and - again - some of them were brighter than others. At 130°C the birefringence vanished and it reappeared during cooling. We can thus claim, that the observed reversible change in length is the consequence of a phase transition from the liquid crystalline to the isotropic phase in an aligned LCE sample. A closer look at figure 3A reveals, that the observed contraction of some rods is more pronounced than of others. Comparison of figure 3A and 3B indicates that the rods with the strongest actuation are also the ones appearing brightest between crossed polarizers. We assume, that these aggregated rods show a stronger change in length than single ones, because they have a smaller surface to volume ratio. As a consequence they experience less friction with the substrate during the actuation process, leading to higher deformations. Figure 3C shows the actuation of a ladder-like object. Due to the fact, that all nanorods actuated simultaneously in the same direction the response was very pronounced. In addition to the objects contraction in width, we also observed an increase of its length, which led to a bending of the structure, probably caused by adhesion to the substrate. This observation is in compliance with the theoretical consideration that the volume of the material has to remain constant during the actuation process. As a result, the contraction of the rod's length is compensated by an increase in their diameter. The increase in thickness of a single rod is too small to be observed by optical microscopy directly, but if the deformations of many rods add up, like in the ladder-structures, the effect becomes visible. When cooled back to the nematic phase, the ladder regained its primal dimensions but obtained a slightly different appearance than before heating. This is most probably due to the softening of the material with heat, leading to coalescence of the single rods. In a second heating-cooling cycle, no further permanent alteration of the structures appearance was observed. In order to demonstrate the speed of the actuation process, we captured one heating and cooling cycle of a ladder-structure in real-time movies, which are available as supplemental information.

These experiments prove the uniform alignment of the mesogenic moieties in the material parallel to the nanowires long axis. Consequently, the confinement induced orientation reported for discotic liquid crystals*[32]* also works for nematics. In this contribution, the authors differentiated two mechanisms of mesogen orientation inside the AAO templates. The first mechanism is surface alignment of the molecules at the interface liquid crystal – aluminum oxide. The second one is the adjustment of the mesogen's alignment to the symmetry of the confined geometry inside the pores. In the case of discotics, these two effect were competing: while the mesogens near the interface tended to align parallel to the pore's surface, the discotic molecules inside the material oriented perpendicular to the surface due to symmetric reasons. This led to a variation of the director field within the nanowires. However, in the case of a nematic mesogen the situation is different.

Considering the fact, that our monomer has a comparable chemical structure, we assume that it adapts a parallel surface alignment to the aluminum oxide as well. Concerning symmetry, the calamitic mesogens should adopt a parallel alignment within the nanowires. Consequently, both effects act in the same direction, leading to the highly ordered structures as observed in our experiments. The high degree of order in the nanowires leads to a strong change of their length during the phase transition. The ability to reversibly change their shape on a micrometer-level after the application of an external stimulus, combined with their uniformity in size, makes these materials very appealing for applications in interdisciplinary science. Thereby they can either be deployed as single rods, allowing the manipulation of movable parts on a microscopic level, or as assemblies, which create stronger forces and larger displacements. Possible fields of utilization are lab-on-chip systems, microfluidics and biomemetics.

Experimental.

Fabrication of AAO templates. High purity aluminum (99.997 %, 0.5 mm thick) for the template fabrication was purchased from Alfa Aesar. Aluminum plates were cleaned by sonication treatment in isopropanol and acetone respectively followed by an electropolishing step in a mixture of ethanol and perchloric acid (v/v 4:1) at 0 °C. The anodization steps were performed in a self-build apparatus. Briefly, the aluminum sheets were mounted on a copper plate serving as the anode. A radial area of 2.27 cm^2 was exposed to an aqueous acidic solution. A platinum wire was used as the cathode. The apparatus was surrounded by a cryostatic bath and the electrolyte solution was rigorously stirred during anodization. The anodization voltage was controlled by a power supply unit with an integrated USB interface. Anodization was performed in an aqueous solution of phosphoric acid (c =1.0 wt%) at 195 V The first anodization step was carried out for 12 h, followed by an etching step in aqueous solution of chromic acid (1.8 wt%) and phosphoric acid (6.0 wt%) at 60 °C for 18 h. The second anodization was performed under the some conditions like the first step. The length of the templates was controlled by the anodization time. A subsequent pore widening was carried out in aqueous phosphoric acid (5 wt%) at 25 °C for 45 min.

Fabrication of LCE wires. The LC monomer **1** was synthesized according to the procedure described in the literature.*[36]* A mixture of **1**, 10 mol% of hexamethylenediacrylate (2) and 2 wt% of the photoinitiator Lucirin TPO was dissolved in dichloromethane (20 wt%). The solution was dropped onto the surface of the AAO template and homogenously spread. After evaporation of the solvent at room temperature, the coated AAO template was pressed between to glass slides and heated up to 90°C for 2 h. After cooling down to room temperature and removing of the glass slides, the residual LC film on top of the template was removed by mechanically scratching with a razor blade and subsequently by a short O_2-plasma treatment (10 min at 100 W). For the crosslinking in the nematic phase the samples were first heated on a hot plate to 90 °C (isotropic phase of **1**) and slowly cooled down to the supercooled nematic phase at 65°C. The temperature was held constant and the sample was UV-irradiated for 20 min by using an Oriel LSH302 500W UV-lamp equipped with a 365 nm line filter. The AAO was selectively removed by treatment with phosphoric acid (5 wt%) for 12 h. The LCE nanowires were separated from the phosphoric acid solution by several centrifugation/sonication-assisted redisperison cycles with water. The wires were stored as an aqueous dispersion. For the heating experiments the wires were redispersed in silicon oil. SEM images were recorded using a Zeiss Leo 1530 at an acceleration voltage of 3.0 kV for AAO membranes and 0.7 kV for polymeric samples. For detection an Inlens detector was used.

Acknowledgements.

We acknowledge the center of Electron Microscopy at the Max-Planck Institute for Polymer Research in Mainz, in particular G. Glasser and I. Lieberwirth, for access to SEM measurements. This research was supported by the International Research Training Group (IRTG 1404) and the Graduate School of Excellence "Material Science in Mainz" (GSC 266) both funded by the German Science Foundation (DFG). This research was supported by WCU (World Class University) program through the National Research Foundation of Korea funded by the Ministry of Education, Science and Technology (R31-10013).

References.

[1] R. Zentel, *Angew. Chem.Int. Edit.* **1989**, *28*, 1407.

[2] H. Finkelmann, H. R. Brand, *Trends in Polymer Science* **1994**, *2*.

[3] E. M. Terentjev, *J. Phys. Condes. Matter* **1999**, *11*, R239.

[4] P. G. de Gennes, *Comptes Rendus Hebdomadaires Des Seances De L Academie Des Sciences Serie B* **1975**, *281*, 101.

[5] C. Ohm, M. Brehmer, R. Zentel, *Advanced Materials* **2010**, *DOI: 10.1002/adma.200904059*.

[6] Y. L. Yu, T. Ikeda, *Angew. Chem. Int. Edit.* **2006**, *45*, 5416.

[7] J. Kupfer, H. Finkelmann, *Makromol. Chem. Rapid Comm.* **1991**, *12*, 717.

[8] M. Brehmer, R. Zentel, G. Wagenblast, K. Siemensmeyer, *Macromol. Chem. Phys.* **1994**, *195*, 1891.

[9] M. H. Li, P. Keller, J. Y. Yang, P. A. Albouy, *Adv. Mater.* **2004**, *16*, 1922.

[10] T. Ikeda, M. Nakano, Y. L. Yu, O. Tsutsumi, A. Kanazawa, *Adv. Mater.* **2003**, *15*, 201.

[11] C. Ohm, C. Serra, R. Zentel, *Adv. Mater.* **2009**, *21*, 4859.

[12] A. Buguin, M. H. Li, P. Silberzan, B. Ladoux, P. Keller, *J. Am. Chem. Soc.* **2006**, *128*, 1088.

[13] Z. Q. Yang, G. A. Herd, S. M. Clarke, A. R. Tajbakhsh, E. M. Terentjev, W. T. S. Huck, *J. Am. Chem. Soc.* **2006**, *128*, 1074.

[14] H. Yang, A. Buguin, J.-M. Taulemesse, K. Kaneko, A. Bergeret, P. Keller, *J. Am. Chem. Soc.* **2009**, *131*, 15000.

[15] C. L. van Oosten, C. W. M. Bastiaansen, D. J. Broer, *Nat. Mater.* **2009**, *8*, 677.

[16] M. Steinhart, *Adv Polym Sci* **2008**, *220*, 123.

[17] T. Wade, J. Wegrowe, *Eur Phys J-Appl Phys* **2005**, *29*, 3.

[18] S.-H. Jeong, S.-H. Jung, K.-H. Lee, *J. Korean Ind. Eng. Chem.* **2005**, *16*, 461.

[19] H. Masuda, K. Fukuda, *Science* **1995**, *268*, 1466.

[20] H. Masuda, H. Yamada, M. Satoh, H. Asoh, M. Nakao, T. Tamamura, *Appl. Phys. Lett.* **1997**, *71*, 2770.

[21] J. Klein, R. Herrick, D. Palmer, M. Sailor, C. Brumlik, C. Martin, *Chem. Mater.* **1993**, *5*, 902.

[22] W. Choi, J. Chu, K. Jeong, E. Bae, J.-W. Lee, J.-J. Kim, J.-O. Lee, *Appl. Phys. Lett.* **2001**, *79*, 3696.

[23] S. Sapp, B. Lakshmi, C. Martin, *Adv. Mater.* **1999**, *11*, 402.

[24] N. Haberkorn, M. C. Lechmann, B. H. Sohn, K. Char, J. S. Gutmann, P. Theato, *Macromol Rapid Comm* **2009**, *30*, 1146.

[25] N. Haberkorn, J. S. Gutmann, P. Theato, *Acs Nano* **2009**, *3*, 1415.

[26] M. Steinhart, J. Wendorff, A. Greiner, R. Wehrspohn, K. Nielsch, J. Schilling, J. Choi, U. Gosele, *Science* **2002**, *296*, 1997.

[27] N. Haberkorn, S. A. L. Weber, R. Berger, P. Theato, *ACS Appl. Mater. Interfaces* **2010**, *2*, 1573.

[28] M. Steinhart, P. Goering, H. Dernaika, M. Prabhukaran, U. Goesele, E. Hempel, T. Thurn-Albrecht, *Phys Rev Lett* **2006**, *97*, 027801.

[29] K. Shin, E. Woo, Y. G. Jeong, C. Kim, J. Huh, K.-W. Kim, *Macromolecules* **2007**, *40*, 6617.

[30] J. S. Kim, Y. Park, D. Y. Lee, J. H. Lee, J. H. Park, J. K. Kim, K. Cho, *Adv Funct Mater* **2010**, *20*, 540.

[31] M. Steinhart, S. Murano, A. Schaper, T. Ogawa, M. Tsuji, U. Gösele, C. Weder, J. Wendorff, *Adv Funct Mater* **2005**, *15*, 1656.

[32] M. Steinhart, S. Zimmermann, P. Goring, A. Schaper, U. Gosele, C. Weder, J. Wendorff, *Nano Lett.* **2005**, *5*, 429.

[33] W. Pisula, T. Zeljko, B. El Hamaoui, M. Watson, T. Pakula, K. Müllen, *Adv Funct Mater* **2005**, *15*, 893.

[34] W. Pisula, M. Kastler, D. Wasserfallen, R. Davies, M.-C. Garcia-Gutierrez, K. Müllen, *J Am Chem Soc* **2006**, *128*, 14424.

[35] J. Wu, W. Pisula, K. Müllen, *Chem. Rev.* **2007**, *107*, 718.

[36] D. Thomsen, P. Keller, J. Naciri, R. Pink, H. Jeon, D. Shenoy, B. Ratna, *Macromolecules* **2001**, *34*, 5868.

[37] J. Naciri, A. Srinivasan, H. Jeon, N. Nikolov, P. Keller, B. R. Ratna, *Macromolecules* **2003**, *36*, 84

6 List of publications

(1) *"Ophthalmic drug delivery utilizing two-photon absorption: A novel approach to treat posterior capsule opacification*." In: Therapeutic Laser Applications and Laser-Tissue Interactions III (ed. A. Vogel). Hee-Cheol Kim, Jens Träger, Matthias Zorn, **Niko Haberkorn**, Norbert Hampp
Proc. SPIE-OSA Biomedical Optics, **2007**, 66321E, 1-8.

(2) "*Synthesis of Nanoobjects Consisting of Reactive Polymers*"
Niko Haberkorn, Katja Nilles, Patrick Theato,
Polymer Preprints, **2008**, *49*, 220-221.

(3) *"Templated Organic and Hybrid Materials for Optoelectronic Applications"*
Niko Haberkorn, Maria C. Lechmann, Byeong Hyeok Sohn, Kookheon Char, Jochen S. Gutmann, Patrick Theato, *Macromol Rapid Comm* **2009**, *30*, 1146

(4) "*Template-Assisted Fabrication of Free-Standing Nanorod Arrays of a Hole-Conducting Cross Linked Triphenylamine Derivative: Toward Ordered Bulk-Heterojunction Solar Cells.",* **Niko Haberkorn**, Jochen S. Gutmann, Patrick Theato, *ACS Nano* **2009**, *3*, 1415.

(5) *"Mapping of Local Conductivity Variations on Fragile Nanopillar Arrays by Scanning Conductive Torsion Mode Microscopy",*
Stefan A. L. Weber, **Niko Haberkorn**, Patrick Theato, Rüdiger Berger, *Nano Lett.* **2010**, *10*, 1194-1197.

(6) *"Template-Assisted Fabrication of Well-Ordered p-Type Nanorod Arrays for Photovoltaic Applications"*
Niko Haberkorn, Patrick Theato, *Polymer Preprints*, **2010**, 51, 246-247.

(7) *"Template-Based Preparation of Free-Standing Semiconducting Polymeric Nanorod Arrays on Conductive Substrates",*
Niko Haberkorn, Stefan A. L. Weber, Rüdiger Berger, Patrick Theato, *ACS Appl. Mater. Interfaces*, **2010,** 2, 1573-1580.

(8) *"Template-Assisted Fabrication of Free-Standing Nanorod Arrays Based upon Organic Semiconductors for Organic Solar Cells",* **Niko Haberkorn**, Patrick Theato, *PMSE Preprint*, **submitted**.

(9) *"Template-Assisted Fabrication of Highly-Ordered Interpenetration Networks of Semi-Conducting Polymers for Photovoltaic Applications",*
Niko Haberkorn, Sehee Kim, Ki-Se Kim, Michael Sommer, Mukudun Thelakkat, Byeong-Hyeok Sohn, Patrick Theato, *Adv. Funct. Mater.* **submitted**.

(10) *"Two Dimensional Self Assembly of Disulfide Functionalized Bis-acylurea: a Nanosheet Template for Gold Nanoparticle Arrays",*
Jong-Uk Kim, Ki-Hyun Kim, **Niko Haberkorn**, Peter J. Roth, Jong-Chan Lee, Patrick Theato, Rudolf Zentel, *Chem. Comm.* **accepted**.

(11) *"Reactive Nanowires Based on Activated Ester Polymers: A Versatile Template-Assisted Approach for the Fabrication of Functional Nanowires "*
Niko Haberkorn, Katja Nilles, Philipp Schattling, Patrick Theato,
Manuscript **in preparation**

(12) *"Template-Based Fabrication of Nanometer-Scaled Actuators from Liquid Crystalline Elastomers"*
Christian Ohm‡ , **Niko Haberkorn**‡, Patrick Theato*, Rudolf Zentel*.
Manuscript **in preparation**
‡: C.O. and N.H. have contributed equally.

(13) "Fabrication of Hierarchically Branched Polymeric Nanorod Arrays by Utilizing Branched Alumina Templates"
Niko Haberkorn, Patrick Theato*
Manuscript **in preparation**

7 Acknowledgements

The work that is presented in this thesis would not have been possible without the collective effort of a number of people that have directly or indirectly supported me during doctoral studies. To these people, I owe my gratitude and thanks.

[redacted]

[redacted]

[redacted]

[redacted]

[redacted]

[redacted]

[redacted]

[redacted]

[redacted]

[redacted]

[redacted]

[redacted]

[redacted]

[redacted]